

# **The immunoregulatory role of amphiregulin in acute and chronic liver disease**

## **Dissertation**

Zur Erlangung des Grades eines Doktors der Naturwissenschaften  
des Fachbereichs Biologie, der Fakultät Mathematik, Informatik und Naturwissenschaften,  
der Universität Hamburg

vorgelegt von:  
Selina Wachtendorf  
aus Delmenhorst

Hamburg 2024

**Tag der Disputation: 11.04.2025**

**Vorsitzende der Prüfungskommission**

Prof. Dr. Julia Kehr  
Universität Hamburg  
Institut für Pflanzenwissenschaften und Mikrobiologie

**Gutachter der Dissertation**

PD Dr. Katrin Neumann  
Universitätsklinikum Hamburg-Eppendorf  
Institut für Zelluläre und Integrative Physiologie

PD Dr. Hartwig Lüthen  
Universität Hamburg  
Institut für Pflanzenwissenschaften und Mikrobiologie

Diese Dissertation ist über die Staats- und Universitätsbibliothek Hamburg veröffentlicht und online verfügbar unter der URN:  
[urn:nbn:de:gbv:18-ediss-127372](https://nbn-resolving.org/urn:nbn:de:gbv:18-ediss-127372)

# Table of contents

<b>Declaration of own contribution to presented published work.....</b>	<b>V</b>
<b>List of publications .....</b>	<b>VII</b>
<b>List of Figures .....</b>	<b>VIII</b>
<b>List of Tables .....</b>	<b>IX</b>
<b>Abbreviations .....</b>	<b>X</b>
<b>1 Introduction.....</b>	<b>1</b>
1.1 The liver: Anatomy, function, and immunological role.....	1
1.2 Autoimmune liver disease.....	5
1.3 The model of Concanavalin A-induced immune-mediated liver disease.....	6
1.4 Chronic liver disease .....	9
1.5 Multidrug resistance p-glycoprotein 2 knockout mice as a model for PSC .....	11
1.6 Regulatory T cells in liver disease.....	13
1.7 Effector function of group 2 innate lymphoid cells in the liver .....	15
1.8 Amphiregulin in acute and chronic liver disease .....	17
1.9 The alarmin IL-33 in autoimmune liver disease.....	19
1.10 Aim of this study .....	21
<b>2 Materials and Methods .....</b>	<b>22</b>
2.1 Materials.....	22
2.1.1 Technical Equipment .....	22
2.1.2 Consumables .....	24
2.1.3 Reagents and Kits .....	25
2.1.4 Cytokines and growth factors .....	29
2.1.5 Buffers and solutions .....	30
2.1.6 Antibodies .....	34
2.1.6.1 Antibodies for enzyme-linked immunosorbent assay (ELISA) .....	34
2.1.6.2 Antibodies for Immunohistochemistry (IHC) .....	35
2.1.6.3 Antibodies for flow cytometry .....	35
2.1.7 Primers.....	37
2.1.8 Software and databases.....	38
2.2 Methods .....	39
2.2.1 Mice .....	39
2.2.2 Animal treatment .....	40
2.2.3 Euthanasia of mice and collection of biological samples .....	40
2.2.4 Analysis of biomarkers of liver disease in blood plasma .....	41
2.2.5 Cytokine determination by enzyme-linked immunosorbent assay (ELISA) .....	42

2.2.6	Quantitative reverse transcription polymerase chain reaction (qRT-PCR)	43
2.2.7	Hydroxyproline assay (HPA)	45
2.2.8	Histology	46
2.2.8.1	Hematoxylin & Eosin staining (H&E)	46
2.2.8.2	Sirius red staining	47
2.2.8.3	Immunohistochemistry (IHC)	48
2.2.9	Isolation of cells	50
2.2.9.1	Isolation of primary hepatocytes for <i>in vitro</i> culture	50
2.2.9.2	Magnetic-activated cell sorting (MACS)	50
2.2.9.3	Isolation of primary LSECs for <i>in vitro</i> culture	51
2.2.9.4	Isolation of CD25 <sup>+</sup> CD4 <sup>+</sup> Tregs for <i>in vitro</i> culture	52
2.2.9.5	Isolation of CD25 <sup>+</sup> CD4 <sup>+</sup> Tregs and CD4 <sup>+</sup> T cells for suppression assay	55
2.2.9.6	Isolation of hepatic non-parenchymal cells	56
2.2.9.7	Fluorescence-activated cell sorting (FACS)	57
2.2.9.8	Isolation of hepatic ILC2s for <i>in vitro</i> culture	57
2.2.10	Cell cultures	59
2.2.10.1	Primary Hepatocyte cell culture	59
2.2.10.2	Primary LSEC cell culture	60
2.2.10.3	Immune cell culture	60
2.2.10.4	Suppression assay	60
2.2.11	Flow cytometry	61
2.2.11.1	Staining and analysis of hepatic non-parenchymal cells	61
2.2.11.2	Gating strategy to identify hepatic ST2 <sup>+</sup> Tregs and ILC2s	63
2.2.12	Statistical analysis	64
<b>3</b>	<b>Results</b>	<b>65</b>
3.1	IL-33-induced AREG expression by hepatic ST2 <sup>+</sup> Tregs and ILC2s	65
3.2	Hepatic ST2 <sup>+</sup> Tregs and ILC2s express AREG in immune-mediated hepatitis	69
3.3	Immune-mediated hepatitis is aggravated in absence of AREG	74
3.4	Exogenous AREG activates ST2 <sup>+</sup> Tregs but inhibits ILC2s	78
3.5	Impaired immunoregulatory capacity of <i>Areg</i> <sup>-/-</sup> Tregs	83
3.6	Reduced capacity of ST2 <sup>+</sup> Tregs to express AREG in chronic liver disease	85
<b>4</b>	<b>Discussion</b>	<b>89</b>
4.1	The EGFR ligands in acute and chronic liver disease	89
4.2	Exogenous IL-33 induces AREG expression in hepatic ST2 <sup>+</sup> Tregs and ILC2s	94
4.3	AREG-expressing cell types in acute immune-mediated hepatitis	96
4.4	Protective role of AREG in acute immune-mediated hepatitis	98
4.5	Differential effect of AREG on ST2 <sup>+</sup> Tregs and ILC2s	100

4.6 The role of AREG in chronic liver disease .....	104
<b>5 Outlook .....</b>	<b>106</b>
<b>6 Summary .....</b>	<b>108</b>
<b>7 Zusammenfassung .....</b>	<b>111</b>
<b>References .....</b>	<b>113</b>
<b>Danksagung.....</b>	<b>137</b>
<b>Affidavit.....</b>	<b>139</b>
<b>Eidesstattliche Versicherung.....</b>	<b>139</b>

## Declaration of own contribution to presented published work

Key findings from the data presented in this thesis have already been published in *Frontiers in Immunology* under the title “The ST2<sup>+</sup> Treg/amphiregulin axis protects from immune-mediated hepatitis” by **Selina Wachtendorf**, Fitriasisari Jonin, Aaron Ochel, Fabian Heinrich, Astrid M. Westendorf, Gisa Tiegs and Katrin Neumann. The authors Selina Wachtendorf and Fitriasisari Jonin contributed equally to this paper and share first authorship. The publication is the result of a collaborative effort to which I substantially contributed in the design and execution of experiments, as well as the analysis and interpretation of data. The manuscript was drafted by Katrin Neumann, with contributions from Fitriasisari Jonin and myself. All authors were involved in the critical revision of the manuscript.

The following outlines my contributions and those of my colleagues to this thesis. Katrin Neumann and Gisa Tiegs planned this project and obtained funding. Matias A. Avila and Max Löhning supported this study by providing mice. I planned, conducted and analyzed most of the experiments, specifically those presented in Figures 6, 7 and 8, Figure 9A, B and C (Bcl-2 and AREG), Figure 10, Figure 11 (ILC2s), Figure 12B, D, E (ST2<sup>+</sup> Tregs, ICOS, CTLA-4 and PD-L1) and F (ILC2s and AREG), Figures 13 and 14, Figure 15A (ST2<sup>+</sup> Tregs), C, D and E (Foxp3<sup>+</sup> Tregs, KLRG1, ICOS, Ki-67, CTLA-4, PD-L1, TIGIT and Bcl-2), and Figures 16, 18, 21, 22 and 23. In complex and time-consuming experiments, I was supported by Elena Tasika and Carsten Rothkegel. Additional data in this thesis originate from experiments that were coordinated, performed and analyzed by colleagues. These include the data shown in Figure 5, Figure 9C (KLRG1, ICOS, IL-10 and PD-L1), Figure 11 (ST2<sup>+</sup> Tregs), and Figures 17, 19 and 20, collected by Fitriasisari Jonin. Data in Figure 12A, C, E (AREG) and F (KLRG1 and IL-13), and Figure 15A (ILC2s), B, E (ST2<sup>+</sup> Tregs) and F were provided by Aaron Ochel. Finally, the data in Figure 9C (ST2<sup>+</sup> Tregs, CTLA-4 and TIGIT) and Figure 12E (KLRG1, IL-10 and TIGIT) were acquired by Fabian Heinrich, and those in Figure 9C (Ki-67) and Figure 12E (Ki-67 and Bcl-2) by Katrin Neumann. I analyzed and interpreted the data and wrote this thesis under the supervision of Katrin Neumann.

Hamburg, den 14.11.2024

---

Place and date

*Selina Wachtendorf*

---

Selina Wachtendorf

Hamburg, den 14.11.2024

---

Place and date

*Katrin Neumann*

---

PD Dr. Katrin Neumann

## List of publications

### Journal articles

**Wachtendorf S\***, Jonin F\*, Ochel A, Heinrich F, Westendorf AM, Tiegs G, Neumann K. The ST2<sup>+</sup> Treg/amphiregulin axis protects from immune-mediated hepatitis. *Front Immunol.* (2024) 15: 1351405. Published 2024 Mar 20. DOI: 10.3389/fimmu.2024.1351405. (\*authors contributed equally and share first authorship)

### Abstracts of congress poster presentations

**Wachtendorf S**, Ochel A, Neumann K, Tiegs G. Immunoregulatory role of the IL-33/amphiregulin axis in acute immune-mediated liver disease. Conference: 37<sup>th</sup> Annual Conference German Association for the Study of the Liver (GASL). Location Virtual. *Z Gastroenterol.* (2021) 59.01: e47.

**Wachtendorf S**, Ochel A, Tiegs G, Neumann K. Immunoregulatory role of the IL-33/amphiregulin axis in acute and chronic liver disease. Conference: 6<sup>th</sup> European Congress of Immunology (ECI). Location Virtual. *Eur J Immunol.* (2021) 51.S1: 247. P-0196.

**Wachtendorf S**, Ochel A, Tiegs G, Neumann K. The IL-33/amphiregulin axis mediates immunoregulation in acute and chronic liver disease. Conference: 38<sup>th</sup> Annual Conference German Association for the Study of the Liver (GASL). Location Virtual. *Z Gastroenterol.* (2022) 60.01: e47.

**Wachtendorf S**, Ochel A, Jonin F, Tiegs G, Neumann K. The role of ILC2s and Tregs in IL-33/amphiregulin-mediated regulation of immune-mediated hepatitis. Conference: Organizing Tissue Homeostasis and Immunity - NK Cell & ILC Meeting. Location Würzburg, Germany. (2023).

**Wachtendorf S**, Ochel A, Jonin F, Tiegs G, Neumann K. IL-33/amphiregulin-mediated regulation of acute immune-mediated hepatitis. Conference: Joint Conference of the French Society for Immunology (SFI) and the German Society for Immunology (DGfI). Location Strasbourg, France. *Eur J Immunol.* (2023) 53.S2: 289. P302.

### Abstracts of congress oral presentations

**Wachtendorf S**, Ochel A, Tiegs G, Neumann K. The IL-33/amphiregulin axis regulates immunity in acute and chronic liver disease. Conference: Joint Meeting of the German Society for Immunology (DGfI) and the Austrian Society for Allergology and Immunology (ÖGAI). Location Hannover, Germany. *Eur J Immunol.* (2022) 52.S1: 32-33. O026.



## List of Figures

Figure 1: Liver anatomy. ....	2
Figure 2: Model of ConA-induced immune-mediated hepatitis. ....	9
Figure 3: Progression of chronic liver disease. ....	11
Figure 4: Model of multidrug resistance p-glycoprotein 2 (MDR2) deficiency. ....	12
Figure 5: Gating strategy and purity of MACS-sorted Tregs for <i>in vitro</i> culture. ....	54
Figure 6: Gating strategy and purity of MACS-sorted CD25 <sup>-</sup> CD4 <sup>+</sup> T cells and CD25 <sup>+</sup> CD4 <sup>+</sup> Tregs for suppression assay. ....	56
Figure 7: Gating strategy and purity of FACS-sorted ILC2 for <i>in vitro</i> culture. ....	59
Figure 8: Gating strategy for flow cytometric analysis of ST2 <sup>+</sup> Tregs and ILC2s. ....	63
Figure 9: IL-33-induced phenotype of hepatic ST2 <sup>+</sup> Tregs. ....	67
Figure 10: IL-33-induced phenotype of hepatic ILC2s. ....	68
Figure 11: Effect of exogenous IL-33 on AREG expression of ST2 <sup>+</sup> Tregs and ILC2s. ....	68
Figure 12: Phenotype of ST2 <sup>+</sup> Tregs and ILC2s in immune-mediated hepatitis. ....	70
Figure 13: AREG expression in the liver tissue in immune-mediated hepatitis. ....	72
Figure 14: AREG expression by hepatocytes. ....	73
Figure 15: <i>Areg</i> <sup>-/-</sup> mice develop more severe immune-mediated hepatitis. ....	75
Figure 16: IL-33-induced phenotype of hepatic ST2 <sup>+</sup> Tregs and ILC2s in the absence of AREG. ....	76
Figure 17: Effect of exogenous IL-33 on ST2 <sup>+</sup> Tregs in the absence of AREG. ....	77
Figure 18: Effect of exogenous AREG on hepatic ILC2s. ....	79
Figure 19: Effect of exogenous AREG on Tregs. ....	81
Figure 20: Effect of exogenous AREG on IL-33-activated ST2 <sup>+</sup> Tregs. ....	83
Figure 21: AREG-dependent immunosuppressive function of Tregs. ....	85
Figure 22: Pathology of the <i>Mdr2</i> <sup>-/-</sup> mouse model of sclerosing cholangitis. ....	87
Figure 23: Phenotype of ILC2s and ST2 <sup>+</sup> Tregs in chronic liver disease. ....	88
Figure 24: Graphical abstract illustrating the proposed role of AREG in acute and chronic liver disease. ....	110

## List of Tables

Table 1: Technical Equipment.....	22
Table 2: Consumables.....	24
Table 3: Reagents and kits .....	25
Table 4: Cytokines and growth factors .....	29
Table 5: Buffers and solutions.....	30
Table 6: Primary and secondary antibodies for Sandwich ELISA.....	34
Table 7: Primary antibodies for IHC .....	35
Table 8: Secondary antibodies for IHC .....	35
Table 9: Antibody for blocking Fc receptors - flow cytometry (anti-mouse).....	35
Table 10: Antibodies for surface staining - flow cytometry (anti-mouse).....	35
Table 11: Antibodies for intracellular analysis by flow cytometry (anti-mouse).....	36
Table 12: Oligonucleotide sequences of primers used in qRT-PCR. ....	37
Table 13: Software and databases .....	38

## Abbreviations

°C	degree Celsius
aa	Amino acid
Ab	antibody
aCD3/CD28	anti-CD3/CD28 Dynabeads
ad	Fill-up to
ADAM	A disintegrin and metalloprotease
AF 647	Alexa Fluor 647
AF 488	Alexa Fluor 488
AIH	Autoimmune hepatitis
AILD	Autoimmune liver disease
ALP	Alkaline phosphatase
ALT	Alanine aminotransferase
ANIT	Alpha-naphthyl-isocyanate
ANOVA	Analysis of variance
AP polymer	Alkaline phosphatase polymer
APC	Antigen-presenting cell
APC	Allophycocyanin
APC-Cy7	Allophycocyanin-cyanin 7
AREG / Areg	Amphiregulin
Bcl-2	B cell lymphoma 2
BLAST	Basic local alignment search tool
BSA	Bovine serum albumin
BTC / Btc	Betacellulin
BV 421	Brilliant Violet 421
BV 605	Brilliant Violet 605
BV 711	Brilliant Violet 711
BV 785	Brilliant Violet 785
CC	Cholangiocarcinoma
CCl <sub>4</sub>	Carbon tetrachloride
CD105	Cluster of differentiation 105
CD11b	Cluster of differentiation 11b
CD11c	Cluster of differentiation 11c
CD16	Cluster of differentiation 16
CD19	Cluster of differentiation 19
CD25	Cluster of differentiation 25
CD32	Cluster of differentiation 32
CD4	Cluster of differentiation 4
CD45R	Cluster of Differentiation 45 receptor
CD49b	Cluster of differentiation 49b
CD8	Cluster of differentiation 8
CD8a	Cluster of differentiation 8 alpha-chain
cDNA	complementary DNA
CFDA-SE	5-(and-6)-carboxyfluorescein diacetate succinimidyl ester
CFSE	5-(and-6)-carboxyfluorescein succinimidyl ester
Col1a1	Collagen type I alpha 1 chain
Col3a1	Collagen type III alpha 1 chain
ConA	Concanavalin A
Ct	Threshold cycle

CTL	Cytotoxic T lymphocyte
CTLA-4	Cytotoxic T lymphocyte-associated protein 4
Cxcl9	Chemokine C-X-C motif ligand 9
Cxcl10	Chemokine C-X-C motif ligand 10
Cxcr3	Chemokine C-X-C motif receptor 3
DAB	3,3'-diaminobenzidine
DAMP	Damage-associated molecular pattern
DDC	3,5-diethoxycarbonyl-1,4-dihydrocollidine
ddH <sub>2</sub> O	double-distilled water
DEPC	Diethyl pyrocarbonate
dL	deciliter
DMAB	4-(Dimethylamino)benzaldehyde
DMSO	Dimethyl sulfoxide
DNA	Deoxyribonucleic acid
dNTP	deoxyribonucleotide triphosphate
ECM	Extracellular matrix
EDTA	Ethylenediamine tetraacetic acid
EGF / Egf	Epidermal growth factor
EGFR / Egfr	Epidermal growth factor receptor
EGTA	Ethylene glycol tetraacetic acid
ELISA	Enzyme-linked immunosorbent assay
EMT	Epithelial-to-mesenchymal transition
EPGN / Epgn	Epigen / Epithelial mitogen
EREG / Ereg	Epiregulin
ERK	Extracellular signal-regulated kinase
FACS	Fluorescence-activated cell sorting
FasL	Fas ligand
FBS	Fetal bovine serum
FIR	Foxp3-IRES-mRFP
FITC	Fluorescein isothiocyanate
FMO	Fluorescence minus one
FSC-A	Forward scatter area
FSC-H	Forward scatter height
Foxp3	Forkhead box protein 3
GATA3	GATA binding protein 3
G	Gauge
g	gram
g	gravity force of centrifuge
GFP	Green fluorescent protein
GITRL	Glucocorticoid-induced tumor necrosis factor receptor ligand
h	hour
H&E	Hematoxylin and eosin
HB-EGF / Hbegf	Heparin binding EGF like growth factor
HBSS	Hank's balanced salt solution
HBV	Hepatitis B virus
HCV	Hepatitis C virus
HCC	Hepatocellular carcinoma
HDL	High-density lipoprotein
HEPES	4-(2-hydroxyethyl)-1-piperazineethanesulfonic acid
HPA	Hydroxyproline

HRP	horseradish peroxidase
HSC	Hepatic stellate cell
i.p.	intraperitoneal
i.v.	intravenous
ICOS	Inducible T cell co-stimulator
IFN $\gamma$ / Ifng	Interferon gamma
Ig	Immunoglobulin
IGF-1	Insulin-like growth factor-1
IHC	Immunohistochemistry
iILC2	Inflammatory group 2 innate lymphoid cell
IL	Interleukin
IL-1RAcP	IL-1 receptor accessory protein
IL-25R	Interleukin 25 receptor
IL-7R	Interleukin 7 receptor
IL12p40	Interleukin-12 subunit p40
IL1RL1	IL-1 receptor-like 1
ILC	Innate lymphoid cell
ILC1/2/3	Group 1/2/3 innate lymphoid cell
IRES	Internal ribosome entry site
IVC	Individually ventilated cage
KHX	Ketamine-Xylazine-Heparin
KLRG1	Killer cell lectin-like receptor subfamily G member 1
KO	Knock out
L	Liters
Ly-6C	Lymphocyte antigen 6C
Ly-6G	Lymphocyte antigen 6G
Ly-76	Lymphocyte antigen 76
lin	Lineage
LSEC	Liver sinusoidal endothelia cell
MACS	Magnetic-activated cell sorting
MAP	Mitogen-activated protein
Mdr2	Multidrug resistance P-glycoprotein 2
mg	milligram
MHC	Major histocompatibility complex
min	minute
mL	milliliters
MMP	Matrix metalloproteinase
mRFP	Monomeric red fluorescent protein
mRNA	messenger RNA
NASH	Nonalcoholic steatohepatitis
NF $\kappa$ B	Nuclear factor kappa-light-chain-enhancer of activated B cells
nILC2	natural group 2 innate lymphoid cell
NK	Natural killer cell
NKT	Natural killer T cell
ns	not significant
PAMP	Pathogen-associated molecular pattern
PBC	Primary biliary cholangitis
PBMC	Peripheral blood mononuclear cell
PBS	Phosphate buffered saline
PCR	Polymerase chain reaction

PD-1	Programmed cell death protein 1
PD-L1	Programmed cell death ligand 1
PE	Phycoerythrin
PE-Cy7	Phycoerythrin-cyanin 7
PerCP-Cy5.5	Peridinin-chlorophyll-protein-cyanin 5.5
PerCP-eF710	Peridinin-chlorophyll-protein-eFluor 710
PFIC3	progressive familial intrahepatic cholestasis type 3 (PFIC3)
PM	Perfusion medium
PMA	Phorbol 12-myristate 13-acetate
PPML	Pre-Perfusion Medium Liver
PSC	Primary sclerosing cholangitis
qPCR	quantitative (real-time) polymerase chain reaction
qRT-PCR	quantitative (real-time) reverse transcription polymerase chain reaction
rm	recombinant murine
RNA	Ribonucleic acid
RT	Room temperature
RT-PCR	Reverse transcription polymerase chain reaction
Sca-1	Stem cell antigen-2
Sec	Second
SEM	Standard error of the mean
SPF	specific pathogen-free
SSC-A	Side scatter area
ST2	Suppression of tumorigenicity 2
TAA	Thioacetamide
TBS	Tris-buffered saline
TCR	T cell receptor
TCR $\beta$	T cell receptor beta-chain
TCR $\gamma/\delta$	T cell receptor gamma/delta-chain
TGF $\alpha$ / Tgfa	Transforming growth factor alpha
TGF $\beta$ / Tgfb1/2	Transforming growth factor beta 1/2
Th	T helper cells
Th1	T helper cells type 1
Th17	T helper cells type 17
Th2	T helper cells type 2
Tiger	Interleukin-ten ires gfp-enhanced reporter
TIGIT	T cell immunoglobulin with ITIM domain
TIMP	Tissue inhibitors of metalloproteinase
TL1A	Tumor necrosis factor-like ligand 1A
TLR4	Toll-like receptor 4
TMB	3,3',5,5'-Tetramethylbenzidine
TNF $\alpha$ / Tnfa	Tumor necrosis factor alpha
TRAIL	TNF-related apoptosis inducing ligand
Treg	regulatory T cell
TSLP	Thymic stromal lymphopoietin
UKE	University medical center Hamburg-Eppendorf
UVB	Ultraviolet B
w/o	without
WT	Wildtype

# 1 Introduction

## 1.1 The liver: Anatomy, function, and immunological role

The liver is the body's largest organ and is located below the diaphragm, primarily in the right hypochondriac and epigastric regions of the abdominal cavity. The organ is incompletely divided into four lobes: the right, left, caudate and quadrate lobes.<sup>1</sup> It is further subdivided into eight macroscopic functional segments with independent vascular and biliary supplies.<sup>1</sup> The blood, hepatic bile duct, lymphatics and nerves enter the liver at its hilus.<sup>1</sup> The blood supply consists of about 20% of well oxygenated blood from the hepatic artery and about 80% of poorly oxygenated blood from the intestines, pancreas and spleen delivered through the portal vein.<sup>1</sup> At the microscopic level, the liver is structured into polygonal units termed hepatic lobules (Figure 1).<sup>1</sup> They are characterized by a central hepatic vein and portal tracts distributed along their peripheral boundaries (Figure 1).<sup>1</sup> Portal tracts contain portal veins and hepatic arteries forming the vascular distribution network, as well as effluent bile ducts (Figure 1).<sup>1</sup> The parenchyma consists of hepatocytes organized in plates along vascular channels called sinusoids, which facilitate blood flow from the portal tracts to the terminal hepatic vein (Figure 1).<sup>1</sup> Hepatic sinusoids are lined with fenestrated liver sinusoidal endothelial cells (LSECs).<sup>1</sup> Unlike most other endothelial cells in the body, they do not rest on a basement membrane, but are separated from hepatocytes by a perisinusoidal space known as the space of Disse (Figure 1).<sup>1</sup> This allows free molecule exchange between blood and hepatocytes.<sup>1</sup> Other non-parenchymal cells adhere to LSECs, including phagocytic Kupffer cells, which attach to the luminal side, and hepatic stellate cells (HSCs), specialized pericytes located in the space of Disse (Figure 1).<sup>1</sup> Hepatocytes are polarized.<sup>1</sup> Their basolateral membrane consists of a basal side with microvilli reaching into the space of disse, and lateral sides facing adjacent hepatocytes (Figure 1).<sup>1</sup> Bile caniculi run directly between neighboring hepatocytes (Figure 1).<sup>1</sup> They form the apical or canalicular surface of hepatocytes, which is also extended by microvilli.<sup>1</sup>

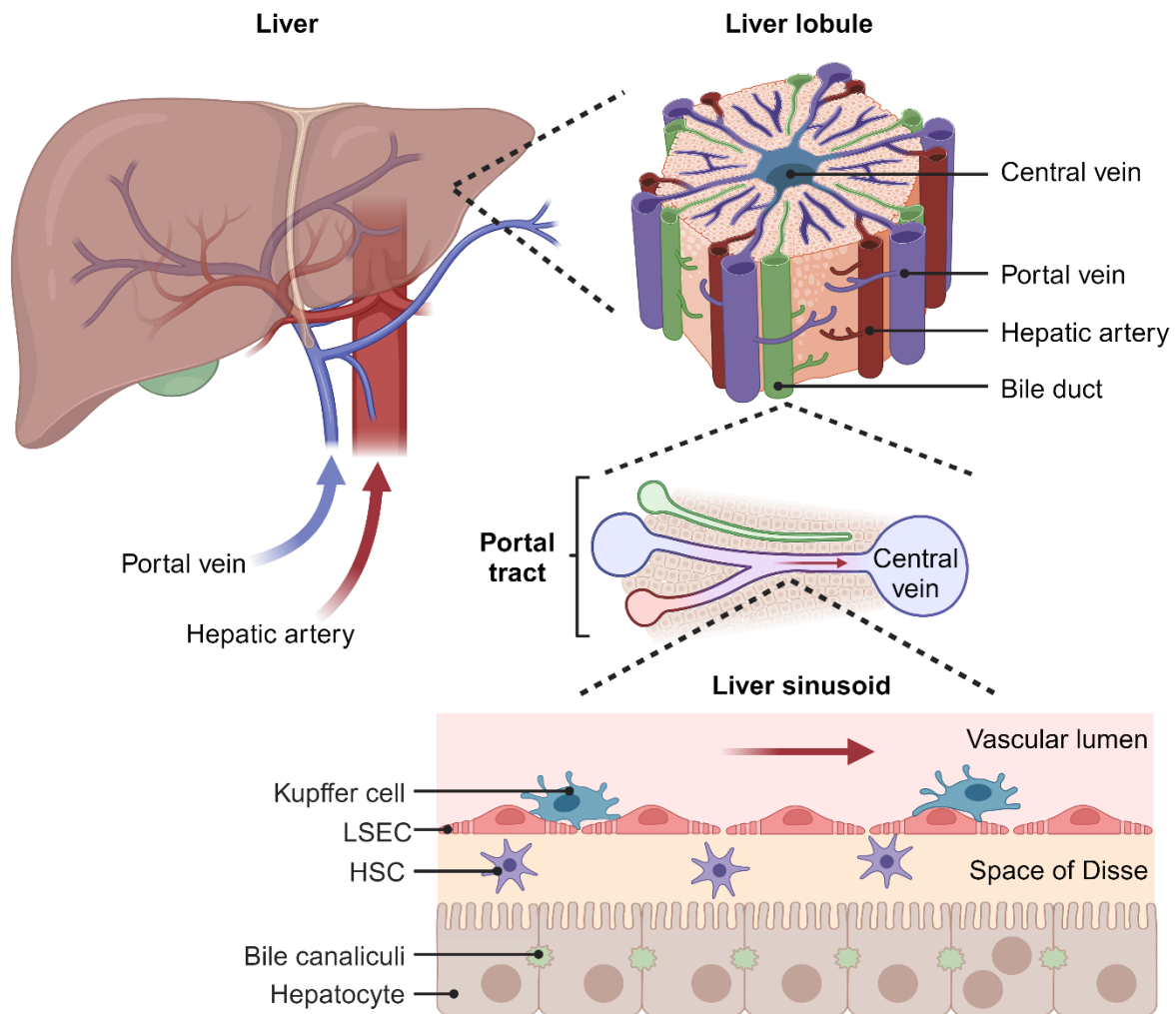


**Figure 1: Liver anatomy.** (Liver) Blood enters the liver via the portal vein and hepatic artery and is distributed to the liver lobes. (Liver lobule) The liver tissue is organized into polygonal lobules with a central hepatic vein and portal tracts along the peripheral borders. The portal tracts contain terminal branches of the bile duct, portal vein and hepatic artery. Blood flows from the portal tracts to the central vein through liver sinusoids. (Liver sinusoid) Liver sinusoids are lined by fenestrated LSECs, allowing blood exchange with the perisinusoidal space termed space of Disse. Phagocytic Kupffer cells adhere to the luminal side of LSECs, and pericytic hepatic HSCs reside in the perisinusoidal space. The liver parenchyma is composed of hepatocytes whose basal surface extends through microvilli into the space of Disse, and whose apical surface forms bile canaliculi between adjacent cells, also extending through microvilli. Created with BioRender.com.

The liver is a multifunctional organ. Hepatocytes secrete alkaline bile into the canaliculi to aid intestinal digestion.<sup>2</sup> The bile contains bile salts (conjugated bile acids), cholesterol, bilirubin, phospholipids, electrolytes and water.<sup>2,3</sup> In addition, the liver is significantly involved in the metabolism of proteins, carbohydrates and fats,<sup>2,3</sup> and stores several minerals and vitamins.<sup>2</sup> The liver is also known for its detoxification function.<sup>2</sup> It excretes and metabolizes toxins, drugs and hormones to reduce and relieve intestinal and renal excretion.<sup>2</sup> Moreover, it can store large amounts of blood in its vascular network or release blood into the circulation depending on arterial and



venous pressure levels.<sup>2,3</sup> The liver also provides hemostatic functions by synthesizing blood coagulation factors.<sup>2</sup>

Finally, the liver is a key site for immune reactions due to its location at the interface between the intestine and the heart and its unique microvascular network with slow sinusoidal blood flow.<sup>4</sup> Since the liver is continuously exposed to large amounts of innocuous dietary and commensal antigens in a healthy state,<sup>5</sup> it characteristically promotes immune tolerance, both locally and systemically.<sup>4</sup> Furthermore, it provides immune surveillance and initiates immune responses by transporting immune signals and antigens to effector immune organs.<sup>4</sup> These immunological functions are mediated by different liver-resident cell populations.<sup>4</sup>

LSECs serve as an adhesion platform.<sup>6</sup> Due to the slow blood flow in the liver sinusoids, circulating leukocytes readily bind to LSECs,<sup>6</sup> which express a variety of adhesion molecules.<sup>7</sup> In addition, LSECs are in constant contact with liver-resident immune cells.<sup>6</sup> LSECs have a high receptor-mediated endocytic capacity, allowing them to clear small colloidal particles, macromolecules and immune complexes from the blood circulation.<sup>7</sup> They also recognize and remove inflammatory pathogen- and damage-associated molecular patterns (PAMPs and DAMPs).<sup>7</sup> LSECs contribute to immune surveillance during infection but also preserve immune tolerance by inhibiting T cell activation and inducing regulatory T cells (Tregs).<sup>6,8</sup> They express molecules promoting presentation of endocytosed antigens<sup>8</sup> and thereby prime cluster of differentiation (CD)4<sup>+</sup> and CD8<sup>+</sup> T cells.<sup>9</sup> However, under steady-state conditions, antigen presentation by LSECs is downregulated by immunoregulatory cytokines, hormones and co-inhibitory molecules.<sup>9</sup>

Antigen presentation is the key process in the initiation of adaptive immune responses.<sup>4</sup> Antigens are presented in the peptide-binding groove of major histocompatibility complex class I (MHC-I) or class II (MHC-II) molecules expressed on the surface of antigen-presenting cells (APCs) and recognized by cognate T cell receptors (TCRs) expressed by T cells.<sup>4</sup> CD8<sup>+</sup> and CD4<sup>+</sup> T cells recognize antigen peptides presented on MHC-I and MHC-II molecules, respectively.<sup>10,11</sup> Peptides loaded on MHC-I originate from endogenous sources, such as viral antigens, whereas MHC-II peptides are derived from endocytosed exogenous proteins.<sup>11</sup> Non-classical pathways

also allow presentation of exogenous antigens on MHC-I (cross-presentation) and presentation of endogenous proteins on MHC-II molecules.<sup>11</sup> Moreover, NKT cells are primed by recognizing endogenous and microbiome-derived lipid antigens presented on the MHC-like molecule CD1.<sup>10</sup> The process of antigen presentation and recognition is regulated by the interaction of co-signaling molecules expressed on the surface of both cells.<sup>4</sup> T cell activation, differentiation and survival are induced by co-stimulatory molecules, whereas co-inhibitory molecules mediate T cell tolerance.<sup>4</sup>

Immunological functions are also mediated by Kupffer cells, the largest population of tissue-resident macrophages.<sup>12</sup> Kupffer cells have phagocytic, antigen-presenting and cytokine-producing capabilities.<sup>12</sup> They are strategically located within the sinusoids to interact with circulating lymphocytes and also migrate to the portal tracts and hepatic lymph nodes.<sup>12</sup> They can suppress antigen-specific T cell activation through the production of prostaglandins, and express the anti-inflammatory cytokines interleukin (IL)-10 and transforming growth factor (TGF) $\beta$  to inhibit inflammatory cytokine production and to stimulate the proliferation and programming of Tregs.<sup>12</sup> In steady-state conditions, Kupffer cells induce tolerance to circulating and hepatocyte-derived antigens.<sup>12</sup> They present antigens to CD4<sup>+</sup> Tregs, inducing their activation and expansion.<sup>13</sup> During liver infection, Kupffer cells present viral antigens to CD4<sup>+</sup> T cells,<sup>14</sup> bacterial antigens to natural killer T (NKT) cells and parasite antigens to CD8<sup>+</sup> T cells to promote antimicrobial immunity.<sup>12</sup>

Another population of liver cells with antigen-presenting capabilities are HSCs.<sup>12</sup> They perform endocytosis and phagocytosis and present antigens to CD8<sup>+</sup> T cells and NKT cells.<sup>12</sup> They also promote homeostatic NKT cell proliferation through IL-15, and induce Treg expansion with the help of IL-2.<sup>12</sup> Moreover, HSCs play a role in wound healing by secretion of extracellular matrix components such as collagens.<sup>15</sup>

Hepatocytes mainly perform metabolic functions.<sup>9</sup> However, they also interact with lymphocytes through direct contact with lymphocyte cytoplasmic extensions that penetrate the fenestrations of the LSECs.<sup>9</sup> Hepatocytes can function as APCs, thereby inducing differentiation of T helper cells type 2 (Th2 cells) from naive CD4<sup>+</sup> T cells, clonal deletion in CD8<sup>+</sup> T cells, and priming NKT cells to induce regulatory CD8<sup>+</sup> T cells.<sup>12</sup>

Even though LSECs, HSCs and hepatocytes are capable of initially activating T cells,<sup>9</sup> they act as non-professional APCs.<sup>4</sup> They lack key co-stimulatory molecules under homeostatic conditions<sup>4</sup> and thus ultimately induce an inactive state or apoptosis in effector T cells.<sup>4,9,12</sup> Thereby, non-professional APCs create an immunotolerogenic environment in the liver.<sup>4</sup>

In addition to tolerogenic APCs, lymphocytes are distributed throughout the liver parenchyma and portal tracts.<sup>8</sup> The intrahepatic lymphocyte population includes CD4<sup>+</sup> and CD8<sup>+</sup> T cells, NKT cells, TCR $\gamma\delta$  T cells, natural killer (NK) cells and B cells.<sup>8</sup> The liver is particularly rich in NKT and NK cells, which are crucial for the initial immune response to pathogens and the recruitment of circulating lymphocytes.<sup>8</sup> Invading lymphocytes are then activated by the liver-resident APCs,<sup>8</sup> which can overcome tolerance induction during microbial infections.<sup>12</sup> The switch from tolerogenic to immunogenic antigen presentation is driven by the upregulation of co-stimulatory molecules on APCs,<sup>12</sup> induced, for instance, on HSCs by inflammatory cytokines,<sup>16</sup> or on hepatocytes by viral infection or interaction with recently activated CD8<sup>+</sup> T cells.<sup>12</sup> However, the mechanisms that override hepatic immune tolerance are still largely unknown.<sup>10</sup>

## 1.2 Autoimmune liver disease

Autoimmune liver diseases (ALDs) are caused by the loss of tolerance toward hepatic self-antigens.<sup>5</sup> Autoimmune reactions in the liver are classified into three diseases: autoimmune hepatitis (AIH), primary sclerosing cholangitis (PSC) and primary biliary cirrhosis (PBC).<sup>5,17</sup> These conditions can develop at any age and persist throughout life as chronic diseases.<sup>17</sup> The annual incidence of each of AIH, PSC and PBC is around 1-2 cases per 100,000 individuals, with variations based on geographical location.<sup>18</sup> For AIH<sup>18,19</sup> and PBC,<sup>18</sup> incidence rates were found to be increasing over time. The ALDs are distinguished by patterns of liver damage, autoantibody profiles, and markers of genetic predisposition.<sup>5,10</sup> AIH is characterized by interface hepatitis, which describes the inflammation and tissue destruction around the portal tracts caused by infiltrating immune cells, particularly cytotoxic T cells and plasma cells.<sup>5</sup> In PSC, immune-mediated injury occurs in the medium and large intra- and extrahepatic bile ducts,<sup>5,10</sup> leading to the development of multifocal bile duct obliteration and

multilayered onion-skin fibrosis.<sup>10</sup> In PBC, inflammatory immune cells damage the small interlobular bile ducts,<sup>10</sup> causing portal tract destruction and biliary cirrhosis.<sup>5</sup> The etiologies of the AILDs are largely unknown, but genetic and environmental factors appear to play a role.<sup>5,17</sup> The most significant genetic susceptibility factors are certain variants of MHC-II molecules, which have an increased capacity to bind and present autoantigenic peptides, leading to the activation of CD4<sup>+</sup> T cells.<sup>5</sup> Environmental risks include smoking, drugs, xenobiotics, and the microbiome.<sup>17</sup> They may induce irregular release of antigens in response to liver damage or alter self-antigens, rendering them immunogenic.<sup>5</sup> In addition, viral or bacterial infections are associated with the development of AILD, possibly due to molecular mimicry, i.e. sequence similarity between microbial and autoantigenic peptides.<sup>5</sup>

The destruction of liver tissue in AILD can be caused directly by innate lymphocytes or by infiltrating activated CD4<sup>+</sup> and CD8<sup>+</sup> T cells, which release inflammatory cytokines and mediate cytotoxicity against hepatocytes or cholangiocytes (biliary epithelial cells).<sup>5</sup> T cells that recognize and respond to self-antigens that are normally tolerated by the immune system are termed autoreactive T cells.<sup>20</sup> During T cell development in the thymus, precursors undergo positive and negative selection processes by encountering a diverse array of self peptide-MHC complexes on thymic APCs.<sup>20</sup> These processes ensure responsiveness to foreign antigens while promoting tolerance to self.<sup>20</sup> Thymocytes that bind self peptide-MHC complexes with high avidity are instructed to undergo apoptosis.<sup>20</sup> However, some autoreactive T cell clones escape negative selection and migrate to the periphery.<sup>20</sup> Under healthy conditions, autoreactive T cells are suppressed in an antigen-specific manner by tolerogenic APCs or anti-inflammatory CD4<sup>+</sup> Tregs.<sup>5,20</sup> Dysregulated tolerance to self-antigens is often driven by an imbalance between effector T cells and protective Tregs.<sup>5</sup> The processes by which this balance is disturbed are not well understood.<sup>5</sup> Tregs were found to be depleted in PSC and PBC patients, and in some patients with AIH, their immunosuppressive function was impaired.<sup>5</sup>

### **1.3 The model of Concanavalin A-induced immune-mediated liver disease**

Concanavalin A (ConA)-induced acute liver inflammation is a well-described model of AIH that resembles the disease mechanisms and pathological changes seen in

patients.<sup>21</sup> ConA is a lectin, which is purified from jack beans (*Canavalia brasiliensis*).<sup>21,22</sup> Lectins are proteins that bind sugar moieties on the surface of various cell types, thereby causing cell clumping, proliferation or cytotoxicity.<sup>22</sup> Acute liver injury is induced in wildtype (WT) mice by a single intravenous injection of ConA.<sup>23</sup> After injection, ConA accumulates specifically in the liver,<sup>24</sup> where its sugar binding sites rapidly adhere to mannose-rich glycoproteins on the surface of LSECs (Figure 2).<sup>24–26</sup> ConA has also been detected to bind to Kupffer cells<sup>25</sup> and to bind and activate neutrophils *in vitro*.<sup>27</sup> However, the preferential binding of ConA to LSECs observed *in vivo* may be explained by modifications of ConA such as binding to plasma proteins and cell-specific variations in mannose receptors.<sup>25</sup> 4 hours later leukocytes progressively stick to LSECs as shown by electron microscopy.<sup>26</sup> As determined by fluorescence microscopy, these include T lymphocytes and neutrophils.<sup>27</sup> At this time macrophages were shown to interact with lymphocytes.<sup>26</sup> ConA is known to bind to MHC molecules on target cells,<sup>28</sup> bridge effector and target cells<sup>29</sup> and activate T lymphocytes that subsequently mediate non-specific cytotoxicity.<sup>30</sup> It is therefore hypothesized that ConA serves as a bridging component, enabling the activation of effector T cells by macrophages through ConA peptides bound to MHC class II molecules.<sup>26</sup> Further, ConA was shown to directly bind to high-mannose glycans on the TCRs of cytotoxic T cells *in vitro*, potentially linking cytotoxic and target cell and inducing antigen-unspecific target cell lysis.<sup>31</sup> Anti-TCR antibodies drastically reduced ConA-mediated cytotoxicity.<sup>31</sup> In the presence of ConA, CD4<sup>+</sup> T cells induce cell death in LSECs within 6 hours, destroying the endothelial membrane and exposing the underlying hepatocytes (Figure 2).<sup>25</sup>

ConA exhibits some direct toxicity to hepatocytes, but lymphocytes are the main drivers of the onset and progression of ConA-induced liver disease.<sup>32</sup> About 8 hours after disease induction, immune cells are activated and recruited, causing inflammation by production of cytokines and severe hepatocyte damage.<sup>21,22,32</sup> Activated CD4<sup>+</sup> T cells, NKT cells, Kupffer cells and neutrophils release pro-inflammatory cytokines such as interferon (IFN) $\gamma$  and tumor necrosis factor (TNF) $\alpha$ ,<sup>22</sup> which promote liver injury in ConA-treated mice (Figure 2).<sup>22,24,33</sup> TNF $\alpha$  can directly induce hepatocyte apoptosis.<sup>22,32</sup> Other mediators of hepatocyte damage in the ConA model include Fas ligand (FasL), perforin and granzyme B, and TNF-related apoptosis inducing ligand (TRAIL), which induces both apoptosis and necroptosis.<sup>22,32</sup> Over 12 hours after ConA

administration, infiltrating CD8<sup>+</sup> cytotoxic T lymphocytes (CTLs) mediate extensive hepatocyte apoptosis and potentially terminal liver failure.<sup>22</sup>

NKT cells induce an upregulation of the nuclear cytokine IL-33 in hepatocytes during ConA hepatitis,<sup>34</sup> and cell damage and necrosis in ConA hepatitis are associated with the hepatic release of IL-33 (Figure 2).<sup>35</sup> IL-33 is an alarmin that can activate a variety of lymphoid and myeloid cells that express the IL-33 receptor suppression of tumorigenicity 2 (ST2), including CD8<sup>+</sup> T cells, CD4<sup>+</sup> Th2 cells, NKT cells, NK cells, macrophages, mast cells, neutrophils, eosinophils, basophils, group 2 innate lymphoid cells (ILC2s) and Tregs.<sup>36</sup> It was shown to accelerate inflammation during ConA-induced liver disease by inducing the activation of hepatic ILC2s, which upregulate the expression of the type 2 cytokines IL-5 and IL-13 and exacerbate disease pathology in response to IL-33 (Figure 2).<sup>35</sup> This was associated with the activation of eosinophils and their recruitment to the liver (Figure 2).<sup>35</sup> However, IL-33 was also shown to expand ST2<sup>+</sup> Forkhead box protein 3 (Foxp3)<sup>+</sup> Tregs in ConA hepatitis (Figure 2), which may regulate the activity of pro-inflammatory immune cells such as ILC2s and contribute to the resolution of immune-mediated hepatitis.<sup>35</sup>

Liver damage in ConA-induced hepatitis is measured by histology and quantification of plasma levels of alanine aminotransferase (ALT)<sup>32</sup> released from the cytoplasm of dying hepatocytes.<sup>22</sup> Elevated ALT levels can be detected as early as 5 hours after ConA treatment.<sup>32</sup> The progression of ConA-induced hepatitis can be monitored from 8 to over 24 hours, followed by regression<sup>32</sup> and the development of tolerance to ConA restimulation within 8 days.<sup>37</sup>

The hormonal state significantly influences the effects of ConA, with female mice tending to exhibit greater susceptibility to ConA and a wider range of disease outcomes.<sup>32</sup> Another important consideration of the experimental design is the dose.<sup>32</sup> Due to its extraction and purification from jack beans, the biological activity of ConA varies between batches.<sup>32</sup> Therefore, it is essential to test each batch to determine the appropriate dose for inducing liver disease.<sup>32</sup> Additionally, the ConA dose must be adjusted according to the body weight of the mouse.<sup>32</sup> Established ConA application protocols use doses of 5-15 mg/kg in C57BL/6 mice.<sup>32</sup>

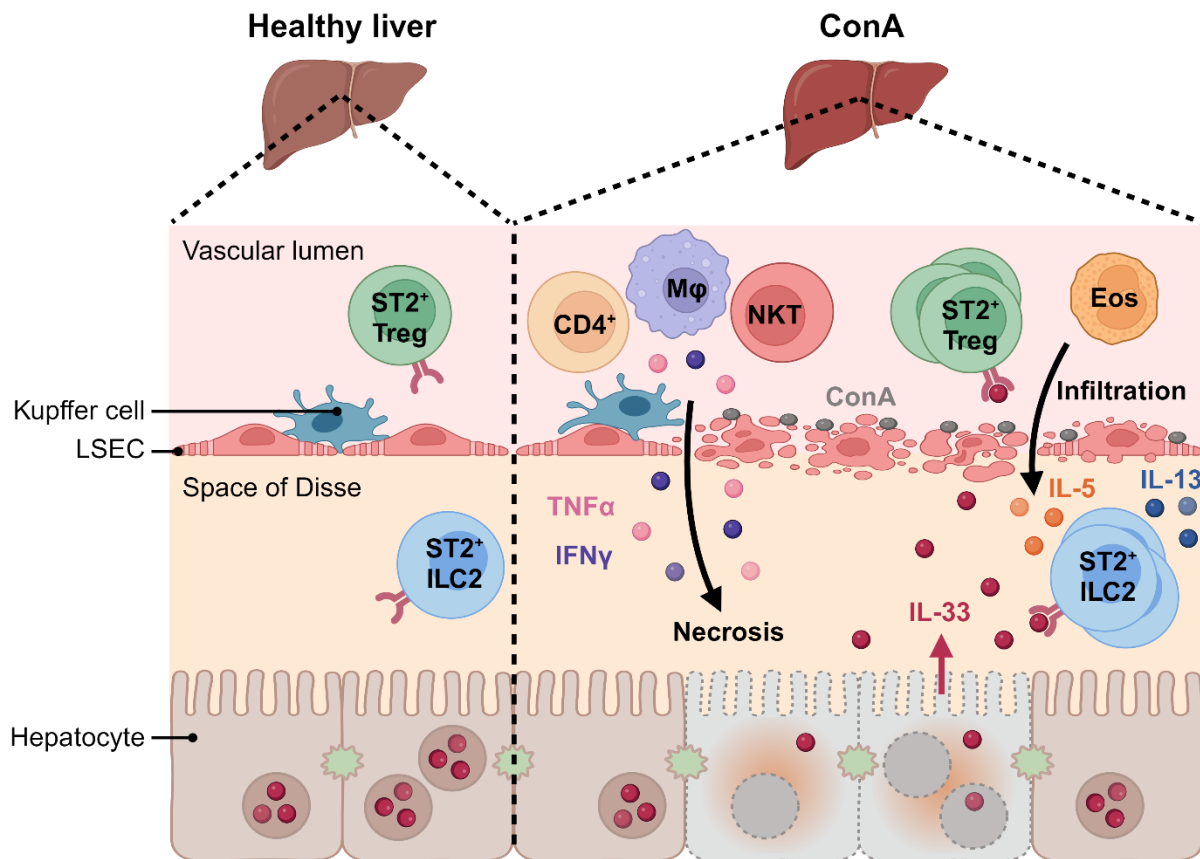


**Figure 2: Model of ConA-induced immune-mediated hepatitis.** ConA binds to LSECs, Kupffer cells and neutrophils. It functions as a bridging component, mediating the activation of effector T cells and linking cytotoxic and target cells. As a result, activated CD4<sup>+</sup> T cells induce apoptotic cell death in LSECs, thereby disrupting the endothelial barrier. More immune cells such as CD4<sup>+</sup> T cells, NKT cells, Kupffer cells and neutrophils are recruited and activated. These cells contribute to inflammation and liver injury through various mechanisms like the production of the pro-inflammatory and cytotoxic cytokines IFNγ and TNFα. Necrotic hepatocyte death results in the release of intranuclear IL-33. The alarmin then activates various pro-inflammatory immune cells, including hepatic ST2<sup>+</sup> ILC2s, which, when stimulated by IL-33, express higher levels of IL-5 and IL-13 and promote eosinophil infiltration. Conversely, IL-33 expands protective ST2<sup>+</sup> Tregs. Created with BioRender.com.

#### 1.4 Chronic liver disease

Autoimmune liver diseases follow a progressive clinical trajectory, potentially culminating in liver fibrosis, cirrhosis, and the development of hepatocellular carcinoma (HCC) or cholangiocarcinoma (CC; Figure 3).<sup>5,10</sup> Hepatic fibrosis is the pathological accumulation of scar-like extracellular matrix (ECM).<sup>38</sup> It develops in response to chronic inflammation and progressive injury of the liver parenchyma (Figure 3).<sup>38,39</sup> Damaged hepatocytes and non-parenchymal cells release signals that recruit and activate cells to acquire a myofibroblast-like phenotype and produce ECM.<sup>15</sup> Hepatic myofibroblasts are mainly derived from resident HSCs, but also from portal fibroblasts,

cells recruited from the bone marrow, and cells that undergo epithelial-to-mesenchymal transition (EMT).<sup>15,38,39</sup> HSC function, activation and transformation are regulated by multiple pro-inflammatory cytokines.<sup>39</sup> The most pro-fibrotic cytokine is TGF $\beta$ , which stimulates collagen I production by HSCs, their differentiation into myofibroblast-like cells and its own production, creating an autocrine feedback loop.<sup>39</sup>

Activated myofibroblasts exhibit a wound-healing response through a variety of biological activities.<sup>15</sup> One important response is the expression of ECM components including fibrillar collagen, mainly collagen types I and III, and non-collagenous components such as fibronectin and proteoglycans.<sup>15</sup> Another response is the production of matrix metalloproteinases (MMPs) and tissue inhibitors of metalloproteinases (TIMPs), which regulate the turnover of ECM proteins by degrading and antagonizing degradation, respectively.<sup>15,39</sup> Liver fibrosis results from an imbalance between ECM synthesis and degradation.<sup>39</sup> During fibrogenesis, fibrillar collagens replace low-density type IV collagens in the space of Disse and the total amount of matrix proteins increases.<sup>38</sup> Fibrillar collagens are mainly distributed in septae, which are broad bands of connective tissue that surround regenerative clusters of hepatocytes called nodules.<sup>38</sup> Thickening of fibrotic septae and enhanced crosslinking of collagen fibrils make the ECM increasingly resistant to breakdown by MMPs.<sup>38,39</sup> In addition, the endothelial porosity is progressively reduced, impairing the exchange of metabolites between hepatocytes and sinusoidal blood.<sup>38</sup> Pronounced fibrosis is characterized by disruption of the liver architecture and the formation of nodules.<sup>38</sup>

As liver damage continues, fibrosis can advance to cirrhosis, which represents the end stage of fibrosis (Figure 3).<sup>39</sup> Cirrhosis is associated with major structural changes in the liver, distortion of the liver vasculature,<sup>39</sup> portal hypertension and impaired liver function.<sup>38</sup> Related complications include ascites, encephalopathy, synthetic dysfunction, and impaired metabolic capacity.<sup>38</sup>

Liver fibrosis is potentially reversible (Figure 3).<sup>39</sup> It often regresses spontaneously after resolution of the primary liver disease.<sup>39</sup> Liver regeneration can restore the liver to a near-normal structure.<sup>39</sup> However, resolution is limited by the extent of collagen cross-linking in advanced fibrosis<sup>38</sup> and there are currently no effective antifibrotic



drugs for the treatment of cirrhosis.<sup>39</sup> Liver fibrosis and cirrhosis are major public health concerns worldwide.<sup>39</sup> Cirrhosis is the primary predictor of liver disease-related morbidity and mortality, increasing the risk of liver failure and primary liver cancer (Figure 3).<sup>39</sup> Liver transplantation is the last treatment option, but its impact is limited by organ shortage, disease recurrence in transplant recipients, and the presence of co-morbidities.<sup>39</sup>

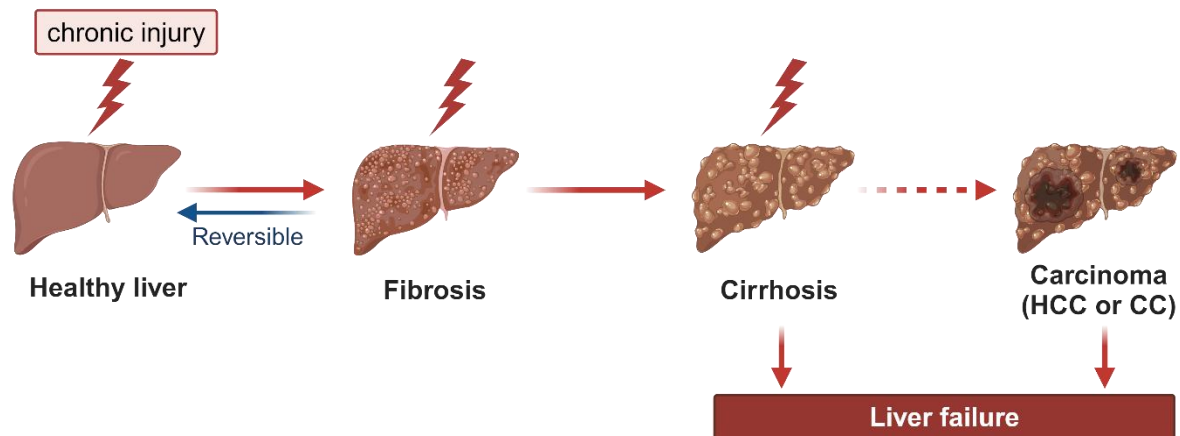


**Figure 3: Progression of chronic liver disease.** Chronic liver injury leads to a pathological accumulation of ECM, known as fibrosis. Without intervention, ongoing liver damage causes fibrosis to progress to end-stage fibrosis, known as cirrhosis. While liver fibrosis can regress, cirrhosis is irreversible and predisposes to the development of primary liver cancer, such as HCC or CC. Advanced liver disease may culminate in the loss of organ function. HCC: Hepatocellular carcinoma; CC: cholangiocarcinoma. Created with BioRender.com.

### 1.5 Multidrug resistance p-glycoprotein 2 knockout mice as a model for PSC

Multidrug resistance p-glycoprotein 2 (*Mdr2*)<sup>-/-</sup> mice develop portal inflammation and liver fibrosis resembling human PSC within a few weeks of birth.<sup>40</sup> The floppase MDR2 transports phosphatidylcholine across the canalicular membrane of hepatocytes into the bile, where it is incorporated into bile acid micelles, reducing their detergent activity and increasing their ability to solubilize cholesterol (Figure 4).<sup>41</sup> In *Mdr2*<sup>-/-</sup> mice, the lack of this transporter leads to abolished biliary phosphatidylcholine excretion and accumulation of non-micellar toxic bile acids and cholesterol in the bile (Figure 4).<sup>40</sup> Within 2 weeks of birth, the bile duct tight junction morphology and basal membrane integrity are severely altered, leading to leaky bile ducts with reflux of toxic bile acids into the periportal tissue.<sup>40</sup> This induces inflammation with infiltration of inflammatory cells and production of pro-inflammatory and pro-fibrotic cytokines such as TNF $\alpha$  and

TGF $\beta$ 1.<sup>40</sup> Initially, neutrophil granulocytes and Kupffer cells are expanded in the portal area, followed by CD4<sup>+</sup> and CD8<sup>+</sup> lymphocytes at 4 to 8 weeks after birth.<sup>40</sup> Inflammatory signals further activate periductal myofibroblasts, which form a periductal fibrotic ring that separates the peribiliary plexus from the biliary epithelium.<sup>40</sup> Periductal fibrosis progresses to onion-skin-like periductal fibrosis by 4 weeks of age.<sup>40</sup> This leads to atrophy and death of the surrounding cholangiocytes, culminating in fibro obliteration of the bile ducts.<sup>40</sup> However, bile flow is not impaired in *Mdr2*<sup>-/-</sup> mice.<sup>40</sup> In the absence of mixed micelles of bile acids and phospholipids, cholesterol solubilization is prevented, resulting in cholesterol supersaturation of the bile (Figure 4) and the formation of cholesterol gallstones.<sup>41</sup> Intraductal cholesterol crystals are observed from the age of 8 weeks.<sup>40</sup>

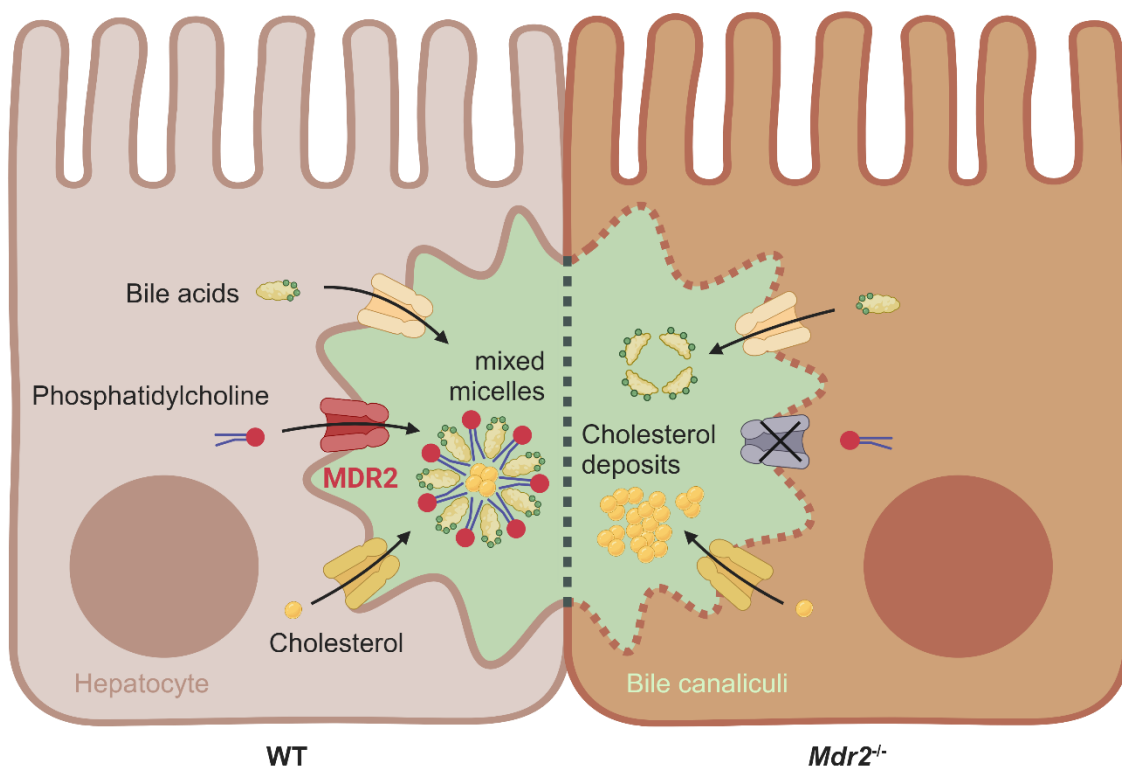


**Figure 4: Model of multidrug resistance p-glycoprotein 2 (MDR2) deficiency.** In WT mice, MDR2 enables the excretion of phosphatidylcholine across the canalicular membrane of hepatocytes. Within the bile canaliculi, mixed micelles containing primary bile acids and phosphatidylcholine are formed and effectively sequester cholesterol. In *Mdr2*<sup>-/-</sup> mice, the transport of phosphatidylcholine into the bile is disrupted, leading to the accumulation of non-micellar toxic bile acids and cholesterol oversaturation. As a result, the integrity of the bile ducts is compromised. Created with BioRender.com.

Disease progression in *Mdr2*<sup>-/-</sup> mice can be measured by various biomarkers. An important indication is characteristic morphological changes and patterns in the liver tissue that can be visualized by histopathological examination.<sup>42</sup> The release of the

cytosolic enzyme ALT into the blood indicates hepatocellular damage and can be measured by determining plasma activity levels.<sup>42</sup> Elevated levels of the membrane-bound ALP are characteristic of cholestatic injury, as the increased concentration of bile acids acts as a detergent, causing the release of ALP from the hepatocellular membrane into the blood.<sup>42</sup> Another marker for bile-induced liver damage is bilirubin.<sup>42</sup> It is formed during the breakdown of hemoglobin from red blood cells and is transported to the liver, released into the bile duct, and stored in the gallbladder.<sup>42</sup> Elevated plasma bilirubin levels may indicate reflux of bilirubin into the bloodstream during advanced cholestatic disease.<sup>42</sup> Furthermore, plasma high-density lipoprotein (HDL) cholesterol levels are reduced in *Mdr2*<sup>-/-</sup> mice.<sup>43</sup> This reduction may be due to decreased cholesterol absorption into the bloodstream or increased fecal cholesterol excretion observed in mice lacking MDR2.<sup>43</sup> However, the exact mechanism remains unknown.<sup>44</sup> Liver fibrosis can be monitored by analyzing the hydroxyproline content in liver tissue, as it is a key component of collagen that accumulates in fibrosis.<sup>45</sup>

## 1.6 Regulatory T cells in liver disease

Tregs are characterized by the expression of CD4, the transcription factor forkhead box protein 3 (Foxp3) and the IL-2 receptor  $\alpha$  chain CD25.<sup>46,47</sup> IL-2 is essential for the survival and expansion of Tregs.<sup>46</sup> They mainly secrete IL-10 and TGF $\beta$ , as well as other cytokines that promote immune tolerance.<sup>47</sup> Tregs also express the function-associated surface molecules killer cell lectin-like receptor subfamily G member 1 (KLRG1),<sup>48</sup> inducible T cell co-stimulator (ICOS),<sup>49</sup> cytotoxic T lymphocyte-associated protein 4 (CTLA-4),<sup>50,51</sup> T cell immunoglobulin with ITIM domain (TIGIT),<sup>52</sup> programmed cell death-ligand (PD-L1)<sup>47</sup> and programmed cell death protein 1 (PD-1).<sup>53</sup> KLRG1 is an established marker of differentiation.<sup>48</sup> While it operates as an inhibitory receptor of effector NK and T cells, Tregs expressing KLRG1 were found to express elevated levels of suppressive molecules, exhibit enhanced inhibitory function, and aggregate at sites of inflammation.<sup>48</sup> ICOS is a co-stimulatory receptor expressed on T cells responsible for T cell activation, proliferation, and differentiation.<sup>49</sup> ICOS expression is linked to Treg functionality.<sup>49</sup> For instance, direct ICOSL-ICOS interaction was required for IL-33-induced accumulation of Tregs in a previous study investigating lung and spleen cells.<sup>54</sup> In addition to these markers of

Treg activation, Tregs express inhibitory molecules, including IL-10. During homeostasis, IL-10 predominantly suppresses the activation and migration of Foxp3<sup>+</sup> Tregs and APCs in a positive feedback loop.<sup>55</sup> In models of autoimmunity, infection, and cancer, IL-10 has been demonstrated to support the function of pro-inflammatory B cells and CD8<sup>+</sup> T cells.<sup>55</sup> However, during inflammation, IL-10 produced by Foxp3<sup>+</sup> Tregs is primarily recognized for its role in inhibiting the pro-inflammatory functions of APCs and CD4<sup>+</sup> T cells.<sup>55</sup> Further, Foxp3<sup>+</sup> Tregs constitutively express CTLA-4 and can thereby alter the function of APCs, such as reducing their capacity to prime effector T cells, by binding to CD80 and CD86 on APCs or removing them from APC surface.<sup>50,51</sup> Upregulated expression of TIGIT on Tregs marks an activated phenotype, which is highly suppressive and may thereby inhibit various types of immune cells.<sup>52</sup> The immunoreceptor TIGIT binds to the ligand CD155 with high affinity, which is mostly expressed on DCs, T cells, B cells and macrophages.<sup>52</sup> Moreover, TIGIT interacts with the ligands CD112 and CD113 with low affinity.<sup>52</sup> To date, TIGIT stimulation was shown to promote the capacity of Tregs to suppress effector T cell proliferation and IFN $\gamma$  expression.<sup>56</sup> Specifically, TIGIT was demonstrated to support the Treg-mediated inhibition of Th1 and Th17 cell, but not Th2 cell responses.<sup>57</sup> In addition, several studies have demonstrated Treg-mediated immunosuppression through PD-L1-driven inhibition of effector lymphocytes expressing the co-inhibitory receptor PD-1.<sup>58</sup> *In vitro* binding of a PD-L1.immunoglobulin fusion protein to PD-1 during T cell activation inhibited T cell proliferation and cytokine secretion.<sup>58</sup> Tregs lacking PD-L1 were impaired in their immunosuppressive function, particularly in suppressing CD4<sup>+</sup> T cell activation *in vitro*.<sup>59,60</sup> Also blocking the PD-1/PD-L1 pathway inhibited Treg-mediated CD4<sup>+</sup> T cell suppression *in vitro*.<sup>61,62</sup> In addition, PD-L1-expressing Tregs were shown to inhibit activation and induce apoptosis of PD-1-expressing autoreactive B cells *in vivo*.<sup>63</sup> Tregs also express PD-1 and elevated levels have previously been shown to mark Treg dysfunction<sup>64</sup> and exhaustion.<sup>65</sup> PD-1 is known to induce an inhibitory signal in lymphocytes after binding its ligand PD-L1,<sup>58,66</sup> expressed by liver-resident cell populations such as LSECs, Kupffer cells,<sup>67</sup> HSCs,<sup>68</sup> hepatocytes<sup>69</sup> and NK cells,<sup>70</sup> or its ligand PD-L2,<sup>71</sup> expressed on dendritic cells (DCs),<sup>72</sup> and on activated macrophages<sup>73</sup> and T cells.<sup>74,75</sup>

The Treg family consists of naturally occurring Tregs (nTregs) and phenotypically similar induced Tregs (iTregs), which are generated *in vitro* from conventional CD4<sup>+</sup>

T cells.<sup>76</sup> The majority of nTregs are differentiated in the thymus (thymus-derived Tregs, tTregs), but under specific conditions Tregs differentiate from conventional T cells in the periphery (peripherally-derived Tregs, pTregs).<sup>76</sup> Although various hepatic APCs such as hepatocytes, DCs and LSECs promote Treg development, the healthy liver typically harbors a relatively low number of CD4<sup>+</sup> Foxp3<sup>+</sup> CD25<sup>+</sup> Tregs compared to the spleen.<sup>12</sup> This may be explained by the tolerogenic environment in the liver, which prevents immune responses and thus the recruitment of Tregs.<sup>12</sup> However, during inflammation, various liver cells are activated and rapidly expand liver-resident Tregs or recruit circulating Tregs to prevent immunopathology.<sup>12</sup> Tregs mediate immune suppression through a variety of mechanisms, including altering APC maturation and function, killing target cells and secreting anti-inflammatory cytokines.<sup>46</sup>

In autoimmune liver diseases, the frequency and/or function of Tregs is reduced.<sup>46</sup> Tregs from patients with AIH have been shown to be reduced in number<sup>77</sup> and functionally impaired in their ability to suppress CD8<sup>+</sup> T cell proliferation and IFN $\gamma$  production,<sup>78</sup> and to induce TGF $\beta$  production by CD4<sup>+</sup> T cells *in vitro*.<sup>79</sup> Further, they increased the activation of monocytes.<sup>80</sup> In addition, Tregs are abundant in fibrotic tissue and play an important role in chronic liver disease by interacting with multiple cell types to exert pro- and anti-fibrotic effects.<sup>47</sup> They release IL-8 to activate HSCs,<sup>81</sup> major drivers of liver fibrosis, which in turn secrete IL-2 to expand Tregs.<sup>47,82</sup> Tregs further promote fibrogenesis by producing TGF $\beta$  to stimulate HSC conversion to myofibroblasts and suppress Kupffer cell expression of ECM-degrading MMPs.<sup>47</sup> In addition, they express TGF $\beta$ , IL-8 and CTLA-4 to protect HSCs from NK cell attack.<sup>47,83</sup> However, Tregs also suppress liver fibrosis by inhibiting inflammatory cell immunity.<sup>47</sup>

### 1.7 Effector function of group 2 innate lymphoid cells in the liver

Innate lymphoid cells (ILCs) are similar to CD4<sup>+</sup> and CD8<sup>+</sup> T cells, but lack the TCR.<sup>84</sup> They are classified into cytotoxic NK cells and helper ILCs, which are further divided into three main lineages according to their ability to secrete type 1, type 2 or type 17 cytokines, namely group 1 ILCs (ILC1s), ILC2s and ILC3s.<sup>84</sup> ILC2s are characterized by the expression of the transcription factor GATA binding protein 3 (GATA3), the IL-2 receptor  $\alpha$  chain CD25, the IL-33 receptor ST2, the IL-25 receptor (IL-25R) and the IL-7 receptor (IL-7R).<sup>84</sup> Further, KLRG1 is recognized as a marker of mature<sup>85</sup> and

inflammatory ILC2s.<sup>86</sup> Activated ILC2s secrete various cytokines including IL-5, IL-13, IL-6, IL-9 and the growth factor amphiregulin (AREG).<sup>87</sup>

ILC2s are mainly activated by the epithelial cell-derived cytokines IL-25 and IL-33.<sup>84,87</sup> This activation is enhanced by various co-stimulatory cytokines,<sup>87</sup> including thymic stromal lymphopoietin (TSLP),<sup>88–90</sup> IL-2,<sup>91,92</sup> IL-4,<sup>93,94</sup> IL-7,<sup>88,95–97</sup> IL-9,<sup>98</sup> tumor necrosis factor-like ligand 1A (TL1A)<sup>99</sup> and glucocorticoid-induced tumor necrosis factor receptor ligand (GITRL).<sup>100</sup> The profiles of produced cytokines vary in different tissues.<sup>87</sup> ILC2s reside in peripheral tissues and rarely migrate between tissues and organs.<sup>101,102</sup> They are renewed and expanded locally with phenotypic differences depending on their local microenvironment.<sup>101,102</sup> IL-33 and IL-25-responsive lung ILC2s are characterized as functionally diverse subsets.<sup>86</sup> ILC2s expressing the IL-33 receptor ST2 are termed tissue-resident natural (n)ILC2s, while IL-25-responsive ILC2s, with high expression of KLRG1 and the pro-inflammatory cytokine IL-17A are described as inflammatory (i)ILC2s.<sup>86</sup> Both subsets produce type 2 cytokines.<sup>86</sup> In response to inflammatory cytokines, iILC2s develop into nILC2-like cells with increased expression of ST2 and reduced expression of IL-17A.<sup>86</sup> Also hepatic ST2<sup>+</sup> ILC2s are strongly activated by IL-33 and produce type 2 cytokines, whereas IL-25 induces the expression of type 2 cytokines and IL-17A.<sup>92</sup> IL-25-mediated IL-17A expression by hepatic ILC2s is inhibited in the presence of IL-33, suggesting suppression of iILC2 development in IL-33-triggered liver diseases.<sup>92</sup>

Elevated IL-33 levels cause the activation of hepatic ILC2s in mouse models of acute immune-mediated hepatitis,<sup>35</sup> viral hepatitis,<sup>103</sup> liver fibrosis,<sup>104</sup> and biliary carcinogenesis.<sup>105</sup> IL-33-activated hepatic ILC2s express the cytokines IL-13 and IL-5, which lead to the activation and recruitment of inflammatory eosinophils into the liver.<sup>35</sup> Through this mechanism, ST2<sup>+</sup> ILC2s were shown to promote inflammation and tissue damage in ConA-induced immune-mediated hepatitis.<sup>35</sup> In different mouse models of chronic liver disease, IL-33-activated hepatic ILC2s mediated pathological tissue remodeling and fibrosis and produced IL-13, which was shown to induce HSC activation and transdifferentiation.<sup>104</sup> Further, the frequency of human intrahepatic ILC2s correlates with the severity of end-stage inflammatory liver disease.<sup>106</sup> These studies describe a pro-inflammatory and pro-fibrotic impact of hepatic ILC2s, increasing the pathogenesis of the liver disease.

## 1.8 Amphiregulin in acute and chronic liver disease

Amphiregulin (AREG) is an epidermal growth factor-like molecule that is constitutively expressed by a variety of epithelial and mesenchymal cell types during development and homeostasis.<sup>107</sup> In the context of inflammation, fibrosis and tumor microenvironments, a number of immune cell populations associated with type 2 immune response and resolution of inflammation have been shown to produce AREG.<sup>107</sup> These include innate basophils, eosinophils, mast cells, neutrophils, ILC2s, and dendritic cells, but also adaptive CD4<sup>+</sup> T cells, Tregs, and tumor-infiltrating CD8<sup>+</sup> T cells.<sup>107</sup> AREG is also produced by various hepatic parenchymal, mesenchymal and immune cell types, namely hepatocytes,<sup>108</sup> cholangiocytes,<sup>109</sup> HSCs<sup>110,111</sup> myfibroblasts,<sup>111</sup> Kupffer cells,<sup>111</sup> and monocyte-derived liver macrophages,<sup>112</sup> Tregs,<sup>113</sup> and ILC2s.<sup>106,114</sup>

AREG is a ligand of the epidermal growth factor receptor (EGFR).<sup>115</sup> The EGFR is a transmembrane protein constitutively expressed in hepatocytes.<sup>116</sup> Moreover, it is expressed in activated HSCs and LSECs in chronic liver disease, as well as in tumor cells, liver macrophages and LSECs in HCC<sup>116</sup> and Tregs under inflammatory conditions.<sup>117</sup> EGFR plays a major hepatoprotective and regenerative role in the liver.<sup>116</sup> In the absence of a ligand, EGFR exists in a catalytically inactive conformation.<sup>118,119</sup> Ligand binding to the EGFR triggers the formation of homo- or heterodimers with the related receptors ErbB2, ErbB3 and ErbB4, and activation of the cytoplasmic bilobular kinase domain.<sup>118,119</sup> Receptor dimers undergo auto- or transphosphorylation on multiple tyrosine residues, leading to the recruitment of enzymes and adaptor proteins subsequently activating downstream signaling components, some of which regulate cellular motility or apoptosis, while others translocate to the nucleus to regulate transcription factors involved in cell cycle progression.<sup>118,119</sup> In mammals, ligands that can bind the EGFR are AREG, epiregulin (EREG), transforming growth factor (TGF) $\alpha$ , betacellulin (BTC), heparin-binding EGF-like growth factor (HB-EGF), epidermal growth factor (EGF), and epigen (EPGN).<sup>115</sup> They are synthesized as type I transmembrane proteins that comprise an amino-terminal extension (pro-region), the EGF module, a short juxtamembrane stalk, a hydrophobic transmembrane domain, and a carboxy-terminal cytoplasmic tail.<sup>115</sup> The EGF domain, whose sequence is responsible for the interaction with the EGFR, is the

central structural and functional feature.<sup>115</sup> The membrane-anchored growth factors are biologically active by contacting and activating receptors on adjacent cells.<sup>115</sup> This mode of intercellular stimulation is known as juxtacrine interaction.<sup>115</sup> Via proteolytic processing, a soluble extracellular fragment containing the EGF module can be released from the membrane surface.<sup>115</sup> This ectodomain shedding occurs in response to diverse agonists, such as a disintegrin and metalloprotease (ADAM) proteins.<sup>115</sup> The soluble growth factor can bind and activate receptors on distant cells (endocrine), neighboring cells (paracrine) or on the cell of its origin (autocrine).<sup>115</sup> This mode of action is assumed to induce a different biological outcome than the juxtacrine stimulation by the membrane-anchored growth factors.<sup>115</sup> All EGFR ligands are potent mitogens, as shown in cultured hepatocytes for AREG,<sup>108</sup> EREG,<sup>120–122</sup> TGF $\alpha$ ,<sup>123</sup> HB-EGF,<sup>124</sup> and EGF,<sup>123,125,126</sup> and non-hepatic cell populations for BTC<sup>127</sup> and EPGN.<sup>128</sup> AREG acts as a bi-functional growth factor that induces proliferation in some cell lines and differentiation in others, as it binds the EGF receptor with low affinity due to a single amino acid difference in its receptor-binding domain compared to other members of the EGF family.<sup>107</sup> In contrast, other EGFR ligands form a stable interaction with the receptor and thereby induce proliferation of the target cell, as well as receptor internalization and degradation.<sup>107</sup>

AREG is barely detectable in the livers of healthy mice, but upregulated upon acute injury,<sup>108,129</sup> cholestatic liver injury,<sup>109</sup> and viral infection<sup>112,130</sup> and remains elevated in chronic liver disease.<sup>108–111</sup> Increased hepatic AREG expression was also detected in patients with liver fibrosis,<sup>110</sup> cirrhosis<sup>108,109</sup> and cholestatic liver disease.<sup>109</sup> However, the function of AREG in liver disease remains unclear. AREG has been shown to protect mice from cholestatic injury<sup>109</sup> and to induce liver regeneration after partial hepatectomy.<sup>108</sup> In contrast, AREG has been demonstrated to impair antiviral immune responses in a mouse model of hepatitis B virus (HBV) infection<sup>130</sup> and to exacerbate liver fibrosis following experimental chronic liver injury.<sup>111</sup>

Treg- and ILC2-derived AREG have been shown to mediate tissue protection, with AREG-expressing Tregs contributing to muscle repair after acute injury<sup>131</sup> and protection against tissue damage during viral lung infection,<sup>132</sup> and AREG-expressing ILC2s promoting tissue repair in infectious lung injury,<sup>133</sup> intestinal inflammation,<sup>134</sup> and biliary atresia.<sup>114</sup> In the liver, AREG has been shown to facilitate tissue regeneration



not only in biliary atresia<sup>114</sup> but also after partial hepatectomy.<sup>108</sup> In addition, AREG can reinforce Treg-mediated immune regulation, as shown for AREG derived from mast cells in colitis, dermatitis and tumor vaccination models,<sup>117</sup> basophils in skin contact hypersensitivity,<sup>135</sup> and hepatic macrophages in HBV infection.<sup>112</sup>

AREG can stimulate its own gene expression, as demonstrated in keratinocytes,<sup>136</sup> HSCs, myofibroblasts,<sup>111</sup> and cell lines of HCC,<sup>137</sup> colon cancer<sup>138</sup> and vascular smooth muscle.<sup>139</sup> Moreover, IL-33 was shown to induce AREG expression in ILC2s<sup>114,133</sup> and Tregs.<sup>132,140,141</sup>

### 1.9 The alarmin IL-33 in autoimmune liver disease

IL-33 is a cytokine of the IL-1 family and the only known ligand of the IL-1 receptor-like 1 (IL1RL1), also known as ST2.<sup>36,142</sup> After its synthesis in the cytosol, IL-33 migrates to the nucleus,<sup>36</sup> where it acts as a transcriptional regulator by binding to chromatin.<sup>143</sup> It exists in two forms: full-length IL-33 (pro-IL-33), localized within the nucleus, and mature IL-33, which lacks the ability to translocate into the nucleus.<sup>36</sup> Following severe tissue damage, the cytokine is passively released from necrotic cells.<sup>36</sup> Once released, pro-IL-33 is frequently cleaved by proteases into mature IL-33, which possesses greater biological potency.<sup>36</sup> Both variants bind to the ST2 receptor, which forms a heterodimeric complex with the IL-1 receptor accessory protein (IL-1RAcP) for signal transduction.<sup>36,144</sup> Signaling via the IL-33 receptor complex leads to activation of the transcription factor nuclear factor kappa-light-chain-enhancer of activated B cells (NFκB) and mitogen-activated protein (MAP) kinases,<sup>142,144</sup> which induce cell activation, differentiation, survival and the production of various cytokines.<sup>36,145</sup>

IL-33 is expressed in endothelial cells, epithelial cells, keratinocytes, fibroblasts, smooth muscle cells, glial cells,<sup>146</sup> and hepatocytes.<sup>34,147,148</sup> It functions as an alarmin that is released in response to cell damage to alert the immune system.<sup>149</sup> IL-33 activates ST2-expressing lymphoid and myeloid cells, including CD8<sup>+</sup> T cells, Th2 cells, Tregs, NKT cells, NK cells, ILC2s, granulocytes, macrophages and mast cells.<sup>36</sup> It stimulates the production of the type 2 cytokines IL-5 and IL-13 in Th2 cells,<sup>142</sup> ILC2s<sup>133,150</sup> and Tregs,<sup>151</sup> as well as the expression of AREG in ILC2s<sup>114,133</sup> and

Tregs.<sup>132,140,141</sup> Moreover, IL-33 increases Treg differentiation and promotes their accumulation and maintenance in peripheral inflamed tissue.<sup>152</sup> It also induces expansion of ST2<sup>+</sup> Tregs and a selective increase in ST2 expression on ST2<sup>+</sup> Tregs,<sup>151,152</sup> an effector subset that preferentially accumulates in non-lymphoid tissues.<sup>151,153</sup> IL-33 has a dual role in modulating immune responses and tissue dynamics.<sup>36</sup> Depending on the disease, it can act as a pro- or anti-inflammatory cytokine.<sup>36</sup> It drives type 1 and type 2 immune responses, but also expands and activates regulatory cells such as Tregs to suppress inflammation.<sup>36</sup> In addition, IL-33 promotes the expression of AREG, which mediates tissue repair and regeneration, but is also implicated in fibrogenesis and carcinogenesis during chronic inflammation.<sup>36</sup>

IL-33 plays a role in the pathology of liver disease.<sup>36</sup> Patients with acute and chronic liver diseases have been found to have elevated serum levels of IL-33,<sup>104,154–160</sup> which correlated positively with disease severity in cases of AIH,<sup>154,156</sup> alcoholic liver disease,<sup>160</sup> chronic hepatitis C virus (HCV) infection,<sup>159</sup> and acute and chronic liver failure.<sup>157</sup> The dual function of IL-33 has also been demonstrated in AIH.<sup>36</sup> In patients with AIH, serum IL-33 levels were positively correlated with liver damage and serum inflammatory cytokines and decreased following treatment with immunosuppressive drugs.<sup>156</sup> In the mouse model of ConA-induced acute hepatitis, NKT cells were shown to induce high expression of IL-33 in hepatocytes,<sup>34</sup> and necrotic tissue damage was associated with the hepatic release of IL-33.<sup>35</sup> This was further associated with the activation of hepatic ILC2s, which expressed IL-5 and IL-13 and exacerbated liver inflammation and tissue injury, and with the activation and infiltration of eosinophils.<sup>35</sup> Administration of IL-33 together with ConA aggravated liver injury, whereas blocking IL-33 signaling attenuated ConA-induced liver disease and reduced T cell and NKT cell activation and IFN $\gamma$  production.<sup>161</sup> Blockage of endogenous IL-33 also ameliorated hepatic injury and inflammatory cytokine production in S-100 antigen-induced experimental AIH.<sup>156</sup> In contrast to its pro-inflammatory role in AIH, IL-33 has also been shown to exert a protective effect in ConA-induced hepatitis.<sup>36</sup> Treatment with IL-33 before administration of ConA prevented the development of immune-mediated hepatitis and expanded hepatic ST2<sup>+</sup> Tregs.<sup>35,162</sup> Correspondingly, IL-33-<sup>147,163</sup> and ST2-deficient mice<sup>162</sup> developed more severe ConA-induced liver injury. In the inflamed livers of mice lacking IL-33, ST2 expression on Tregs was reduced,<sup>163</sup> and in the absence of ST2, ConA-induced expansion of hepatic Tregs was diminished.<sup>162</sup>

### 1.10 Aim of this study

AREG is associated with tissue repair and immunosuppressive functions in acute liver disease, but is also involved in fibrogenesis in chronic liver disease. AREG produced by Tregs and ILC2s has been shown to mediate tissue protection, and the alarmin IL-33 can induce the activation of pro-inflammatory ILC2s and immunosuppressive Tregs expressing the IL-33 receptor ST2, as well as their production of AREG. However, the expression and function of AREG in immune-mediated hepatitis remained unclear. To better understand the signaling pathways of the IL-33/AREG axis in hepatic immune regulation, this study first assessed the production of AREG by hepatic ILC2s and ST2<sup>+</sup> Tregs after treatment with IL-33, in the mouse model of ConA-induced immune-mediated hepatitis, and in *Mdr2*<sup>-/-</sup> mice with sclerosing cholangitis. Furthermore, the gene expression levels of *Egfr*, *Areg*, and other members of the EGF family were determined in liver tissue from mice with these acute and chronic liver diseases. This study further aimed to gain insight into the role of AREG in the regulation of hepatic inflammation. To this end, the pathology of acute immune-mediated hepatitis was examined in *Areg*<sup>-/-</sup> mice compared to C57BL/6J (WT) controls. Moreover, the activation of hepatic ST2<sup>+</sup> Tregs and ILC2s from AREG-deficient mice were detected following induction of acute hepatitis or administration of IL-33. In another approach, the effect of exogenous AREG on the activation and effector cytokine expression of naïve and IL-33-activated hepatic ILC2s and ST2<sup>+</sup> Tregs was investigated. In this context, the effect of exogenous AREG on the Treg phenotype was also determined in Tregs lacking endogenous expression of AREG or ST2. AREG has also been shown to strengthen the immunoregulatory function of hepatic Tregs. To analyze the effect of AREG on the capacity of Tregs to inhibit T cell proliferation, suppression assays were performed with Tregs in the presence or absence of exogenous AREG, as well as with Tregs from *Areg*<sup>-/-</sup> compared to WT mice. Overall, this study provides insight into the immunoregulatory role of AREG in both acute and chronic liver disease.

## 2 Materials and Methods

### 2.1 Materials

#### 2.1.1 Technical Equipment

Table 1: Technical Equipment

EQUIPMENT	SUPPLIER
<b>Balances:</b>	
Acculab ATILON ATL-423-I analytical balance	Sartorius, Göttingen
TE124S analytical balance	Sartorius, Göttingen
<b>Centrifuges:</b>	
Centrifuge 5417 R	Eppendorf, Hamburg
Centrifuge 5430 R	Eppendorf, Hamburg
Centrifuge 5810 R	Eppendorf, Hamburg
Mini Centrifuge 6x 1.5/2.0 mL tubes	neoLab, Heidelberg
Mini Centrifuge 2x 8x 0.2 mL strips	neoLab, Heidelberg
DragonLab D1008 Palm Micro Centrifuge	DLAB Scientific, Beijing, China
<b>Clean benches:</b>	
Airflow-control EN 14175	Airflow Lufttechnik, Rheinbach
Hera Safe Clean Bench	Heraeus, Hanau
MSC Advantage™ clean bench	Thermo Fisher Scientific, Waltham, USA
<b>Flow Cytometers:</b>	
BD FACSAria™ Fusion cell sorter	BD Biosciences, Franklin Lakes, USA
BD LSRFortessa™ cell analyzer	BD Biosciences, Franklin Lakes, USA
<b>Heating blocks and baths:</b>	
Mixing Block MB-102 Thermomixer	Bioer Technology, Hangzhou, China
Shaking water bath	GFL - Gesellschaft für Labortechnik, Burgwedel
Thermoleader Dry Block Heat Bath	UniEquip, Martinsried
Thermo Scientific™ Digital Dry Bath/Block Heater	Thermo Fisher Scientific, Waltham, USA
<b>Histology equipment:</b>	
Automated Rotary Microtome Leica RM2255	Leica Biosystems, Wetzlar
Cooling Plate COP 30	MEDITE Medical, Burgdorf
Embedding machine Leica TP1020	Leica Biosystems, Wetzlar
Embedding workstation HistoStar™	Thermo Fisher Scientific, Waltham, USA
Microwave 900 & Grill	Severin, Sundern
Tissue Float Bath GFL 1052	GFL - Gesellschaft für Labortechnik, Burgwedel

<b>EQUIPMENT</b>	<b>SUPPLIER</b>
<b>Incubators:</b>	
Galaxy® 48R CO <sub>2</sub> Incubator	New Brunswick Scientific, Eppendorf, Hamburg
Innova® CO-48 CO <sub>2</sub> Incubator	New Brunswick Scientific, Eppendorf, Hamburg
<b>Microplate Washer:</b>	
HydroFlex™ microplate washer	Tecan, Männedorf, Switzerland
<b>Microscopes:</b>	
Axio Observer 7 Microscope	Zeiss, Oberkochen
Olympus CK40 microscope	Olympus, Shinjuku City, Japan
<b>Non-technical equipment:</b>	
BD IMag™ Cell Separation Magnet	BD Biosciences, Franklin Lakes, USA
BLAUBRAND® Neubauer Improved Counting chambers	Brand, Wertheim
MACS® MultiStand	Miltenyi Biotec, Bergisch Gladbach
OctoMACS™ Separator	Miltenyi Biotec, Bergisch Gladbach
QuadroMACS™ Separator	Miltenyi Biotec, Bergisch Gladbach
Stainless steel 5 mm metal beads	Qiagen, Hilden
<b>pH meter:</b>	
SevenGo pH meter	Mettler Toledo, Columbus, USA
<b>Photometric Analyzers:</b>	
Cobas Integra® 400 plus biochemical analyzer	Roche, Basel, Switzerland
Infinite® M200 microplate reader	Tecan, Männedorf, Switzerland
NanoDrop® Spectrophotometer ND-1000	Peqlab Biotechnologie, Erlangen
<b>Pipettes:</b>	
Eppendorf Research® plus mechanical pipettes 2.5, 10, 20, 100, 200, 1000	Eppendorf, Hamburg
HandyStep® touch repetitive pipettes	Brand, Wertheim
Pipetboy acu 2 pipette controller for glass and plastic pipettes	Integra Biosciences, Zizers, Switzerland
<b>Pumps:</b>	
TL peristaltic pump	Medorex Biotech, Nörten-Hardenberg
VACUSAFE comfort Laboratory vacuum pump	Integra, Princeton, USA
<b>Shaker:</b>	
Dual-Action Shaker KL 2	Edmund Bühler, Bodelshausen
MTS 2/4 digital microtiter shaker	IKA, Staufen
TissueLyser II	Qiagen, Hilden
<b>Stirrers:</b>	
M 22 Magnetic stirrer	Ingenieurbüro CAT, Ballrechten-Dottingen
OMNILAB MR 2002 magnetic stirrer	Heidolph Instruments, Schwabach

EQUIPMENT	SUPPLIER
<b>Thermocyclers:</b>	
Biometra TAdvanced Twin 48	Analytik Jena, Jena
Biometra TProfessional TRIO 48	Analytik Jena, Jena
Biometra TRIO 48	Analytik Jena, Jena
QuantStudio™ 7 Flex Real-Time PCR System	Thermo Fisher Scientific, Waltham, USA
<b>Vortexers:</b>	
Analog Vortex Mixers	VWR, Radnor, USA
Reax 1R Vortex Mixers	Heidolph Instruments, Schwabach

## 2.1.2 Consumables

Table 2: Consumables

CONSUMABLES	SUPPLIER
24-well Cell culture plates, tissue culture treated, flat bottom	Eppendorf, Hamburg
48-well Microplates, Nunclon™ Delta Surface, flat bottom	Thermo Fisher Scientific, Waltham, USA
96-well Microplates, Nunclon™ Delta Surface, round (U) bottom	Thermo Fisher Scientific, Waltham, USA
96-well Microplates, transparent, Microlon, high binding, flat bottom (Tecan)	Greiner Bio-One, Kremsmünster, Austria
Bemis™ Parafilm™ M Laboratory film	Ancor, Zurich, Switzerland
Bottle top filter Filtropur BT50, 500 mL (0.2 µm)	Sarstedt, Nümbrecht
CD146 (LSEC) MicroBeads, mouse	Miltenyi Biotec, Bergisch Gladbach
Cell scrapers M, 2-position blade	Sarstedt, Nümbrecht
Cell strainers Corning® (100 µm)	Corning, Corning, USA
Cell strainers LABSOLUTE® (70 µm)	Th. Geyer, Renningen
CellTrics™ Disposable Filters (30 µm)	Sysmex, Kobe, Japan
Cover slips (21 x 26 mm, 24 x 60 mm)	Gerhardt Menzel, Braunschweig
Falcon Tubes (15 mL)	Corning, Corning, USA
Falcon Tubes (15 mL, 50 mL)	Sarstedt, Nümbrecht
Falcon Tubes (50 mL)	Greiner Bio-One, Kremsmünster, Austria
Filter papers MN 615 ¼	Machery-Nagel, Duren
Flow Cytometry Polystyrene tubes (5 mL)	Sarstedt, Nümbrecht
Cuvettes COBAS INTEGRA	Roche, Basel, Switzerland
Histology Embedding cassettes Universal	Sanowa, Leimen
MACS® Separation Columns LS	Miltenyi Biotec, Bergisch Gladbach
MACS® Separation Columns MS	Miltenyi Biotec, Bergisch Gladbach
MicroAmp™ Optical 384-Well Reaction Plate (RT-PCR)	Thermo Fisher Scientific, Waltham, USA

<b>CONSUMABLES</b>	<b>SUPPLIER</b>
MicroAmp™ Optical Adhesive Film (RT-PCR)	Thermo Fisher Scientific, Waltham, USA
HistoBond® Adhesive Microscope slides (26 x 76 mm)	Paul Marienfeld, Lauda-Königshofen
Quali-PCR-Tubes (0.2 mL)	Kisker Biotech, Steinfurt
Reaction tubes (1.5 mL)	Sarstedt, Nümbrecht
Reaction tubes Biosphere® SafeSeal (1.5 mL)	Sarstedt, Nümbrecht
Reaction tubes SafeSeal (2 mL)	Sarstedt, Nümbrecht
Reaction tubes SafeSeal (5 mL)	Sarstedt, Nümbrecht
Petri dishes	Greiner Bio-One, Kremsmünster, Austria
Pipette tips Biosphere® Filter (20 µL)	Sarstedt, Nümbrecht
Pipette tips Biosphere® Filter (200 µL, extra-long)	Sarstedt, Nümbrecht
Pipette tips Biosphere® Filter (1000 µL)	Sarstedt, Nümbrecht
Pipette tips SafeSeal SurPhob® Filter (200 µL)	Biozym, Hessisch Oldendorf
Pipette tips SafeSeal SurPhob® Filter (1250 µL)	Biozym, Hessisch Oldendorf
Pipette tips Sapphire Filter (1250 µL)	Greiner Bio-One, Kremsmünster, Austria
Pipette tips without Filter (10 µL)	Biozym, Hessisch Oldendorf
Pipette tips without Filter (200 µL)	Sarstedt, Nümbrecht
Precision dispenser (PD)-tips II (5 mL)	Brand, Wertheim
Sealing Tape, optically clear (ELISA)	Sarstedt, Nümbrecht
Serological pipettes (5 mL, 10 mL, 25 mL)	Sarstedt, Nümbrecht
Sterican® injection cannulas (0.4 x 12 mm (27 G x ½”), 0.55 x 25 mm (24 G x 1”), 0.9 x 40 mm (20 G x 1½”))	B. Braun, Melsungen
Surgical blades No. 20	Feather, Osaka, Japan
Syringe filters Rotilabo® CME (0.22 µm)	Roth, Karlsruhe
Syringes Inject®-F (1 mL)	B. Braun, Melsungen
Syringes Omnifix®-F (1 mL)	B. Braun, Melsungen
Syringes BD Discardit™ II (2 mL)	BD Biosciences, Franklin Lakes, USA

### 2.1.3 Reagents and Kits

**Table 3: Reagents and kits**

<b>REAGENTS AND KITS</b>	<b>SUPPLIER</b>
1-Propanol CHEMSOLUTE® (N-Propanol, Min. 99,5%)	Th. Geyer, Renningen
2-Mercaptoethanol (50 mM)	Thermo Fisher Scientific, Waltham, USA
4-(Dimethylamino)benzaldehyde (DMAB)	Merck, Darmstadt

REAGENTS AND KITS	SUPPLIER
Acetic acid (100%)	Roth, Karlsruhe
ALT reagent (ALTL, Alanine Aminotransferase COBAS INTEGRA)	Roche, Basel, Switzerland
ALP reagent (ALP2S, ALP IFCC Gen.2 Small COBAS INTEGRA)	Roche, Basel, Switzerland
Ammonium Chloride (NH <sub>4</sub> Cl)	Avantor, Radnor, USA
Anti-APC MicroBeads	Miltenyi Biotec, Bergisch Gladbach
Anti-PE MicroBeads	Miltenyi Biotec, Bergisch Gladbach
Antibody Diluent	Agilent, Santa Clara, USA
Antibody Diluent	Zytomed Systems, Berlin
BD OptEIA™ TMB Substrate Reagent Set (ELISA)	BD Biosciences, Franklin Lakes, USA
Bilirubin reagent (BILD2, Bilirubin Direct Gen.2 COBAS INTEGRA)	Roche, Basel, Switzerland
Albumin bovine fraction V (Bovine serum albumin, BSA)	Serva Electrophoresis, Heidelberg
Brefeldin A (BFA)	Sigma-Aldrich, St. Louis, USA
Calcium chloride dehydrate (CaCl <sub>2</sub> x 2 H <sub>2</sub> O)	Sigma-Aldrich, St. Louis, USA
Calibrator for automated systems (C.f.a.s. COBAS)	Roche, Basel, Switzerland
CC/Mount™ tissue mounting medium	Sigma-Aldrich, St. Louis, USA
CD4 <sup>+</sup> T Cell Isolation Kit mouse	Miltenyi Biotec, Bergisch Gladbach
CFSE Cell Division Tracker Kit	BioLegend, San Diego, USA
Chloramine T trihydrate	Roth, Karlsruhe
Cholesterol reagent (CHOL2, Cholesterol Gen.2 COBAS INTEGRA)	Roche, Basel, Switzerland
Citric acid anhydrous	Merck, Darmstadt
Cleaner Cassette (CLEAN COBAS INTEGRA)	Roche, Basel, Switzerland
Collagenase from <i>Clostridium histolyticum</i>	Sigma-Aldrich, St. Louis, USA
Collagen R solution (0.2%)	Roche, Basel, Switzerland
Concanavalin A (ConA) from <i>Canavalia ensiformis</i> (Jack bean)	Sigma-Aldrich, St. Louis, USA
D-(-)-Fructose	Sigma-Aldrich, St. Louis, USA
D-(+)-Glucose	Sigma-Aldrich, St. Louis, USA
α-D-(+)-Glucose monohydrate	Roth, Karlsruhe
Diethyl pyrocarbonate (DEPC)	Sigma-Aldrich, St. Louis, USA
Di-Sodium hydrogen phosphate dihydrate (Na <sub>2</sub> HPO <sub>4</sub> x 2 H <sub>2</sub> O)	Roth, Karlsruhe
DMEM (1x) +GlutaMAX™-I (+ 4.5 g/L D-Glucose, + Pyruvate)	Thermo Fisher Scientific, Waltham, USA
DMEM (1x) high glucose (+ 4.5 g/L D-Glucose, + L-Glutamine)	Thermo Fisher Scientific, Waltham, USA



REAGENTS AND KITS	SUPPLIER
DNA-free™ Kit	Thermo Fisher Scientific, Waltham, USA
Dulbecco's Phosphate Buffered Saline (DPBS, 1x, with MgCl <sub>2</sub> and CaCl <sub>2</sub> , for cell culture) <i>for ConA treatment</i>	Sigma-Aldrich, St. Louis, USA
Dulbecco's Phosphate Buffered Saline (DPBS, 10x, +CaCl <sub>2</sub> + MgCl <sub>2</sub> ) <i>for Hepatocyte culture</i>	Thermo Fisher Scientific, Waltham, USA
Dynabeads™ Mouse T-Activator CD3/CD28	Thermo Fisher Scientific, Waltham, USA
eBioscience™ Foxp3/Transcription Factor Staining Buffer Set	Thermo Fisher Scientific, Waltham, USA
Ethylenediamine tetraacetic acid (EDTA)	Roth, Karlsruhe
Ethylene glycol tetraacetic acid (EGTA)	Roth, Karlsruhe
Entellan® rapid mounting medium for microscopy	Sigma-Aldrich, St. Louis, USA
Eosin Y (yellowish) Certistain®	Merck, Darmstadt
Ethanol absolute CHEMSOLUTE® (Min. 99.5%)	Th. Geyer, Renningen
Ethanol denatured CHEMSOLUTE® (99%)	Th. Geyer, Renningen
Fetal bovine Serum (FBS)	Thermo Fisher Scientific, Waltham, USA
Fetal bovine Serum (FBS) <i>for LSEC-PBS</i>	Sigma-Aldrich, St. Louis, USA
Formalin Solution 10% (v/v) [=4% (w/v)] neutralized	Avantor, Radnor, USA
Glycine	Roth, Karlsruhe
Hemalum solution acid acc. to Mayer	Roth, Karlsruhe
HEPES PUFFERAN®	Roth, Karlsruhe
HEPES buffer solution (1 M)	Thermo Fisher Scientific, Waltham, USA
Hydrochloric acid fuming (HCl, 37%) ROTIPURAN®	Roth, Karlsruhe
Heparin-Sodium solution (25000 IU/5 mL)	LEO Pharma, Ballerup, Denmark
Hydrogen peroxide ROTIPURAN® (H <sub>2</sub> O <sub>2</sub> , 30%)	Roth, Karlsruhe
Hydroxyproline stock solution (1 mg/mL)	Sigma-Aldrich, St. Louis, USA
Ionomycin Calcium Salt from <i>Streptomyces conglobatus</i>	Sigma-Aldrich, St. Louis, USA
Ketamine Ketamidor® (100 mg/mL)	WDT, Garbsen
L-Alanine	Roth, Karlsruhe
L-Aspartic acid	Roth, Karlsruhe
L-Glutamine (200 mM)	Thermo Fisher Scientific, Waltham, USA
L-Glutamic acid	Roth, Karlsruhe
L-Serine	Roth, Karlsruhe
L-Threonine	Roth, Karlsruhe
Liberase™ TM Research Grade	Roche, Basel, Switzerland

REAGENTS AND KITS	SUPPLIER
LIVE/DEAD™ Fixable Red Dead Cell Stain Kit (PE-TR)	Thermo Fisher Scientific, Waltham, USA
Liquid DAB + Substrate Chromogen System	Agilent, Santa Clara, USA
MEM Non-essential Amino Acid Solution (100x)	Sigma-Aldrich, St. Louis, USA
Magnesium chloride hexahydrate ( $\text{MgCl}_2 \times 6 \text{ H}_2\text{O}$ )	Roth, Karlsruhe
Magnesium chloride ( $\text{MgCl}_2$ )	Roth, Karlsruhe
Magnesium sulfate heptahydrate ( $\text{MgSO}_4 \times 7 \text{ H}_2\text{O}$ )	Merck, Darmstadt
Monensin Solution (1,000X)	BioLegend, San Diego, USA
Mouse Amphiregulin DuoSet® ELISA Development System	R&D Systems, Minneapolis, USA
NaCl Diluent 9% COBAS INTEGRA	Roche, Basel, Switzerland
Naphthol-AS-BI-Phosphate	Sigma-Aldrich, St. Louis, USA
New Fuchsin	MP Biomedicals, Santa Ana, USA
N,N-Dimethylformamide (min. 99%)	Sigma-Aldrich, St. Louis, USA
Normal Swine serum	Jackson ImmunoResearch, West Grove, USA
Nuclease-free water	Thermo Fisher Scientific, Waltham, USA
NucleoSpin® RNA, Mini Kit for RNA purification	Machery-Nagel, Duren
Nycodenz®	Serumwerk Bernburg, Bernburg
Penicillin / Streptomycin (10.000 U/mL)	Thermo Fisher Scientific, Waltham, USA
Percoll™	Cytiva, Marlborough, USA
PeriControl ClinChem Multi 1 (COBAS)	Roche, Basel, Switzerland
PeriControl ClinChem Multi 2 (COBAS)	Roche, Basel, Switzerland
Perchloric acid ( $\text{HClO}_4$ , 60%)	Merck, Darmstadt
Phorbol 12-myristate 13-acetate (PMA)	Sigma-Aldrich, St. Louis, USA
Picric acid, water saturated	Morphisto, Offenbach am Main
Potassium hydrogen carbonate ( $\text{KHCO}_3$ )	Roth, Karlsruhe
Potassium chloride (KCl)	Roth, Karlsruhe
Potassium phosphate monobasic ( $\text{KH}_2\text{PO}_4$ )	Sigma-Aldrich, St. Louis, USA
PowerUp™ SYBR™ Green Master Mix	Thermo Fisher Scientific, Waltham, USA
RNeasy® Micro Kit, for RNA purification	Qiagen, Hilden
RPMI Medium 1640 (1X) + GlutaMAX™-I	Thermo Fisher Scientific, Waltham, USA
Direct Red 80 (Sirius red)	Sigma-Aldrich, St. Louis, USA
Sodium acetate 3-hydrate ( $\text{CH}_3\text{COONa} \times 3 \text{ H}_2\text{O}$ )	ITW Reagents, Castellar del Vallès, Spain
Sodium azide ( $\text{NaN}_3$ )	Roth, Karlsruhe
Sodium chloride (NaCl)	ITW Reagents, Castellar del Vallès, Spain

REAGENTS AND KITS	SUPPLIER
Sodium hydrogen carbonate ( $\text{NaHCO}_3$ )	Roth, Karlsruhe
Sodium hydroxide ( $\text{NaOH}$ )	Roth, Karlsruhe
Sodium nitrite ( $\text{NaNO}_2$ )	Sigma-Aldrich, St. Louis, USA
Sodium phosphate monobasic monohydrate ( $\text{NaH}_2\text{PO}_4 \times \text{H}_2\text{O}$ )	Sigma-Aldrich, St. Louis, USA
Sodium pyruvate (100 mM)	Thermo Fisher Scientific, Waltham, USA
Streptavidin-HRP	R&D Systems, Minneapolis, USA
Sucrose	Thermo Fisher Scientific, Waltham, USA
Sulphuric acid ( $\text{H}_2\text{SO}_4$ , 96%)	Roth, Karlsruhe
Target Retrieval solution (10x), pH6	Agilent, Santa Clara, USA
Trichloroacetic acid (min. 98%)	Sigma-Aldrich, St. Louis, USA
TRIS-hydrochloride (Tris-HCl)	Roth, Karlsruhe
PUFFERAN®	
Trizma® base (Tris-base)	Sigma-Aldrich, St. Louis, USA
Trypan blue	Sigma-Aldrich, St. Louis, USA
TWEEN® 20	Sigma-Aldrich, St. Louis, USA
VECTASTAIN® ABC-HRP Kit, Peroxidase (Standard)	Vector Laboratories, Newark, USA
Verso cDNA Synthesis Kit	Thermo Fisher Scientific, Waltham, USA
Xylazine (20 mg/mL)	WDT, Garbsen
Xyloersatz-Medium (HS200-5, XEM)	DiaTec, Bamberg
William's Medium E (1x) +GlutaMAX™-I	Thermo Fisher Scientific, Waltham, USA
Zombie NIR™ Fixable Viability Kit (APC-Cy7)	BioLegend, San Diego, USA
ZytoChem Plus (AP) Polymer Kit	Zytomed Systems, Berlin

#### 2.1.4 Cytokines and growth factors

Table 4: Cytokines and growth factors

CYTOKINES AND GROWTH FACTORS	SUPPLIER
recombinant murine (rm)AREG	R&D Systems, Minneapolis, USA
rmIFN $\gamma$	R&D Systems, Minneapolis, USA
rmIL-1 $\beta$	BioLegend, San Diego, USA
rmIL-2	R&D Systems, Minneapolis, USA
rmIL-33	BioLegend, San Diego, USA
rmTGF $\beta$ 1	BioLegend, San Diego, USA
rmTNF $\alpha$	Sino Biological, Beijing, China

### 2.1.5 Buffers and solutions

**Table 5: Buffers and solutions**

<b>BUFFERS AND SOLUTIONS</b>	<b>COMPOUNDS</b>
Acetate citrate buffer	0.88 M Sodium acetate 3-hydrate 0.24 M Citric acid 0.2 M Acetic acid 0.85 M NaOH ddH <sub>2</sub> O pH 6.5
ACK lysis buffer (10x)	1.5 M NH <sub>4</sub> Cl 0.1 M KHCO <sub>3</sub> 1 mM EDTA
Ammonium chloride (NH <sub>4</sub> Cl) buffer	19 mM Tris-HCl 140 mM NH <sub>4</sub> Cl ddH <sub>2</sub> O pH 7.2
Calcium-deprived buffer	0.1 mM L-Aspartic acid 0.2 mM L-Threonine 0.3 mM L-Serine 0.5 mM Glycine 0.6 mM L-Alanine 0.9 mM L-Glutamic acid 0.9 mM L-Glutamine 20 mM D-Glucose 20 mM D-Fructose 197 mM Sucrose 3 mM KCl 0.7 mM NaH <sub>2</sub> PO <sub>4</sub> x H <sub>2</sub> O 0.5 mM MgCl <sub>2</sub> 10 mM HEPES 24 mM NaHCO <sub>3</sub> ddH <sub>2</sub> O pH 7.4
Calcium-deprived buffer + Collagenase	1:100 mixture of: Calcium-deprived buffer + Collagenase (50 mg/mL)
CFSE stock solution (5 mM)	100 µg CFSE 36 µL DMSO
CFSE working solution (5 µM, 1 mL)	1 µL CFSE stock solution (5 mM) 1 mL PBS (1x)
Chloramine-T solution (10 mL)	127 mg Chloramine T trihydrate 2 mL N-Propanol (50%) 8 mL Acetate citrate buffer

<b>BUFFERS AND SOLUTIONS</b>	<b>COMPOUNDS</b>
DMEM <sup>4+</sup> medium	DMEM (1x) high glucose 8% FBS 2% L-Glutamine 1% Penicillin/Streptomycin
Ehrlich's reagent (10 mL)	1.5 g DMAB 10 mL N-Propanol/perchloric acid-mix (2:1)
ELISA reagent dilution buffer	1% BSA 1x PBS pH 7.2-7.4
ELISA wash buffer (1 L)	100 mL PBS (10x) 900 mL ddH <sub>2</sub> O 0,5 mL TWEEN® 20 pH 7.2-7.4
Eosin Y (1%, 1L)	10 g Eosin Y 1 L Ethanol (96 %)
Fluorescence activated cell sorting buffer (FACS Buffer; 1L)	100 mL PBS (10x) 20 mL FBS (heat-inactivated) 2 mL NaN <sub>3</sub> (10%) ddH <sub>2</sub> O pH 7.2-7.4
GBSS + Collagenase	1:125 mixture of: GBSS + Collagenase (50 mg/mL)
Gey's balanced salt solution (GBSS)	137 mM NaCl 5 mM KCl 1.6 mM CaCl <sub>2</sub> x 2 H <sub>2</sub> O 0.9 mM MgCl <sub>2</sub> x 6 H <sub>2</sub> O 0.3 mM MgSO <sub>4</sub> x 7 H <sub>2</sub> O 0.2 mM KH <sub>2</sub> PO <sub>4</sub> 1.7 mM Na <sub>2</sub> HPO <sub>4</sub> 2.7 mM NaHCO <sub>3</sub> 5.5 mM D-Glucose 50 mM HEPES ddH <sub>2</sub> O pH 7.4

<b>BUFFERS AND SOLUTIONS</b>	<b>COMPOUNDS</b>
Hank's balanced salt solution (HBSS)	5.4 mM KCl 0.3 mM Na <sub>2</sub> HPO <sub>4</sub> x 2 H <sub>2</sub> O 0.4 mM KH <sub>2</sub> PO <sub>4</sub> 4.2 mM NaHCO <sub>3</sub> 1.3 mM CaCl <sub>2</sub> x 2 H <sub>2</sub> O 0.5 mM MgCl <sub>2</sub> x 6 H <sub>2</sub> O 0.6 mM MgSO <sub>4</sub> x 7 H <sub>2</sub> O 137 mM NaCl 5.6 mM D-Glucose monohydrate ddH <sub>2</sub> O pH 7.4
Hydroxyproline working solution (0.5 mg/mL)	1:1 mixture of: Hydroxyproline stock solution (1 mg/mL) 12 M HCl
Ketamine-Xylazine-Heparin (KHx)	240 mg/kg Ketamine 32 mg/kg Xylazine 16666 IU/kg Heparin
Liberase stock solution (1 mg/mL)	5 mg Liberase™ 5 mL PM
LSEC <sup>4+</sup> medium	DMEM (1x) +GlutaMAX™-I 8% LSEC-FBS 2% L-Glutamine 1% P/S
LSEC-PBS	1x PBS 1% LSEC-FBS
Magnetic-activated cell sorting buffer (MACS buffer)	1x PBS 0.5% BSA 2 mM EDTA ddH <sub>2</sub> O pH 7.2-7.4
New Fuchsin solution	300 mg NaNO <sub>2</sub> 7.5 mL ddH <sub>2</sub> O 300 µL New Fuchsin standard solution 150 mL TNT buffer 20 mg Naphthol-AS-BI-Phosphate 795 µL NN-Dimethylformamide solution
New Fuchsin standard solution (3.5 mL)	175 mg New Fuchsin 3.5 mL HCl (2 M)
Percoll solution for Primary Hepatocyte Isolation (24 mL)	21.6 mL Percoll™ 2.4 mL DPBS (10x, +CaCl <sub>2</sub> +MgCl <sub>2</sub> )
Percoll working solution (4 mL)	3.7 mL Percoll™ 0.288 mL PBS (10x) 0.048 mL NaHCO <sub>3</sub> in ddH <sub>2</sub> O (7.5%)

<b>BUFFERS AND SOLUTIONS</b>	<b>COMPOUNDS</b>
Percoll-HBSS solution (10 mL)	4 mL Percoll working solution 6 mL HBSS 0.2 mL Heparin
Phosphate buffered saline (PBS, 10x, 1 L)	80 g NaCl 11,6 g Na <sub>2</sub> HPO <sub>4</sub> x 2 H <sub>2</sub> O 2 g KH <sub>2</sub> PO <sub>4</sub> 2 g KCl ddH <sub>2</sub> O pH 7.4
Perfusion medium (PM, 1 L)	190 mg MgSO <sub>4</sub> x 7 H <sub>2</sub> O 190 mg MgCl <sub>2</sub> x 6 H <sub>2</sub> O 60 mg Na <sub>2</sub> HPO <sub>4</sub> x 2 H <sub>2</sub> O 60 mg KH <sub>2</sub> PO <sub>4</sub> 400 mg KCl 2,38 g HEPES 8 g NaCl 2 g D-Glucose 220 mg CaCl <sub>2</sub> 2 g BSA (in ddH <sub>2</sub> O) pH 7.4
Pre-perfusion medium liver (PPML, 1 L)	400 mg KCl 58 mg KH <sub>2</sub> PO <sub>4</sub> 350 mg NaHCO <sub>3</sub> 8.06 g NaCl 68 mg Na <sub>2</sub> HPO <sub>4</sub> x 2 H <sub>2</sub> O 1 g D-Glucose 190 mg EGTA 11.91 g HEPES pH 7.35
RNAse-free water (1 L)	1 mL DEPC 1 L ddH <sub>2</sub> O
RPMI medium for FACS-Sorting	RPMI Medium 1640 (1X) +GlutaMAX™-I 2% Penicillin/Streptomycin
RPMI <sup>5+</sup> medium	RPMI Medium 1640 (1X) +GlutaMAX™-I 10% FBS 1% Sodium pyruvate (100 mM) 1% Penicillin/Streptomycin 0.1% 2-mercaptoethanol

BUFFERS AND SOLUTIONS	COMPOUNDS
RPMI <sup>7+</sup> medium	RPMI Medium 1640 (1X) +GlutaMAX™-I 10% FBS 1% Sodium pyruvate (100 mM) 1% Penicillin/Streptomycin 0.1% 2-mercaptoethanol 0.5% HEPES buffer solution (1 M) 1x Non-essential amino acids (100x)
Sirius red solution	0.1% Direct Red 80 (Sirius red) Picric acid
TNT buffer (1L)	6.35 g Tris-base 9 g NaCl 1 mL TWEEN® 20 1 L ddH <sub>2</sub> O pH 8.2-8.4
Tris-buffered saline (TBS, 10x, 1L)	1.5 M NaCl 1 M Tris-base 1 L ddH <sub>2</sub> O pH 7.4
William's medium E <sup>4+</sup>	William's Medium E (1x) +GlutaMAX™-I 1% L-Glutamine 10% FBS 1% Penicillin/Streptomycin

## 2.1.6 Antibodies

### 2.1.6.1 Antibodies for enzyme-linked immunosorbent assay (ELISA)

Table 6: Primary and secondary antibodies for Sandwich ELISA

TAREGT	REFERENCE	SPECIES	CONJUGATE	DILUTION	SUPPLIER
NUMBER					
<b>Capture antibody</b>					
mouse AREG	DuoSet DY989 #842047	Goat	-	1:180	R&D Systems, Minneapolis, USA
<b>Detection antibody</b>					
mouse AREG	DuoSet DY989 #842048	Goat	Biotin	1:180	R&D Systems, Minneapolis, USA

According to the manufacturer's protocol, the primary capture antibody was diluted in phosphate buffered saline (PBS) and the secondary detection antibody was diluted in ELISA reagent diluent buffer.



### 2.1.6.2 Antibodies for Immunohistochemistry (IHC)

**Table 7: Primary antibodies for IHC**

#	TARGET	REFERENCE NUMBER	SPECIES	CLONE	DILUTION	SUPPLIER
1	AREG	PA5-109404	Rabbit	polyclonal	1:100	Thermo Fisher Scientific, Waltham, USA
2	AREG	orb4539	Rabbit	polyclonal	1:100 / 1:200	Biorbyt, Cambridge, UK
3	AREG	AF989	Goat	polyclonal	1:20	R&D Systems, Minneapolis, USA

For detection using DAB substrate chromogen system containing hydrogen peroxidase, all primary antibodies were diluted in Agilent antibody diluent. For detection with ZytoChem Plus alkaline phosphatase (AP) polymer kit and New Fuchsin chromogen, the primary antibodies #1 and #2 were diluted in Zytomed antibody diluent.

**Table 8: Secondary antibodies for IHC**

TARGET	REFERENCE NUMBER	SPECIES	CLONE	DILUTION	SUPPLIER
Rabbit	E0353	Swine	polyclonal	1:200	Agilent, Santa Clara, USA
Goat	E0466	Rabbit	polyclonal	1:200	Agilent, Santa Clara, USA

The secondary antibodies were diluted in Agilent antibody diluent.

### 2.1.6.3 Antibodies for flow cytometry

**Table 9: Antibody for blocking Fc receptors - flow cytometry (anti-mouse)**

NAME	TARGET	CLONE	DILUTION	SUPPLIER
TrueStain FcX antibody	CD16/32	93	1:100	BioLegend, San Diego, USA

The blocking antibody was diluted in MACS buffer for MACS sorting (see 2.2.9.4, 2.2.9.5 and 2.2.9.8) or in PBS for immune cells analysis by flow cytometry (see 2.2.11.1).

To block unspecific binding of staining antibodies to Fc receptors

**Table 10: Antibodies for surface staining - flow cytometry (anti-mouse)**

TARGET	CONJUGATE	CLONE	DILUTION	SUPPLIER
TCR $\beta$	FITC, PE-Cy7	H57-597	1:200	BioLegend, San Diego, USA
CD4	BV 711	RM4-5	1:200	BioLegend, San Diego, USA

TARGET	CONJUGATE	CLONE	DILUTION	SUPPLIER
Sca-1	Pacific Blue	D7	1:100	BioLegend, San Diego, USA
ST2	PE-Cy7, PerCP-eF710	RMST2-2	1:100	Thermo Fisher Scientific, Waltham, USA
CD25	PE	PC-61	1:200	BioLegend, San Diego, USA
ICOS	FITC	7E.17G9	1:200	Thermo Fisher Scientific, Waltham, USA
KLRG1	BV 605	2F1/KLRG1	1:200	BioLegend, San Diego, USA
PD-1	APC-Cy7	29F.1A12	1:200	BioLegend, San Diego, USA
PD-L1	BV 421	10F.9G2	1:200	BioLegend, San Diego, USA
TIGIT	BV 421	1G9	1:200	BioLegend, San Diego, USA
Mouse Lineage Antibody cocktail (CD3e, CD11b, CD45R, Ly-76, Ly-6G/Ly-6C)	APC	145-2C11, M1/70, RA3-6B2, TER-119, RB6-8C5	1:150	BD Biosciences, Franklin Lakes, USA
L CD3e	APC	145-2C11	1:200	BioLegend, San Diego, USA
i CD11b	APC	M1/70	1:200	BioLegend, San Diego, USA
n CD45R	APC	RA3-6B2	1:200	BioLegend, San Diego, USA
e Ly-76	APC	TER-119	1:200	BioLegend, San Diego, USA
a Ly-6G / g Ly-6C	APC	RB6-8C5	1:200	BioLegend, San Diego, USA

All antibodies for surface staining were diluted in PBS.

**Table 11: Antibodies for intracellular analysis by flow cytometry (anti-mouse)**

TARGET	CONJUGATE	CLONE	DILUTION	SUPPLIER
Foxp3	AF 647	MF-14	1:200	BioLegend, San Diego, USA
	PerCP-Cy5.5	FJK-16s	1:100	Thermo Fisher Scientific, Waltham, USA
AREG	Biotin	polyclonal	1:200	R&D Systems, Minneapolis, USA
Streptavidin	BV 785	-	1:200	BioLegend, San Diego, USA
Bcl-2	PE	BCL/10C4	1:10	BioLegend, San Diego, USA
CTLA-4	PE	UC10- 4F10-11	1:200	BD Pharmingen, San Diego, USA
IL-13	AF 488	eBio13A	1:100	Thermo Fisher Scientific, Waltham, USA
Ki-67	FITC	REA183	1:100	Miltenyi Biotec, Bergisch Gladbach

All antibodies for intracellular staining were diluted in Permeabilization buffer from Foxp3/Transcription Factor Staining Buffer Set.

IL-10 and, in some experiments, Foxp3 were detected not by antibody staining, but by using FIR x *tiger* double reporter mice (Foxp3-IRES-mRFP [FIR] x IL-10-IRES-GFP [*tiger*]). These mice were engineered with an internal ribosome entry site (IRES) monomeric red fluorescent protein (mRFP) element knocked into the *Foxp3* locus,<sup>164</sup> and an IRES green fluorescent protein (GFP) element inserted into the *Il10* locus.<sup>165</sup>

### 2.1.7 Primers

**Table 12: Oligonucleotide sequences of primers used in qRT-PCR.**

<b>TARGET (REFERENCE)</b>	<b>FORWARD PRIMER (5' → 3') REVERSE PRIMER (3' → 5')</b>	<b>ANNEALING TEMPERATURE</b>
<i>Actb</i> (NM_007393)	TATTGGCAACGAGCGGTTCC GGCATAGAGGTCTTTACGGATGTC	60°C
<i>Areg</i> (NM_009704.4)	GGTCTTAGGCTCAGGCCATTA AGAGTTCACTGCCAGAAGGC	60°C
<i>Btc</i> (NM_007568.5)	AGCACAGTTGATGGACCCAA TGGAGAATTGCAAGACCCAGG	60°C
<i>Col1a1</i> (NM_007742)	GAGCGGAGAGTACTGGATCG TACTCGAACGGGAATCCATC	60°C
<i>Col3a1</i> (NM_009930)	GTCCACGAGGTGACAAAGGT GATGCCCACTTGTTCCATCT	60°C
<i>Cxcl9</i> (NM_008599.4)	TGGAGCAGTGTGGAGTTCCG GTAGTGGATCGTGCCTCGG	60°C
<i>Cxcl10</i> (NM_021274)	GCCGTCATTTTCTGCCTCAT TGCAGCGGACCGTCCTT	60°C
<i>Cxcr3</i> (NM_009910.3)	GCTAGATGCCTCGGACTTTG CGCTGACTCAGTAGCACAGC	60°C
<i>Egf</i> (NM_207655.2)	GAGGTCCGCTAGAGAAATGTCA TGGGGCATGTGCAGTGATAG	60°C
<i>Egfr</i> (NM_207655.2)	CATAGTGGTGGTGGCCCTTG GAGGTTCCACGAGCTCTCTC	60°C
<i>Epgn</i> (NM_053087.2)	TTGGCGTCGGATTGCTAATT TCCCTCCAGAGCAGATGATGT	60°C
<i>Ereg</i> (NM_007950.2)	CGCTGCTTTGTCTAGGTTCC CGGGGATCGTCTTCCATCTG	61°C
<i>Hbegf</i> (NM_010415.2)	GTACTCCCTCTTGCAAATGCC TCCACTGGTAGAGTCAGCCC	60°C
<i>Ifng</i> (NM_008337.4)	ACAGCAAGGCGAAAAAGGATG TCTTCCCCACCCCGAATCA	60°C

<b>TARGET (REFERENCE)</b>	<b>FORWARD PRIMER (5'→3') REVERSE PRIMER (3'→5')</b>	<b>ANNEALING TEMPERATURE</b>
<i>Il10</i> (NM_010548.2)	GGCCCAGAAATCAAGGAGCA ACAGGGGAGAAATCGATGACAG	60°C
<i>Il12p40</i> (NM_001303244.1)	AGACCCTGCCCATTGAACTG GGCGGGTCTGGTTTGATGAT	60°C
<i>Il33</i> (NM_001164724.1)	ATGGGAAGAAGCTGATGGTG CCGAGGACTTTTTGTGAAGG	60°C
<i>Tgfa</i> (NM_031199.5)	CCACTCTGAGACAGTGGTCTG TTGGTTGGGCTGTCATAGGC	60°C
<i>Tgfb1</i> (NM_011577.2)	ACTGGAGTTGTACGGCAGTG GGGGCTGATCCCGTTGATT	60°C
<i>Tgfb2</i> (NM_009367.4)	TCCCCTCCGAAAATGCCATC TGCTATCGATGTAGCGCTGG	60°C
<i>Tnfa</i> (NM_013693)	GATCGGTCCCCAAAGGGATG GCTACAGGCTTGTCACCTCGAA	60°C

Primers were designed using the Primer Basic Local Alignment Search Tool (Primer-BLAST) from NCBI (Bethesda, USA). Primers detecting exon-overlapping amplicons were selected and purchased from Metabion (Planegg, Germany).

### 2.1.8 Software and databases

Table 13: Software and databases

<b>SOFTWARE</b>	<b>SUPPLIER</b>
Adobe Photoshop CS5 v12.0	Adobe, San Jose, USA
BD FACSDiva™	BD Biosciences, Franklin Lakes, USA
BioRender	BioRender, Science Suite, Toronto, Canada
ChatGPT GPT-4o	OpenAI, San Francisco, USA
DeepL Write	DeepL, Cologne, Germany
FlowJo™ v10.6.1	BD Biosciences, Franklin Lakes, USA
GraphPad Prism 7	GraphPad, San Diego, USA
Mendeley Desktop V.1.19.8	Elsevier, Amsterdam, Netherlands
MS Office 2016	Microsoft, Redmond, USA
NanoDrop ND-1000 V3.5.2	Peqlab Biotechnologie, Erlangen
Primer-BLAST	NCBI, Bethesda, USA
QuantStudio™ Real-Time PCR System v1.3	Thermo Fisher Scientific, Waltham, USA
TBASE v17.4	4D Deutschland GmbH, Eching
Tecan Magellan™ 6.5	Tecan, Männedorf, Switzerland
Windows 11	Microsoft, Redmond, USA
ZEN 3.5 (blue edition)	Zeiss, Oberkochen

## 2.2 Methods

### 2.2.1 Mice

C57BL/6J (WT) mice were used to analyze the phenotype of hepatic ST2<sup>+</sup> Tregs and ILC2s in response to IL-33 treatment or in ConA-induced immune-mediated hepatitis. WT mice were also used to isolate hepatic ILC2s for *in vitro* culture and study their phenotype in the presence of exogenous AREG, IL-33 or IL-33/AREG. Additionally, we isolated primary hepatocytes and LSECs from WT mice to measure their AREG production in response to inflammatory stimuli. Further, WT mice were used as controls in experiments with transgenic mice.

FIR x *tiger* mice (Foxp3-IRES-mRFP [FIR] x IL-10-IRES-GFP [*tiger*])<sup>165</sup> were used to detect IL-10 expression by ST2<sup>+</sup> Tregs in response to IL-33 and ConA treatment and for isolation of Tregs for *in vitro* culture experiments with AREG, IL-33 or both. In experiments with genetic knockouts on the FIR x *tiger* mouse background, FIR x *tiger* mice are indicated as WT controls.

To test whether AREG selectively activates ST2<sup>+</sup> Tregs, Tregs were isolated from FIR x *tiger* x *Il1rl1*<sup>-/-</sup> mice lacking the IL-33 receptor ST2 and cultured in the presence of AREG. *Il1rl1*<sup>-/-</sup> mice (*Il1rl1*<sup>tm1Anjm</sup>) were provided by Max Löhning (Experimental Immunology and Osteoarthritis Research, Department of Rheumatology and Clinical Immunology, Charité - Universitätsmedizin Berlin, Berlin, Germany).

In addition, we used FIR x *tiger* x *Areg*<sup>-/-</sup> mice to isolate Tregs for cell culture with exogenous AREG, IL-33 or both and thereby investigate the effect of exogenous AREG on Tregs lacking endogenous AREG expression. *Areg*<sup>-/-</sup> mice were used to analyze the role of AREG in ConA-induced immune-mediated hepatitis, as well as in IL-33-treated mice. We assessed the disease severity in ConA-treated mice and the phenotype of hepatic ST2<sup>+</sup> Tregs and ILC2s in the absence of AREG. Further, we isolated Tregs from *Areg*<sup>-/-</sup> mice to analyze their immunoregulatory function in the absence of AREG by performing suppression assays with CD4<sup>+</sup> responder T cells. *Areg*<sup>-/-</sup> mice (*Areg*<sup>tm1Dle/J</sup>) were provided by Matias A. Avila (Hepatology Program, CIMA, Universidad de Navarra, Pamplona, Spain).

To analyze the phenotype of hepatic ST2<sup>+</sup> Tregs and ILC2s in chronic liver injury, we used 12-week-old *Mdr2*<sup>-/-</sup> mice deficient in the MDR2-dependent phosphatidylcholine transport into the bile.<sup>41</sup> *Mdr2*<sup>-/-</sup> mice develop sclerosing cholangitis with portal inflammation and liver fibrosis within a few weeks of birth.<sup>40</sup>

Age- and sex-matched littermates were used for all experiments with mice aged 7-22 weeks at the time of the experiments. Male mice were included in the *in vivo* studies and a mixture of males and females in the *in vitro* studies. Genotypes of the transgenic mice were regularly screened by PCR analysis. All experiments were approved by the institutional review board (Behörde für Justiz und Verbraucherschutz, Hamburg, Germany) and conducted in accordance with the German animal welfare act. All mice were bred in the animal facility of the University Medical Center Hamburg-Eppendorf (Hamburg, Germany) according to the guidelines of the Federation of European Laboratory Animal Science Association. Mice received human care as described in the “Guide for the Care and Use of Laboratory Animals”. They were kept in individually ventilated cages (IVCs) under controlled conditions (specific pathogen-free (SPF), 22°C, 55% humidity, and 12-hour day/night cycle) and given a standard laboratory chow (LASvendi, Altromin, Germany) and water ad libitum.

### 2.2.2 Animal treatment

To study the effect of exogenous IL-33 on hepatic ST2<sup>+</sup> Tregs and ILC2s, mice were injected intraperitoneally (i.p.) with recombinant murine (rm)IL-33 (0.3 µg/mouse) on three or four consecutive days. Controls were treated with PBS. Mice were sacrificed and analyzed one day after the last injection. For induction of immune-mediated hepatitis, mice received ConA (7 mg/kg) intravenously (i.v.) through the tail vein. Controls received PBS. Mice were sacrificed and analyzed 24 h later.

### 2.2.3 Euthanasia of mice and collection of biological samples

Mice were anesthetized by exposure to a CO<sub>2</sub>/O<sub>2</sub> mixture or by injection of a ketamine (240 mg/kg)-xylazine (32 mg/kg)-heparin (16666 IU/kg) solution (10 µL/g mouse) into the tail vein. Subsequently, mice were sacrificed by cervical dislocation.

For biological sampling, the abdominal cavity was opened and the diaphragm was removed. For the assessment of hepatic biomarkers by biochemical analyzer and AREG concentrations by ELISA, heart blood was collected with syringes (0.4 x 12 mm cannula) into 1.5 mL reaction tubes and placed on ice. The blood was then centrifuged at maximum speed (20800 g) for 5 min at 4°C. The plasma was carefully separated from the cell pellet and stored at -20°C until further analysis. After removing the gallbladder, the liver was dissected according to further use. For the quantification of hepatic mRNA and hydroxyproline content, small liver samples were shock-frozen in liquid nitrogen. For histological analysis of liver tissue, the lobus quadratus was transferred into a histology embedding cassette and fixed in 4% formalin solution. For flow cytometric analysis of hepatic Tregs and ILC2s, the remaining liver was removed and transferred to 50 mL tubes containing 5 mL HBSS on room temperature (RT).

For isolation of Tregs and CD4<sup>+</sup> T cells for *in vitro* culture experiments, lymph nodes and spleen were collected and transferred to 50 mL tubes containing 5 mL HBSS on ice. First, the fur was pulled from the skin to excise the mandibular, cervical, brachial, axillary, and inguinal lymph nodes. Thereafter, the abdominal cavity was opened to remove the mesenteric, lumbar, iliac and renal lymph nodes and the spleen.

The isolation of primary hepatocytes and LSECs by liver perfusion for *in vitro* culture is described in sections 2.2.9.1 and 2.2.9.3, respectively.

#### **2.2.4 Analysis of biomarkers of liver disease in blood plasma**

To investigate hepatic tissue injury in mice treated with IL-33 or ConA, as well as in untreated *Mdr2*<sup>-/-</sup> mice and WT controls, we determined the plasma levels of alanine aminotransferase (ALT).<sup>166</sup> To analyze disease progression in *Mdr2*<sup>-/-</sup> compared to WT mice, we further assessed cholestatic injury by quantifying plasma levels of alkaline phosphatase (ALP) and bilirubin,<sup>42</sup> and evaluated cholesterol homeostasis by measuring plasma cholesterol levels.<sup>43</sup> Prior to analysis, plasma samples were diluted 1:10 in ddH<sub>2</sub>O. Plasma activities (U/L) of ALT and ALP, and plasma concentrations (mg/dL) of bilirubin and cholesterol were measured with Cobas Integra 400 plus.

### 2.2.5 Cytokine determination by enzyme-linked immunosorbent assay (ELISA)

Sandwich enzyme-linked immunosorbent assay (ELISA) was performed to quantify AREG protein levels in the blood plasma of ConA-treated mice, that developed immune-mediated hepatitis, and in the supernatants of primary hepatocyte and LSEC cultures that were stimulated with cytokines known to be upregulated in ConA-induced immune-mediated hepatitis.

During Sandwich ELISA, an antigen is 'sandwiched' between two antibodies in a microplate well.<sup>167</sup> First, the well is coated with an antigen-specific capture antibody, followed by blocking of remaining binding sites.<sup>167</sup> The samples, standard and negative controls (blank) are then added in separate wells.<sup>167</sup> This is followed by a conjugated detection antibody.<sup>167</sup> In the ELISA used in this study, the detection antibody is haptenized and binds an anti-hapten-conjugated enzyme. Upon final incubation with a specific substrate, the enzyme catalyzes a color signal proportional to the antigen present in the sample.<sup>167</sup> The color signal is detected by measuring the optical density using a microplate reader.<sup>167</sup>

The assay was conducted using the Mouse Amphiregulin DuoSet ELISA Development System according to the manufacturer's protocol and a HydroFlex microplate washer. In brief, transparent 96-well microplate wells were coated with 100  $\mu$ L of capture antibodies (see Table 6) overnight at RT. The next day, plates were washed 4 times with 200  $\mu$ L of ELISA wash buffer and then blocked with 250  $\mu$ L of ELISA reagent diluent buffer for 1 h at RT on a shaker. The plates were washed again before 100  $\mu$ L of plasma samples (undiluted), cell culture supernatants (undiluted) or standard samples (0 to 500 pg/mL, serial diluted in ELISA reagent diluent buffer) were added. Deviating from the manufacturer's instructions, they were incubated overnight at 4°C instead of 2 h at RT. Subsequently, plates were washed and 100  $\mu$ L of detection antibodies (see Table 6) were added and allowed to bind for 2 h at RT on a shaker. The samples were washed again and then incubated with 100  $\mu$ L of streptavidin-horseradish peroxidase (streptavidin-HRP) for 20 min at RT on a shaker. After a final washing step, samples were incubated with 100  $\mu$ L of chromogenic 3,3',5,5'-Tetramethylbenzidine (TMB) substrate reagent containing hydrogen peroxide ( $H_2O_2$ ) for 20 min at RT in the dark. In the presence of  $H_2O_2$ , HRP catalyzes the



oxidation of TMB to a blue-colored product.<sup>168</sup> The colometric reaction was stopped with 50  $\mu$ L of 1 M sulfuric acid ( $\text{H}_2\text{SO}_4$ ), changing the color to bright yellow. Optical densities were measured immediately using an Infinite M200 microplate reader set to 450 nm against 570 nm wavelength correction and analyzed with Magellan software. The software generated a standard curve by plotting the known standard concentrations against the measured absorbance values. It then calculated the concentrations of the samples by interpolating their absorbance values to the corresponding concentrations on the standard curve.

### 2.2.6 Quantitative reverse transcription polymerase chain reaction (qRT-PCR)

To quantify the mRNA levels of genes of interest in ConA-induced immune-mediated hepatitis and in chronic liver disease in *Mdr2*<sup>-/-</sup> mice, we performed RNA isolation from mouse livers, followed by cDNA synthesis and quantitative real-time (q)PCR using primers spanning exon-exon junctions. Specifically, we analyzed the gene expression of the EGF receptor (*Egfr*) and its ligands (*Areg*, *Ereg*, *Tgfa*, *Btc*, *Hbegf*, *Egf* and *Ep gn*). In immune-mediated hepatitis, we further analyzed the gene expression of pro- and anti-inflammatory cytokines (*Il33*, *Tnfa*, *Ifng*, *Il12p40*, *Il10*), as well as chemokines and chemokine receptors mediating immune cell recruitment (chemokine c-x-c motif ligand 9 (*Cxcl9*), *Cxcl10*, and chemokine c-x-c motif receptor 3 (*Cxcr3*)). In chronic liver disease, we determined the expression of genes involved in inflammation (*Il33*, *Tnfa*, *IL12p40*) and fibrosis (*Tgfb1*, *Tgfb2*, *Col1a1*, *Col3a1*).

Quantitative real-time reverse transcription polymerase chain reaction (qRT-PCR) is an analytical method used to quantify gene expression changes.<sup>169</sup> It involves two main steps: reverse transcription (RT), which converts RNA into complementary DNA (cDNA), and subsequent quantitative real-time PCR (qPCR), which amplifies and quantifies the cDNA.<sup>169</sup> In this study, we performed a two-step qRT-PCR, where RT and qPCR were completed separately.<sup>169</sup> During RT, the RNA template is transcribed into single-stranded cDNA using a reverse transcriptase enzyme, primers annealing to the RNA, and deoxynucleotide triphosphates (dNTPs).<sup>169</sup> During the qPCR step, the generation of amplification products is monitored in real-time using fluorescent receptor molecules.<sup>169,170</sup> In this study, the fluorescent dye SYBR Green was used. During PCR cycles, double-stranded cDNA is denaturized at 95°C, followed by primer

annealing to single-stranded DNA at 55-65°C, and DNA polymerization at 72°C.<sup>169</sup> SYBR Green shows minimal fluorescence in solution.<sup>170</sup> During DNA extension, SYBR green non-specifically intercalates into the double-stranded DNA, which increases the fluorescent signal.<sup>169</sup> The fluorescence emitted is therefore proportional to the amount of DNA synthesized.<sup>169,170</sup>

Since dye intercalation is non-specific, primer specificity is verified by analysis of the PCR product using a melting curve.<sup>169,170</sup> A melting curve displays fluorescence peaks at the specific melting temperatures ( $T_m$ ) of the amplicons produced.<sup>170</sup> For analysis, samples are heated to 95°C to melt (dissociate) double-stranded DNA, equilibrated at a lower temperature and then melted again by slow reheating to 95°C.<sup>170</sup> The DNA product of interest is indicated by one specific melting peak at its respective  $T_m$ , whereas multiple peaks represent primer-dimer artifacts or non-specific amplicons.<sup>169,170</sup>

Real-time monitoring of the qPCR generates an amplification curve that plots the fluorescence signal against the number of cycles.<sup>169,170</sup> The key parameter is the cycle threshold ( $C_t$ ) value, which is the cycle fraction at which fluorescence passes a fixed detection threshold.<sup>170</sup> The threshold is set when fluorescence is first reliably detected at some point during the exponential growth phase.<sup>169,170</sup> The lower the  $C_t$  value, the higher the initial copy number of the target DNA.<sup>170</sup> In this study, data were analyzed by relative quantification to a reference gene, an endogenous control with a stable expression across all samples, unaffected by biological conditions.<sup>169</sup> To calculate the ratio of the RNA of interest to the reference, the delta delta  $C_t$  method ( $\Delta\Delta C_t$ ) is used.<sup>169</sup> First, the  $C_t$  of the reference is subtracted from the  $C_t$  of the target.<sup>169</sup> The resulting  $\Delta C_t$  value is then normalized to a control group to obtain the  $\Delta\Delta C_t$ .<sup>169</sup>

Murine liver samples were homogenized with TissueLyser II at a frequency of 30/sec for 1 min before total liver RNA was extracted using the NucleoSpin RNA Mini Kit according to the manufacturer's instructions. The kit includes a DNase for digestion of genomic DNA. The RNA concentrations were determined using the NanoDrop spectrophotometer and diluted below 500 µg/mL before further digestion of genomic DNA using the DNA-free Kit according to the manufacturer's protocol. Before RT, the RNA concentrations were determined again. In addition, we analyzed *Areg* mRNA

expression by primary hepatocyte cultures in response to inflammatory stimuli. Total RNA was isolated from each well using the RNeasy Micro Kit, which also contains a DNase, according to the manufacturer's protocol. For RT of RNA to cDNA we used 1 µg of RNA from mouse livers and all isolated RNA from hepatocyte cultures. The RT was performed using the Verso cDNA Synthesis Kit according to the manufacturer's protocol and a thermal cycler.

For qRT-PCR, 1 µL of cDNA, 0.7 µL each of forward and reverse primer (diluted 1:20 in RNase-free water), 5 µL of PowerUp SYBR Green Master Mix and 2.6 µL of RNase-free water were added to a 384-well plate. Each sample was analyzed in triplicate. Depending on the expression level of the respective target, cDNA was used either undiluted or diluted 1:10 in RNase-free water. Primer sequences and the respective annealing temperatures are listed in Table 12. Melting curve analyses were carried out using a melting temperature of 10°C above the annealing temperature. The reaction was performed using the QuantStudio 7 Flex Real-Time PCR System. To calculate x-fold changes in relative mRNA expression, resulting Ct values were normalized to the reference gene  $\beta$ -actin and the respective control group using the  $\Delta\Delta C_t$  method.

### 2.2.7 Hydroxyproline assay (HPA)

To measure the progression of liver fibrosis in *Mdr2*<sup>-/-</sup> mice and WT controls, we determined the concentration of hydroxyproline (HPA) in the liver tissue, a key component of collagen.<sup>45</sup> Murine liver samples were accurately weighed to 100 mg each in 2 mL reaction tubes and homogenized with 900 µL of ice-cold autoclaved water and one metal bead using the TissueLyser II for 2 min at 30 Hz. The blended contents were transferred to new 2 mL reaction tubes, mixed with 125 µL each of 50 % trichloroacetic acid and incubated on ice to precipitate proteins. After 20 min, the samples were centrifuged at 3824 g for 10 min at 4°C and the supernatants were discarded. 1000 µL of ice-cold ethanol (100%) were added and vortexed vigorously. The resulting pellets were disrupted using one metal bead per sample and the TissueLyser II for 30 sec at 30 Hz. The homogenized contents were transferred into new 2 mL reaction tubes and centrifuged at 3824 g for 10 min at 4°C. The pellets were mixed with 1000 µL each of ice-cold ethanol (100%) and centrifuged again at 3824 g

for 10 min at 4°C. To dry the precipitate, the reaction tubes were opened and incubated upside down for 5-10 min. Afterwards, 800 µL of 6 M HCl were added to each sample, followed by sonication for about 10 min until no large solid pieces remained. The samples were then incubated in a heating block at 110°C for 18 h. The next day, the samples were cooled to RT, vortexed and centrifuged at 20817 g for 10 min at RT. The supernatants were collected using 1 mL syringes with needles and transferred through 0.22 µm filters into new reaction tubes. The volumes of the supernatants were documented. For reference, HPA standards were prepared by diluting Hydroxyproline working solution (0.5 mg/mL) with 6 M HCl to 0.25, 0.124, 0.0625, 0.0313, 0.0156, 0.0078, 0.0039 and 0 mg/mL.

For the oxidation of HPA, 40 µL each of the filtered samples and hydroxyproline standards were transferred to new 1.5 mL reaction tubes and 10 µL of 10 M NaOH and 450 µL of chloramine-T solution were added. Samples and standards were incubated for 25-30 min at RT. For colometric reaction of modified HPAs, samples and standards were mixed with 500 µL of Ehrlich's reagent, incubated for 20 min at 65°C. After cooling to RT, 200 µL of each sample and standard were added in triplicate to a 96-well microplate (flat bottom). The HPA content was measured in µg/mL using the Infinite M200 microplate reader at 560 nm excitation. The HPA concentration in µg/mg liver was calculated as  $\frac{\text{HPA content (}\mu\text{g/mL)}}{\text{weight liver (}\sim 100 \text{ mg)}} \times \frac{\text{volume supernatant (<0.8 mL)}}{\text{volume supernatant transferred (0.04)}}$ . To obtain the x-fold change, HPA concentrations were normalized to the WT control group.

## 2.2.8 Histology

### 2.2.8.1 Hematoxylin & Eosin staining (H&E)

Hematoxylin-eosin (H&E) staining was performed to detect necrotic tissue in ConA-treated WT and *Areg*<sup>-/-</sup> mice and fibrotic areas in *Mdr2*<sup>-/-</sup> mice. H&E staining provides an overview of tissue structure.<sup>171</sup> Hematoxylin is a basic dye that stains the cell nuclei blue, while eosin is an acidic dye that binds to proteins, staining the cytoplasm pink.<sup>171</sup>

The quadratus lobes of mouse livers were fixed in 4% formalin for 24 h and embedded in paraffin. Paraffin blocks were hardened on a cooling plate and then stored at RT. For sectioning, they were cooled to -20°C overnight, placed on a cooling plate and cut

into 3  $\mu\text{m}$  sections using a Microtome. The liver slices were stretched in a water bath at RT, straightened in a tissue float bath at 45°C, placed on glass slides and dried at 37°C overnight.

Tissue sections were deparaffinized twice in XEM for 10 min each, followed by a gradual rehydration process. This consisted of immersing the slides in decreasing concentrations of ethanol (100%, 96%, 80%, 70%, 50%) for 4 min each. After washing in dH<sub>2</sub>O for 2 min, they were incubated in hemalum for 5 min. Hemalum staining solution contains aluminum ions and hematein formed by oxidation of hematoxylin.<sup>172</sup> During staining, electrostatic forces attract the red cationic aluminum-hematein complex to the anionic DNA.<sup>172</sup> Next, tissue sections were blued by rinsing under running tap water for 5 min. Blueing is the process by which the soluble red color of the hemalum is converted to an insoluble blue color by washing at pH > 5.5.<sup>172,173</sup> This step removes acidic protons that compete with hemalum for binding sites, thereby allowing stronger binding.<sup>172,173</sup> Tissues were then differentiated in 1% Ethanol/HCl for 2 sec. Since acidic protons again compete with aluminum for binding sites in the tissue, the color is removed from components other than nuclear chromatin.<sup>172,173</sup> To remove the acidic protons and restore the binding symmetry of hemalum,<sup>173</sup> the tissues sections were then blued a second time under running tap water for 5 min. Afterwards, they were incubated in 1% Eosin Y for 7 min. Finally, the slides were dehydrated in increasing concentrations of ethanol (90%, 96%, 100%) for 1 min each and then incubated in XEM for at least 10 min to remove ethanol and brighten the tissue. Thereafter, they were covered with Entellan mounting medium and a cover slip and allowed to set for more than 1 h. H&E staining of liver tissue sections was analyzed by light microscopy.

#### 2.2.8.2 Sirius red staining

Sirius red staining was performed to visualize fibrosis in liver tissue samples from *Mdr2*<sup>-/-</sup> mice and WT controls. The Sirius red dye selectively stains collagen through a reaction between its sulphonic acid groups and basic groups within the collagen molecules.<sup>174</sup> The dye molecules bind to the fibers in a parallel orientation, increasing birefringence.<sup>174</sup>

The quadratus lobes of mouse livers were removed, fixed in 4% formalin for 24 h, embedded in paraffin and cut into 3  $\mu$ m sections using a Microtome. The tissue sections were stretched and straightened in two water baths, first at RT and then at 45°C. They were then positioned onto glass slides and left to dry overnight at 37°C.

Tissue sections were deparaffinized twice in XEM for 10 min each and then rehydrated progressively by immersion in decreasing concentrations of ethanol (100%, 96%, 80%, 70%, 50%) for 5 min each. Subsequently, they were washed in dH<sub>2</sub>O for 2 min. Tissue slides were then stained with Sirius red solution for 90 min at RT. To remove non-specific staining, slides were washed in 0.01 N HCl for 15 sec. Afterwards, slides were dehydrated in a series of increasing ethanol concentrations (50% for 30 sec, 70% for 1 min, 100% for 4 min). To remove ethanol and lighten the tissue sections, slides were incubated twice in XEM for 3 min each. Finally, they were coated with Entellan mounting medium, covered with a cover slip and cured for a minimum of 1 h. Sirius red staining of liver tissue sections was analyzed by light microscopy.

#### **2.2.8.3 Immunohistochemistry (IHC)**

To investigate AREG expression by hepatocytes in immune-mediated hepatitis, we performed immunohistochemical (IHC) staining for AREG using liver tissue samples from mice treated with PBS or ConA. After removal, the quadratus lobes of mouse livers were fixed in 4% formalin for 24 h, embedded in paraffin and sectioned into 3  $\mu$ m slices using a Microtome. The liver sections were stretched and straightened in two water baths, first at RT and then at 45°C, placed on glass slides and dried overnight at 37°C.

Tissue sections were then deparaffinized twice in XEM for 10 min each, rehydrated in a series of decreasing ethanol concentrations (100%, 90%, 70%, 50%) for 4 min each and washed in dH<sub>2</sub>O three times. For antigen retrieval, sectioned liver slides were heated in target retrieval solution (citrate buffer) for 10 min at 740 watts in a microwave. After cooling to RT for approximately 20 min, the slides were washed with TBS for 5 min.

Blocking was performed in a wet chamber for 30 min at RT with 50  $\mu$ L of swine serum diluted 1:20 in Agilent antibody diluent. Remaining blocking solution was decanted from the slides. Next, 50  $\mu$ L of the primary anti-mouse AREG antibody solution (Ab #1: Rabbit anti-AREG, Thermo Fisher Scientific, 1:100; Ab #2: Rabbit anti-AREG, Biorbyt, 1:100; Ab #3: Goat anti-AREG, R&D Systems, 1:20; see Table 7) was applied to the tissue slides and incubated overnight in the wet chamber at 4°C. The next day, slides were washed three times in TBS for 5 min each at RT, covered with the corresponding biotinylated secondary antibodies (Swine anti-rabbit, 1:200; Rabbit anti-goat, 1:200; see Table 8) and incubated in the wet chamber for 30 min at RT. They were then washed three times in TBS for 5 min each at RT. For detection, liver tissue slides were treated with 50  $\mu$ L of avidin-biotin complex (ABC) HRP reagent (ABC-HRP Kit) in the wet chamber for 30 min at RT, followed by a washing step in TBS for 5 min and incubation with 50  $\mu$ L of substrate working solution of Liquid DAB + substrate chromogen system in the wet chamber for 10 min at RT. Thereafter, samples were washed twice in dH<sub>2</sub>O for 5 min each.

Alternatively, antigen retrieval was followed by blocking of endogenous phosphatases and peroxidases in 5% H<sub>2</sub>O<sub>2</sub> for 3 min at RT. The slides were washed in TBS for 5 min and then blocked in a wet chamber for 30 min at RT with 50  $\mu$ L of swine serum diluted 1:20 in Zytomed antibody diluent. Subsequently, the tissue slides were treated with 50  $\mu$ L of the primary antibody solution (Ab #1: Rabbit anti-AREG, Thermo Fisher Scientific, 1:100; Ab #2: Rabbit anti-AREG, Biorbyt, 1:200; see Table 7) overnight in the wet chamber at 4°C. The next day, slides were washed three times in TBS for 5 min each at RT. For detection, liver tissues were first incubated with 50  $\mu$ L of alkaline phosphatase (AP) polymer in the wet chamber for 30 min at 37°C. After three washing steps with TBS for 5 min each at RT, slides were rinsed under running tap water for 2 min and with dH<sub>2</sub>O for 3 min. The slides were then immersed in fresh New Fuchsin chromogen solution in the dark for 30 min at RT and subsequently rinsed for 1 min under running tap water.

In both protocols, the cell nuclei were then counterstained with hemalum (50%) for 5-120 sec and the slides were blued for 5 min by rinsing under running tap water. For preservation of tissue sections, the slides were fixed with CC/Mount medium and left to dry for more than 90 min. Finally, they were covered with Entellan mounting medium

and a cover slip and allowed to dry for at least 1 h. IHC AREG signal on liver tissue sections was analyzed by light microscopy.

## **2.2.9 Isolation of cells**

### **2.2.9.1 Isolation of primary hepatocytes for *in vitro* culture**

Primary hepatocytes for *in vitro* culture (see 2.2.10.1) were isolated from anesthetized naïve C57BL/6J mice by liver perfusion. The superior vena cava was clamped and the vena portae exposed, fixed, and punctured with a 27 G syringe attached to the hose of a peristaltic pump. The liver was then perfused with 10 mL of PPML prewarmed to 42°C, followed by 26 mL PM prewarmed to 42°C, containing 1 mL Liberase stock solution. As the liver became lighter in color, the inferior vena cava was cut and then intermittently occluded to facilitate Liberase action. After completed *in situ* digestion, the liver was removed and placed in a Petri dish containing approximately 25 mL of warm PM. The liver capsules were gently disrupted and shaken with forceps to release hepatocytes. The dissociated liver cells were collected and filtered through a 100 µm cell strainer before being incubated at RT for 20 min to sediment.

For primary hepatocyte isolation, the cells were mixed with 24 mL of cold Percoll solution and centrifuged at 72 g for 5 min at 5°C to isolate living hepatocytes. The hepatocyte pellets were washed with 30 mL William's medium E<sup>4+</sup>, centrifuged again at 72 g for 5 min at 5°C, and pooled in 15 mL William's medium E<sup>4+</sup>. Finally, hepatocytes were counted and seeded in 24-well plates at a density of 2 x10<sup>5</sup> cells per well. They were then incubated overnight at 37°C in 40% O<sub>2</sub> and 5% CO<sub>2</sub>, to allow the cells to adhere to the bottom of the wells and form a monolayer. The medium was changed after 4 hours.

### **2.2.9.2 Magnetic-activated cell sorting (MACS)**

Magnetic-activated cell sorting (MACS, also magnetic cell separation) is a technique for the isolation of a specific cell type from a mixed cell population.<sup>175,176</sup> It is based on cell labeling with small colloidal superparamagnetic beads and subsequent cell separation using high-gradient ferromagnetic columns placed in an external magnetic field.<sup>175,176</sup>



Cells are incubated with fluorochrome-conjugated primary antibodies targeting specific cell surface markers, followed by microbead-conjugated secondary antibodies.<sup>176</sup> Alternatively, cells are labeled with antibodies conjugated directly to microbeads, or with a haptenized antibody and anti-hapten-conjugated microbeads.<sup>176</sup> The cell-bead suspensions are applied to the separation column placed in an external magnet.<sup>175</sup> Cells labeled with superparamagnetic beads attach to the column matrix within the magnetic field, while unlabeled cells are eluted.<sup>175</sup> The labeled cells are eluted from the column when it is removed from the external magnetic field.<sup>175</sup> Cells are sorted by two different methods, either by positive selection, which is the enrichment of magnetically labeled target cells, or by negative selection, which is the depletion of unwanted cells by magnetic labeling.<sup>176</sup>

### 2.2.9.3 Isolation of primary LSECs for *in vitro* culture

Primary LSECs for *in vitro* culture (see 2.2.10.2) were isolated from anesthetized naïve C57BL/6J mice by liver perfusion, followed by density gradient centrifugation and MACS. The liver was perfused through the vena portae using a peristaltic pump pre-filled with 2 mL of Calcium-deprived buffer + collagenase per liver. When the livers became lighter in color, they were removed and transferred to 50 mL tubes containing 1x PBS. The livers were placed in Petri dishes where they were scraped out with a curved scissor and cut into small pieces. The liver homogenates were transferred to 50 mL tubes and supplemented with 3 mL GBSS + collagenase per liver after it had been used to rinse the Petri dishes. For digestion, the homogenates were incubated for 20 min at 37°C in a shaking water bath. Thereafter, the liver homogenates were mashed with the plungers of 2 mL syringes, rinsed twice with 20 mL of GBSS, transferred to a new 50 mL tube and centrifuged at 500 g for 10 min at RT.

To perform density gradient centrifugation fat that could interfere with the gradient was removed by washing the pellets twice with 30 mL of GBSS and centrifuging at 500 g for 10 min at RT. After the second wash, most of the supernatant was removed and the pellets were resuspended in a small volume of the remaining GBSS. The suspensions were mixed with 1.23 times the volume of Nycodenz (30%, dissolved in ddH<sub>2</sub>O) each, transferred to 15 mL tubes, covered with 1 mL of 1x PBS and centrifuged at 1400 g for 20 min at RT (acceleration: 7, brake: 1). The resulting interfaces were transferred to

new 50 mL tubes, washed with 30 mL cold MACS buffer and centrifuged at 500 g for 10 min at RT.

For positive selection of CD146<sup>+</sup> LSECs using MACS, the pellets were resuspended in 200 µL MACS buffer. 24 µL of magnetic CD146 microbeads were added per liver, incubated for 15 min at 4°C, washed with 20 mL MACS buffer and centrifuged at 500 g for 10 min at RT. MACS separation columns LS were placed in a magnetic QuadroMACS separator and rinsed with 3 mL of MACS buffer. Up to three liver cell pellets per column were resuspended in 500 µL of MACS buffer and pipetted onto the LS column through a 30 µm filter. The columns were washed three times with 3 mL of MACS buffer. The columns were then removed from the separation magnet, placed on a 15 mL tube and LSECs were eluted with 5 mL of MACS buffer using plungers. Afterwards, they were centrifuged at 500 g for 5 min at RT and resuspended in DMEM<sup>4+</sup> medium.

Finally, the LSECs were counted and seeded in 24-well plates at a density of 1 x10<sup>6</sup> cells per well in 1 mL LSEC<sup>4+</sup> medium. They were cultured at 37°C in 5% CO<sub>2</sub> overnight to form a monolayer at the bottom of the wells. The next morning, medium was changed by adding 1 mL warm LSEC-PBS per well and gently washing the cells by pipetting up and down. The medium was then removed and replaced with LSEC-PBS to wash cells. This step was repeated until no dead cells were remaining as visible through the microscope. In the end, LSECs were resuspended in 1 mL of LSEC<sup>4+</sup> medium and again cultured at 37°C in 5% CO<sub>2</sub>.

#### **2.2.9.4 Isolation of CD25<sup>+</sup> CD4<sup>+</sup> Tregs for *in vitro* culture**

CD25<sup>+</sup> CD4<sup>+</sup> Tregs for *in vitro* culture (see 2.2.10.3) were isolated from spleens and lymph nodes of naïve FIR x *tiger*, FIR x *tiger* x *Il1rl1*<sup>-/-</sup> and FIR x *tiger* x *Areg*<sup>-/-</sup> mice. First, we obtained single cell suspensions of the organs. Then, we performed MACS to enrich CD4<sup>+</sup> T cells by negative selection, followed by positive selection of CD4<sup>+</sup> CD25<sup>+</sup> T cells.

Spleens and lymph nodes were homogenized separately by passing them through 70 µm cell strainers with plungers of 2 mL syringes and rinsing with cold HBSS. They

were then centrifuged at 500 g for 5 min at 4°C and the cell pellet was resuspended in 3 mL ACK lysis buffer for 3 min at RT to disrupt erythrocytes. The lysis was stopped with 40 mL HBSS and centrifugation. The cells were then resuspended in MACS buffer and spleens and lymph nodes, as well as samples from individual mice with the same genotype, were pooled. Finally, the cells were counted using Neubauer chamber and trypan blue staining for selection of living cells.

To perform MACS, the single cell suspension was first centrifuged and the supernatant was discarded. To block unspecific binding of staining antibodies to Fc receptors, cells were incubated for 10 min at 4°C with 50  $\mu\text{L}/1 \times 10^6$  cells of TrueStain FcX antibody (see Table 9) specific for the common epitope of the IgG Fc receptor III (FcR III, CD16) and FcR II (CD32). The incubation was stopped by the addition of MACS buffer and centrifugation. For negative selection of CD4<sup>+</sup> T cells, all other cells were then labeled using the CD4<sup>+</sup> T cell isolation kit according to the manufacturer's instructions. The kit contains a cocktail of biotin-conjugated antibodies against CD8a, CD11b, CD11c, CD19, CD45R, CD49b, CD105, MHC class II, Ly-76 and TCR $\gamma/\delta$  and anti-biotin microbeads. In brief, the cell pellet was resuspended in 40  $\mu\text{L}/1 \times 10^7$  cells of MACS buffer and incubated with 10  $\mu\text{L}/1 \times 10^7$  cells of biotin-antibody cocktail for 10 min at 4°C. Next, 39.45  $\mu\text{L}/1 \times 10^7$  cells of MACS buffer were added with 20  $\mu\text{L}/1 \times 10^7$  cells of the magnetic anti-biotin microbeads. In preparation for later positive selection of CD25<sup>+</sup> CD4<sup>+</sup> T cells, 0.55  $\mu\text{L}/1 \times 10^7$  cells of anti-CD25-PE antibody was also added at this step (see Table 10). The cell suspension was incubated for 15 min at 4°C and then washed with MACS buffer and centrifuged. The cells were resuspended in 500  $\mu\text{L}/1 \times 10^8$  labeled cells of MACS buffer. Then, the cells labeled with magnetic microbeads were captured in the magnetic MACS column LS placed in a QuadroMACS separator. 500  $\mu\text{L}/\text{column}$  of cell solution was pipetted onto the columns through a 30  $\mu\text{m}$  filter, followed by washing with 3 mL of MACS buffer. The eluted CD4<sup>+</sup> T cells were collected in 15 mL tubes on ice and counted using a Neubauer chamber with trypan blue staining.

Next, positive selection of CD25<sup>+</sup> CD4<sup>+</sup> T cells was performed. The CD4<sup>+</sup> T cell suspension was centrifuged. The cell pellet was incubated with 90  $\mu\text{L}/1 \times 10^7$  cells of MACS buffer and 10  $\mu\text{L}/1 \times 10^7$  cells of anti-PE microbeads for 15 min at 4°C. The incubation was stopped with MACS buffer and centrifugation. The cells were resuspended in 500  $\mu\text{L}/1 \times 10^7$  labeled cells of MACS buffer. Then, the CD25<sup>+</sup> CD4<sup>+</sup>

T cells labeled with magnetic PE-microbeads were captured in the MACS column MS placed in a magnetic OctoMACS separator. 500  $\mu$ L/column of cell solution was pipetted onto the columns through a 30  $\mu$ m filter, followed by washing twice with 500  $\mu$ L of MACS buffer each. The columns were then removed from the magnetic field of the OctoMACS separator and CD4<sup>+</sup> CD25<sup>+</sup> Tregs were eluted with 1 mL of MACS buffer using plungers. To increase purity, the cells were sorted through a second round of MS columns and finally eluted in 1 mL of PBS. The eluted Tregs were then counted using a Neubauer chamber with trypan blue staining.

To check the purity of the isolated Tregs, small cell samples were taken from the cell suspension before and after MACS and stored in PBS at 4°C. The cells were centrifuged at 500 g for 5 min at 4°C and stained with 50  $\mu$ L of a solution containing Zombie NIR viability dye (APC-Cy7, 1:1000) and the surface antibodies TCR $\beta$  (PE-Cy7), CD4 (BV 711) and CD25 (PE; see Table 10) for 30 min at 4°C. They were then washed with 1 mL of PBS, centrifuged, and resuspended in 350  $\mu$ L of FACS buffer. Finally, the frequency of CD25<sup>+</sup> CD4<sup>+</sup> TCR $\beta$ <sup>+</sup> cells and their expression of Foxp3 (mRFP) was determined by flow cytometry using BD LSRFortessa. The gating strategy is shown in Figure 5. The frequency of CD25<sup>+</sup> CD4<sup>+</sup> Tregs (% of TCR $\beta$ <sup>+</sup>) was on average 76%, with more than 90% expressing Foxp3<sup>+</sup> (Figure 5).

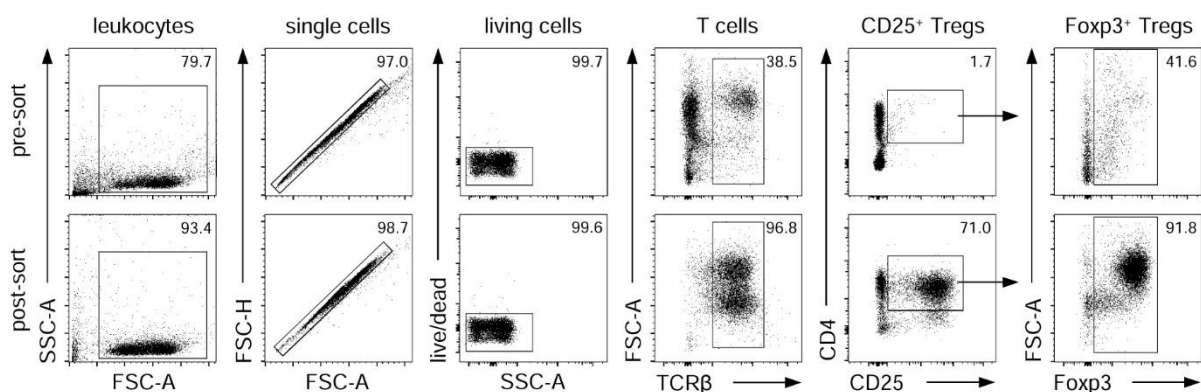


**Figure 5: Gating strategy and purity of MACS-sorted Tregs for *in vitro* culture.** Utilizing MACS, CD25<sup>+</sup> CD4<sup>+</sup> Tregs were isolated from lymph nodes and spleens of FIR x *tiger* mice. The expression of Foxp3 by CD25<sup>+</sup> CD4<sup>+</sup> TCR $\beta$ <sup>+</sup> T cells is displayed. Frequencies of Tregs before and after sort are shown in representative dot plots of at least two experiments.

### 2.2.9.5 Isolation of CD25<sup>+</sup> CD4<sup>+</sup> Tregs and CD4<sup>+</sup> T cells for suppression assay

CD25<sup>+</sup> CD4<sup>+</sup> Tregs and CD25<sup>-</sup> CD4<sup>+</sup> T cells for the suppression assay (see 2.2.10.4) were isolated from spleens and lymph nodes of naïve C57BL/6J mice. In addition, CD25<sup>+</sup> CD4<sup>+</sup> Tregs were obtained from *Areg*<sup>-/-</sup> mice. Single cells were isolated from organs and CD4<sup>+</sup> T cells were enriched by negative selection using MACS as described in section 2.2.9.4. Subsequently, MACS was used to isolate CD25<sup>-</sup> CD4<sup>+</sup> T cells by negative selection and CD25<sup>+</sup> CD4<sup>+</sup> Tregs by positive selection. The procedure for the positive selection of CD25<sup>+</sup> CD4<sup>+</sup> Tregs was performed as detailed in section 2.2.9.4, but in addition, the flowthroughs from the initial round of MACS columns MS were collected to obtain CD25<sup>-</sup> CD4<sup>+</sup> conventional T cells.

To assess the purity of the isolated cells, a fraction of Tregs and conventional CD4<sup>+</sup> T cells was collected before and after MACS and stored in PBS at 4°C. The cells were then centrifuged at 500 g for 5 min at 4°C and incubated for 30 min at 4°C with 50 µL of a staining solution containing Zombie NIR viability dye (APC-Cy7, 1:1000) and the surface antibodies TCRβ (FITC), CD4 (BV 711) and CD25 (PE; see Table 10). The stained cells were washed with 1 mL of PBS, centrifuged, and resuspended in 350 µL of FACS buffer. The frequencies of both T cell populations were determined by flow cytometry using BD LSRFortessa according to the gating strategies shown in Figure 6. The frequency of CD25<sup>+</sup> CD4<sup>+</sup> TCRβ<sup>+</sup> T cells (% of TCRβ<sup>+</sup>) was between 84 and 92% and that of CD25<sup>+</sup> CD4<sup>+</sup> Tregs (% of TCRβ<sup>+</sup>) between 58 and 89% (Figure 6). For suppression assay, the corrected cell numbers of conventional T cells and Tregs were determined by multiplying the cell purity (% CD25<sup>+/-</sup> CD4<sup>+</sup> of living cells) with the number of isolated cells counted.

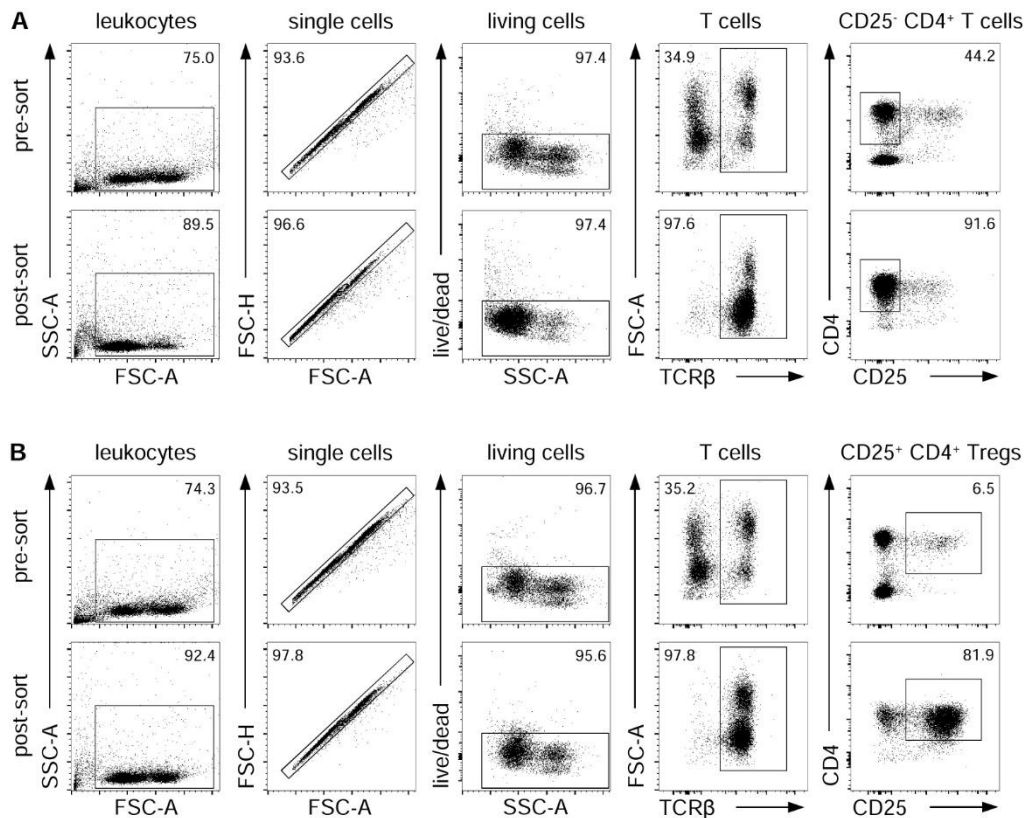


**Figure 6: Gating strategy and purity of MACS-sorted CD25<sup>-</sup> CD4<sup>+</sup> T cells and CD25<sup>+</sup> CD4<sup>+</sup> Tregs for suppression assay.** Using MACS, (A) CD25<sup>-</sup> CD4<sup>+</sup> T cells and (B) CD25<sup>+</sup> CD4<sup>+</sup> Tregs were extracted from lymph nodes and spleens of C57BL/6J mice. Frequencies before and after sort are displayed in representative dot plots of at least two experiments.

### 2.2.9.6 Isolation of hepatic non-parenchymal cells

Non-parenchymal cells were isolated from mouse livers to subsequently purify ILC2s for *in vitro* culture (see 2.2.9.6) or to directly analyze ST2<sup>+</sup> Tregs and ILC2s by flow cytometry (see 2.2.11). The livers were homogenized by squashing them in scratched petri dishes with the plungers of 2 mL syringes. The tissues were then filtered through 100 μm cell strainers, rinsed with HBSS and centrifuged at 500 g for 5 min at RT. To isolate non-parenchymal cells, the pellets were resuspended in 10 mL each of Percoll-HBSS solution (containing 100 IU/mL heparin-sodium solution), followed by density gradient centrifugation at 800 g for 20 min at RT (brake: 7) as described previously.<sup>177</sup> Percoll is a colloid solution containing silica particles.<sup>178</sup> The gradient is formed during centrifugation by sedimentation of silica particles while at the same time the cells move in the direction of gravity and separate according to size and density.<sup>178</sup> Leukocytes and erythrocytes aggregate at the bottom due to their high buoyant density. Hepatocytes, which are larger and contain more intracellular fluid and organelles, have

a lower buoyant density and therefore form a layer at the top of the gradient along with cell debris. The supernatant was discarded and the pellet was resuspended in 10 mL ammonium chloride (NH<sub>4</sub>Cl) buffer for 10 min at RT to lyse the erythrocytes. The lysis was stopped by the addition of cold HBSS and centrifugation at 500 g for 5 min at 4°C. For MACS-sort (see 2.2.9.8), cells were then pooled and resuspended in MACS buffer. For flow cytometric analysis (see 2.2.11), cells were resuspended in 1 mL HBSS per liver. Finally, they were counted using a Neubauer counting chamber with trypan blue staining for selection of living cells.

### 2.2.9.7 Fluorescence-activated cell sorting (FACS)

Fluorescence-activated cell sorting (FACS) is a process in which live cells are sorted based on electrical charge and fluorescence.<sup>179</sup> The method is a variant of flow cytometry (see 2.2.11), performed on flow cytometers specifically designed for cell sorting.<sup>179</sup> In this study, the BD FACSAria Fusion cell sorter was used, which provides multicolor detection.

Prior to analysis, cells are stained with fluorochrome-labeled antibodies.<sup>179</sup> During FACS sorting, they are then diverted into a single stream passing through a nozzle.<sup>179</sup> At an interrogation point, cells are illuminated with a laser to measure cell size and fluorescence with light detectors.<sup>180,181</sup> Based on the gating strategy, the cells are assigned to a specific charge.<sup>179</sup> After the detection zone, the stream breaks up into droplets carrying single cells.<sup>181</sup> Droplets containing cells that meet the sorting criteria are charged and then sorted as they pass through deflector plates that influence the direction of the droplet.<sup>179,181</sup>

### 2.2.9.8 Isolation of hepatic ILC2s for *in vitro* culture

For the isolation of hepatic ILC2s for *in vitro* culture (see 2.2.10.3), livers were obtained from C57BL/6J mice treated with rmlL-33 on four consecutive days to enrich the hepatic ILC2 population. Hepatic non-parenchymal cells were isolated as described in section 2.2.9.6. We then purified ILC2s as described below by enriching lineage-negative (lin<sup>-</sup>) cells using MACS and subsequent FACS of ST2<sup>+</sup> Sca-1<sup>+</sup> lin<sup>-</sup> ILC2s.

The counted single non-parenchymal cell suspension was centrifuged at 300 g for 8 min at 4°C, resuspended in 50  $\mu\text{L}/1 \times 10^6$  cells of TrueStain FcX antibody (see Table 9) and incubated for 10 min at 4°C to block unspecific binding of staining antibodies. The incubation was stopped by the addition of MACS buffer and centrifugation and the cell pellet was resuspended in 50  $\mu\text{L}/1 \times 10^6$  cells of MACS buffer. To remove lineage-positive ( $\text{lin}^+$ ) cells, such as  $\text{CD3}^+$  T cells,  $\text{CD45 receptor (CD45R)}^+$  B cells,  $\text{CD11b}^+$  macrophages, monocytes and NK cells, lymphocyte antigen ( $\text{Ly-76}^+$ ) erythrocytes and  $\text{CD11b}^+$   $\text{Ly-6G}^+$   $\text{Ly-6C}^+$  granulocytes, the surface proteins mentioned were marked with a mixture of targeted APC-conjugated antibodies (see Table 10, “Lineage”). 0.33  $\mu\text{L}/1 \times 10^6$  cells of the prepared antibody mixture was added to the cell suspension and incubated for 15 min at 4°C. After centrifugation, the cell pellet was resuspended in 80  $\mu\text{L}/1 \times 10^7$  cells of MACS buffer and 20  $\mu\text{L}/1 \times 10^7$  cells of magnetic anti-APC microbeads. The cell suspension was then incubated for 15 min at 4°C to facilitate binding of microbeads to APC antibodies on  $\text{lin}^+$  cells. Unbound microbeads were removed by washing with MACS buffer and centrifugation. The cells were resuspended in 500  $\mu\text{L}/1 \times 10^8$  labeled cells of MACS buffer. Next,  $\text{lin}^-$  cells were isolated by capturing  $\text{lin}^+$  cells labeled with magnetic microbeads in a magnetic column. Magnetic LS columns were placed in the magnetic field of a QuadroMACS separator and 500  $\mu\text{L}/\text{column}$  of cell solution was pipetted onto the columns through a 30  $\mu\text{m}$  filter, followed by washing three times with 3 mL of MACS buffer each. The eluted solution containing  $\text{lin}^-$  cells was collected in 15 mL tubes placed on ice and cells were counted with Neubauer chamber and trypan blue staining for selection of living cells.

Next,  $\text{lin}^-$  cells were stained for the surface markers ST2 (Pacific Blue) and Sca-1 (PerCP-eF710) to identify ILC2s during FACS sorting (see Table 10). After centrifugation, the cell pellet was incubated in 50  $\mu\text{L}/1 \times 10^6$  cells antibody solution for 20 min at 4°C. Cells were washed with cold PBS, centrifuged, resuspended in PBS and passed through a 30  $\mu\text{m}$  filter. Finally,  $\text{lin}^-$   $\text{Sca-1}^+$   $\text{ST2}^+$  ILC2s were sorted by FACS (BD FACSAria Fusion cell sorter) and collected in RPMI medium for FACS-sorting containing 2% Penicillin/Streptomycin. The cell number of isolated ILC2s was counted with Neubauer chamber and trypan blue staining.

To control the purity of isolated ILC2s, small cell samples were withdrawn from the cell suspension before and after FACS and stored in PBS at 4°C. The cells were



centrifuged at 500 g for 5 min at 4°C and stained with 50 µL of Zombie NIR viability dye (APC-Cy7, 1:1000) for 30 min at 4°C. Afterwards, they were washed with 1 mL of PBS, centrifuged and resuspended in 350 µL of FACS buffer to be analyzed by flow cytometry using BD LSRFortessa. The gating strategy is displayed in Figure 7. We regularly detected ILC2 purities (% ST2<sup>+</sup> Sca-1<sup>+</sup> lin<sup>-</sup> of living cells) above 95% (Figure 7).

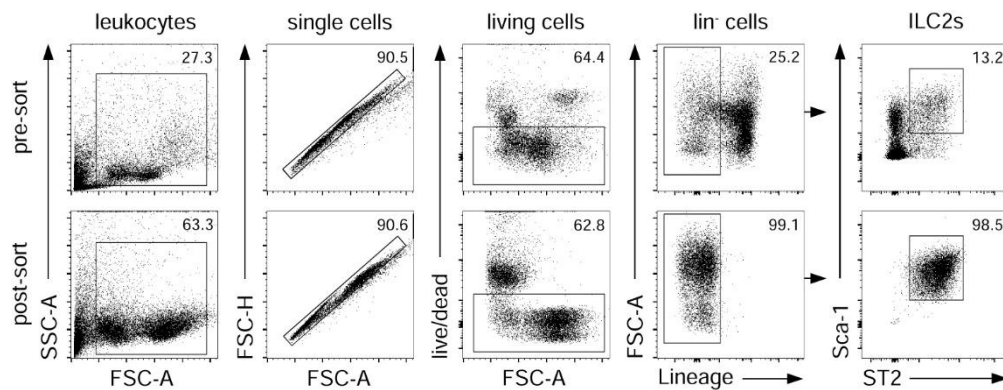


**Figure 7: Gating strategy and purity of FACS-sorted ILC2 for *in vitro* culture.** C57BL/6J mice were subjected to IL-33 treatment on four consecutive days. Hepatic lineage (CD3e, CD11b, CD45R, Ly-76, Ly-6G/Ly-6C)-negative (lin<sup>-</sup>) cells were enriched through MACS, previous to isolation of ST2<sup>+</sup> Sca-1<sup>+</sup> lin<sup>-</sup> ILC2s via FACS. Frequencies of ILC2 before and after sort are shown. Representative dot plots of at least two experiments are shown.

## 2.2.10 Cell cultures

### 2.2.10.1 Primary Hepatocyte cell culture

Primary hepatocytes isolated from naïve C57BL/6J mice and pre-cultured overnight in 24-well plates at a density of  $2 \times 10^5$  cells/well (see 2.2.9.1) were incubated with 250 µL of fresh William's medium E<sup>4+</sup> per well, alone or supplemented with rmIL-33 (10 ng/mL), rmAREG (40 ng/mL), rmTNFα (50 ng/mL), rmIFNγ (50 ng/mL), rmIL-1β (10 ng/mL), or rmTGFβ (10 ng/mL) for 0, 1, 4, 8 or 24 h at 37°C in 40% O<sub>2</sub> and 5% CO<sub>2</sub>. For AREG protein analysis by ELISA, 200 µL of supernatant was collected from each well (see 2.2.4). For Areg mRNA analysis by qRT-PCR, cells were washed twice with 1 mL of PBS before RNA purification (see 2.2.5).

### 2.2.10.2 Primary LSEC cell culture

Primary LSECs isolated from naïve C57BL/6J mice and pre-cultured overnight in 24-well plates at a density of  $1 \times 10^6$  cells/well (see 2.2.9.3) were incubated with 250  $\mu$ L of fresh LSEC-medium per well, alone or supplemented with rmTNF $\alpha$  (50 ng/mL), rmIFN $\gamma$  (50 ng/mL), rmIL-1 $\beta$  (10 ng/mL), or rmTGF $\beta$  (10 ng/mL) for 0, 8 or 24 h at 37°C in 5% CO<sub>2</sub>. To analyze AREG protein levels by ELISA, 200  $\mu$ L of supernatant was collected from each well (see 2.2.4).

### 2.2.10.3 Immune cell culture

ILC2s were isolated from livers of IL-33-treated C57BL/6J mice (see 2.2.9.8).  $1.5 \times 10^4$  ILC2s were cultured in 200  $\mu$ L RPMI<sup>7+</sup> medium with rmIL-2 (1 U/mL) in the presence or absence of rmIL-33 (10 ng/mL), rmAREG (10 ng/mL) or both in a round-bottom 96-well microplate at 37°C in 5% CO<sub>2</sub>. After 3.5 days, cells were counted using a Neubauer chamber with trypan blue, followed by antibody staining and analysis using flow cytometry (see 2.2.11).

CD25<sup>+</sup> CD4<sup>+</sup> Tregs were isolated from spleens and lymph nodes of naïve FIR x *tiger*, FIR x *tiger* x *Il1rl1*<sup>-/-</sup> and FIR x *tiger* x *Areg*<sup>-/-</sup> mice (see 2.2.9.4). They were cultured in a round-bottom 96-well microplate at a density of  $2 \times 10^4$  cells in 200  $\mu$ L RPMI<sup>7+</sup> medium supplemented with rmIL-2 (100 U/mL) for 1.5 days at 37°C in 5% CO<sub>2</sub>. They were either cultured alone or stimulated with rmIL-33 (10 ng/mL), rmAREG (10 ng/mL) or both. Following incubation, cells were stained with antibodies and analyzed by flow cytometry (see 2.2.11).

### 2.2.10.4 Suppression assay

CD25<sup>-</sup> CD4<sup>+</sup> responder T cells were isolated from spleens and lymph nodes of naïve C57BL/6J mice (see 2.2.9.5). To determine proliferation, they were labeled with 5-(and 6)-carboxyfluorescein succinimidyl ester (CFSE) using the CFSE Cell Division Tracker Kit according to the manufacturer's instructions. CD25<sup>+</sup> CD4<sup>+</sup> Tregs were isolated from spleens and lymph nodes of naïve C57BL/6J and *Areg*<sup>-/-</sup> mice (see 2.2.9.5).  $1 \times 10^5$  CD4<sup>+</sup> responder T cells were cultured in the presence or absence of  $1 \times 10^5$  Tregs in 200  $\mu$ L RPMI<sup>7+</sup> medium in a round-bottom 96-well microplate for

2.5 days at 37°C in 5% CO<sub>2</sub>. They were cultured alone or supplemented with rmAREG (100 or 500 ng/mL). For CD4<sup>+</sup> responder T cell activation, 0.5x10<sup>5</sup> Dynabeads (Dynabeads Mouse T-Activator CD3/CD28) were added to the co-culture. Following incubation, cells were stained with antibodies and analyzed by flow cytometry (see 2.2.11).

The proliferation of Foxp3<sup>-</sup> CD4<sup>+</sup> responder T cells was measured by analyzing the CFSE signal. During gating, CFSE<sup>-</sup> Tregs were excluded before identifying CFSE<sup>low</sup> proliferated responder T cells. The percentage of inhibition was calculated as  $\frac{(\text{highest value \% proliferated cells} - x)}{\text{highest value \% proliferated cells}} \times 100$ .

### 2.2.11 Flow cytometry

Flow cytometry is a method used to quantify and phenotype cells suspended in a fluid by labeling them with fluorochrome-coupled antibodies.<sup>180</sup> Cells are separated into a single-cell stream by hydrodynamic focusing.<sup>180</sup> Singularized cells pass through a laser beam which excites the fluorochrome.<sup>180</sup> The emitted light is received by a detector and converted into digital data points that are graphically displayed in flow plots.<sup>180</sup> This allows for single-cell analysis, facilitating the evaluation of specific cell types within heterogeneous populations and their expression of various proteins.<sup>180</sup> In addition, optical detectors recognize light scatter.<sup>182</sup> The forward scatter (FSC) channel captures light scattered in the forward direction, serving as an indicator of cell size.<sup>182</sup> The side scatter (SSC) channel detects light scattered perpendicular to the laser, offering information about cellular granularity and complexity.<sup>182</sup> Cytometers are equipped with multiple excitation lasers, emitting light at distinct wavelengths.<sup>182</sup> In this study, flow cytometry analyses were conducted using the BD LSRFortessa which contains violet (405 nm), blue (488 nm), yellow-green (561 nm) and red (640 nm) lasers and multiple filters to detect up to 18 colors.

#### 2.2.11.1 Staining and analysis of hepatic non-parenchymal cells

Hepatic non-parenchymal cells were isolated as described in section 2.2.9.6 for direct staining and analysis by flow cytometry. In addition, Tregs, CD4<sup>+</sup> conventional T cells and ILC2s were isolated (2.2.9.4, 2.2.9.5 and 2.2.9.8) and used for different *in vitro*

experiments (2.2.10.3 and 2.2.10.4) before they were stained and analyzed by flow cytometry. The latter remained in 96-well plates throughout the staining process and were therefore treated with smaller volumes as indicated in brackets in the following section.

First, the cells were centrifuged at 500 g for 5 min at 4°C. For the analysis of intracellular cytokine production, they were resuspended in 500 µL (200 µL) of restimulation medium containing phorbol 12-myristate 13-acetate (PMA, 20 ng/mL) and ionomycin (1 µg/mL) and transferred into 48-well microplates (or kept in 96-well microplates). Cells were restimulated for 4 h, or for 6 h when IL-13 was included in the staining panel. PMA and ionomycin non-specifically stimulate cytokine production by T cells.<sup>183</sup> After 30 min (or 60 min for IL-13 staining), brefeldin A (1 µg/ml) and monensin (2 µM) were added. Both act as protein transport inhibitors, preventing cytokine secretion and thus leading to their intracellular accumulation.<sup>183</sup> After restimulation, the cells were transferred into flow cytometry tubes (or kept in 96-well plates).

Prior to antibody staining, cells were incubated with 50 µL (25 µL) of TrueStain FcX antibody (see Table 9) for 10 min at 4°C to block unspecific binding. They were then washed with 1 mL (150 µL) of PBS and centrifuged. To exclude dead cells, cells were incubated for 10 min at 4°C with 50 µL (25 µL) of viability dye from LIVE/DEAD Fixable Red Dead Cell Stain Kit (PE-TR, 1:5000). Cells were washed again and centrifuged. Alternatively, dead cells were stained with Zombie NIR Fixable Viability Kit (APC-Cy7, 1:1000) during cell surface antibody staining. For cell surface analysis, cells were incubated with 50 µL (25 µL) of fluorochrome-conjugated antibodies listed in Table 10 for 30 min at 4°C. The cells were then washed with PBS and centrifuged.

Intracellular and intranuclear staining was performed using the Foxp3/Transcription factor staining buffer set. Cells were fixed with 300 µL (100 µL) of Fix/Perm solution for 30 min at 4°C, washed with PBS and centrifuged. Then they were washed twice with Permeabilization buffer, first with 2 mL (200 µL) and then with 1 mL (100 µL), and centrifuged. Thereafter, the cells were incubated with 50 µL of fluorochrome-labeled antibodies listed in Table 11 for 40 min in Permeabilization buffer at 4°C and then washed with 2 mL (150 µL) of Permeabilization buffer. To detect AREG using a biotin-

conjugated antibody, cells were subjected to a second round of intracellular staining with anti-streptavidin antibody (Table 11). They were then washed with PBS, centrifuged and resuspended in 350  $\mu$ L of FACS buffer. Cells from 96-well microplates were transferred to flow cytometry tubes during the final washing step. Finally, the cells were analyzed using BD LSRFortessa and FACSDiva software.

### 2.2.11.2 Gating strategy to identify hepatic ST2<sup>+</sup> Tregs and ILC2s

To identify hepatic ST2<sup>+</sup> Foxp3<sup>+</sup> CD4<sup>+</sup> Tregs and ST2<sup>+</sup> Sca-1<sup>+</sup> lin<sup>-</sup> ILC2s, we analyzed the flow cytometry data using FlowJo software with the gating strategy depicted in Figure 8. First, leukocytes were identified by size (FSC area, FSC-A) and granularity (SSC area, SSC-A). Within the leukocyte compartment, single cells were characterized by linear correlation of FSC-A and FSC height (FSC-H). Dead cells were excluded by gating on cells negative for LIVE/DEAD Fixable Red Dead Cell Stain (PE-TR) or Zombie NIR Fixable Viability dye (APC-Cy7) signal. On the basis of gated living cells, we identified both Tregs and ILC2s. Tregs were determined by gating for CD4<sup>+</sup> (BV 711) Foxp3<sup>+</sup> (AF 647 / PerCP-Cy5.5) cells. This was followed by gating for ST2<sup>+</sup> Tregs (PE-Cy-7 / PerCP-eF710; Figure 8). To identify ILC2s, living cells were analyzed for the expression signals of lineage markers (APC) and lin<sup>+</sup> cells were excluded. Finally, ILC2s were defined by co-expression of ST2 (PE-Cy7 / PerCP-eF710) and Sca-1 (Pacific Blue; Figure 8).

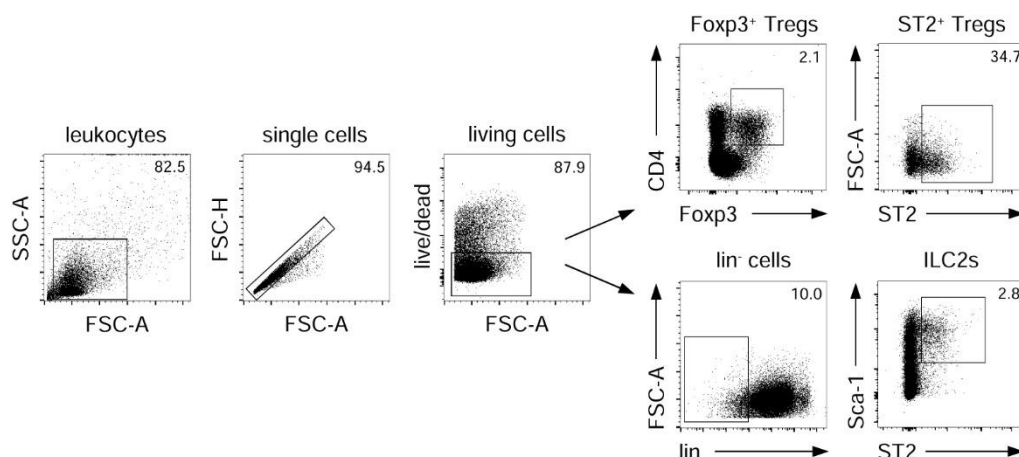


**Figure 8: Gating strategy for flow cytometric analysis of ST2<sup>+</sup> Tregs and ILC2s.** Hepatic leukocytes were isolated from C57BL/6J mice and stained for CD4, Foxp3, and ST2 to identify ST2<sup>+</sup> Tregs and for lineage markers (CD3e, CD11b, CD45R, Ly-76, Ly-6G/Ly-6C), Sca-1, and ST2 to isolate ILC2s. Frequencies are shown in representative dot plots.

### 2.2.12 Statistical analysis

Statistical analysis was performed using the GraphPad Prism software. All data are presented as mean  $\pm$  standard error of the mean (SEM). The non-parametric Mann-Whitney U test was performed to compare two groups. For comparison between more than two groups, we used the one-way ANOVA with Tukey's post-hoc test. Statistical significance was defined as a p-value of less than 0.05. Increasing numbers of asterisks represent specific levels of significance with the following ranges: \* $p < 0.05$ , \*\* $p < 0.01$ , \*\*\* $p < 0.001$ , and \*\*\*\* $p < 0.0001$ .

### 3 Results

#### 3.1 IL-33-induced AREG expression by hepatic ST2<sup>+</sup> Tregs and ILC2s

To investigate the immunoregulatory function of the IL-33/AREG axis in immune-mediated hepatitis and the role of ST2<sup>+</sup> Foxp3<sup>+</sup> Tregs and ILC2s in this system, we assessed the phenotype of these lymphocytes in response to exogenous IL-33 by flow cytometry. In particular, we aimed to determine whether the alarmin induces AREG expression by hepatic ST2<sup>+</sup> Tregs and ILC2s as IL-33 is known to stimulate the expression of AREG in Tregs<sup>132,140,141</sup> and ILC2s<sup>114,133</sup> from various organs. WT mice were injected intraperitoneally with IL-33 on four consecutive days, while the control mice received PBS. Since endogenous IL-33 functions as a danger signal released in response to liver tissue damage and exerts both pro- and anti-inflammatory responses by targeting various immune cells,<sup>36</sup> our initial objective was to determine whether exogenous IL-33 has any hepatotoxic effects. To analyze hepatic tissue injury, we measured the plasma levels of alanine aminotransferase (ALT), a liver enzyme released from damaged hepatocytes.<sup>166</sup> The biomarker was present at physiological levels<sup>184</sup> in both IL33 (32 ± 4 U/L) and PBS-treated mice (38 ± 7 U/L; Figure 9A). Moreover, liver tissue sections of IL-33-treated mice were stained with H&E and compared to those of mice treated with PBS. The representative images from both groups exhibit liver lobules with healthy parenchyma, characterized by well-organized hepatocyte plates separated by sinusoids, without any signs of abnormalities, such as inflammation or necrosis (Figure 9B). Therefore, the administration of IL-33 did not induce liver injury or tissue damage.

The administered IL-33 elevated the frequency of hepatic ST2<sup>+</sup> Foxp3<sup>+</sup> Tregs in WT mice (PBS: 18.6 ± 2.3%, IL-33: 53.4 ± 2.1%; Figure 9C). For phenotype analysis, we have assessed hepatic ST2<sup>+</sup> Treg activation and differentiation (KLRG1, ICOS), proliferation (Ki-67), inhibitory molecule expression (CTLA-4, IL-10, PD-L1, TIGIT), apoptosis (Bcl-2) and AREG expression. In response to IL-33, hepatic ST2<sup>+</sup> Tregs upregulated the expression of KLRG1 (PBS: 44.1 ± 3.5%, IL-33: 66.9 ± 0.9%), ICOS (PBS: 9.5 ± 3.1%, IL-33: 62.4 ± 3.4%) and Ki-67 (PBS: 76.5 ± 1.2%, IL-33: 80.2 ± 1.2%; Figure 9C). Additionally, the expression of several inhibitory molecules was elevated on hepatic ST2<sup>+</sup> Tregs from IL-33-treated mice compared to control mice (Figure 9C).

These include CTLA-4 (PBS:  $72.9 \pm 1.6\%$ , IL-33:  $88.2 \pm 0.6\%$ ), PD-L1 (PBS:  $16.9 \pm 3.0\%$ , IL-33:  $44.0 \pm 4.4\%$ ) and TIGIT (PBS:  $51.7 \pm 3.9\%$ , IL-33:  $67.4 \pm 3.4\%$ ; Figure 9C). However, the production of IL-10 by ST2<sup>+</sup> Tregs was not changed in response to administered IL-33 (Figure 9C). In addition, the expression of the anti-apoptotic molecule Bcl-2 was elevated on hepatic ST2<sup>+</sup> Tregs upon IL-33 treatment (PBS:  $23.2 \pm 1.4\%$ , IL-33:  $94.9 \pm 0.8\%$ ; Figure 9C). Importantly, we found elevated AREG expression in response to IL-33 treatment in hepatic ST2<sup>+</sup> Tregs (PBS:  $8.2 \pm 2.6\%$ , IL-33:  $25.1 \pm 1.9\%$ ; Figure 9C). In summary, IL-33 induced enhanced expansion and activation of hepatic ST2<sup>+</sup> Tregs, as well as increased expression of inhibitory molecules and AREG.



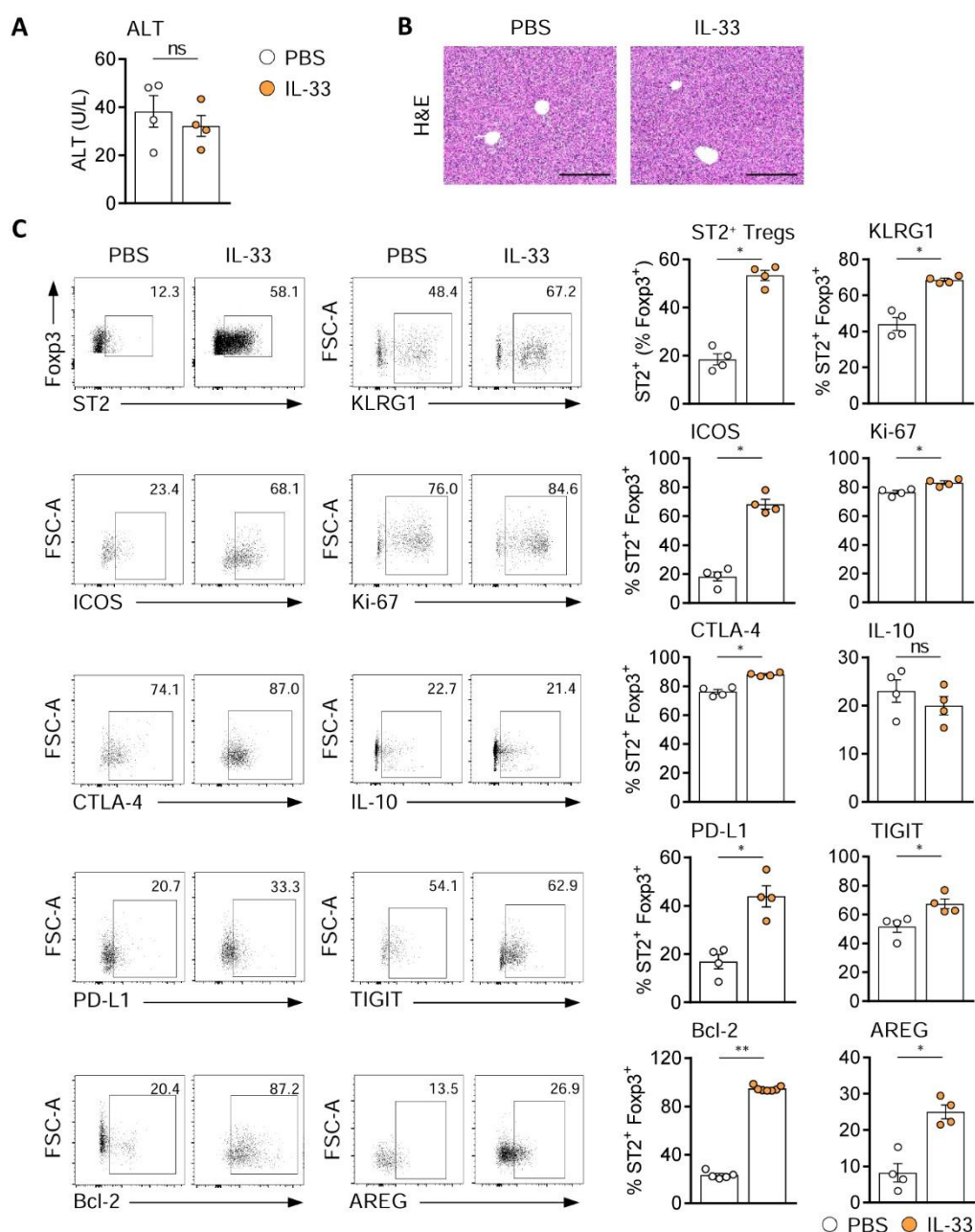


**Figure 9: IL-33-induced phenotype of hepatic ST2<sup>+</sup> Tregs.** WT mice received IL-33 on four consecutive days. Controls received PBS. (A) Plasma ALT levels were assessed. (B) H&E staining of liver sections is depicted. (C) The frequency and phenotype of hepatic ST2<sup>+</sup> Fxp3<sup>+</sup> CD4<sup>+</sup> Tregs were determined. Representative dot plots are presented. Bars represent 200 μm. Means ± SEM of one out of two experiments are shown. \**p* < 0.05; \*\**p* < 0.01; ns: not significant.

Furthermore, consistent with our prior publications,<sup>35,92</sup> the frequency of ILC2s was elevated in the livers of IL-33- compared to PBS-treated mice (PBS: 3.8 ± 0.4%, IL-33: 53.4 ± 3.6%; Figure 10). This was accompanied by an increase in their activation, as indicated by upregulated expression of KLRG1 (PBS: 23.3 ± 1.0%, IL-33: 91.5 ± 0.7%), along with the effector cytokine IL-13 (PBS: 3.4 ± 0.6%, IL-33: 23.8 ± 2.9%; Figure 10). Finally, we observed increased AREG production in hepatic ILC2s of mice injected with

IL-33 (PBS:  $20.1 \pm 2.4\%$ , IL-33:  $49.4 \pm 3.1\%$ ; Figure 10). Thus, exogenous IL-33 induced increased activation and AREG production of both hepatic ST2<sup>+</sup> Tregs and ILC2s.

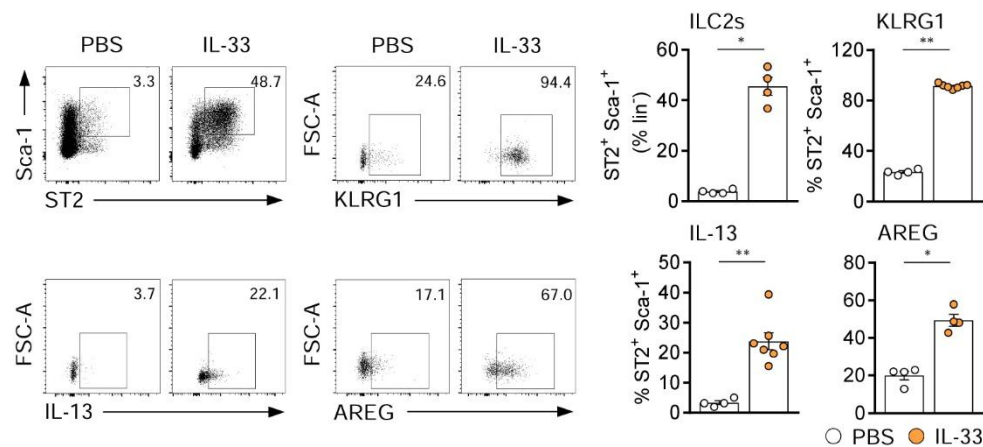


**Figure 10: IL-33-induced phenotype of hepatic ILC2s.** WT mice were treated with IL-33 on four consecutive days. Controls received PBS. The frequency and phenotype of hepatic ST2<sup>+</sup> Sca1<sup>+</sup> lin<sup>−</sup> ILC2s were analyzed. Representative dot plots are presented. Means  $\pm$  SEM of one out of two experiments are shown. \* $p < 0.05$ ; \*\* $p < 0.01$ .

Further, we sought to confirm the IL-33-mediated upregulation of AREG expression in ST2<sup>+</sup> Tregs and ILC2s *in vitro*. To this end, CD25<sup>+</sup> CD4<sup>+</sup> Tregs were isolated from the lymph nodes and spleens of naïve WT mice using MACS and cultured for 1.5 days in the presence or absence of IL-33. ILC2s were FACS-isolated from the livers of WT mice that had been treated with IL-33 on four consecutive days for cell expansion. The ILC2s were then cultured for 3.5 days in the presence or absence of IL-33. AREG expression by ST2<sup>+</sup> Foxp3<sup>+</sup> Tregs and ILC2s was analyzed by flow cytometry. Indeed, we found that exogenous IL-33 induced increased AREG expression by ST2<sup>+</sup> Tregs (w/o:  $28.4 \pm 0.8\%$ , IL-33:  $38.6 \pm 3.5\%$ ) and ILC2s (w/o:  $43.9 \pm 2.9\%$ , IL-33:  $70.1 \pm 2.6\%$ ; Figure 11) *in vitro*.

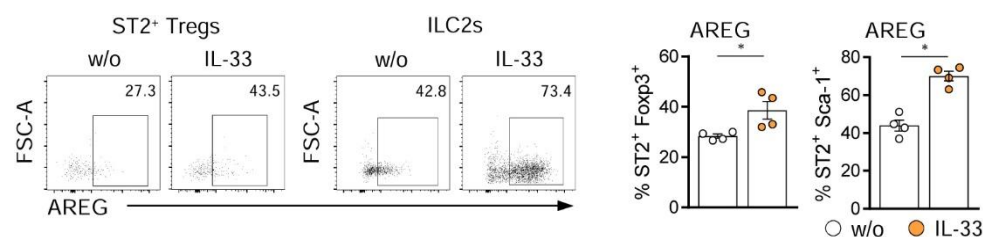


**Figure 11: Effect of exogenous IL-33 on AREG expression of ST2<sup>+</sup> Tregs and ILC2s.** CD25<sup>+</sup> CD4<sup>+</sup> Tregs were isolated from lymph nodes and spleens of naïve WT mice using MACS and cultured in presence or absence of IL-33 for 1.5 days. To expand hepatic ILC2s, WT mice were treated with IL-33 on four consecutive days. Hepatic ST2<sup>+</sup> Sca1<sup>+</sup> ILC2s were isolated via FACS and cultured in presence or absence of IL-33 for 3.5 days. AREG expression by ST2<sup>+</sup> Foxp3<sup>+</sup> CD4<sup>+</sup> Tregs and ST2<sup>+</sup> Sca1<sup>+</sup> ILC2s was assessed. Representative dot plots are displayed. Means  $\pm$  SEM of one out of two experiments are shown. \* $p < 0.05$ ; w/o: without.

### 3.2 Hepatic ST2<sup>+</sup> Tregs and ILC2s express AREG in immune-mediated hepatitis

Since AREG has previously been shown to be induced during acute liver injury<sup>108,129</sup> or HBV infection,<sup>112,130</sup> we aimed to explore its expression and potential role in the regulation of immune-mediated hepatitis. Acute immune-mediated hepatitis was induced in WT mice by intravenous administration of ConA. Control mice received PBS. Previously, we have shown an accumulation of ST2<sup>+</sup> Foxp3<sup>+</sup> Tregs in the inflamed livers of ConA-treated mice, as well as expansion and activation of pro-inflammatory ST2<sup>+</sup> ILC2s.<sup>35</sup> To explore the role of these lymphocytes in immune-mediated hepatitis with regard to AREG expression, we assessed their activation and phenotype by flow cytometry.

ConA-treated mice developed severe liver injury and tissue damage within 24 hours, as measured by elevated ALT values (PBS:  $34 \pm 1$  U/L, ConA:  $2291 \pm 408$  U/L) in the blood plasma (Figure 12A) and the formation of necrotic areas in the liver tissue (Figure 12B). Crucially, immune-mediated hepatitis coincided with highly increased serum AREG levels in ConA-treated compared to PBS-treated mice (Figure 12C). We also investigated the hepatic gene expression of the EGF receptor and its ligands in ConA-induced acute hepatitis, as previous studies indicate a major role of the EGFR signaling axis in acute liver disease and liver regeneration.<sup>116</sup> Our findings revealed that *Areg* is one of the most upregulated ligands of the EGF receptor in the livers of mice treated with ConA compared to healthy controls ( $7.4 \pm 2.2$ -fold; Figure 12D). In addition, mRNA expression of the growth factors *Ereg*, *Hbegf* and *Epgn* was increased in acute hepatitis. In contrast, *Egfr* expression was downregulated after induction of hepatitis (Figure 12D). Consistent with our earlier findings<sup>35</sup> and similar to the effects of administered IL-33 (Figure 9C), the frequency of hepatic ST2<sup>+</sup> Foxp3<sup>+</sup> Tregs was elevated in ConA-induced immune-mediated hepatitis (PBS:  $16.2 \pm 2.8\%$ , ConA:  $34.8 \pm 0.9\%$ ; Figure 12E). Notably, ST2<sup>+</sup> Tregs showed increased expression of KLRG1 (PBS:  $62.8 \pm 1.0\%$ , ConA:  $77.6 \pm 1.1\%$ ), ICOS (PBS:  $82.8 \pm 2.7\%$ , ConA:  $90.6 \pm 0.7\%$ ), CTLA-4 (PBS:  $55.9 \pm 11.8\%$ , ConA:  $92.4 \pm 1.3\%$ ), PD-L1 (PBS:  $21.9 \pm 6.6\%$ , ConA:  $64.7 \pm 4.2\%$ ), TIGIT (PBS:  $60.7 \pm 2.4\%$ , ConA:  $87.7 \pm 0.5\%$ ) and Bcl-2 (PBS:  $23.2 \pm 1.4\%$ , ConA:  $76.7 \pm 2.0\%$ ; Figure 12E). The expression of Ki-67 by hepatic ST2<sup>+</sup> Tregs was reduced (PBS:  $75.5 \pm 1.4\%$ , ConA:  $62.9 \pm 2.0\%$ ) and their production of IL-10 was not altered (Figure 12E). Importantly, the ST2<sup>+</sup> Treg-derived expression of AREG was

upregulated in the livers of ConA-treated mice compared to PBS-treated controls (PBS:  $19.2 \pm 2.3\%$ , ConA:  $35.8 \pm 1.3\%$ ; Figure 12E). Similarly, the frequency of hepatic ILC2s was elevated in immune-mediated hepatitis (PBS:  $1.0 \pm 0.2\%$ , ConA:  $2.8 \pm 0.2\%$ ), as well as their expression of KLRG1 (PBS:  $3.3 \pm 1.1\%$ , ConA:  $8.6 \pm 1.1\%$ ), IL-13 (PBS:  $2.6 \pm 1.0\%$ , ConA:  $10.9 \pm 1.1\%$ ), and AREG (PBS:  $12.5 \pm 2.0\%$ , ConA:  $31.9 \pm 3.6\%$ ; Figure 12F). Thus, both ST2<sup>+</sup> Tregs and ILC2s exhibited a more activated phenotype in ConA-induced immune-mediated hepatitis and upregulated the expression of AREG.

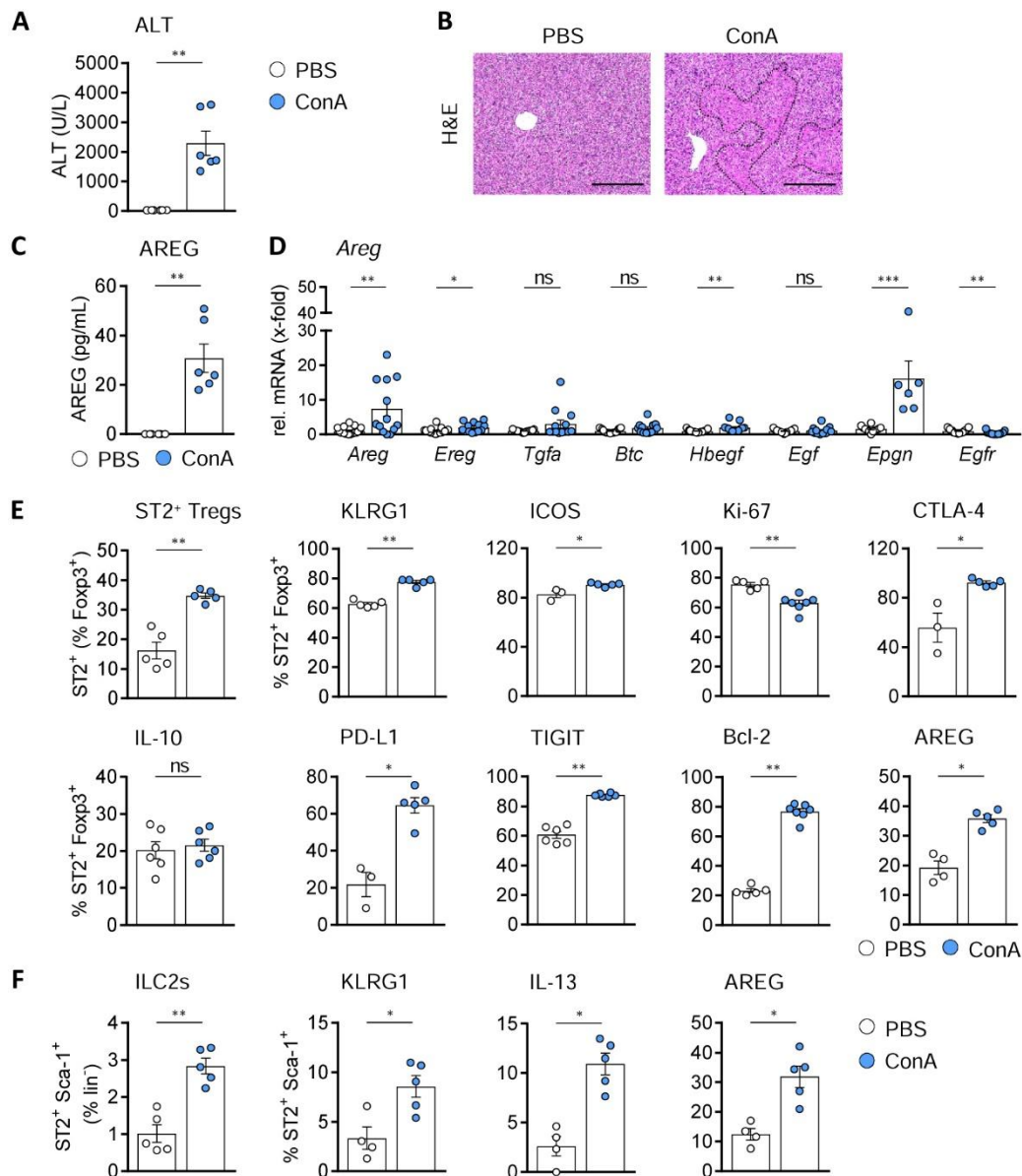


**Figure 12: Phenotype of ST2<sup>+</sup> Tregs and ILC2s in immune-mediated hepatitis.** WT mice received ConA and were examined 24 hours later. Controls received PBS. (A) Plasma levels of ALT were assessed. (B) H&E staining was performed with liver sections to visualize regions of necrosis (dotted line). (C) Plasma AREG levels were determined. (D) Hepatic mRNA expression of EGFR ligands and *Egfr* was assessed. (E+F) The frequency and phenotype of hepatic (E) ST2<sup>+</sup> Foxp3<sup>+</sup> CD4<sup>+</sup> Tregs and (F) ST2<sup>+</sup> Sca-1<sup>+</sup> lin<sup>-</sup> ILC2s were assessed. Bars represent 200  $\mu$ m. Means  $\pm$  SEM of one out of two experiments are shown. \* $p < 0.05$ ; \*\* $p < 0.01$ ; \*\*\* $p < 0.001$ ; \*\*\*\* $p < 0.0001$ ; ns: not significant.

Besides hepatic lymphocytes such as Tregs<sup>113</sup> and ILC2s<sup>106,114</sup>, hepatocytes were shown to express AREG *in vitro* in response to inflammatory stimuli.<sup>108,109</sup> Moreover, AREG production by hepatocytes was detected in hepatitis B virus (HBV)-infected mice,<sup>130</sup> nonalcoholic steatohepatitis (NASH) mice,<sup>110</sup> and in mice and patients with cholestatic liver injury.<sup>109</sup> To assess whether tissue cells like hepatocytes also express AREG in immune-mediated hepatitis, we performed immunohistochemical (IHC) staining for AREG using liver tissue samples from PBS- and ConA-treated WT mice. To determine the specificity of AREG staining, we used hepatic tissue from ConA-treated *Areg*<sup>-/-</sup> mice. Of the few commercially available anti-mouse AREG antibodies, we tested three antibodies from different companies that correspond to different immunogens covering human and mouse AREG. All three antibodies are described to recognize mouse AREG. Sectioned liver slides were treated with a primary anti-mouse AREG antibody (Figure 13: Ab #1: Rabbit anti-AREG, Thermo Fisher Scientific, immunogen: human AREG aa20-252, reactivity: human, mouse, rat; Ab #2: Rabbit anti-AREG, Biorbyt, immunogen: human AREG aa185-252, reactivity: human, mouse, rat; Ab #3: Goat anti-AREG, R&D Systems, immunogen: mouse AREG aa94-191, reactivity: mouse; see Table 7), followed by incubation with a biotinylated secondary antibody. Detection was conducted using the avidin-biotin-peroxidase complex (ABC) method and DAB substrate chromogen reagent containing hydrogen peroxidase. Alternatively, primary antibody (Figure 13: Ab #1-2; see Table 7) binding was followed by incubation with alkaline phosphatase (AP) polymer and New Fuchsin chromogen solution. The presence of the target antigen AREG is indicated by brown (DAB) or pink (New Fuchsin) reaction products. AREG staining was nearly absent in liver samples from healthy, PBS-treated mice, whereas it was strongly elevated in inflamed liver tissues from WT mice treated with ConA (Figure 13). Unfortunately, all antibodies tested exhibited non-specific binding to necrotic areas in damaged livers, as evidenced by prominent staining in liver sections from ConA-treated *Areg*<sup>-/-</sup> mice (Figure 13). Therefore, histological analysis of AREG expression in the liver tissue was not possible.



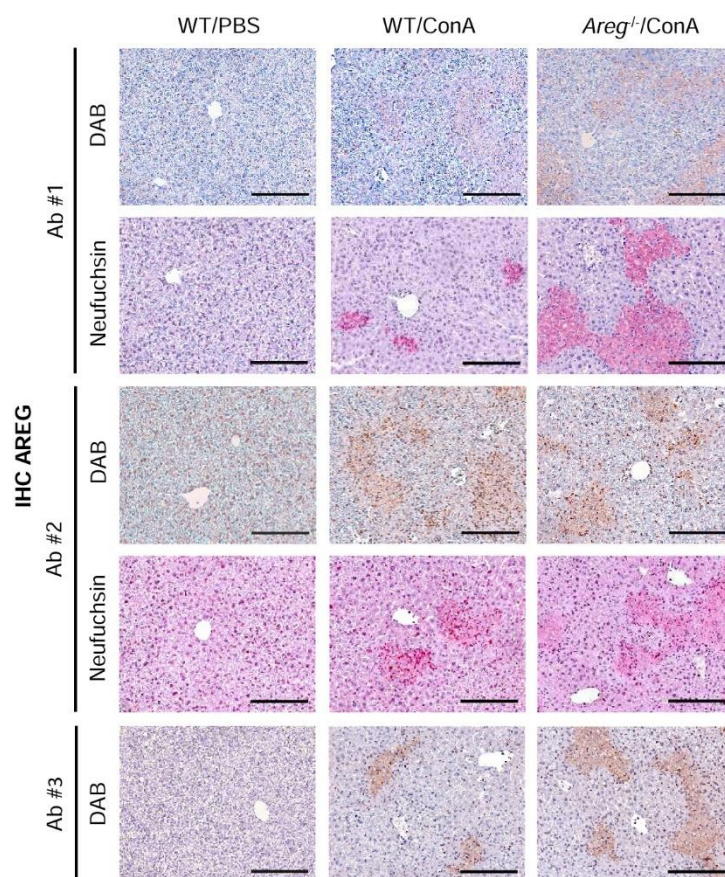


**Figure 13: AREG expression in the liver tissue in immune-mediated hepatitis.** WT and *Areg*<sup>-/-</sup> mice were treated with ConA 24 hours before analysis. Controls received PBS. Immunohistochemical (IHC) staining of AREG was performed on the respective liver sections. Representative images from at least two experiments are pictured. Bars represent 200  $\mu$ m.

Furthermore, we aimed to identify inflammatory stimuli that play a role in ConA-induced immune-mediated hepatitis and might affect hepatocyte-derived AREG expression. For this study, we selected several cytokines that are upregulated in ConA-induced immune-mediated hepatitis: IL-33,<sup>34,35</sup> TNF $\alpha$ ,<sup>24,33</sup> IFN $\gamma$ ,<sup>24,33</sup> IL-1 $\beta$ ,<sup>185,186</sup> TGF $\beta$ <sup>187</sup> and AREG itself (Figure 12C+D). In addition, IL-33,<sup>114,132,133,140,141</sup> TNF $\alpha$ ,<sup>188–190</sup> IFN $\gamma$ ,<sup>191</sup> IL-1 $\beta$ ,<sup>108,188,192</sup> TGF $\beta$ ,<sup>193</sup> and AREG<sup>111,136–139</sup> are known to induce AREG expression in various cell types and organs. To determine whether stimulation with these cytokines directly affects AREG production by primary hepatocytes, we performed *in vitro* culture experiments with primary hepatocytes isolated from naive WT mice. Initially, we investigated AREG expression in homeostasis by measuring AREG concentrations in the supernatants of unstimulated hepatocyte cultures over a period of 24 hours using ELISA. Next, primary hepatocytes were incubated with the cytokines mentioned above. After 8 hours of stimulation, the concentration of AREG protein in the culture supernatant was analyzed by ELISA. Furthermore, *Areg* mRNA expression was

determined after 1 hour of stimulation by RNA isolation from hepatocytes and subsequent qRT-PCR analysis.

Interestingly, AREG was produced by unstimulated hepatocytes, as demonstrated by its accumulation over 24 hours in the supernatant of *in vitro* cell cultures (Figure 14A). However, none of the tested cytokines induced an increased AREG production after 8 hours (Figure 14B). In fact, AREG levels were even reduced in response to IL-33, TNF $\alpha$ , IFN $\gamma$ , or TGF $\beta$  (Figure 14B). The assessment of AREG protein expression upon AREG treatment was precluded by the experimental design, as any supplementation to the culture medium would introduce spurious AREG concentrations in the analyzed supernatant, leading to false positive data. Therefore, we focused on *Areg* mRNA expression in hepatocytes. Importantly, *Areg* mRNA levels in hepatocytes significantly increased following AREG treatment compared to untreated cells ( $1.67 \pm 0.09$ -fold; Figure 14C), suggesting a self-induction mechanism. Further, incubation with IL-33 resulted in reduced *Areg* mRNA levels ( $0.75 \pm 0.07$ -fold; Figure 14C). The remaining cytokines tested had no effect on *Areg* mRNA levels (Figure 14C). In summary, primary hepatocytes produced AREG *in vitro*, and *Areg* mRNA levels were increased in response to exogenous AREG in a self-induction mechanism. However, exogenous IL-33 and other cytokines associated with immune-mediated hepatitis did not stimulate AREG expression.

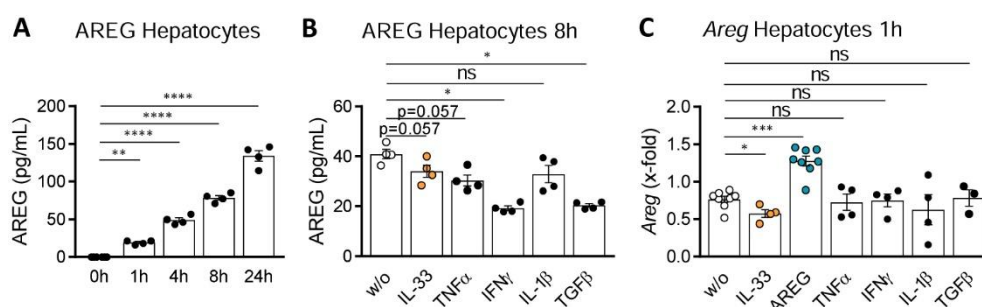


**Figure 14: AREG expression by hepatocytes.** Primary hepatocytes were isolated from naïve WT mice for cultivation. (A) AREG concentrations were analyzed in the supernatants over a period of 24 hours. (B+C) Hepatocyte cultures were incubated with depicted cytokines. (B) AREG protein production after 8 hours, and (C) *Areg* mRNA expression after 1 hour were determined. *Areg* mRNA levels were normalized to gene expression at 0-hour stimulation. Representative images from at least two experiments are pictured. Means  $\pm$  SEM of one out of two experiments are shown. \* $p < 0.05$ ; \*\* $p < 0.01$ ; \*\*\* $p < 0.001$ ; \*\*\*\* $p < 0.0001$ ; ns: not significant; h: hours; w/o: without.

To assess a potential immunoregulatory role of AREG produced by non-lymphocytic liver cells other than hepatocytes in immune-mediated hepatitis, we also investigated

the induction of AREG expression by LSECs, the most abundant non-parenchymal cells in the liver.<sup>8</sup> To analyze AREG expression by LSECs, we isolated LSECs from naïve WT mice and cultured them with TNF $\alpha$ , IFN $\gamma$ , IL-1 $\beta$  or TGF $\beta$  for 8 or 24 hours. However, in contrast to hepatocytes, LSECs did not express AREG under homeostatic conditions and none of the stimuli tested induced AREG expression in LSECs (data not shown).

### 3.3 Immune-mediated hepatitis is aggravated in absence of AREG

After demonstrating that hepatic ST2<sup>+</sup> Tregs and ILC2s expressed AREG in immune-mediated hepatitis, we wanted to investigate its immunomodulatory function in acute liver injury. Therefore, we induced immune-mediated hepatitis in *Areg*<sup>-/-</sup> mice, where AREG expression was absent in hepatic ST2<sup>+</sup> Foxp3<sup>+</sup> Tregs and ILC2s (Figure 15A), and analyzed the frequency and phenotype of hepatic ST2<sup>+</sup> Foxp3<sup>+</sup> Tregs and ILC2s by flow cytometry, as well as disease pathology. Interestingly, these mice developed more pronounced hepatic tissue damage than WT mice, as indicated by elevated plasma ALT levels (WT: 1269  $\pm$  383 U/L, KO: 11374  $\pm$  2446 U/L; Figure 15B) and increased necrotic areas in H&E stained liver tissue (Figure 15C). In line with this, mRNA expression of the inflammatory cytokines *Tnfa* and *Ifng*, crucial mediators of liver damage in immune-mediated hepatitis,<sup>24,33</sup> was elevated in the absence of AREG (Figure 15D). However, gene expression levels of the alarmin *Il33*, and *Il12p40*, subunit of the IFN $\gamma$ -inducing cytokine IL-12, were not changed (Figure 15D). Interestingly, anti-inflammatory *Il10* mRNA expression was increased as well (Figure 15D). IFN $\gamma$  is known to induce *Cxcl9* and *Cxcl10* in immune-mediated hepatitis.<sup>194</sup> In accordance, we found higher mRNA levels of both chemokines, along with their receptor *Cxcr3*, in ConA-treated *Areg*<sup>-/-</sup> compared to WT mice (Figure 15D).



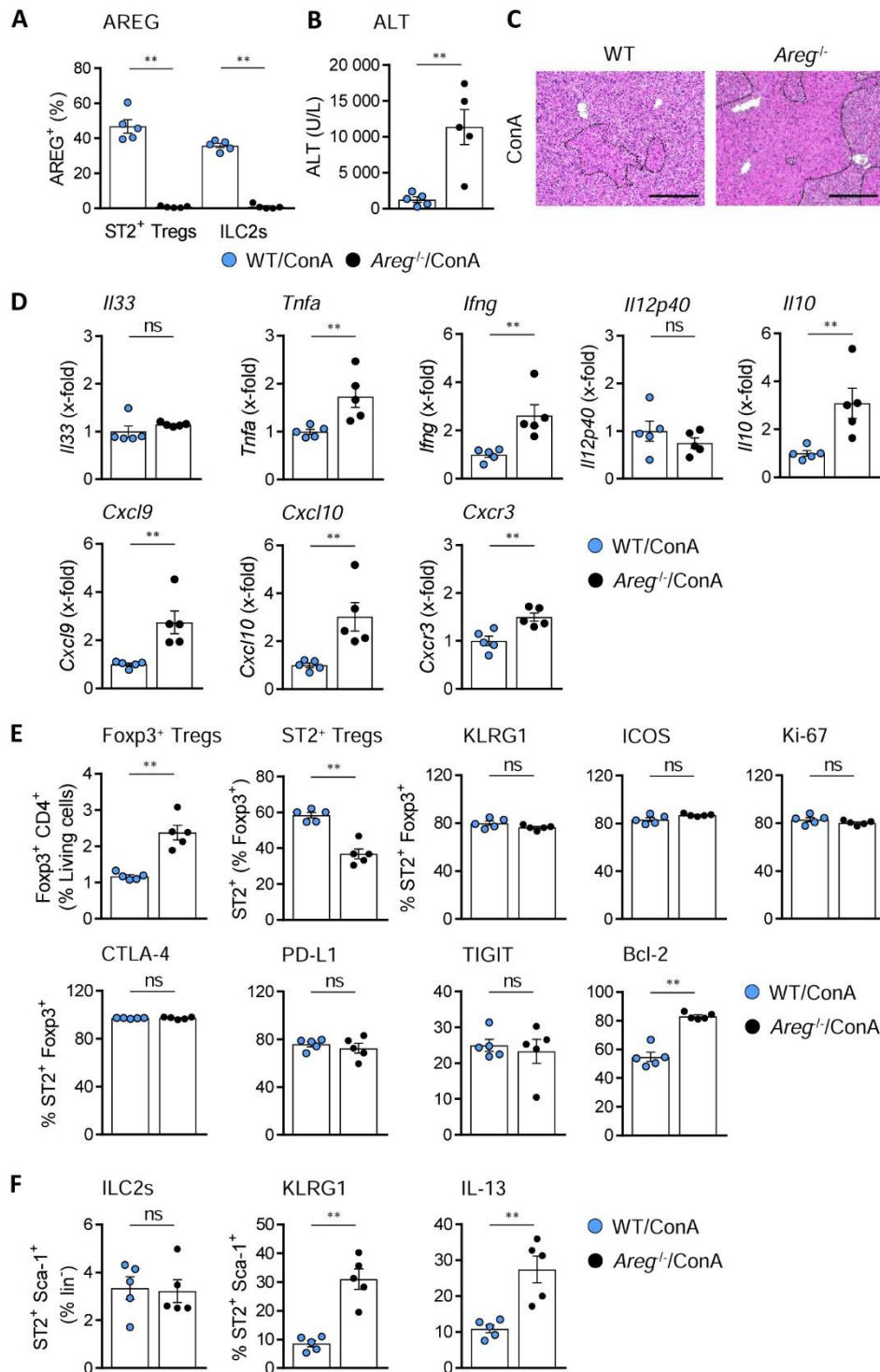


**Figure 15: *Areg*<sup>-/-</sup> mice develop more severe immune-mediated hepatitis.** WT and *Areg*<sup>-/-</sup> mice received ConA 24 hours before analysis. (A) AREG expression of hepatic ST2<sup>+</sup> Foxp3<sup>+</sup> CD4<sup>+</sup> Tregs and ST2<sup>+</sup> Sca-1<sup>+</sup> lin<sup>-</sup> ILC2s was analyzed. (B) Plasma ALT activity was determined. (C) Liver sections were subjected to H&E staining for the visualization of necrotic areas (dotted line). (D) Hepatic mRNA expression of critical cytokines was determined. (E+F) The frequency and phenotype of hepatic (E) ST2<sup>+</sup> Foxp3<sup>+</sup> CD4<sup>+</sup> Tregs and (F) ST2<sup>+</sup> Sca-1<sup>+</sup> ILC2s were analyzed. Bars represent 200 μm. Means ± SEM of one out of two experiments are shown. \*\*p < 0.01; ns: not significant.

Further, the absence of AREG in acute hepatitis resulted in an elevated frequency of total hepatic Foxp3<sup>+</sup> CD4<sup>+</sup> Tregs (WT: 1.18 ± 0.04%, KO: 2.38 ± 0.20%; Figure 15E).

In contrast, the frequency of hepatic ST2<sup>+</sup> Foxp3<sup>+</sup> Tregs was diminished (WT: 58.4 ± 1.5%, KO: 36.9 ± 2.8%; Figure 15E). Phenotype analysis of ST2<sup>+</sup> Tregs in the inflamed livers of *Areg*<sup>-/-</sup> mice showed similar activation (KLRG1, ICOS), proliferation (Ki-67), and inhibitory molecule expression (CTLA-4, PD-L1, TIGIT) compared to ST2<sup>+</sup> Tregs from WT mice, but elevated expression of the anti-apoptotic protein Bcl-2 (WT: 54.7 ± 3.2%, KO: 83.2 ± 1.0%; Figure 15E). The lack of AREG did not alter the frequency of hepatic ILC2s in immune-mediated hepatitis, but resulted in stronger activation of ILC2s, determined by enhanced expression of the activation marker KLRG1 (WT: 8.6 ± 1.1%, KO: 31.0 ± 3.5%) and the type 2 cytokine IL-13 (WT: 10.9 ± 1.1%, KO: 27.5 ± 3.7%; Figure 15F).

To determine whether the absence of AREG affects the activating effect of exogenous IL-33 on hepatic ST2<sup>+</sup> Foxp3<sup>+</sup> Tregs and ILC2s (Figure 9-11), we treated *Areg*<sup>-/-</sup> mice and WT controls with IL-33 on four consecutive days and analyzed the frequency and phenotype of both immune cell populations by flow cytometry. Similar to the results in immune-mediated hepatitis, the frequency of hepatic ST2<sup>+</sup> Tregs was reduced in IL-33-treated *Areg*<sup>-/-</sup> compared to WT mice (WT: 64.8 ± 2.1%, KO: 56.5 ± 1.9%; Figure 16A). The lack of endogenous AREG did not affect the activation of ST2<sup>+</sup> Tregs or their expression of Bcl-2 or inhibitory molecules (Figure 16A). However, the expression of the proliferation marker Ki-67 was increased (WT: 85.7 ± 1.9%, KO: 90.9 ± 0.7%; Figure 16A). In contrast, the frequency of ILC2s remained unchanged in IL-33-treated *Areg*<sup>-/-</sup> compared to WT mice, as did ILC2 activation and IL-13 expression (Figure 16B).

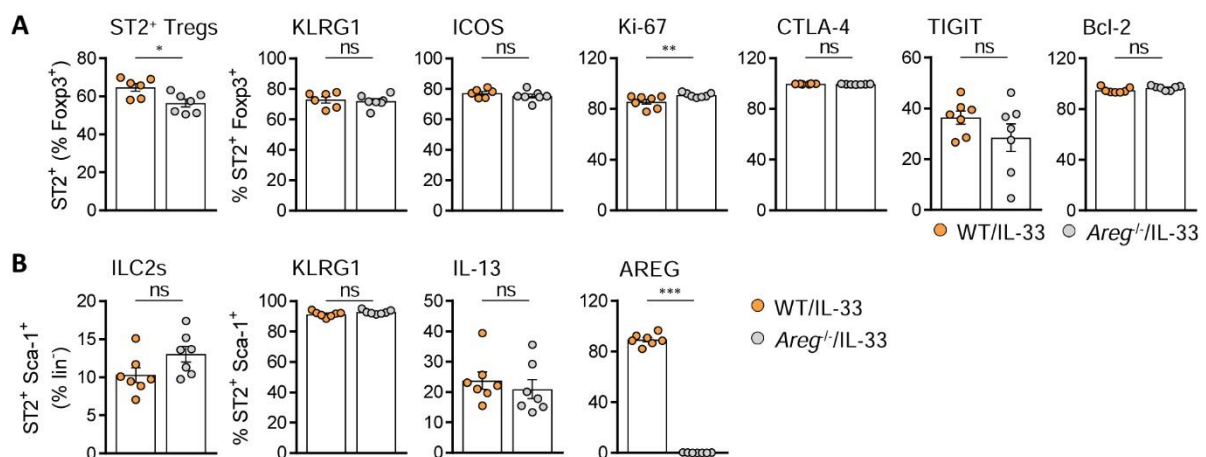


**Figure 16: IL-33-induced phenotype of hepatic ST2<sup>+</sup> Tregs and ILC2s in the absence of AREG.** (A+B) WT and *Areg*<sup>-/-</sup> mice were treated with IL-33 on four consecutive days. The frequency and phenotype of hepatic (A) ST2<sup>+</sup> Foxp3<sup>+</sup> CD4<sup>+</sup> Tregs and (B) ST2<sup>+</sup> Sca-1<sup>+</sup> lin<sup>-</sup> ILC2s were determined. Means ± SEM of one out of two experiments are shown. \*p < 0.05; \*\*p < 0.01; \*\*\*p < 0.001; ns: not significant.

To verify the reduced frequency of exogenous IL-33-induced Tregs in the absence of AREG, we isolated CD25<sup>+</sup> CD4<sup>+</sup> Tregs from lymph nodes and spleens of naïve *Areg*<sup>-/-</sup> mice and WT controls using MACS and cultured Tregs in the presence or absence of IL-33. After 1.5 days, the frequency and phenotype of ST2<sup>+</sup> Foxp3<sup>+</sup> CD4<sup>+</sup> Treg were determined by flow cytometry. We observed IL-33-induced expansion of *Areg*<sup>-/-</sup> and WT ST2<sup>+</sup> Tregs, along with an upregulation of ICOS and TIGIT in both groups (Figure 17). However, consistent with the *in vivo* results, the frequency of IL-33-activated ST2<sup>+</sup> Tregs was lower in cell cultures from *Areg*<sup>-/-</sup> compared to WT mice (WT: 26.6 ± 0.6%, KO: 15.0 ± 0.7%; Figure 17). Moreover, the lack of AREG resulted in a reduced IL-33-induced expression of the inhibitory molecule IL-10 in ST2<sup>+</sup> Tregs (WT: 20.0 ± 0.3%, KO: 13.1 ± 0.8%; Figure 17). However, the expression of KLRG1, PD-L1, TIGIT and Bcl-2 were not altered, and the expression of the activation marker ICOS was increased in the absence of AREG (WT: 30.2 ± 1.9%, KO: 38.3 ± 1.7%; Figure 17).

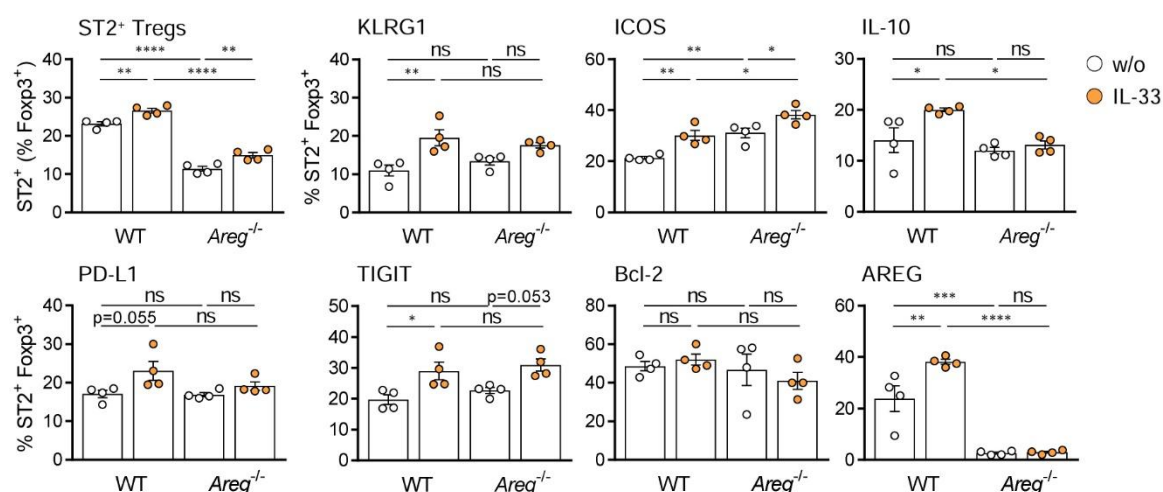


**Figure 17: Effect of exogenous IL-33 on ST2<sup>+</sup> Tregs in the absence of AREG.** CD25<sup>+</sup> CD4<sup>+</sup> Tregs sorted using MACS from lymph nodes and spleens of naïve WT and *Areg*<sup>-/-</sup> mice were cultured in the presence of IL-33 for 1.5 days. ST2<sup>+</sup> Foxp3<sup>+</sup> CD4<sup>+</sup> Treg frequency and phenotype were assessed. Means ± SEM of one out of two experiments are shown. \*p< 0.05; \*\*p< 0.01; \*\*\*p< 0.001; \*\*\*\*p< 0.0001; ns: not significant; w/o: without.

Taken together, AREG deficiency in immune-mediated hepatitis was associated with exacerbated disease pathology, reduced frequency of hepatic ST2<sup>+</sup> Tregs and increased activation of hepatic ILC2s. Furthermore, the lack of AREG resulted in a decreased frequency of hepatic ST2<sup>+</sup> Tregs in IL-33-treated mice and IL-33-stimulated Tregs *in vitro*, accompanied by a diminished *in vitro* expression of IL-10 by IL-33-activated Tregs.

### 3.4 Exogenous AREG activates ST2<sup>+</sup> Tregs but inhibits ILC2s

To further investigate AREG-mediated regulation of ILC2s and Tregs, we performed cell culture experiments in which these immune cells were stimulated with AREG. To assess the role of the IL-33 receptor ST2 in AREG-mediated regulation of Tregs, we also compared the effect of AREG stimulation on ST2<sup>-</sup> and ST2<sup>+</sup> Foxp3<sup>+</sup> Tregs from WT mice and on Foxp3<sup>+</sup> Tregs from WT and *Il1rl1*<sup>-/-</sup> mice lacking ST2. In addition, we cultured ST2<sup>+</sup> Foxp3<sup>+</sup> Tregs from *Areg*<sup>-/-</sup> mice in the presence or absence of AREG to analyze whether exogenous AREG can compensate the lack of endogenous AREG. Finally, ILC2s and WT or *Areg*<sup>-/-</sup> ST2<sup>+</sup> Foxp3<sup>+</sup> Tregs were cultured in the presence or absence of IL-33 and IL-33/AREG to elucidate the effect of AREG on IL-33-activated ILC2s and Tregs. ST2<sup>+</sup> Sca-1<sup>+</sup> ILC2s were FACS-isolated from livers of WT mice treated with IL-33 for cell expansion. Hepatic ILC2s were cultured in the presence or absence of AREG, IL-33 or IL33/AREG for 3.5 days. CD25<sup>+</sup> CD4<sup>+</sup> Tregs were isolated from lymph nodes and spleens of naïve WT, *Il1rl1*<sup>-/-</sup> or *Areg*<sup>-/-</sup> mice by MACS and cultured in the presence or absence of AREG, IL-33 or IL-33/AREG for 1.5 days. The phenotype of harvested ILC2s and Foxp3<sup>+</sup> Tregs were analyzed by flow cytometry.

Interestingly, the number of hepatic ILC2s was decreased in the presence of AREG (w/o: 3198 ± 170 ILC2s, AREG: 2451 ± 156 ILC2s), as well as their activation (KLRG1: w/o: 3077 ± 49 ILC2s, AREG: 2389 ± 9 ILC2s) and expression of IL-13 (w/o: 2462 ± 40 ILC2s, AREG: 1719 ± 110 ILC2s, Figure 18A). The expression of AREG was not increased in response to exogenous AREG (Figure 18A). Next, we assessed the effect of AREG on IL-33-stimulated hepatic ILC2s. Exogenous IL-33 resulted in increased ILC2 number (w/o: 3198 ± 170 ILC2s, IL-33: 22526 ± 4467 ILC2s), activation (KLRG1: w/o: 3077 ± 49 ILC2s, IL-33: 12412 ± 640 ILC2s) and expression of IL-13 (w/o: 2462 ± 40 ILC2s, IL-33: 9286 ± 459 ILC2s) and AREG (w/o: 1623 ± 70 ILC2s, IL-33: 14450 ± 1065 ILC2s; Figure 18B). The addition of AREG reduced the IL-33-induced activation of ILC2s (KLRG1: IL-33: 12412 ± 640 ILC2s, IL-33/AREG: 7717 ± 125 ILC2s) and their expression of IL-13 (IL-33: 9286 ± 459 ILC2s, IL-33/AREG: 5633 ± 334 ILC2s) and AREG (IL-33: 14450 ± 1065 ILC2s, IL-33/AREG: 8691 ± 240 ILC2s; Figure 18B).

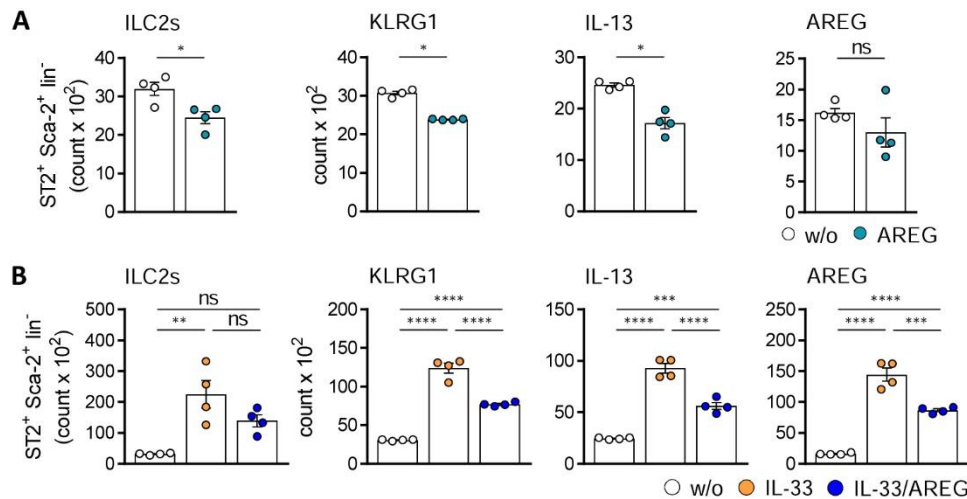


**Figure 18: Effect of exogenous AREG on hepatic ILC2s.** (A+B) ST2<sup>+</sup> Sca-1<sup>+</sup> lin<sup>-</sup> ILC2s were isolated from livers of IL-33-treated WT mice by FACS, and cultured in presence or absence of (A) AREG or (B) IL-33 and IL-33/AREG. After 3.5 days, the number and phenotype of ILC2s were determined. Means  $\pm$  SEM of one out of two experiments are shown. \* $p$  < 0.05; \*\* $p$  < 0.01; \*\*\* $p$  < 0.001; \*\*\*\* $p$  < 0.0001; ns: not significant; w/o: without.

The frequency of ST2<sup>+</sup> Foxp3<sup>+</sup> Tregs was elevated in presence of AREG (w/o:  $6.0 \pm 0.5\%$ , AREG:  $7.8 \pm 0.3\%$ ), whereas the frequency of ST2<sup>-</sup> Foxp3<sup>+</sup> Tregs was reduced (Figure 19A). Furthermore, exogenous AREG induced activation of ST2<sup>+</sup> but not ST2<sup>-</sup> Foxp3<sup>+</sup> Tregs, which was characterized by elevated expression of KLRG1 (w/o:  $18.2 \pm 1.4\%$ , AREG:  $24.7 \pm 0.9\%$ ) and the inhibitory molecules IL-10 (w/o:  $13.3 \pm 1.2\%$ , AREG:  $17.0 \pm 0.7\%$ ), PD-L1 (w/o:  $17.1 \pm 1.0\%$ , AREG:  $24.0 \pm 1.6\%$ ) and TIGIT (w/o:  $30.4 \pm 1.2\%$ , AREG:  $35.3 \pm 0.9\%$ ), as well as AREG itself (w/o:  $28.4 \pm 0.8\%$ , AREG:  $41.6 \pm 1.0\%$ ; Figure 19A). Independent of ST2-expression, the frequency of ICOS<sup>+</sup> and Bcl-2<sup>+</sup> Foxp3<sup>+</sup> Tregs was not altered in response to AREG (Figure 19A). To verify whether AREG selectively activates ST2<sup>+</sup> Foxp3<sup>+</sup> Tregs, we also cultured Tregs from *Il1rl1*<sup>-/-</sup> mice lacking the IL-33 receptor ST2 in the presence of AREG. Indeed, Foxp3<sup>+</sup> Tregs from WT but not *Il1rl1*<sup>-/-</sup> mice were expanded (w/o:  $9.3 \pm 0.6\%$ , AREG:  $12.4 \pm 0.6\%$ ) and activated by AREG, as indicated by increased expression of KLRG1 (w/o:  $9.1\% \pm 0.3\%$ , AREG:  $11.3 \pm 0.4\%$ ), PD-L1 (w/o:  $29.7 \pm 2.3\%$ , AREG:  $36.9 \pm 1.2\%$ ), TIGIT (w/o:  $20.8 \pm 1.5\%$ , AREG:  $26.8 \pm 1.4\%$ ) and AREG (w/o:  $12.0 \pm 0.9\%$ , AREG:  $17.7 \pm 1.0\%$ ; Figure 19B). In both WT and *Il1rl1*<sup>-/-</sup> mice, AREG did not affect the expression levels of ICOS and Bcl-2 by Foxp3<sup>+</sup> Tregs (Figure 19B). To assess ST2-specific AREG recognition and signaling on Tregs, we examined the expression of its receptor EGFR in the presence or absence of ST2. Interestingly, EGFR expression was comparable

in Foxp3<sup>+</sup> Tregs from WT and *Il1rl1*<sup>-/-</sup> mice, as well as in ST2<sup>-</sup> and ST2<sup>+</sup> Foxp3<sup>+</sup> Tregs from WT mice (Figure 19C).

Furthermore, we observed that exogenous AREG failed to induce the expansion of ST2<sup>+</sup> Foxp3<sup>+</sup> Tregs from *Areg*<sup>-/-</sup> mice (Figure 19D). While the expression of KLRG1 (w/o: 13.4 ± 1.0%, AREG: 18.1 ± 0.3%) and TIGIT (w/o: 22.7 ± 1.0%, AREG: 27.9 ± 1.2%) was upregulated in response to AREG in *Areg*<sup>-/-</sup> ST2<sup>+</sup> Tregs, the expression of the inhibitory molecules IL-10 and PD-L1 was not altered compared to unstimulated cells (Figure 19D). Similar to ST2<sup>+</sup> Tregs from WT mice, the expression levels of ICOS and Bcl-2 in *Areg*<sup>-/-</sup> ST2<sup>+</sup> Tregs were not changed in response to AREG (Figure 19D).



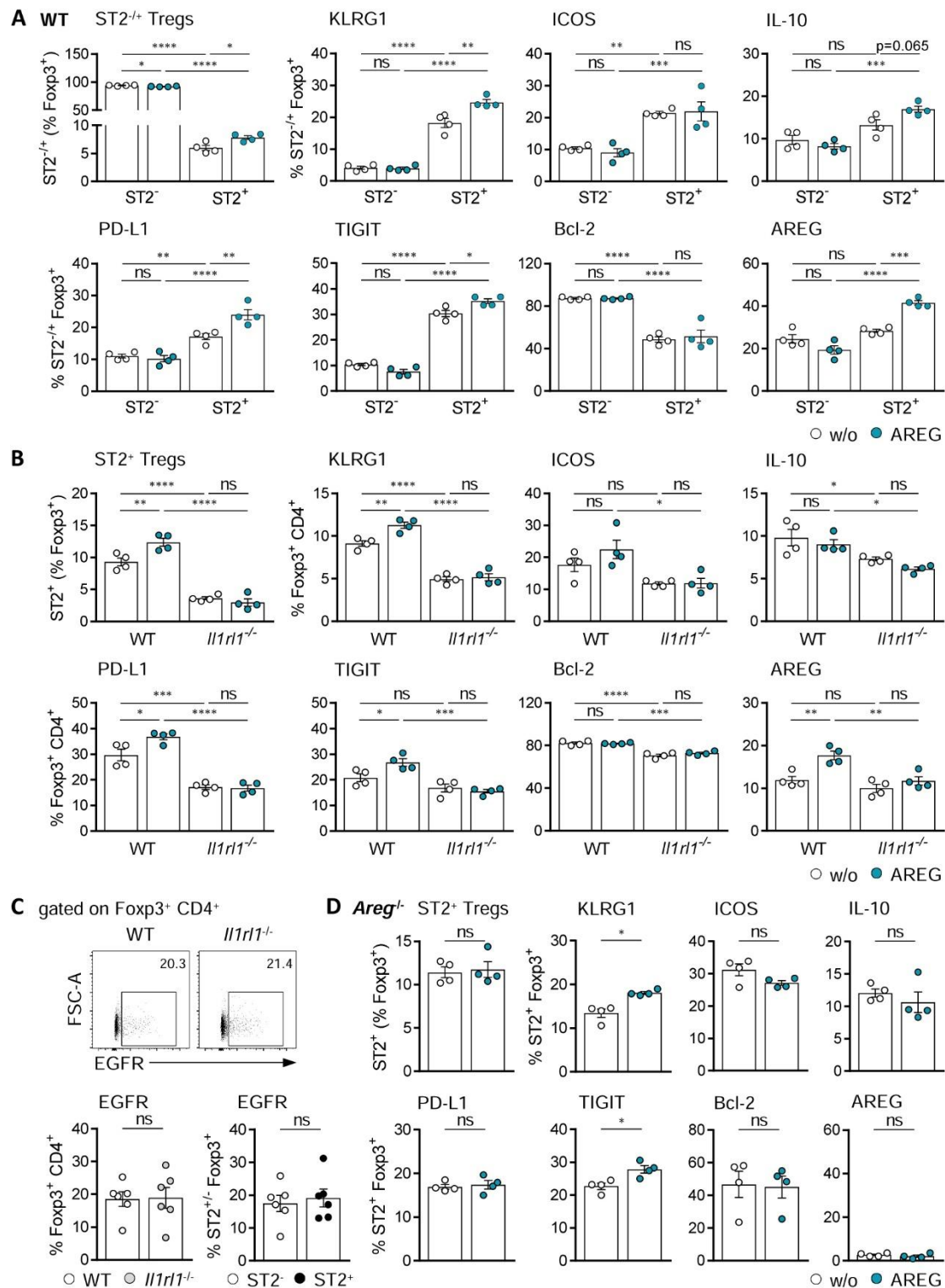


**Figure 19: Effect of exogenous AREG on Tregs.** (A+B) MACS-sorted CD25<sup>+</sup> CD4<sup>+</sup> Tregs from lymph nodes and spleens of (A+B) WT and (B) *Il1rl1*<sup>-/-</sup> mice were cultured in presence or absence of AREG. After 1.5 days, ST2<sup>+</sup> Foxp3<sup>+</sup> CD4<sup>+</sup> Treg frequency and Foxp3<sup>+</sup> CD4<sup>+</sup> Treg phenotype were determined. (C) EGFR expression was analyzed in hepatic Foxp3<sup>+</sup> CD4<sup>+</sup> Tregs from WT and *Il1rl1*<sup>-/-</sup> mice. Representative dot plots are shown. Besides, EGFR expression by hepatic ST2<sup>+</sup> and ST2<sup>-</sup> Foxp3<sup>+</sup> CD4<sup>+</sup> Tregs from WT mice is depicted. (D) MACS-sorted CD25<sup>+</sup> CD4<sup>+</sup> Tregs from *Areg*<sup>-/-</sup> mice, cultured with or without AREG for 1.5 days, were assessed for ST2<sup>+</sup> Foxp3<sup>+</sup> CD4<sup>+</sup> Treg frequency and phenotype. Means ± SEM of one out of two experiments are shown. \**p* < 0.05; \*\**p* < 0.01; \*\*\**p* < 0.001; \*\*\*\**p* < 0.0001; ns: not significant; w/o: without.

Finally, we compared the effect of AREG on ST2<sup>+</sup> Foxp3<sup>+</sup> Tregs *in vitro* in the presence or absence of IL-33. Exogenous IL-33 induced expansion and activation of ST2<sup>+</sup> Tregs, as evidenced by increased cell frequency (w/o:  $6.0 \pm 0.5\%$ , IL-33:  $10.1 \pm 0.3\%$ ) and expression of KLRG1 (w/o:  $11.0 \pm 1.4\%$ , IL-33:  $19.6 \pm 2.1\%$ ), ICOS (w/o:  $21.4 \pm 0.6\%$ , IL-33:  $30.2 \pm 1.9\%$ ), IL-10 (w/o:  $14.1 \pm 2.4\%$ , IL-33:  $20.0 \pm 0.3\%$ ), PD-L1 (w/o:  $15.6 \pm 1.4\%$ , IL-33:  $28.5 \pm 3.1\%$ ), TIGIT (w/o:  $20.9 \pm 2.6\%$ , IL-33:  $36.3 \pm 4.6\%$ ), and AREG (w/o:  $28.4 \pm 0.8\%$ , IL-33:  $38.6 \pm 3.5\%$ ; Figure 20A). Of the markers analyzed, only Bcl-2 was not altered by IL-33 (Figure 20A). However, the addition of AREG to IL-33 did not result in further ST2<sup>+</sup> Treg activation beyond that induced by IL-33 alone (Figure 20A). In *Areg*<sup>-/-</sup> mice, exogenous IL-33 had a limited effect, only increasing the expression of KLRG1 (w/o:  $13.4 \pm 1.0\%$ , IL-33:  $17.6 \pm 0.7\%$ ) without inducing the expansion of ST2<sup>+</sup> Tregs or the expression of ICOS, Bcl-2, or the inhibitory molecules IL-10, PD-L1 and TIGIT (Figure 20B). Exogenous AREG did not further activate IL-33-stimulated *Areg*<sup>-/-</sup> ST2<sup>+</sup> Tregs (Figure 20B).

Collectively, the *in vitro* data demonstrate antagonistic effects of AREG stimulation on ILC2s and ST2<sup>+</sup> Tregs. Exogenous AREG reduced the number and activation of unstimulated or IL-33-stimulated hepatic ILC2s. In contrast, it increased the frequency and activation of unstimulated ST2<sup>+</sup> Tregs but could not further activate IL-33-stimulated ST2<sup>+</sup> Tregs. Exogenous AREG-mediated activation of Tregs was dependent on ST2 expression and the activating effect of exogenous AREG was diminished in AREG-deficient ST2<sup>+</sup> Tregs.



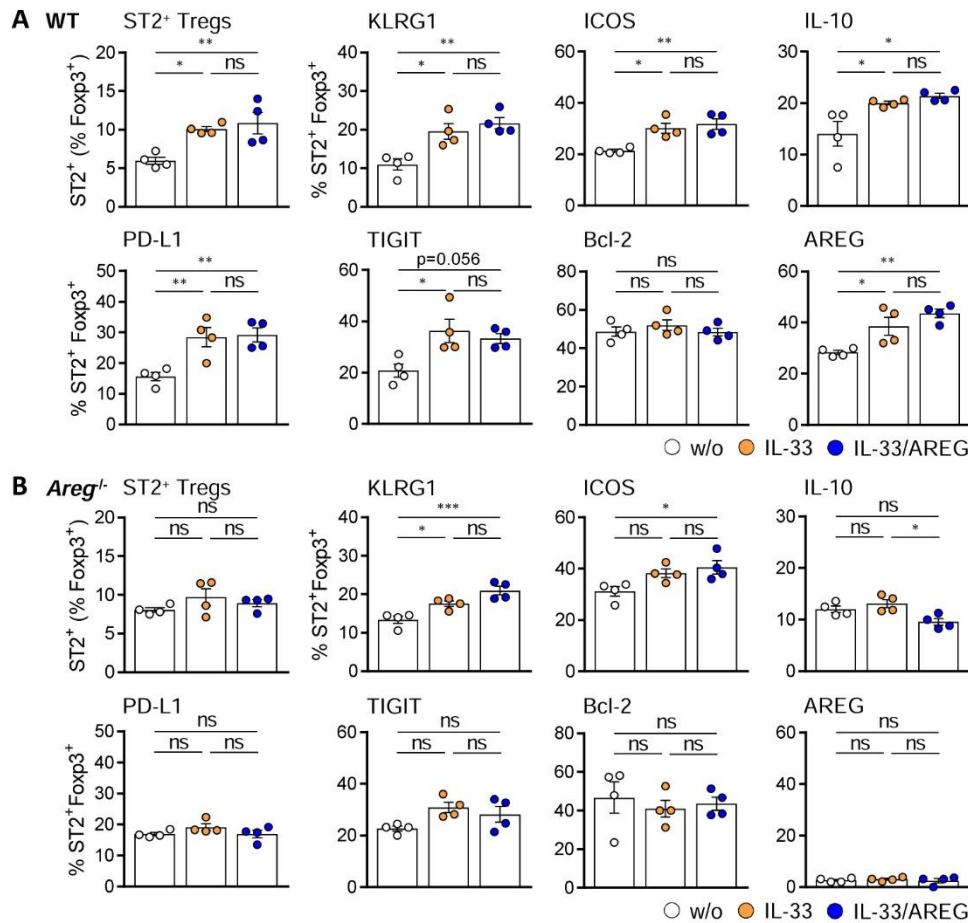


**Figure 20: Effect of exogenous AREG on IL-33-activated ST2<sup>+</sup> Tregs.** (A+B) Cell cultures of MACS-sorted CD25<sup>+</sup> CD4<sup>+</sup> Tregs from lymph nodes and spleens of naïve (A) WT and (B) *Areg*<sup>-/-</sup> mice were incubated in presence or absence of IL-33 or IL-33/AREG for 1.5 days. ST2<sup>+</sup> Foxp3<sup>+</sup> CD4<sup>+</sup> Treg frequency and phenotype were analyzed. Means ± SEM of one out of two experiments are shown. \*p< 0.05; \*\*p< 0.01; ns: not significant; w/o: without.

### 3.5 Impaired immunoregulatory capacity of *Areg*<sup>-/-</sup> Tregs

To elucidate the functional relevance of AREG expression in Treg-mediated immune regulation, we performed suppression assays with WT or *Areg*<sup>-/-</sup> Tregs and CD4<sup>+</sup> responder T cells. Suppression assays are co-cultures used to quantitatively analyze the capacity of Tregs to inhibit the proliferation of responder T cells.<sup>195</sup> To facilitate monitoring of proliferation, isolated responder T cells are labeled with an intracellular fluorescent dye prior to culture.<sup>196</sup> Cells are incubated with the membrane-permeant 5-(and-6)-carboxyfluorescein diacetate succinimidyl ester (CFDA-SE), which converts intracellularly to fluorescent 5-(and-6)-carboxyfluorescein succinimidyl ester (CFSE), stably marking cells by covalent binding to long-lived intracellular molecules.<sup>196,197</sup> CFSE is evenly distributed to the progeny cells, with the fluorescence being

sequentially halved with each cell division.<sup>198</sup> Therefore, flow cytometric analysis of responder T cell CFSE signal displays distinct peaks of fluorescence intensity, representing the respective cell cycle generations.<sup>196,198</sup> In this study, both CD25<sup>-</sup> CD4<sup>+</sup> responder T cells and CD25<sup>+</sup> CD4<sup>+</sup> Tregs were isolated by MACS from lymph nodes and spleens of naïve mice, responder T cells from WT mice and Tregs from WT or *Areg*<sup>-/-</sup> mice. To verify the functionality of the assay, a control group in which no Tregs were added was included in addition to the WT and *Areg*<sup>-/-</sup> Treg groups. Responder T cells were activated by the addition of anti-CD3/CD28 coated Dynabeads to the *in vitro* culture. After 2.5 days, cells were harvested and the frequency and AREG expression of Foxp3<sup>+</sup> CD4<sup>+</sup> Tregs was analyzed by flow cytometry, as well as the CFSE signal of Foxp3<sup>-</sup> CD4<sup>+</sup> responder T cells. The percentage inhibition of responder T cell proliferation was calculated by normalizing the frequency of proliferated CFSE<sup>low</sup> Foxp3<sup>-</sup> CD4<sup>+</sup> T cells to the control group without Tregs. We detected significant AREG expression in Foxp3<sup>+</sup> CD4<sup>+</sup> Tregs from WT mice, whereas deficient expression was confirmed in Tregs from *Areg*<sup>-/-</sup> mice (Figure 21A). Although the frequency of *Areg*<sup>-/-</sup> Tregs did not differ from their WT counterparts (Figure 21A), the frequency of proliferated CFSE<sup>low</sup> responder T cells was elevated in assays with *Areg*<sup>-/-</sup> Tregs compared to WT Tregs (Figure 21B, left). Therefore, the percentage inhibition of responder T cell proliferation was reduced in the absence of AREG-producing Tregs (Figure 21B, right).

To test whether the suppressive function of WT Tregs can be enhanced by exogenous AREG, we also cultured CD25<sup>+</sup> CD4<sup>+</sup> Tregs and CFSE-labeled CD25<sup>-</sup> CD4<sup>+</sup> responder T cells with Dynabeads in the presence or absence of exogenous AREG. After 2.5 days, the frequency of Foxp3<sup>+</sup> CD4<sup>+</sup> Tregs was analyzed by flow cytometry and the percentage inhibition of Foxp3<sup>-</sup> CD4<sup>+</sup> responder T cell proliferation was calculated. The frequency of Foxp3<sup>+</sup> Tregs was not altered in response to AREG (Figure 21C). Interestingly, supplementation with 100 ng/mL exogenous AREG did not increase the Treg-mediated inhibition of CD4<sup>+</sup> T cell proliferation (Figure 21D). The experiment was repeated with a second AREG concentration, 500 ng/mL, confirming the initial finding that exogenous AREG had no effect on the percentage of inhibition mediated by Tregs (data not shown). Thus, Treg-mediated suppression of CD4<sup>+</sup> T cell proliferation could not be reinforced by exogenous AREG but was impaired in the absence of endogenous AREG.

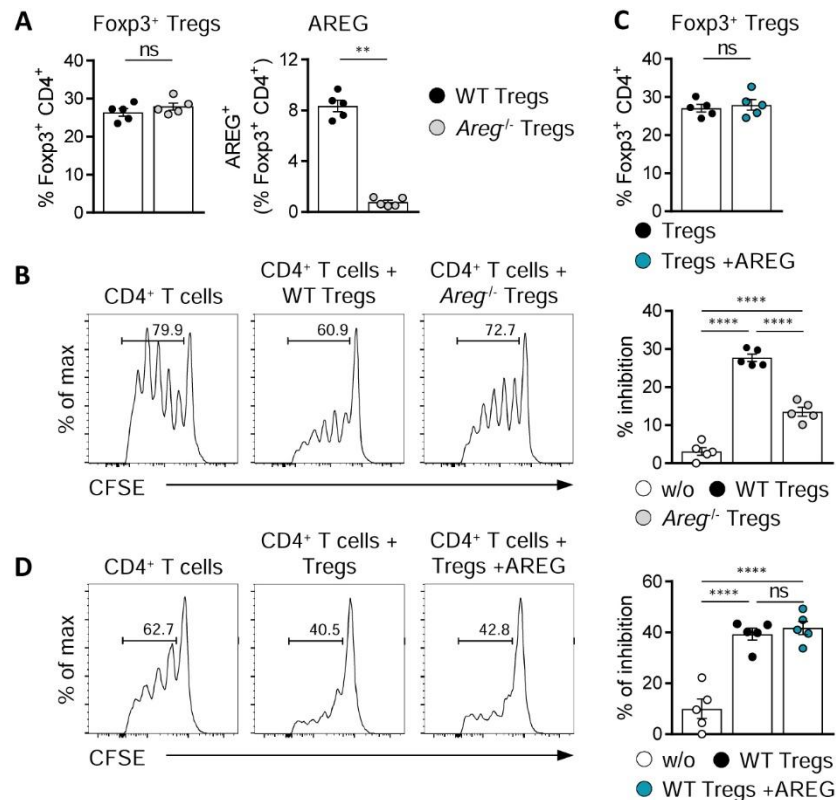


**Figure 21: AREG-dependent immunosuppressive function of Tregs.** CD25<sup>-</sup> CD4<sup>+</sup> responder T cells and WT or *Areg*<sup>-/-</sup> CD25<sup>+</sup> CD4<sup>+</sup> Tregs were MACS-sorted from lymph nodes and spleens of naïve WT or *Areg*<sup>-/-</sup> mice. (A+B) CFSE-labeled CD25<sup>-</sup> CD4<sup>+</sup> T cells were incubated with Dynabeads for 2.5 days in presence or absence of CD25<sup>+</sup> CD4<sup>+</sup> Tregs from WT and *Areg*<sup>-/-</sup> mice. (A) Frequency and AREG expression of Foxp3<sup>+</sup> CD4<sup>+</sup> Tregs were analyzed. (B) Representative histograms show frequencies of proliferating Foxp3<sup>+</sup> CD4<sup>+</sup> T cells. Besides, the percentage inhibition of Foxp3<sup>+</sup> CD4<sup>+</sup> T cell proliferation is displayed. (C+D) CD25<sup>-</sup> CD4<sup>+</sup> T cells were labeled with CFSE and activated in presence or absence of CD25<sup>+</sup> CD4<sup>+</sup> Tregs and AREG for 2.5 days. (C) The frequency of Foxp3<sup>+</sup> CD4<sup>+</sup> Tregs was determined. (D) Frequencies of proliferating Foxp3<sup>+</sup> CD4<sup>+</sup> T cells are depicted in representative histograms. Percentage inhibition of Foxp3<sup>+</sup> CD4<sup>+</sup> T cell proliferation was assessed. Means  $\pm$  SEM of one out of two experiments are shown. \* $p$  < 0.05; \*\* $p$  < 0.01; \*\*\* $p$  < 0.001; \*\*\*\* $p$  < 0.0001; ns: not significant; w/o: without.

### 3.6 Reduced capacity of ST2<sup>+</sup> Tregs to express AREG in chronic liver disease

Demonstrating the immunoregulatory role of AREG in acute hepatitis, we were also interested in investigating its involvement in chronic liver disease. In this context, AREG has previously been implicated as a driver of liver fibrogenesis.<sup>111</sup> In this study, we investigated the activation and AREG expression of hepatic ILC2s and ST2<sup>+</sup> Tregs by flow cytometry in a murine model of chronic liver disease. We used 12-week-old *Mdr2*<sup>-/-</sup> mice, a stage at which they fully develop portal inflammation and liver fibrosis resembling human PSC.<sup>40</sup> To determine disease progression in *Mdr2*<sup>-/-</sup> compared to WT mice, we analyzed different markers that identify specific disease characteristics. These include plasma ALT, which marks hepatocellular damage,<sup>42</sup> ALP and bilirubin,

which are characteristic of cholestatic injury,<sup>42</sup> and cholesterol, whose reduction in *Mdr2*<sup>-/-</sup> mice indicates altered cholesterol kinetics.<sup>43</sup> Further, we analyzed the concentration of hydroxyproline in liver tissue, a key component of collagen that accumulates in liver fibrosis.<sup>45</sup> To assess morphological changes in the liver tissue we also performed histological analysis of liver sections, including H&E staining, which provides an overview of tissue structure,<sup>171</sup> and selective staining of collagen fibers using Sirius red to visualize fibrotic areas.<sup>174</sup> In addition, we measured the gene expression of hepatic collagen type I  $\alpha$  1 chain (*Col1a1*) and type III  $\alpha$  1 chain (*Col3a1*), *Tgfb1* and *Tgfb2*, isoforms of the mediator of liver fibrosis TGF $\beta$ ,<sup>199</sup> and the inflammatory cytokines *Tnfa* and *Il12p40*.

We detected elevated plasma levels of ALT (WT:  $30 \pm 5$  U/L, KO:  $250 \pm 71$  U/L), ALP (WT:  $91 \pm 7$  U/L, KO:  $207 \pm 40$  U/L) and bilirubin in *Mdr2*<sup>-/-</sup> compared to WT mice (WT:  $0.05 \pm 0.01$  mg/dL, KO:  $0.41 \pm 0.21$  mg/dL; Figure 22A). Plasma cholesterol concentrations were reduced (WT:  $67.6 \pm 4.1$  mg/dL, KO:  $49.5 \pm 3.1$  mg/dL; Figure 22A). Further, we found elevated hydroxyproline levels in *Mdr2*<sup>-/-</sup> mice ( $3.2 \pm 0.2$ -fold; Figure 22B). H&E staining-revealed fibrotic patterns exclusively in the liver of *Mdr2*<sup>-/-</sup> mice, whereas WT tissue displayed a healthy structure (Figure 22C). Sirius red staining clearly visualized fibrotic regions in *Mdr2*<sup>-/-</sup> mice that were absent in WT mice (Figure 22C). These observations were confirmed by quantitative analysis of Sirius red staining (WT:  $10534 \pm 927$   $\mu\text{m}^2/\text{image}$ , KO:  $99252 \pm 16428$   $\mu\text{m}^2/\text{image}$ , Figure 22C). In accordance, the mRNA levels of collagen type I (*Col1a1*,  $18.3 \pm 9.1$ -fold) and III (*Col3a1*,  $9.6 \pm 3.2$ -fold) were upregulated in livers of fibrotic *Mdr2*<sup>-/-</sup> mice (Figure 22D). Moreover, chronic liver damage in *Mdr2*<sup>-/-</sup> mice was accompanied by increased mRNA levels of hepatic *Tgfb1* ( $1.8 \pm 0.3$ -fold) and *Tgfb2* ( $6.5 \pm 2.1$ -fold; Figure 22D). Finally, we observed elevated gene expression of *Tnfa* ( $5.9 \pm 0.7$ -fold) and *Il12p40* ( $3.7 \pm 1.0$ -fold) in the diseased livers (Figure 22E). Thus, at 12 weeks of age *Mdr2*<sup>-/-</sup> mice developed chronic liver disease characterized by increased hepatocellular damage, hepatic expression of inflammatory cytokines, altered cholesterol kinetics, cholestatic injury, and liver fibrosis.

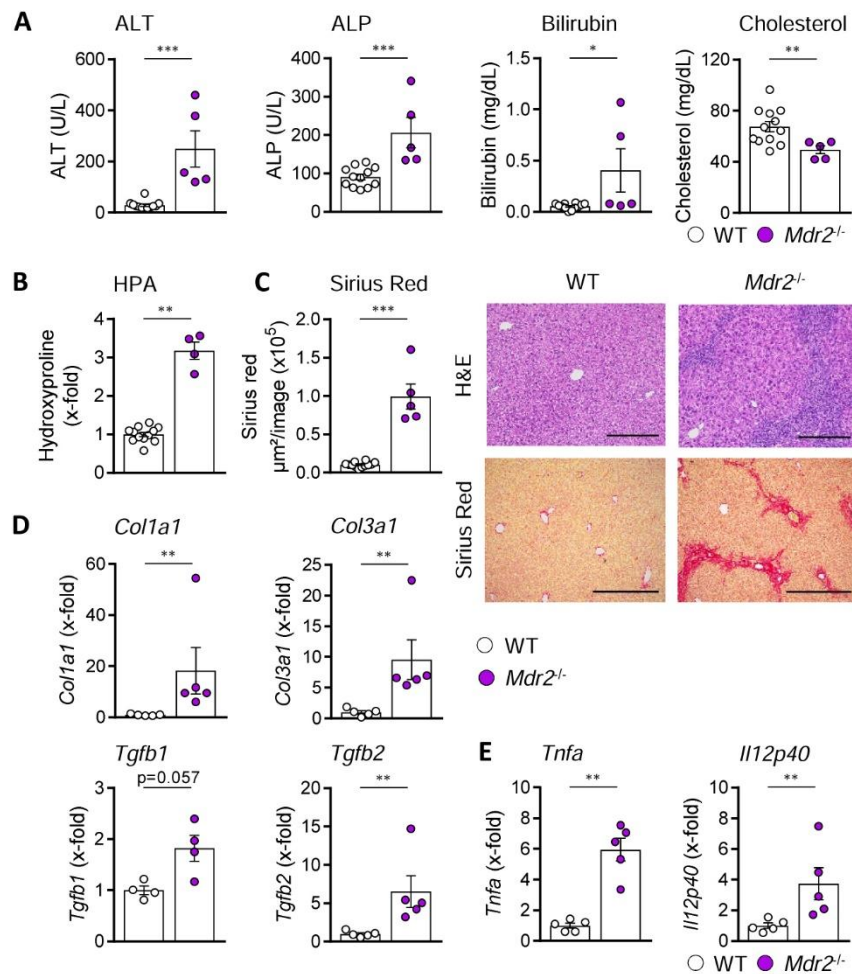


**Figure 22: Pathology of the *Mdr2*<sup>-/-</sup> mouse model of sclerosing cholangitis.** WT and *Mdr2*<sup>-/-</sup> mice were analyzed at the age of 12 weeks. (A) Plasma ALT, ALP, bilirubin, and cholesterol levels were measured. (B) Hydroxyproline (HPA) levels in the liver were assessed. (C) Liver sections were stained with H&E and Sirius Red to visualize fibrotic regions. Sirius red staining was quantified. (D) Liver mRNA expression of collagen type I (*Col1a1*) and III (*Col3a1*), and the TGF- $\beta$  isoforms *Tgfb1* and *Tgfb2* were detected. (E) Liver mRNA expression of *Tnfa* and *Il12p40* was analyzed. Bars indicate 200  $\mu$ m for H&E and 500  $\mu$ m for Sirius red staining. Means  $\pm$  SEM of one out of two experiments are shown. \* $p < 0.05$ ; \*\* $p < 0.01$ ; \*\*\* $p < 0.001$ .

Chronic liver injury in sclerosing cholangitis was associated with elevated expression of *Il33* mRNA ( $1.7 \pm 0.2$ -fold; Figure 23A). Furthermore, analysis of the EGFR ligands revealed an increased expression of *Areg*, *Btc*, and *Hbegf* mRNA in the livers of *Mdr2*<sup>-/-</sup> mice, with *Areg* being the most prominently upregulated growth factor ( $7.3 \pm 0.9$ -fold; Figure 23B). Similar to acute hepatitis, chronic liver injury resulted in an elevated frequency of hepatic ILC2s (WT:  $0.9 \pm 0.1\%$ , KO:  $2.7 \pm 0.2\%$ ; Figure 23C). However, the activation of hepatic ILC2s was not changed, as demonstrated by similar expression levels of KLRG1, IL-13 and AREG in *Mdr2*<sup>-/-</sup> and WT mice (Figure 23C). Also the frequency of ST2<sup>+</sup> Foxp3<sup>+</sup> Tregs was increased in *Mdr2*<sup>-/-</sup> compared to WT mice (WT:  $13.1 \pm 1.0\%$ , KO:  $17.9 \pm 0.9\%$ ; Figure 23D). The expression of KLRG1 was

not altered. Notably, the expression of the co-inhibitory receptor PD-1 by ST2<sup>+</sup> Tregs was upregulated in sclerosing cholangitis (WT: 15.4 ± 3.4%, KO: 36.3 ± 5.7%), whereas their production of AREG was substantially reduced (WT: 11.6 ± 1.6%, KO: 5.5 ± 1.2%; Figure 23D). Thus, chronic liver injury in *Mdr2*<sup>-/-</sup> mice was associated with an increased frequency of hepatic ILC2s and ST2<sup>+</sup> Tregs. In addition, ST2<sup>+</sup> Tregs exhibited elevated expression of PD-1 and reduced expression of AREG.

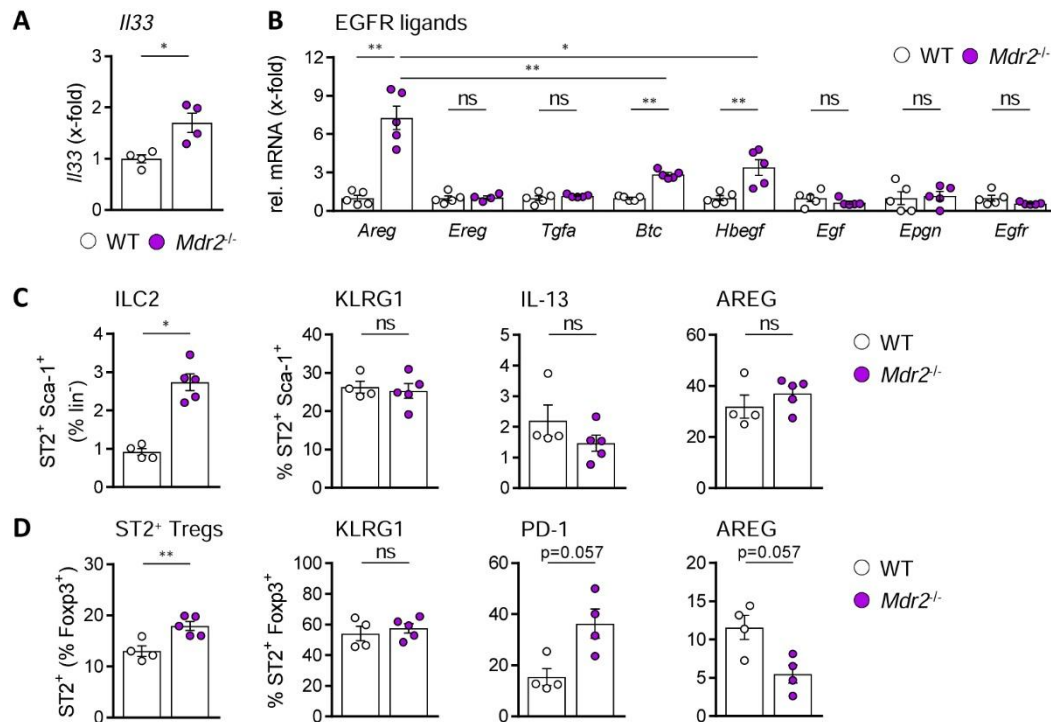


**Figure 23: Phenotype of ILC2s and ST2<sup>+</sup> Tregs in chronic liver disease.** WT and *Mdr2*<sup>-/-</sup> mice were analyzed at 12 weeks of age. (A-B) Liver mRNA expression of (A) *Il33*, as well as of (B) EGFR ligands and *Egfr* was analyzed. (C+D) The frequency and phenotype of hepatic (C) ST2<sup>+</sup> Sca-1<sup>+</sup> lin<sup>-</sup> ILC2s and (D) ST2<sup>+</sup> Foxp3<sup>+</sup> CD4<sup>+</sup> Tregs were assessed. Means ± SEM of one out of two experiments are shown. \*p < 0.05; \*\*p < 0.01; ns: not significant.

## 4 Discussion

Autoimmune liver diseases, including AIH and PSC, follow a progressive clinical trajectory that can lead to fibrosis, cirrhosis and ultimately liver cancer.<sup>10</sup> They significantly impact patient morbidity and mortality with limited treatment options available.<sup>17</sup> This highlights the need for a better understanding of the cellular and molecular processes that drive and regulate liver inflammation to develop targeted and effective therapeutic strategies. In AIH, the immune system targets and damages the liver parenchyma, whereas PSC is characterized by immune-mediated injury to the bile ducts.<sup>5,10</sup> Tissue destruction in AIH results in the release of IL-33 from necrotic hepatocytes.<sup>35,36</sup> Extracellular IL-33 can bind and activate various immune cells expressing the IL-33 receptor ST2 such as pro-inflammatory ILC2s and immunosuppressive Tregs,<sup>36</sup> which both express AREG following activation.<sup>114,132,133,140,141</sup> AREG is associated with the repair and regeneration of liver tissue<sup>108,114</sup> and immunosuppressive functions in viral liver infection,<sup>112,130</sup> but also with cholestatic liver disease,<sup>109</sup> fibrogenesis<sup>111</sup> and carcinogenesis<sup>137,189,200–206</sup> in chronic liver inflammation. However, the expression and function of AREG in acute and chronic immune-mediated liver diseases are still largely unknown. In this study, we described the immunoregulatory role of AREG in the mouse model of ConA-induced immune-mediated hepatitis, which shares some similarities with acute AIH,<sup>23</sup> and demonstrated differential effects on hepatic ILC2s and ST2<sup>+</sup> Tregs. Additionally, we observed exhausted hepatic ST2<sup>+</sup> Tregs with reduced AREG expression in *Mdr2*<sup>-/-</sup> mice with sclerosing cholangitis and liver fibrosis resembling human PSC.<sup>40</sup>

### 4.1 The EGFR ligands in acute and chronic liver disease

Since previous studies have indicated a major role of the EGF receptor and its ligands in liver regeneration after acute and chronic liver injury, as well as in fibrosis and cirrhosis,<sup>116</sup> we examined their gene expression and regulation in ConA-induced acute immune-mediated hepatitis and *Mdr2*<sup>-/-</sup> mice with chronic liver disease.

Acute liver injury (Figure 12A+B) was associated with an upregulation of the growth factors *Areg*, *Ereg*, *Hbegf* and *Ep gn* (Figure 12D). In this study, we focused on the role of AREG, which was one of the most upregulated members of the EGF family in

immune-mediated hepatitis (Figure 12D). In addition, we found significantly elevated serum AREG levels in ConA-treated compared to healthy PBS-treated mice (Figure 12C). Our findings are congruous with AREG expression levels in other models of acute liver disease and regeneration. AREG protein and mRNA levels were also strongly upregulated in Fas-mediated acute liver injury,<sup>129</sup> as was *Areg* gene expression in carbon tetrachloride (CCl<sub>4</sub>)-induced acute liver injury.<sup>207</sup> Also after partial hepatectomy and partial liver transplantation, both established models of liver regeneration, elevated levels of AREG protein and mRNA were detected in the liver.<sup>108,208</sup> Moreover, hepatic AREG protein and mRNA levels were increased in mice with cholestatic liver injury after bile duct ligation or alpha-naphthyl-isocyanate (ANIT) gavage,<sup>109</sup> and bile acids induced *Areg* gene expression in primary mouse hepatocytes and cholangiocytes.<sup>109</sup> Furthermore, elevated levels of AREG protein have been observed in the serum and liver following HBV infection.<sup>112,130</sup> Specifically, increased AREG mRNA and protein expression after HBV infection has been determined in intrahepatic macrophages and hepatocytes.<sup>130</sup> The role of AREG in acute liver disease and regeneration has previously been studied in various experimental models. Analysis of naïve *Areg*<sup>-/-</sup> mice revealed signs of chronic liver injury, and the survival of *Areg*<sup>-/-</sup> mice was reduced following lethal doses of Fas-agonist antibody.<sup>129</sup> However, sublethal Fas-mediated liver injury was reduced in mice lacking AREG, possibly because pre-existing liver damage can precondition hepatocytes against cell death.<sup>129</sup> AREG pretreatment abrogated Fas-mediated liver injury and apoptosis in WT and *Areg*<sup>-/-</sup> mice.<sup>129</sup> Furthermore, AREG has been shown to act as a primary mitogen through the EGFR in cultured rat hepatocytes,<sup>108</sup> and *Areg*<sup>-/-</sup> rats exhibited diminished proliferative responses after partial hepatectomy.<sup>108</sup> After partial liver transplantation in mice, AREG neutralizing antibody impaired regeneration in 50% liver grafts, while AREG treatment enhanced regeneration, function, and survival of 30% liver grafts.<sup>208</sup> AREG has also been reported to protect against cholestatic liver injury.<sup>109,114</sup> *Areg*<sup>-/-</sup> mice developed more severe cholestatic liver injury after bile duct ligation and ANIT gavage, while AREG treatment alleviated ANIT-induced cholestatic liver injury and attenuated bile acid synthesis and toxicity in primary mouse hepatocytes.<sup>109</sup> In addition, AREG promoted tissue repair in rotavirus-induced experimental biliary atresia.<sup>114</sup> Finally, AREG has been demonstrated to reinforce the immunosuppressive activity of hepatic Tregs following HBV infection in mice, thereby inhibiting antiviral immune responses.<sup>112,130</sup> Taken together, AREG plays a multifaceted role in acute liver



conditions by mitigating bile acid toxicity and hepatocyte apoptosis, promoting hepatocyte proliferation and liver regeneration, and enhancing the immunoregulatory function of Tregs.

The elevated gene expression of *Ereg* in ConA-induced hepatitis also aligns with previous findings in other models of acute liver disease and regeneration. *Ereg* mRNA expression was upregulated after Fas- and CCl<sub>4</sub>-mediated acute liver injury,<sup>129,207</sup> as was EREG protein expression in remnant livers after partial hepatectomy.<sup>120</sup> Moreover, hepatic EREG protein and mRNA, as well as serum EREG levels, were elevated following 3,5-diethoxycarbonyl-1,4-dihydrocollidine (DDC)-induced liver injury in mice, with hepatic EREG expressed around ductular structures close to the portal area.<sup>209</sup> Similarly, serum EREG levels were increased in patients with acute liver failure but not in patients with acute hepatitis.<sup>209</sup> Functionally, EREG has been shown to stimulate the proliferation of cultured mouse liver progenitor cells<sup>209</sup> and rat hepatocytes.<sup>120,122</sup> Finally, overexpression of EREG in mouse liver has been reported to induce liver progenitor cells and enhance DNA synthesis in hepatocytes.<sup>209</sup>

The elevated hepatic *Hbegf* expression found in this study is also consistent with previous findings. HB-EGF protein and mRNA have also been shown to be increased after partial hepatectomy in rats.<sup>210</sup> Specifically, *Hbegf* gene expression has been detected in LSECs and Kupffer cells, but not in HSCs or hepatocytes.<sup>210</sup> In addition, mRNA and protein levels were induced in injured rat livers following CCl<sub>4</sub> treatment, as was hepatic *Hbegf* mRNA in rat D-galactosamine-<sup>211</sup> and mouse CCl<sub>4</sub>-induced liver injury.<sup>207</sup> However, gene expression of *Hbegf* was unchanged in Fas-mediated liver injury in mice.<sup>129</sup> HB-EGF has been found to stimulate DNA synthesis *in vivo* in mouse hepatocytes<sup>212</sup> and *in vitro* in primary rat hepatocyte cultures.<sup>124,213</sup> Moreover, HB-EGF treatment reduced TNF $\alpha$ -induced apoptosis and facilitated wound healing of a mouse hepatocyte cell line.<sup>207</sup> Upregulation of *Hbegf* gene expression has been reported to precede the start of DNA replication following two-thirds partial hepatectomy in mice.<sup>214</sup> In contrast, *Hbegf* levels were not increased following one-third partial hepatectomy with little DNA replication.<sup>214</sup> Similarly, plasma HB-EGF levels were elevated in patients who underwent large partial hepatectomy, but not in those who had minor partial hepatectomy.<sup>215</sup> Congruently, hepatocyte DNA replication following two-thirds partial hepatectomy was delayed in *Hbegf*<sup>-/-</sup> mice, and hepatocyte DNA replication after

one-third partial hepatectomy in mice was improved by HB-EGF treatment.<sup>214</sup> Liver-specific overexpression of HB-EGF in transgenic mice promoted hepatocyte proliferation and liver regeneration after partial hepatectomy.<sup>216</sup> CCl<sub>4</sub>-induced liver injury was exacerbated in the absence of hepatic HB-EGF in conditional knockout mice,<sup>207</sup> while injection of HB-EGF prevented liver injury and apoptosis of Fas-mediated fulminant hepatic failure.<sup>217</sup> Furthermore, adenoviral HB-EGF gene transduction inhibited liver injury and apoptosis in Fas-induced liver injury,<sup>218</sup> reduced acute cholestatic liver injury after bile duct ligation,<sup>219</sup> and enhanced hepatocyte proliferation in both conditions.<sup>218,219</sup> Overall, HB-EGF is a hepatotropic factor that exhibits anti-apoptotic properties and mediates regeneration and hepatocyte proliferation following acute liver injury or resection. Thus, it may also exert these functions in acute immune-mediated hepatitis.

*Epgn* mRNA has previously been detected in the murine liver and has been shown to stimulate the proliferation of a keratinocyte cell line.<sup>128</sup> However, the expression of EPGN mRNA or protein, as well as its functional role, have not been investigated in the context of liver disease. The increase in *Epgn* mRNA levels in immune-mediated hepatitis observed in this study suggests a potential role in liver disease and highlights the need for further research to elucidate its functional implications and underlying mechanisms.

In *Mdr2*<sup>-/-</sup> mice, the EGFR ligands *Areg*, *Btc* and *Hbegf* were upregulated, with *Areg* showing a significantly higher level of upregulation compared with the other EGFR ligands (Figure 23B). In line with our findings, Santamaria E et al. demonstrated an age-dependent increase in hepatic *Areg* gene expression in *Mdr2*<sup>-/-</sup> mice aged 4-17 months, likely indicating disease progression.<sup>109</sup> Moreover, *Areg* mRNA was elevated in the livers of cirrhotic patients<sup>108</sup> and in CCl<sub>4</sub>-induced fibrotic mouse<sup>111</sup> and cirrhotic rat livers.<sup>108</sup> AREG protein and mRNA levels were also upregulated in the livers of fibrotic patients with severe NASH, as well as *Areg* mRNA in the livers of mice with diet-induced NASH.<sup>110</sup> In addition, elevated levels of AREG protein have specifically been observed in HSCs isolated from mice with diet-induced NASH.<sup>110</sup> Finally, hepatic AREG protein and mRNA levels were increased in patients with cirrhotic PBC and PSC.<sup>109</sup> Functionally, AREG has been shown to promote liver fibrosis. CCl<sub>4</sub>-induced liver fibrosis was attenuated in *Areg*<sup>-/-</sup> mice.<sup>111</sup> While Tregs have been found to be a

major producer of *Areg* mRNA among immune cells in CCl<sub>4</sub>-treated inflamed livers, the lack of Treg-derived AREG in Foxp3<sup>Cre</sup> x Areg<sup>fl/fl</sup> mice did not affect the development of liver fibrosis.<sup>113</sup> However, direct treatment of liver fibrogenic cells with AREG stimulated cell activation and proliferation, suppressed apoptosis, and induced the expression of fibrogenic markers.<sup>110,111</sup>

Consistent with our findings in *Mdr2*<sup>-/-</sup> mice with chronic liver disease, elevated hepatic *Btc* gene expression has also been reported in mouse models of CCl<sub>4</sub>-induced liver fibrosis and western diet-induced NASH, as well as in patients with NASH<sup>220</sup> and liver cancer.<sup>220,221</sup> Functionally, BTC has been shown to stimulate the proliferation of an HSC cell line and induce the production of TGFβ2 and collagen.<sup>220</sup> It also supported microbial signals in the induction of integrin production by macrophages *in vitro*.<sup>220</sup> These findings suggest that BTC plays a significant role in promoting liver fibrosis and inflammation.<sup>220</sup>

Unlike the pro-fibrotic role of AREG, the role of HB-EGF in chronic liver disease is contradictory. In accordance with the elevated expression of hepatic *Hbegf* mRNA in fibrotic *Mdr2*<sup>-/-</sup> mice observed in this study, its expression was also increased in bile duct ligation-induced fibrotic livers in mice.<sup>222</sup> *Hbegf* mRNA in primary HSCs and hepatic HB-EGF protein were also upregulated in CCl<sub>4</sub>-induced liver fibrosis.<sup>223</sup> Moreover, *Hbegf* gene expression positively correlated with the degree of liver fibrosis in chronic liver disease patients.<sup>222</sup> In addition, *Hbegf* levels were elevated in rat hepatocytes during thioacetamide (TAA)-induced liver fibrosis.<sup>224</sup> Contrarily, hepatic *Hbegf* has been shown to be reduced in TAA-induced liver fibrosis in mice and in primary hepatocyte cultures in response to the pro-fibrotic cytokine TGFβ1.<sup>225</sup> However, this study also found HB-EGF to decrease its own gene expression in primary cultured HSCs, suggesting a negative feedback loop and potentially explaining its downregulation.<sup>225</sup> Interestingly, *Hbegf*<sup>-/-</sup> mice exhibited increased fibrosis in response to TAA- and CCl<sub>4</sub>-induced chronic liver injury<sup>225</sup> and conditional loss of hepatic HB-EGF resulted in enhanced liver fibrosis after bile duct ligation.<sup>222</sup> Adenoviral HB-EGF gene transduction reduced biliary infarcts, hepatocyte apoptosis, fibrotic lesions and cholangiocyte proliferation during the chronic phase of bile duct ligation-induced cholestatic liver injury.<sup>219</sup> Furthermore, HB-EGF attenuated the expression of fibrosis-related genes in murine primary cultured HSCs<sup>222,225</sup> and promoted their

migration.<sup>225</sup> In contrast to its anti-fibrotic effects in chronic liver disease, HB-EGF has also been demonstrated to exert pro-fibrotic effects. Specifically, transgenic mice overexpressing HB-EGF developed more severe liver fibrosis in response to CCl<sub>4</sub> treatment or bile duct ligation.<sup>223</sup>

These results indicate distinct roles of the EGFR ligands during liver disease and regeneration. This study, in line with previous studies in a variety of acute and chronic liver conditions, showed upregulated AREG and HB-EGF expression in both acute and chronic liver disease. Both growth factors are known to function protective and regenerative after acute liver injury, and pro-fibrotic during chronic liver disease. However, HB-EGF, has previously been shown to be regulated differentially depending on the specific chronic liver disease and act either pro- or anti-inflammatory. Moreover, according to the current state in research, the anti-inflammatory role of AREG is unique among the EGFR ligands. In this study, EREG and EPGN were only upregulated during acute-immune mediated hepatitis, while BTC was only upregulated during chronic liver disease. Thus, AREG appears to play diverse roles in various acute and chronic liver conditions, while other growth factors may exhibit more distinct expression patterns and functions. In this study, we further focused on the immunoregulatory role of AREG in acute immune-mediated hepatitis and chronic sclerosing cholangitis.

#### 4.2 Exogenous IL-33 induces AREG expression in hepatic ST2<sup>+</sup> Tregs and ILC2s

In order to better understand the signaling pathways of the IL-33/AREG axis in hepatic immune regulation, we were interested in investigating the cell-specific expression of AREG by lymphocytes in the livers of mice treated with IL-33. Since Tregs<sup>132,140,141</sup> and ILC2s<sup>114,133,226</sup> have previously been shown to express AREG in different organs in response to IL-33, we focused on these two hepatic lymphocyte populations. Recently, IL-33-induced AREG expression by ILC2s has been reported in the liver.<sup>114</sup> Also hepatic Tregs have been shown to express AREG in fibrotic mice.<sup>113</sup> However, the contribution of IL-33 to AREG expression in hepatic Tregs has not been specifically investigated.<sup>113</sup>

IL-33 is well-documented to promote the expansion<sup>151,152</sup> and activation<sup>151,227</sup> of ST2<sup>+</sup> Tregs *in vitro*. In this study, we confirmed the direct stimulatory effect of exogenous

IL-33 on ST2<sup>+</sup> Tregs *in vitro* (Figure 17). Furthermore, we observed an expansion of ST2<sup>+</sup> Tregs in the livers of mice treated with IL-33 (Figure 9C), consistent with previous findings in both healthy<sup>228,229</sup> and diseased tissues,<sup>227,230–234</sup> including the healthy liver.<sup>235</sup> Moreover, IL-33 is known to activate Tregs that upregulate markers such as ICOS and CTLA-4 in the healthy spleen<sup>228,229</sup> and Ki-67 in both healthy<sup>235</sup> and diseased liver.<sup>233</sup> In our study, we extended these observations by demonstrating that IL-33 promotes activation, proliferation and survival of hepatic Tregs expressing the IL-33 receptor ST2. Specifically, we found increased expression levels of the activation markers KLRG1 and ICOS, the inhibitory molecules CTLA-4, PD-L1 and TIGIT, the proliferation marker Ki-67, and the anti-apoptotic protein Bcl-2 (Figure 9C). Most interestingly, we discovered an increased expression of AREG by ST2<sup>+</sup> Tregs in IL-33- compared to PBS-treated mice (Figure 9C), describing for the first time the stimulatory effect of IL-33 on AREG expression by hepatic Tregs. Finally, our *in vitro* experiments confirmed that exogenous IL-33 directly induces AREG expression in ST2<sup>+</sup> Tregs (Figure 11).

Exogenous IL-33 also expands<sup>92,236,237</sup> and activates ILC2s,<sup>92,95,133,150,226,236,237</sup> as shown *in vitro*. Moreover, ILC2s are known to expand<sup>35,92,226,231,238–241</sup> and become activated<sup>92,237,239,242</sup> in various organs and tissues in response to IL-33 treatment. In line with previous publications from our working group,<sup>35,92</sup> this study demonstrates an expansion of hepatic ILC2s following administration of IL-33 (Figure 10). Steinmann S et al. also showed an increased activation of hepatic ILC2s in response to IL-33 treatment, with an elevated frequency of the activation marker KLRG1.<sup>92</sup> In addition to confirming this finding, we also found elevated levels of the effector cytokine IL-13 in IL-33- compared to PBS-treated mice (Figure 10). Most importantly, we observed increased AREG expression by hepatic ILC2s in response to IL-33 treatment (Figure 10), a finding first described by Russi AE et al.<sup>114</sup> Finally, we also determined the stimulatory effect of exogenous IL-33 on hepatic ILC2s *in vitro*. Consistent with Steinmann S et al.,<sup>92</sup> IL-33 directly stimulated the expansion and activation of hepatic ILC2s (Figure 18B). Furthermore, we found elevated AREG expression in response to exogenous IL-33 (Figure 11), demonstrating its direct function in inducing AREG production by ILC2s.

### 4.3 AREG-expressing cell types in acute immune-mediated hepatitis

Since hepatic ST2<sup>+</sup> Tregs and ILC2s express AREG in response to exogenous IL-33 (Figure 9-11) and IL-33 is released from necrotic hepatocytes during tissue destruction in AIH,<sup>35,36</sup> we aimed to determine whether AREG is induced in these immune cells in ConA-induced immune-mediated hepatitis. Our research group has previously demonstrated that ST2<sup>+</sup> Tregs accumulate in the inflamed livers of ConA-treated mice, along with an increase in pro-inflammatory ST2<sup>+</sup> ILC2s, which upregulate their effector cytokines IL-5 and IL-13.<sup>35</sup> To further elucidate the role of ST2<sup>+</sup> Tregs and ILC2s in acute immune-mediated hepatitis, we examined their expression of AREG along with their activation status and phenotypic profiles. AREG derived from mast cells,<sup>117</sup> basophils,<sup>135</sup> and hepatic macrophages<sup>112</sup> has previously been shown to strengthen Treg-mediated immune suppression. In addition, AREG is associated with the repair and regeneration of liver tissue.<sup>108,114</sup> To focus on the immunoregulatory role of AREG, we specifically analyzed the early inflammatory stage of the disease, before the onset of liver regeneration processes.<sup>243</sup>

Similar to the response observed with IL-33 treatment (Figure 9-10), both hepatic ST2<sup>+</sup> Tregs and ILC2s expanded, showed a more activated state and increased AREG expression in immune-mediated hepatitis (Figure 12). AREG expression by hepatic Tregs has also previously been observed in the inflamed and fibrotic livers of CCl<sub>4</sub>-treated mice.<sup>113</sup> Hepatic ILC2s have also been shown to express AREG in patients with end-stage inflammatory liver diseases.<sup>106</sup>

In the liver, AREG is produced not only by lymphocytes such as Tregs<sup>113</sup> and ILC2s,<sup>106,114</sup> but also by parenchymal and mesenchymal cells, including hepatocytes,<sup>108</sup> cholangiocytes<sup>109</sup> and HSCs.<sup>110,111</sup> In this study, we performed immunohistochemical staining of AREG in liver tissue to determine whether tissue cells like hepatocytes, cholangiocytes and HSCs produce AREG and to gain insight into the localization of its expression in immune-mediated hepatitis. However, all of the antibodies tested showed non-specific binding to necrotic regions in the livers of ConA-treated mice, as demonstrated by pronounced staining in liver sections from ConA-treated *Areg*<sup>-/-</sup> mice (Figure 13). Consequently, it was not feasible to determine the localization of AREG expression in the liver tissue. Non-specific staining could not

have been detected without the use of samples from *Areg*<sup>-/-</sup> mice, as there were strong differences in AREG staining between the healthy and diseased groups (Figure 13), and no staining was detected in negative controls in which either primary or secondary antibodies were not applied (data not shown). Previously, AREG expression has been detected immunohistochemically in cholangiocytes and hepatocytes of mouse liver after cholestatic injury (same immunogen as antibody #2, Figure 13, Table 7).<sup>109</sup> In patients with PBC and PSC, AREG was expressed by hepatocytes located mainly at the edge of regenerative nodules and surrounding fibrotic tissue, and by cholangiocytes of small bile ducts in fibrotic tissues (same immunogen as antibody #2, Figure 13, Table 7).<sup>109</sup> Moreover, AREG was stained in CD3<sup>+</sup> and CD3<sup>-</sup> cells from healthy human liver tissue from end-stage liver disease patients (immunogen: human AREG aa1-155)<sup>106</sup> and in HSCs from severely fibrotic NASH patients (antibody not commercially available).<sup>110</sup> AREG has also been immunohistochemically stained in other organs, such as rat prostate (immunogen: human AREG aa1-155),<sup>244</sup> mouse lung (antibody #1, Figure 13, Table 7)<sup>245</sup> and ear skin from transgenic mice with a cutaneous psoriasis-like phenotype (antibody not commercially available),<sup>246,247</sup> as well as in human colon (antibody #2, Figure 13, Table 7),<sup>248</sup> breast carcinoma (antibodies not commercially available)<sup>249,250</sup> and cranial nerve schwannoma (immunogen: human AREG aa1-155).<sup>251</sup> However, none of the animal studies included liver samples from *Areg*<sup>-/-</sup> rats or mice as controls. Among the limited number of commercially available anti-mouse AREG antibodies, in this study we evaluated three antibodies from different suppliers, each targeting distinct immunogens (Figure 13, Table 7). The non-specific binding of antibodies to necrotic liver tissues may result from changes in tissue architecture that expose various epitopes, enabling interactions with unintended targets. Necrosis and the inflammatory environment may also induce the expression of proteins structurally similar to AREG, while enhancing antibody binding affinity for these proteins, leading to cross-reactivity. The quality of the antibodies, including specificity, purity, and polyclonality, may contribute to these binding challenges. Future studies using more specific antibodies will be valuable to examine AREG expression in the inflamed liver during immune-mediated hepatitis. Investigating the localization of AREG may reveal patterns of accumulation at sites of inflammation and necrosis.

Further, we analyzed AREG production by primary hepatocyte cultures. Interestingly, AREG accumulated over 24 hours in the supernatant of unstimulated hepatocytes (Figure 14A). Next, we investigated whether inflammatory cytokines that play a role in ConA-induced immune-mediated hepatitis stimulate *Areg* mRNA and AREG protein expression by primary hepatocytes *in vitro*. Of the stimuli tested - IL-33, TNF $\alpha$ , IFN $\gamma$ , IL-1 $\beta$ , TGF $\beta$  and AREG - *Areg* mRNA levels increased only in response to exogenous AREG, suggesting a self-induction mechanism (Figure 14C). AREG protein expression was not upregulated by any of the cytokines analyzed (Figure 14B). However, the effect of AREG stimulation on AREG protein expression could not be assessed due to the experimental limitation of distinguishing between supplemented and endogenously produced AREG. AREG has previously been shown to induce its own gene expression in a human HCC cell line,<sup>137</sup> a human HSC cell line, primary mouse HSCs and myofibroblasts,<sup>111</sup> secondary human keratinocytes,<sup>136</sup> human metastatic colon cancer cell lines<sup>138</sup> and a rat vascular smooth muscle cell line.<sup>139</sup> Aside from AREG, neither exogenous IL-33 nor the other cytokines linked to immune-mediated hepatitis induced AREG expression by primary hepatocytes *in vitro* (Figure 14B+C). This is surprising since IL-33,<sup>114,132,133,140,141</sup> TNF $\alpha$ ,<sup>188–190</sup> IFN $\gamma$ ,<sup>191</sup> IL-1 $\beta$ ,<sup>108,188,192</sup> and TGF $\beta$ <sup>193</sup> are known to induce AREG expression in various other cell types and organs. Notably, AREG protein and *Areg* mRNA levels were even decreased in response to exogenous IL-33 (Figure 14B+C). This demonstrates a differential effect of exogenous IL-33 on AREG expression by hepatocytes compared to hepatic ST2<sup>+</sup> Tregs and ILC2s (Figure 11).

#### 4.4 Protective role of AREG in acute immune-mediated hepatitis

Having established that hepatic ST2<sup>+</sup> Tregs and ILC2s upregulate AREG expression in ConA-induced immune-mediated hepatitis (Figure 12E+F), we next examined its role in modulating immune responses during the acute phase of the disease. Interestingly, we observed that *Areg*<sup>-/-</sup> mice treated with ConA exhibited more severe liver tissue damage compared to WT counterparts (Figure 15B+C), suggesting that AREG may have a protective function in mitigating acute liver injury. Consistently, the absence of AREG was associated with increased hepatic mRNA levels of *Tnfa*, *Ifng*, *Cxcl9*, *Cxcl10* and *Cxcr3* (Figure 15D). TNF $\alpha$  and IFN $\gamma$  are key drivers of liver damage in immune-mediated hepatitis.<sup>24,33</sup> CXCL9 and CXCL10, which are induced by IFN $\gamma$  in immune-mediated hepatitis,<sup>194</sup> are chemokines that can be secreted by hepatocytes,



HSCs, and LSECs at sites of inflammation and tissue damage to attract specific immune cells expressing the receptor CXCR3, such as T cells or NKT cells.<sup>252</sup> Moreover, CXCL10 was shown to drive Toll-like receptor 4 (TLR4)-mediated hepatocyte apoptosis independently of CXCR3 in ConA-induced acute liver injury.<sup>253</sup> In contrast, the gene expression of the anti-inflammatory cytokine *Il10* was also upregulated in *Areg*<sup>-/-</sup> mice compared to WT mice (Figure 15D), suggesting an inflammation-induced immunoregulatory response. This may be mediated by Tregs, as IL-10 is a key cytokine produced by these regulatory cells.<sup>47</sup>

In line with the increased disease severity observed in *Areg*<sup>-/-</sup> mice (Figure 15B+C), pro-inflammatory ILC2s were more activated in the inflamed livers of these mice, characterized by higher expression of the activation marker KLRG1 and the effector cytokine IL-13 (Figure 15F). IL-33-activated ILC2s are known to aggravate liver inflammation and liver tissue damage in ConA-treated mice.<sup>35</sup> Furthermore, the frequency of total hepatic Foxp3<sup>+</sup> Tregs was increased in the absence of AREG during immune-mediated hepatitis (Figure 15E), likely contributing to the elevated levels of *Il10* mRNA (Figure 15D). However, the frequency of hepatic ST2<sup>+</sup> Foxp3<sup>+</sup> Tregs was reduced in ConA-treated *Areg*<sup>-/-</sup> mice compared to WT mice (Figure 15E). These Tregs also exhibited higher levels of the anti-apoptotic protein Bcl-2 (Figure 15E), likely compensating for their reduced frequency by enhancing their stability in the absence of AREG. This suggests that AREG may play a role in supporting the survival of protective ST2<sup>+</sup> Tregs.

AREG is also known for its role in tissue repair and recovery. It has been demonstrated to prevent liver cell death<sup>129</sup> and support liver regeneration by stimulating hepatocyte proliferation.<sup>108</sup> In addition, ILC2-derived AREG has been shown to mediate tissue protection in models of infectious lung injury,<sup>133</sup> intestinal inflammation,<sup>134</sup> and biliary atresia.<sup>114</sup> Similarly, AREG produced by Tregs contributed to protective effects in acute muscle injury,<sup>131</sup> viral lung infection,<sup>132</sup> and ischemic brain injury.<sup>254</sup> AREG functions through ligand binding to the EGFR on the cell surface.<sup>115</sup> Ligand binding to the EGFR can activate intracellular signaling pathways that regulate cellular motility, apoptosis and cell cycle progression.<sup>118,119</sup> AREG is known to exert two distinct effects: it drives proliferation in certain cell types<sup>107,255</sup> while promoting differentiation in others.<sup>107,131</sup> Both functions may facilitate tissue repair by inducing the expansion of surviving tissue

cells and the differentiation of tissue-resident progenitor cells. However, the mechanism by which AREG mediates these differential effects remain unknown.<sup>107</sup> Unlike most other EGFR ligands, AREG binds to the EGFR with low affinity, which prevents receptor internalization and enables sustained downstream signaling.<sup>107</sup> This prolonged signaling results in stable extracellular signal-regulated kinase (ERK) activation, promoting growth arrest and cell differentiation.<sup>107</sup> High-affinity EGFR ligands, in contrast, induce EGFR internalization and degradation, creating negative feedback loops and repetitive ERK activation, ultimately generating a mitogenic signal in the recipient cell.<sup>107</sup> AREG might collaborate with other mitogens to mediate a potent mitogenic stimulus. In this context, it is suggested that it supports the activity of the epithelial mitogen insulin-like growth factor-1 (IGF-1).<sup>107</sup> AREG may also exert a tissue-protective effect in immune-mediated hepatitis. However, this effect does not play a role in this study, as we specifically examined the early inflammatory phase of immune-mediated hepatitis, which precedes the onset of liver regeneration processes.<sup>243</sup>

#### 4.5 Differential effect of AREG on ST2<sup>+</sup> Tregs and ILC2s

Next, we conducted a series of experiments to assess the effect of endogenous and exogenous AREG on ST2<sup>+</sup> Tregs and hepatic ILC2s. In addition to examining its role in ConA-induced immune-mediated hepatitis, we investigated whether IL-33-mediated activation of ST2<sup>+</sup> Tregs and ILC2s depends on endogenous AREG expression by analyzing the consequences of AREG deficiency on these cells in IL-33-treated *Areg*<sup>-/-</sup> mice. To further elucidate the effect of AREG on these cells, we performed cell culture experiments in which naïve or IL-33-activated ST2<sup>+</sup> Tregs or ILC2s were incubated with exogenous AREG. These experiments were performed with ST2<sup>+</sup> Tregs from WT and *Areg*<sup>-/-</sup> mice. Moreover, we determined the impact of exogenous AREG or lack of endogenous AREG on the capacity of Tregs to suppress CD4<sup>+</sup> T cell proliferation. Interestingly, we showed distinct effects of AREG on ST2<sup>+</sup> Tregs and ILC2s.

We found that the frequency of hepatic ST2<sup>+</sup> Foxp3<sup>+</sup> Tregs was diminished in *Areg*<sup>-/-</sup> compared to WT mice following both ConA (Figure 15E) and IL-33 treatment (Figure 16A). This reduction occurred despite an overall increase in Foxp3<sup>+</sup> Treg numbers and elevated expression of the anti-apoptotic protein Bcl-2 in hepatic ST2<sup>+</sup>

Tregs during acute hepatitis (Figure 15E), as well as enhanced proliferation of these cells in IL-33-treated mice (Figure 16A). Furthermore, *Areg*<sup>-/-</sup> Tregs exhibited a reduced efficacy in suppressing CD4<sup>+</sup> T cell activation (Figure 21B). These findings indicate that the survival and function of ST2<sup>+</sup> Tregs rely on the intrinsic expression of AREG.

AREG has previously been associated with increased immunosuppressive function of Tregs. Efficient Treg function in mouse models of colitis, dermatitis, and tumor vaccination has been linked to AREG produced by bone marrow-derived mast cells.<sup>117</sup> Basophil-derived AREG was found to play a crucial role in ultraviolet B (UVB) irradiation-induced Treg-mediated suppression of skin hypersensitivity in mice.<sup>135</sup> Moreover, hepatic macrophage-derived AREG has been observed to enhance the immunosuppressive activity of Tregs during HBV infection both *in vitro* and *in vivo*.<sup>112</sup> Similarly, AREG was upregulated in cultured HCC cells and HCC mouse xenografts and promoted the immunoregulatory function of intratumoral Tregs *in vitro*.<sup>202</sup> AREG knockdown in these xenografts led to reduced intratumoral Treg activation and improved the anti-tumor activity of CD8<sup>+</sup> T cells.<sup>202</sup> In addition, AREG was overexpressed in sera, tumor tissues, and effusions from lung or gastric cancer patients, and reinforced the suppressive activity of Tregs *in vitro*.<sup>256</sup> Furthermore, AREG/EGFR signaling supported the Treg suppressive function *in vitro* and in a tumor metastasis model.<sup>256</sup> Also ILC2s were shown to strengthen the suppressive function of Tregs *in vitro*, but AREG has not been investigated as a potential mediator.<sup>257</sup> Since EGFR ligands, such as AREG, can potentially activate the EGFR at the own cell membrane by autocrine mechanisms,<sup>115</sup> and tissue-resident Tregs produce AREG themselves (Figure 9C, Figure 12E, Figure 23D),<sup>113,131,132,141,254</sup> the reinforcement of Treg function through Treg-derived AREG in an autocrine manner has long been suspected but, to date, remained unconfirmed.<sup>107</sup> In contrast to our experiments, in which spleen and lymph node Tregs from naïve *Areg*<sup>-/-</sup> mice displayed a reduced immunosuppressive capacity *in vitro* (Figure 21B), Arpaia N et al. reported that AREG deficiency did not impair the suppressive function of naïve spleen and lymph node Tregs *in vitro*, nor did Treg-specific AREG deficiency affect antiviral immune responses in the spleen, lung, or lung-draining lymph nodes during influenza virus infection.<sup>132</sup> This discrepancy may be due to differences in the experimental design, such as the genetic background of Tregs (*Areg*<sup>-/-</sup> and WT mice vs. CD4<sup>Cre-</sup> x *Areg*<sup>fl/fl</sup> and CD4<sup>Cre+</sup> x *Areg*<sup>fl/fl</sup> mice), gating strategies for responder T cells (CD4<sup>+</sup> CD25<sup>-</sup> T cells vs.

CD4<sup>+</sup> CD44<sup>lo</sup> CD62L<sup>hi</sup> T cells), numbers of each Tregs and responder T cells (10x10<sup>4</sup> cells vs. 4x10<sup>4</sup>), methods of responder T cell activation (anti-CD3/CD28 coated Dynabeads vs. irradiated T cell-depleted splenocytes and anti-CD3 antibody), culture duration (~60 h vs. 80 h) and proliferation detection methods (fluorescence-based detection of cell division (CFSE dilution) during the entire culture time vs. radioactivity-based detection of DNA synthesis ([<sup>3</sup>H]-thymidine incorporation) during the final 8 h of culture).

Our results further revealed that exogenous AREG specifically activated ST2<sup>+</sup> Tregs but not ST2<sup>-</sup> Tregs (Figure 19A) or Tregs from *Il1rl1*<sup>-/-</sup> mice lacking the ST2 receptor (Figure 19B). AREG has previously been reported to reinforce the immunoregulatory function of Tregs expressing the EGFR *in vitro*.<sup>117,130</sup> However, in our study, EGFR expression was similar in Tregs from both WT and *Il1rl1*<sup>-/-</sup> mice, and in both ST2<sup>-</sup> and ST2<sup>+</sup> Tregs from WT mice (Figure 19C). These findings indicate that the stimulatory effect of exogenous AREG on ST2<sup>+</sup> Tregs is independent of EGFR. Therefore, mechanisms by which AREG acts independently of EGFR remain to be identified.

While the lack of intrinsic AREG expression diminished the immunosuppressive activity of Tregs on CD4<sup>+</sup> responder T cell proliferation *in vitro* (Figure 21B), stimulation with exogenous AREG did not affect the suppressive function of WT Tregs (Figure 21D). In contrast to our findings with Tregs from naïve lymph nodes and spleens (Figure 21D), Zaiss DMW et al. demonstrated that AREG stimulation markedly enhanced the function of Tregs from healthy human blood in inhibiting CD4<sup>+</sup> T cell proliferation, as well as splenic Tregs from naïve mice in suppressing CD8<sup>+</sup> T cell proliferation.<sup>117</sup> Similarly, Wang S et al. found that exogenous AREG promoted the regulatory function of Tregs isolated from peripheral blood and tumor-derived effusion mononuclear cells of cancer patients *in vitro*, thereby limiting the proliferation of CD4<sup>+</sup> T cells.<sup>256</sup> Additionally, Yuan CH et al. reported that exogenous AREG improved intratumoral Treg function, leading to attenuation of the tumor-killing molecules IFN $\gamma$ , TNF $\alpha$ , perforin and granzyme B in CD8<sup>+</sup> T cells *in vitro*.<sup>202</sup> It is important to note that we stimulated Tregs or ILC2s with 10 ng/mL AREG in the cell culture experiments (Figure 18-20), while using higher concentrations of 100 (Figure 21C+D) and 500 ng/mL (data not shown) in the suppression assay. However, similar concentrations of AREG were used in the before-mentioned studies: 100 ng/mL AREG by Zaiss DMW et al. and Yuan CH et

al.<sup>117,202</sup> and 50, 100, and 200 ng/mL AREG with a dose-dependent effect by Wang S et al.<sup>256</sup> These findings suggest that exogenous AREG promotes the immunosuppressive function of Tregs in some environments, whereas in others, Treg function relies more on intrinsic AREG expression. Thus, Tregs from the lymph nodes and spleen may depend on intrinsic AREG to suppress CD4<sup>+</sup> T cell proliferation (Figure 21B+D), whereas exogenous AREG is sufficient to support their capacity to inhibit the proliferation of CD8<sup>+</sup> T cells in the spleen<sup>117</sup> and CD4<sup>+</sup> T cells in the peripheral blood<sup>117,256</sup> and tumor environment.<sup>256</sup>

Notably, the AREG-mediated activation of cultured ST2<sup>+</sup> Tregs (Figure 19A+B) was diminished in *Areg*<sup>-/-</sup> ST2<sup>+</sup> Tregs (Figure 19D), suggesting that exogenous AREG is incapable of fully compensating for the lack of intrinsic AREG in these cells, which stimulates their activation in an autocrine manner. This was further confirmed by the limited IL-33-induced expansion and IL-10 expression of AREG-deficient ST2<sup>+</sup> Tregs *in vitro* (Figure 17) and the inability of exogenous AREG to enhance IL-33-induced activation of *Areg*<sup>-/-</sup> ST2<sup>+</sup> Tregs (Figure 20B). Therefore, exogenous IL-33 and AREG promote AREG production by ST2<sup>+</sup> Tregs, which in turn enhances their viability, activation and function. Importantly, the strong stimulatory effects of exogenous IL-33 and AREG are mediated only in the presence of endogenous AREG expression.

In contrast to ST2<sup>+</sup> Tregs, ILC2s exhibited elevated activation and cytokine expression in the inflamed livers of *Areg*<sup>-/-</sup> mice treated with ConA (Figure 15F). Accordingly, exogenous AREG suppressed hepatic ILC2 activation and cytokine production (Figure 18A), as well as IL-33-induced activation and cytokine release from ILC2s *in vitro* (Figure 18B). Thus, AREG-producing ILC2s (Figure 12F) may enhance the function of ST2<sup>+</sup> Tregs while limiting their own effector activity in immune-mediated liver disease. In line with this, Rauber S et al. have previously demonstrated a stimulatory effect of ILC2s on the suppressive function of Tregs *in vitro*.<sup>257</sup> In addition, ST2<sup>+</sup> Tregs, which upregulate AREG expression during acute hepatitis (Figure 12E), may play a role in regulating pro-inflammatory ILC2s. Consistently, Tregs were reported to suppress cytokine production by ILC2s *in vitro*<sup>258,259</sup> and in a mouse model of allergic lung inflammation,<sup>259</sup> and Treg-mediated ILC2 inhibition attenuated airway hyperreactivity.<sup>258</sup> Interestingly, hepatic ILC2 activation remained unchanged in

IL-33-treated *Areg*<sup>-/-</sup> mice (Figure 16B), suggesting that, unlike Tregs, ILC2 function is independent of intrinsic AREG expression.

#### 4.6 The role of AREG in chronic liver disease

After demonstrating the immunoregulatory function of ST2<sup>+</sup> Treg and ILC2/AREG signaling in acute immune-mediated hepatitis, we further aimed to explore its role in chronic liver disease. It has previously been shown that mice lacking AREG develop less severe CCl<sub>4</sub>-induced chronic hepatitis, implicating AREG as a driver of liver fibrogenesis.<sup>111</sup> In this study, chronic liver disease in *Mdr2*<sup>-/-</sup> mice, marked by upregulated hepatic inflammatory cytokines (Figure 22E), hepatocellular and cholestatic injury, impaired cholesterol metabolism (Figure 22A), and liver fibrosis (Figure 22B-D), was associated with increased hepatic *Il33* and *Areg* mRNA levels (Figure 23A+B). Elevated AREG expression has previously also been demonstrated in various rat,<sup>108</sup> murine<sup>109–111</sup> and human<sup>108–110</sup> chronic liver diseases (see 4.1). Notably, consistent with our findings in early stages of cholestatic liver disease using 12-week-old *Mdr2*<sup>-/-</sup> mice, Santamaria E et al. reported increased *Areg* mRNA levels in later disease stages in 4- to 17-month-old *Mdr2*<sup>-/-</sup> mice compared to WT controls,<sup>109</sup> which are known to develop cirrhosis and HCC.<sup>260</sup> Furthermore, they observed a gradual upregulation of hepatic *Areg* mRNA expression in *Mdr2*<sup>-/-</sup> mice with advancing age.<sup>109</sup>

Furthermore, chronic liver injury in *Mdr2*<sup>-/-</sup> mice was associated with expansion of hepatic ILC2s (Figure 23C) and ST2<sup>+</sup> Tregs (Figure 23D). However, in contrast to the elevated expression of AREG by hepatic ST2<sup>+</sup> Tregs in acute hepatitis (Figure 12E), the capacity of hepatic ST2<sup>+</sup> Tregs to express AREG was substantially reduced in *Mdr2*<sup>-/-</sup> mice with sclerosing cholangitis (Figure 23D). Interestingly, hepatic ST2<sup>+</sup> Tregs also exhibited an exhausted phenotype, characterized by elevated expression of the co-inhibitory receptor PD-1 (Figure 23D), a marker linked to Treg dysfunction<sup>64</sup> and exhaustion.<sup>65</sup> As demonstrated in this study, ST2<sup>+</sup> Tregs depend on intrinsic production of AREG, which functions in an autocrine loop to support their survival, activation and function (Figure 15E, 16A, 17, 19D, 20B, 21B, see 4.5). Thus, the reduced AREG expression in ST2<sup>+</sup> Tregs of *Mdr2*<sup>-/-</sup> mice may reflect a diminished immunosuppressive functionality of these cells in PSC. In this context, a study by Ikeno Y et al. using

transgenic mice with selective deletion of AREG expression from Tregs found that Treg-derived AREG was not essential for preventing CCl<sub>4</sub>-induced liver inflammation and fibrosis.<sup>113</sup> Therefore, the functional role of Treg-derived AREG in chronic liver disease needs to be further elucidated.

In addition to the reduced AREG expression by hepatic ST2<sup>+</sup> Tregs in *Mdr2*<sup>-/-</sup> compared to WT mice (Figure 23D), hepatic ILC2-derived AREG expression remained unaltered (Figure 23C). Since the increased *Areg* mRNA levels in the liver tissue of mice with sclerosing cholangitis (Figure 23A+B) could not be attributed to AREG released from hepatic ST2<sup>+</sup> Tregs or ILC2s (Figure 23C+D), this suggests that parenchymal cells might be responsible for the upregulated AREG expression. They may produce AREG in response to the inflammatory environment, thereby suppressing the immune response and exerting a protective effect against ongoing tissue damage. The cellular localization of AREG production could be investigated further by immunohistochemical staining of liver sections, provided that specific AREG antibodies are available to ensure accurate detection.

## 5 Outlook

This thesis aimed to elucidate the role of the growth factor AREG in acute and chronic liver disease, using the mouse model of ConA-induced immune-mediated hepatitis, which shares some similarities with acute AIH,<sup>23</sup> and *Mdr2*<sup>-/-</sup> mice with sclerosing cholangitis and liver fibrosis resembling human PSC.<sup>40</sup> The presented data demonstrate an immunoregulatory function of AREG in acute immune-mediated hepatitis, and elevated levels in the liver during acute and chronic liver disease. In immune-mediated hepatitis, AREG expression was upregulated by hepatic ILC2s and ST2<sup>+</sup> Tregs, and the absence of AREG aggravated disease progression. Moreover, AREG was shown to differentially affect hepatic ILC2s and ST2<sup>+</sup> Tregs, inhibiting ILC2s but activating Tregs and reinforcing their immunosuppressive function. In chronic liver disease, hepatic ST2<sup>+</sup> Tregs exhibited reduced production of AREG and an exhausted phenotype.

However, this study has some limitations. We observed exacerbated liver damage in mice lacking endogenous AREG. Therefore, it would be interesting to analyze whether treatment of mice with exogenous AREG before induction of hepatitis can exert a protective effect. Furthermore, we demonstrated the impact of exogenous AREG on ST2<sup>+</sup> Tregs and hepatic ILC2s *in vitro*. Thus, future research should investigate the phenotype of hepatic ST2<sup>+</sup> Tregs and ILC2s *in vivo* following administration of AREG. In addition, the specific functional significance of AREG expressed by ST2<sup>+</sup> Tregs or ILC2s in immune-mediated hepatitis remains unclear. Adoptive transfer experiments using Tregs or hepatic ILC2s from *Areg*<sup>-/-</sup> mice could be conducted to evaluate the disease pathology of ConA-induced hepatitis in the absence of AREG expression in these cells. Given the inhibitory effect of AREG on hepatic ILC2s and its stimulatory effect on ST2<sup>+</sup> Tregs found in this study, we propose that both AREG-producing ST2<sup>+</sup> Tregs and ILC2s may enhance the function of ST2<sup>+</sup> Tregs while inhibiting the activity of ILC2s. Co-culture experiments with Tregs and ILC2 in the presence or absence of AREG can give insights into their direct effect on each other.

Mice were shown to develop less severe CCl<sub>4</sub>-induced chronic hepatitis in the absence of AREG.<sup>111</sup> In this study, we determined AREG expression in *Mdr2*<sup>-/-</sup> mice with sclerosing cholangitis and liver fibrosis. However, functional data regarding the role of



AREG in other chronic liver disease models are still lacking. Hence, examining the disease pathology in *Areg*<sup>-/-</sup> x *Mdr2*<sup>-/-</sup> mice would be an important direction for future studies.

Finally, we used mouse models of AIH and PSC to perform functional analyses of ST2<sup>+</sup> Treg and ILC2/AREG signaling in hepatic immune regulation. However, our findings need to be further investigated in patients with acute and chronic liver diseases. Future investigations could measure serum AREG levels in patients with AIH and PSC and correlate them with disease severity or clinical outcomes. Moreover, AREG expression could be assessed in liver biopsies from patients through immunohistochemistry or qRT-PCR analysis. Additionally, single-cell RNA sequencing can elucidate *Areg* expression and its associated signaling pathways in ST2<sup>+</sup> Tregs or ILC2s, within the liver or peripheral blood mononuclear cells (PBMCs) from patients. Human PBMCs may also be used to perform flow cytometric analysis of AREG expression by systemic ST2<sup>+</sup> Tregs and ILC2s. Lastly, functional studies to explore the immunoregulatory role of AREG could be conducted using human PBMCs *in vitro* or in humanized mouse models - mice engrafted with human immune cells.

In conclusion, this thesis reveals an immunoregulatory role of AREG in immune-mediated hepatitis, demonstrating distinct effects on hepatic ST2<sup>+</sup> Tregs and ILC2s. In addition, our findings provide novel insights into AREG expression in immune cells in sclerosing cholangitis. Nevertheless, the functional significance of AREG specifically expressed by ST2<sup>+</sup> Tregs or ILC2s in acute immune-mediated hepatitis, its role in chronic liver disease, and its potential as a therapeutic target remain unknown and require further investigation.

## 6 Summary

Autoimmune liver diseases such as autoimmune hepatitis (AIH) and primary sclerosing cholangitis (PSC) often progress to fibrosis, cirrhosis and liver cancer. These conditions contribute significantly to patient morbidity and mortality, and treatment options remain limited. Gaining a deeper insight into the cellular and molecular processes in immune-mediated liver diseases is essential for the development of more effective and targeted therapies. The growth factor amphiregulin (AREG) has been shown to contribute to tissue repair and Treg function in acute liver disease, but to fibrogenesis in chronic liver disease. AREG expression is induced in pro-inflammatory group 2 innate lymphoid cells (ILC2s) and immunosuppressive regulatory T cells (Tregs) in response to the alarmin interleukin (IL)-33, which is released from necrotic hepatocytes following tissue damage. Due to the limited knowledge of the function of AREG produced by these immune cells, this thesis addressed its immunoregulatory role in acute and chronic immune-mediated liver diseases. For this, we used the mouse model of concanavalin (ConA)-induced immune-mediated hepatitis, resembling human acute AIH, and multidrug resistance p-glycoprotein 2 (*Mdr2*<sup>-/-</sup>) mice with chronic cholestatic liver disease similar to human PSC.

The presented data demonstrate elevated levels of plasma AREG and hepatic *Areg* mRNA in immune-mediated hepatitis. Additionally, hepatic *Areg* mRNA was upregulated in fibrotic *Mdr2*<sup>-/-</sup> mice with sclerosing cholangitis. Flow cytometry analysis further revealed increased frequencies of hepatic ILC2s and Tregs expressing the IL-33 receptor suppression of tumorigenicity 2 (ST2) in both ConA- and IL-33-treated mice, as well as in *Mdr2*<sup>-/-</sup> mice. In mice treated with ConA or IL-33, hepatic ST2<sup>+</sup> ILC2s and ST2<sup>+</sup> Tregs showed enhanced activation and AREG expression. In contrast, hepatic ST2<sup>+</sup> Tregs from *Mdr2*<sup>-/-</sup> mice displayed reduced AREG production and an exhausted phenotype. Also hepatocytes expressed AREG *in vitro*, but the expression was not upregulated in response to cytokines linked to immune-mediated hepatitis. However, exogenous AREG stimulated *Areg* mRNA expression in cultured primary hepatocytes in a self-inducing mechanism. The functional role of AREG was further explored in immune-mediated hepatitis. *Areg*<sup>-/-</sup> mice exhibited more pronounced ConA-induced liver tissue damage than WT mice, as indicated by elevated plasma levels of the cytosolic liver enzyme alanine aminotransferase (ALT) and increased

necrotic areas in H&E-stained liver sections. This was accompanied by a higher activation of hepatic ILC2s and a lower frequency of hepatic ST2<sup>+</sup> Tregs. AREG also differentially affected hepatic ILC2s and ST2<sup>+</sup> Tregs *in vitro*. Exogenous AREG reduced the number and activation of hepatic ILC2s, as well as their IL-33-mediated activation. In contrast, exogenous AREG induced the expansion and activation of ST2<sup>+</sup> Tregs, but not ST2<sup>-</sup> Tregs. Interestingly, this stimulatory effect was mediated independently of the epidermal growth factor receptor (EGFR), since its expression levels were similar in ST2<sup>+</sup> and ST2<sup>-</sup> Tregs. Moreover, the activating effect of exogenous AREG was diminished in AREG-deficient ST2<sup>+</sup> Tregs, showing that exogenous AREG could not compensate for the lack of intrinsic AREG. Finally, suppression assays demonstrated that the loss of intrinsic AREG also reduced the capacity of Tregs to inhibit CD4<sup>+</sup> T cell proliferation. Thus, ST2<sup>+</sup> Tregs rely on intrinsic AREG production to maintain their survival, activation, and function through an autocrine mechanism.

Overall, this thesis describes an immunoregulatory role of the ST2<sup>+</sup> Treg/AREG axis in immune-mediated liver disease, demonstrating its dual function: supporting the maintenance and immunosuppressive function of ST2<sup>+</sup> Tregs while suppressing the effector function of hepatic ILC2s.

The role of AREG in acute and chronic liver disease, as proposed in this thesis, is illustrated in the graphical abstract presented in Figure 24.

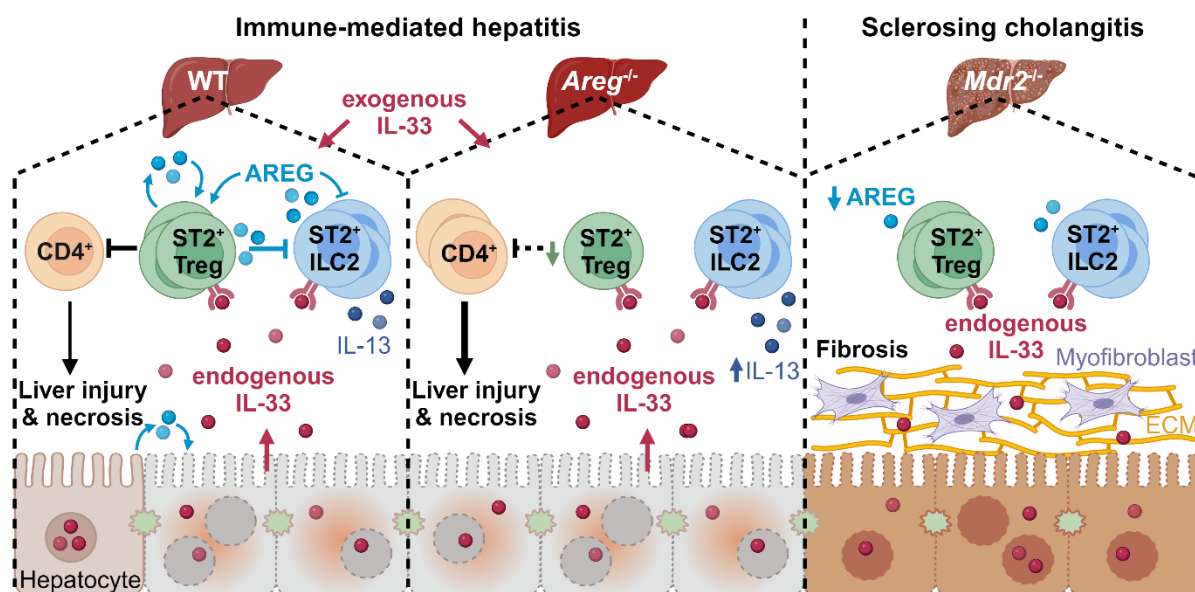


**Figure 24: Graphical abstract illustrating the proposed role of AREG in acute and chronic liver disease.** During ConA-induced immune-mediated hepatitis, immune cells, including CD4<sup>+</sup> T cells, are known to contribute to liver injury and necrosis. IL-33 is released from necrotic hepatocytes and binds to the IL-33 receptor ST2 on various immune cells. In this study, IL-33 and ConA treatment induced the expansion and activation of hepatic ST2<sup>+</sup> Tregs and ILC2s, as well as the production of the immunoregulatory growth factor AREG. Exogenous AREG further promoted the expansion, activation and AREG expression of ST2<sup>+</sup> Tregs. However, ST2<sup>+</sup> Tregs primarily depended on intrinsic AREG, which acted in an autocrine manner to support their survival, activation and ability to suppress CD4<sup>+</sup> T cell proliferation. In addition, exogenous AREG inhibited the activation and effector function of pro-inflammatory hepatic ILC2s. Hepatocytes produced AREG as well, which further drove its expression in these cells through a positive feedback loop. *Areg*<sup>-/-</sup> mice developed more severe immune-mediated hepatitis compared to WT mice. In the absence of AREG, the frequency of hepatic ST2<sup>+</sup> Tregs was decreased, while the activation and IL-13 expression of hepatic ILC2s was increased. *Mdr2*<sup>-/-</sup> mice developed sclerosing cholangitis. Chronic inflammation and progressive injury of the liver parenchyma lead to the recruitment and activation of extracellular matrix (ECM)-producing myofibroblasts, ultimately resulting in fibrosis due to pathological ECM accumulation. Similar to immune-mediated hepatitis, hepatic IL-33 levels were elevated in *Mdr2*<sup>-/-</sup> mice compared to WT mice, potentially stimulating ST2<sup>+</sup> Tregs and ILC2s, both of which were expanded. However, ST2<sup>+</sup> Tregs produced lower levels of AREG and exhibited an exhausted phenotype. Created with BioRender.com.

## 7 Zusammenfassung

Autoimmunbedingte Lebererkrankungen wie die autoimmune Hepatitis (AIH) und die primär sklerosierende Cholangitis (PSC) führen häufig zu Fibrose, Zirrhose und Leberkrebs. Diese Erkrankungen tragen erheblich zur Morbidität und Mortalität der Patienten bei, und die Behandlungsmöglichkeiten sind nach wie vor begrenzt. Ein tieferer Einblick in die zellulären und molekularen Prozesse immunvermittelter Lebererkrankungen ist für die Entwicklung wirksamerer und gezielterer Therapien unerlässlich. Der Wachstumsfaktor Amphiregulin (AREG) trägt in akuten Lebererkrankungen nachweislich zur Gewebereparatur und Treg-Funktion bei, in chronischen Lebererkrankungen jedoch zur Fibrogenese. Die Expression von AREG wird in proinflammatorischen angeborenen lymphoiden Zellen der Gruppe 2 (ILC2s) und immunsuppressiven regulatorischen T-Zellen (Tregs) als Reaktion auf das Alarmin Interleukin (IL)-33 induziert, das nach einer Gewebeschädigung aus nekrotischen Hepatozyten freigesetzt wird. Da die Funktion des von diesen Immunzellen produzierten AREG nur wenig bekannt ist, wurde in dieser Arbeit seine immunregulatorische Rolle in akuten und chronischen immunvermittelten Lebererkrankungen untersucht. Hierzu verwendeten wir das Mausmodell der Concanavalin (ConA)-induzierten immunvermittelten Hepatitis, die der akuten AIH des Menschen ähnelt, und Multidrug-Resistenz P-Glykoprotein 2 (*Mdr2*)<sup>-/-</sup> Mäuse mit chronischer cholestatischer Lebererkrankung, die Merkmale der menschlichen PSC aufweist.

Die vorgestellten Daten zeigen erhöhte Spiegel von Plasma-AREG und hepatischer *Areg*-mRNA in immunvermittelter Hepatitis. Außerdem war die hepatische *Areg*-mRNA in fibrotischen *Mdr2*<sup>-/-</sup> Mäusen mit sklerosierender Cholangitis hochreguliert. Durchflusszytometrie-Analysen zeigten zudem eine erhöhte Häufigkeit von hepatischen ILC2s und Tregs, die den IL-33-Rezeptor Suppression der Tumorigenität 2 (ST2) exprimieren, in ConA- und IL-33-behandelten Mäusen als auch in *Mdr2*<sup>-/-</sup> Mäusen. In Mäusen, die mit ConA oder IL-33 behandelt wurden, wiesen hepatische ST2<sup>+</sup> ILC2s und ST2<sup>+</sup> Tregs eine erhöhte Aktivierung und AREG-Expression auf. Im Gegensatz dazu zeigten hepatische ST2<sup>+</sup> Tregs aus *Mdr2*<sup>-/-</sup> Mäusen eine verminderte AREG-Produktion und einen erschöpften Phänotyp. Auch Hepatozyten exprimierten AREG *in vitro*, jedoch wurde die Expression nach der

Stimulation mit Zytokinen, die mit immunvermittelter Hepatitis in Verbindung stehen, nicht hochreguliert. Exogenes AREG hingegen stimulierte die Expression von *Areg*-mRNA in kultivierten primären Hepatozyten über einen selbstinduzierenden Mechanismus. Die funktionelle Rolle von AREG wurde im Weiteren in der immunvermittelten Hepatitis untersucht. *Areg*<sup>-/-</sup> Mäuse wiesen eine ausgeprägtere ConA-induzierte Schädigung des Lebergewebes auf als WT-Mäuse, was sich in erhöhten Plasmaspiegeln des zytosolischen Leberenzym Alanin-Aminotransferase (ALT) und vermehrten nekrotischen Bereichen in H&E-gefärbten Leberschnitten zeigte. Dies ging mit einer stärkeren Aktivierung der hepatischen ILC2s und einer verringerten Häufigkeit hepatischer ST2<sup>+</sup> Tregs einher. AREG hatte auch *in vitro* unterschiedliche Effekte auf hepatische ILC2s und ST2<sup>+</sup> Tregs. Exogenes AREG reduzierte die Anzahl und Aktivierung der hepatischen ILC2s sowie deren IL-33-vermittelte Aktivierung. Im Gegensatz dazu induzierte exogenes AREG die Expansion und Aktivierung von ST2<sup>+</sup> Tregs, aber nicht von ST2<sup>-</sup> Tregs. Interessanterweise wurde diese stimulierende Wirkung unabhängig vom epidermalen Wachstumsfaktor-Rezeptor (EGFR) vermittelt, da dessen Expressionsniveau in ST2<sup>+</sup> und ST2<sup>-</sup> Tregs ähnlich war. Darüber hinaus war die aktivierende Wirkung von exogenem AREG in AREG-defizienten ST2<sup>+</sup> Tregs vermindert, was zeigt, dass exogenes AREG den Mangel an intrinsischem AREG nicht kompensieren konnte. Schließlich demonstrierten Suppressionsassays, dass der Verlust von intrinsischem AREG auch die Fähigkeit der Tregs verringerte, die Proliferation von CD4<sup>+</sup> T-Zellen zu hemmen. Somit sind ST2<sup>+</sup> Tregs auf die intrinsische Produktion von AREG angewiesen, um ihre Überlebensfähigkeit, Aktivierung und Funktion durch einen autokrinen Mechanismus aufrechtzuerhalten.

Insgesamt beschreibt diese Dissertation eine immunregulatorische Rolle der ST2<sup>+</sup> Treg/AREG-Achse in immunvermittelten Lebererkrankungen und zeigt ihre duale Funktion auf: Sie unterstützt die Erhaltung und immunsuppressive Funktion der ST2<sup>+</sup> Tregs und unterdrückt gleichzeitig die Effektorfunktion der hepatischen ILC2s.

## References

1. Qin L and Crawford JM. Anatomy and cellular functions of the liver. In: Zakim and Boyer's Hepatology: A textbook of liver disease. 7th ed. Editors: Sanyal AJ, Boyer TD, Lindor KD, Terrault NA. Elsevier, Philadelphia. (2018): 2–19.
2. Ozougwu JC. Physiology of the liver. *International Journal of Research in Pharmacy and Biosciences*. (2017) 4.8: 13–24.
3. Mitra V and Metcalf J. Metabolic functions of the liver. *Anaesth Intensive Care Med*. (2009) 10.7: 334–5.
4. Szabo G, Saha B, and Ambade A. The Liver as an Immune Organ. In: Zakim and Boyer's Hepatology: A textbook of liver disease. 7th ed. Editors: Sanyal AJ, Boyer TD, Lindor KD, Terrault NA. Elsevier, Philadelphia. (2018): 66–76.
5. Doherty DG. Immunity, tolerance and autoimmunity in the liver: A comprehensive review. *J Autoimmun*. (2016) 66: 60–75.
6. Knolle PA and Wohlleber D. Immunological functions of liver sinusoidal endothelial cells. *Cell Mol Immunol*. (2016) 13.3: 347–53.
7. Pandey E, Nour AS, and Harris EN. Prominent receptors of liver sinusoidal endothelial cells in liver homeostasis and disease. *Front Physiol*. (2020) 11: 547714.
8. Racanelli V and Rehermann B. The liver as an immunological organ. *Hepatology*. (2006) 43.S1: S54–62.
9. Tiegs G and Lohse AW. Immune tolerance: What is unique about the liver. *J Autoimmun*. (2010) 34.1: 1–6.
10. Horst AK, Kumashie KG, Neumann K, Diehl L, and Tiegs G. Antigen presentation, autoantibody production, and therapeutic targets in autoimmune liver disease. *Cell Mol Immunol*. (2021) 18.1: 92–111.
11. Neefjes J, Jongsma MLM, Paul P, and Bakke O. Towards a systems understanding of MHC class I and MHC class II antigen presentation. *Nat Rev Immunol*. (2011) 11.12: 823–36.
12. Thomson AW and Knolle PA. Antigen-presenting cell function in the tolerogenic liver environment. *Nat Rev Immunol*. (2010) 10.11: 753–66.
13. Heymann F, Peusquens J, Ludwig-Portugall I, Kohlhepp M, Ergen C, et al. Liver inflammation abrogates immunological tolerance induced by Kupffer cells. *Hepatology*. (2015) 62.1: 279–91.

14. You Q, Cheng L, Kedl RM, and Ju C. Mechanism of T cell tolerance induction by murine hepatic Kupffer cells. *Hepatology*. (2008) 48.3: 978–90.
15. Marra F and Parola M. Cells in the liver - Functions in Health and disease. In: Chronic Liver Failure - Mechanisms and Management. Editors: Ginès P, Kamath PS, Arroyo V. Humana Press Springer, New York. (2011): 3–32.
16. Viñas O, Bataller R, Sancho-Bru P, Ginès P, Berenguer C, et al. Human hepatic stellate cells show features of antigen-presenting cells and stimulate lymphocyte proliferation. *Hepatology*. (2003) 38.4: 919–29.
17. Arndtz K and Hirschfield GM. The pathogenesis of autoimmune liver disease. *Dig Dis*. (2016) 34.4: 327–33.
18. Jepsen P, Grønbaek L, and Vilstrup H. Worldwide incidence of autoimmune liver disease. *Dig Dis*. (2015) 33.Suppl 2: 2–12.
19. Hahn JW, Yang HR, Moon JS, Chang JY, Lee K, et al. Global incidence and prevalence of autoimmune hepatitis, 1970–2022: a systematic review and meta-analysis. *EClinicalMedicine*. (2023) 65: 102280.
20. Tsai S and Santamaria P. MHC class II polymorphisms, autoreactive T-cells, and autoimmunity. *Front Immunol*. (2013) 4: 321.
21. Wang HX, Liu M, Weng SY, Li JJ, Xie C, et al. Immune mechanisms of concanavalin A model of autoimmune hepatitis. *World J Gastroenterol*. (2012) 18.2: 119–25.
22. Ballegeer M and Libert C. Different cell types involved in mediating concanavalin A induced liver injury: A comprehensive overview. *J Gastroenterol Hepatology Res*. (2016) 1.1: 100001.
23. Erhardt A and Tiegs G. Tolerance induction in response to liver inflammation. *Dig Dis*. (2010) 28.1: 86–92.
24. Gantner F, Leist M, Lohse AW, Germann PG, and Tiegs G. Concanavalin A-induced T-cell-mediated hepatic injury in mice: The role of tumor necrosis factor. *Hepatology*. (1995) 21.1: 190–8.
25. Knolle PA, Gerken G, Löser E, Dienes HP, Gantner F, et al. Role of sinusoidal endothelial cells of the liver in concanavalin A-induced hepatic injury in mice. *Hepatology*. (1996) 24.4: 824–9.
26. Tiegs G, Hentschel J, and Wendel A. A T cell-dependent experimental liver injury in mice inducible by concanavalin A. *J Clin Invest*. (1992) 90.1: 196–203.



27. Bonder CS, Ajuebor MN, Zbytnuik LD, Kubes P, and Swain MG. Essential role for neutrophil recruitment to the liver in concanavalin A-induced hepatitis. *J Immunol.* (2004) 172.1: 45–53.
28. Keren Z and Berke G. Selective binding of concanavalin A to target cell major histocompatibility antigens is required to induce nonspecific conjugation and lysis by cytolytic T lymphocytes in lectin-dependent cytotoxicity. *Cell Immunol.* (1984) 89.2: 458–77.
29. Parker WL and Martz E. Lectin-induced nonlethal adhesions between cytolytic tumor cells and nonspecific “triggering” of cytotoxicity. *J Immunol.* (1980) 124.1: 25–35.
30. Asherson GL, Ferluga J, Janossy G, and HAI M. Non-specific cytotoxicity by T cells activated with plant mitogens in vitro and the requirement for plant agents during the killing reaction. *Clin Exp Immunol.* (1973) 15.4: 573–89.
31. Hubbard SC, Kranz DM, Longmore GD, Sitkovsky M V, and Eisent HN. Glycosylation of the T-cell antigen-specific receptor and its potential role in lectin-mediated cytotoxicity. *Proc Natl Acad Sci U S A.* (1986) 83.6: 1852–6.
32. Heymann F, Hamesch K, Weiskirchen R, and Tacke F. The concanavalin A model of acute hepatitis in mice. *Lab Anim.* (2015) 49.S1: 12–20.
33. Küsters S, Gantner F, Kunstle G, and Tiegs G. Interferon gamma plays a critical role in T cell-dependent liver injury in mice initiated by concanavalin A. *Gastroenterology.* (1996) 111.2: 462–71.
34. Arshad MI, Rauch M, L’Helgoualc’h A, Julia V, Leite-de-Moraes MC, et al. NKT cells are required to induce high IL-33 expression in hepatocytes during ConA-induced acute hepatitis. *Eur J Immunol.* (2011) 41.8: 2341–8.
35. Neumann K, Karimi K, Meiners J, Voetlaue R, Steinmann S, et al. A proinflammatory role of type 2 innate lymphoid cells in murine immune-mediated hepatitis. *J Immunol.* (2017) 198.1: 128–37.
36. Neumann K, Schiller B, and Tiegs G. NLRP3 inflammasome and IL-33: Novel players in sterile liver inflammation. *Int J Mol Sci.* (2018) 19.9: 1–26.
37. Erhardt A, Biburger M, Papadopoulos T, and Tiegs G. IL-10, regulatory T cells, and Kupffer cells mediate tolerance in concanavalin A-induced liver injury in mice. *Hepatology.* (2007) 45.2: 475–85.
38. Bechmann LP and Friedman SL. Fibrosis as a major mechanism of chronic liver disease. In: *Chronic Liver Failure - Mechanisms and Management*. Editors:

- Ginès P, Kamath PS, Arroyo V. Humana Press Springer, New York. (2011): 91–108.
39. Xu R, Zhang Z, and Wang FS. Liver fibrosis: Mechanisms of immune-mediated liver injury. *Cell Mol Immunol*. (2012) 9.4: 296–301.
  40. Fickert P, Fuchsbichler A, Wagner M, Zollner G, Kaser A, et al. Regurgitation of bile acids from leaky bile ducts causes sclerosing cholangitis in Mdr2 (Abcb4) knockout mice. *Gastroenterology*. (2004) 127.1: 261–74.
  41. Oude Elferink RPJ and Paulusma CC. Function and pathophysiological importance of ABCB4 (MDR3 P-glycoprotein). *Pflugers Arch*. (2007) 453.5: 601–10.
  42. Pieters A, Gijbels E, Cogliati B, Annaert P, Devisscher L, et al. Biomarkers of cholestasis. *Biomark Med*. (2021) 15.6: 437–54.
  43. Voshol PJ, Havinga R, Wolters H, Ottenhoff R, Princen HMG, et al. Reduced plasma cholesterol and increased fecal sterol loss in multidrug resistance gene 2 p-glycoprotein-deficient mice. *Gastroenterology*. (1998) 114.5: 1024–34.
  44. Fuchs M and Stange EF. Cholesterol and cholestasis: a lesson from the Mdr2 (-/-) mouse. *J Hepatol*. (2001) 34.2: 339–41.
  45. Gabr SA, Alghadir AH, Sherif YE, and Ghfar AA. Hydroxyproline as a biomarker in liver disease. In: Biomarkers in Liver Disease, Biomarkers in Disease: Methods, Discoveries and Applications. Editor: V.R. Preedy. Springer, Dordrecht. (2016): 1–26.
  46. Liberal R, Grant CR, Longhi MS, Mieli-Vergani G, and Vergani D. Regulatory T cells: Mechanisms of suppression and impairment in autoimmune liver disease. *IUBMB Life*. (2015) 67.2: 88–97.
  47. Wu K jia, Qian Q fei, Zhou J ren, Sun D lin, Duan Y fei, et al. Regulatory T cells (Tregs) in liver fibrosis. *Cell Death Discov*. (2023) 9.1: 53.
  48. Borys SM, Bag AK, Brossay L, and Adeegbe DO. The Yin and Yang of targeting KLRG1+ Tregs and effector cells. *Front Immunol*. (2022) 13.April: 1–8.
  49. Wikenheiser DJ and Stumhofer JS. ICOS co-stimulation: Friend or foe? *Front Immunol*. (2016) 7.AUG: 1–16.
  50. Walker LSK and Sansom DM. Confusing signals: Recent progress in CTLA-4 biology. *Trends Immunol*. (2015) 36.2: 63–70.

51. Wing K, Yamaguchi T, and Sakaguchi S. Cell-autonomous and -non-autonomous roles of CTLA-4 in immune regulation. *Trends Immunol.* (2011) 32.9: 428–33.
52. Harjunpää H and Guillerey C. TIGIT as an emerging immune checkpoint. *Clin Exp Immunol.* (2020) 200.2: 108–19.
53. Francisco LM, Sage PT, and Sharpe AH. The PD-1 pathway in tolerance and autoimmunity. *Immunol Rev.* (2010) 236.1: 219–42.
54. Molofsky AB, Van Gool F, Liang HE, Van Dyken SJ, Nussbaum JC, et al. Interleukin-33 and Interferon- $\gamma$  counter-regulate group 2 innate lymphoid cell activation during immune perturbation. *Immunity.* (2015) 43.1: 161–74.
55. Bedke T, Muscate F, Soukou S, Gagliani N, and Huber S. IL-10-producing T cells and their dual functions. *Semin Immunol.* (2019) 44.August: 101335.
56. Lucca LE, Axisa PP, Singer ER, Nolan NM, Dominguez-Villar M, et al. TIGIT signaling restores suppressor function of Th1 Tregs. *JCI Insight.* (2019) 4.3: e124427.
57. Joller N, Lozano E, Burkett PR, Patel B, Xiao S, et al. Treg cells expressing the coinhibitory molecule TIGIT selectively inhibit proinflammatory Th1 and Th17 cell responses. *Immunity.* (2014) 40.4: 569–81.
58. Freeman GJ, Long AJ, Iwai Y, Bourque K, Chernova T, et al. Engagement of the PD-1 immunoinhibitory receptor by a novel B7 family member leads to negative regulation of lymphocyte activation. *J Exp Med.* (2000) 192.7: 1027–34.
59. Habicht A, Dada S, Jurewicz M, Fife BT, Yagita H, et al. A link between PDL1 and T regulatory cells in fetomaternal tolerance. *J Immunol.* (2007) 179.8: 5211–9.
60. Neumann K, Ostmann A, Breda PC, Ochel A, Tacke F, et al. The co-inhibitory molecule PD-L1 contributes to regulatory T cell-mediated protection in murine crescentic glomerulonephritis. *Sci Rep.* (2019) 9.1: 1–13.
61. Kitazawa Y, Fujino M, Wang Q, Kimura H, Azuma M, et al. Involvement of the programmed death-1/programmed death-1 ligand pathway in CD4+CD25+ regulatory T-cell activity to suppress alloimmune responses. *Transplantation.* (2007) 83.6: 774–82.
62. Sharma MD, Baban B, Chandler P, Hou DY, Singh N, et al. Plasmacytoid dendritic cells from mouse tumor-draining lymph nodes directly activate mature Tregs via indoleamine 2,3-dioxygenase. *J Clin Invest.* (2007) 117.9: 2570–82.

63. Gotot J, Gottschalk C, Leopold S, Knolle PA, Yagita H, et al. Regulatory T cells use programmed death 1 ligands to directly suppress autoreactive B cells in vivo. *Proc Natl Acad Sci U S A*. (2012) 109.26: 10468–73.
64. Lowther DE, Goods BA, Lucca LE, Lerner BA, Raddassi K, et al. PD-1 marks dysfunctional regulatory T cells in malignant gliomas. *JCI Insight*. (2016) 1.5: e85935.
65. Xiao J, Zhang L, Dong Y, Liu X, Peng L, et al. PD-1 upregulation is associated with exhaustion of regulatory T cells and reflects immune activation in HIV-1-infected individuals. *AIDS Res Hum Retroviruses*. (2019) 35.5: 444–52.
66. Dong H, Zhu G, Tamada K, and Chen L. B7-H1, a third member of the B7 family, co-stimulates T-cell proliferation and interleukin-10 secretion. *Nat Med*. (1999) 5.12: 1365–9.
67. Iwai Y, Terawaki S, Ikegawa M, Okazaki T, and Honjo T. PD-1 inhibits antiviral immunity at the effector phase in the liver. *J Exp Med*. (2003) 198.1: 39–50.
68. Yu MC, Chen CH, Liang X, Wang L, Gandhi CR, et al. Inhibition of T-cell responses by hepatic stellate cells via B7-H1-mediated T-cell apoptosis in mice. *Hepatology*. (2004) 40.6: 1312–21.
69. Mühlbauer M, Fleck M, Schütz C, Weiss T, Froh M, et al. PD-L1 is induced in hepatocytes by viral infection and by interferon- $\alpha$  and - $\gamma$  and mediates T cell apoptosis. *J Hepatol*. (2006) 45.4: 520–8.
70. Zhou J, Peng H, Li K, Qu K, Wang B, et al. Liver-resident NK cells control antiviral activity of hepatic T cells via the PD-1-PD-L1 axis. *Immunity*. (2019) 50.2: 403–17.
71. Latchman Y, Wood CR, Chernova T, Chaudhary D, Borde M, et al. PD-L2 is a second ligand for PD-1 and inhibits T cell activation. *Nat Immunol*. (2001) 2.3: 261–8.
72. Inaba K, Witmer-Pack M, Inaba M, Hathcock KS, Sakuta H, et al. The tissue distribution of the B7-2 costimulator in mice: Abundant expression on dendritic cells in situ and during maturation in vitro. *J Exp Med*. (1994) 180.5: 1849–60.
73. Yamazaki T, Akiba H, Iwai H, Matsuda H, Aoki M, et al. Expression of programmed death 1 ligands by murine T cells and APC. *J Immunol*. (2002) 169.10: 5538–45.
74. Lesterhuis WJ, Steer H, and Lake RA. PD-L2 is predominantly expressed by Th2 cells. *Mol Immunol*. (2011) 49.1–2: 1–3.

75. Messal N, Serriari NE, Pastor S, Nunès JA, and Olive D. PD-L2 is expressed on activated human T cells and regulates their function. *Mol Immunol.* (2011) 48.15–16: 2214–9.
76. Ohkura N and Sakaguchi S. Transcriptional and epigenetic basis of Treg cell development and function: its genetic anomalies or variations in autoimmune diseases. *Cell Res.* (2020) 30.6: 465–74.
77. Longhi MS, Ma Y, Bogdanos DP, Cheeseman P, Mieli-Vergani G, et al. Impairment of CD4+CD25+ regulatory T-cells in autoimmune liver disease. *J Hepatol.* (2004) 41.1: 31–7.
78. Longhi MS, Ma Y, Mitry RR, Bogdanos DP, Heneghan M, et al. Effect of CD4+CD25+ regulatory T-cells on CD8 T-cell function in patients with autoimmune hepatitis. *J Autoimmun.* (2005) 25.1: 63–71.
79. Longhi MS, Hussain MJ, Mitry RR, Arora SK, Mieli-Vergani G, et al. Functional study of CD4+CD25+ regulatory T cells in health and autoimmune hepatitis. *J Immunol.* (2006) 176.7: 4484–91.
80. Longhi MS, Mitry RR, Samyn M, Scalori A, Hussain MJ, et al. Vigorous activation of monocytes in juvenile autoimmune liver disease escapes the control of regulatory T-cells. *Hepatology.* (2009) 50.1: 130–42.
81. Langhans B, Krämer B, Louis M, Nischalke HD, Hüneburg R, et al. Intrahepatic IL-8 producing Foxp3+CD4+ regulatory T cells and fibrogenesis in chronic hepatitis C. *J Hepatol.* (2013) 59.2: 229–35.
82. Jiang G, Yang HR, Wang L, Wildey GM, Fung J, et al. Hepatic stellate cells preferentially expand allogeneic CD4+CD25+FoxP3+ regulatory T cells in an IL-2-dependent manner. *Transplantation.* (2008) 86.11: 1492–502.
83. Langhans B, Alwan AW, Krämer B, Glässner A, Lutz P, et al. Regulatory CD4+ T cells modulate the interaction between NK cells and hepatic stellate cells by acting on either cell type. *J Hepatol.* (2015) 62.2: 398–404.
84. Annunziato F, Romagnani C, and Romagnani S. The 3 major types of innate and adaptive cell-mediated effector immunity. *J Allergy Clin Immunol.* (2015) 135.3: 626–35.
85. Hoyler T, Klose CSN, Souabni A, Turqueti-Neves A, Pfeifer D, et al. The transcription factor GATA-3 controls cell fate and maintenance of type 2 innate lymphoid cells. *Immunity.* (2012) 37.4: 634–48.

86. Huang Y, Guo L, Qiu J, Chen X, Hu-Li J, et al. IL-25-responsive, lineage-negative KLRG1<sup>hi</sup> cells are multipotential “inflammatory” type 2 innate lymphoid cells. *Nat Immunol.* (2015) 16.2: 161–9.
87. Kabata H, Moro K, and Koyasu S. The group 2 innate lymphoid cell (ILC2) regulatory network and its underlying mechanisms. Vol. 286, *Immunol Rev.* Blackwell Publishing Ltd. (2018) 286.1: 37–52.
88. Halim TYF, Krauß RH, Sun AC, and Takei F. Lung natural helper cells are a critical source of Th2 cell-type cytokines in protease allergen-induced airway inflammation. *Immunity.* (2012) 36.3: 451–63.
89. Kim BS, Siracusa MC, Saenz SA, Noti M, Monticelli LA, et al. TSLP elicits IL-33-independent innate lymphoid cell responses to promote skin inflammation. *Sci Transl Med.* (2013) 5.170: 170ra16.
90. Mjösberg J, Bernink J, Golebski K, Karrich JJ, Peters CP, et al. The transcription factor GATA3 is essential for the function of human type 2 innate lymphoid cells. *Immunity.* (2012) 37.4: 649–59.
91. Roediger B, Kyle R, Tay SS, Mitchell AJ, Bolton HA, et al. IL-2 is a critical regulator of group 2 innate lymphoid cell function during pulmonary inflammation. *J Allergy Clin Immunol.* (2015) 136.6: 1653–63.
92. Steinmann S, Schoedsack M, Heinrich F, Breda PC, Ochel A, et al. Hepatic ILC2 activity is regulated by liver inflammation-induced cytokines and effector CD4<sup>+</sup> T cells. *Sci Rep.* (2020) 10.1: 1–13.
93. Kim BS, Wang K, Siracusa MC, Saenz SA, Brestoff JR, et al. Basophils promote innate lymphoid cell responses in inflamed skin. *J Immunol.* (2014) 193.7: 3717–25.
94. Motomura Y, Morita H, Moro K, Nakae S, Artis D, et al. Basophil-derived interleukin-4 controls the function of natural helper cells, a member of ILC2s, in lung inflammation. *Immunity.* (2014) 40.5: 758–71.
95. Moro K, Yamada T, Tanabe M, Takeuchi T, Ikawa T, et al. Innate production of TH2 cytokines by adipose tissue-associated c-Kit<sup>+</sup> Sca-1<sup>+</sup> lymphoid cells. *Nature.* (2010) 463.7280: 540–4.
96. Satoh-Takayama N, Kato T, Motomura Y, Kageyama T, Taguchi-Atarashi N, et al. Bacteria-induced group 2 innate lymphoid cells in the stomach provide immune protection through induction of IgA. *Immunity.* (2020) 52.4: 635–49.

97. Sheikh A, Lu J, Melese E, Seo JH, and Abraham N. IL-7 induces type 2 cytokine response in lung ILC2s and regulates GATA3 and CD25 expression. *J Leukoc Biol.* (2022) 112.5: 1105–13.
98. Wilhelm C, Hirota K, Stieglitz B, Van Snick J, Tolaini M, et al. An IL-9 fate reporter demonstrates the induction of an innate IL-9 response in lung inflammation. *Nat Immunol.* (2011) 12.11: 1071–7.
99. Yu X, Pappu R, Ramirez-Carrozzi V, Ota N, Caplazi P, et al. TNF superfamily member TL1A elicits type 2 innate lymphoid cells at mucosal barriers. *Mucosal Immunol.* (2014) 7.3: 730–40.
100. Nagashima H, Okuyama Y, Fujita T, Takeda T, Motomura Y, et al. GITR cosignal in ILC2s controls allergic lung inflammation. *J Allergy Clin Immunol.* (2018) 141.5: 1939–43.
101. Gasteiger G, Fan X, Dikiy S, Lee SY, and Rudensky AY. Tissue residency of innate lymphoid cells in lymphoid and nonlymphoid organs. *Science* (1979). (2015) 350.6263: 981–5.
102. Moro K, Kabata H, Tanabe M, Koga S, Takeno N, et al. Interferon and IL-27 antagonize the function of group 2 innate lymphoid cells and type 2 innate immune responses. *Nat Immunol.* (2016) 17.1: 76–86.
103. Liang Y, Jie Z, Hou L, Aguilar-Valenzuela R, Vu D, et al. IL-33 induces nuocytes and modulates liver injury in viral hepatitis. *J Immunol.* (2013) 190.11: 5666–75.
104. Mchedlidze T, Waldner M, Zopf S, Walker J, Rankin AL, et al. Interleukin-33-dependent innate lymphoid cells mediate hepatic fibrosis. *Immunity.* (2013) 39.2: 357–71.
105. Nakagawa H, Suzuki N, Hirata Y, Hikiba Y, Hayakawa Y, et al. Biliary epithelial injury-induced regenerative response by IL-33 promotes cholangiocarcinogenesis from peribiliary glands. *Proc Natl Acad Sci U S A.* (2017) 114.19: E3806–15.
106. Jeffery HC, McDowell P, Lutz P, Wawman RE, Roberts S, et al. Human intrahepatic ILC2 are IL-13 positive amphiregulin positive and their frequency correlates with model of end stage liver disease score. *PLoS One.* (2017) 12.12: 1–16.
107. Zaiss DMW, Gause WC, Osborne LC, and Artis D. Emerging functions of amphiregulin in orchestrating immunity, inflammation, and tissue repair. *Immunity.* (2015) 42.2: 216–26.

108. Berasain C, García-Trevijano ER, Castillo J, Erroba E, Lee DC, et al. Amphiregulin: An early trigger of liver regeneration in mice. *Gastroenterology*. (2005) 128.2: 424–32.
109. Santamaría E, Rodríguez-Ortigosa CM, Uriarte I, Latasa MU, Urtasun R, et al. The epidermal growth factor receptor ligand amphiregulin protects from cholestatic liver injury and regulates bile acids synthesis. *Hepatology*. (2019) 69.4: 1632–47.
110. McKee C, Sigala B, Soeda J, Mouralidarane A, Morgan M, et al. Amphiregulin activates human hepatic stellate cells and is upregulated in non alcoholic steatohepatitis. *Sci Rep*. (2015) 5: 1–10.
111. Perugorria MJ, Latasa MU, Nicou A, Cartagena-Lirola H, Castillo J, et al. The epidermal growth factor receptor ligand amphiregulin participates in the development of mouse liver fibrosis. *Hepatology*. (2008) 48.4: 1251–61.
112. Dai K, Huang L, Sun X, Yang L, and Gong Z. Hepatic CD206-positive macrophages express amphiregulin to promote the immunosuppressive activity of regulatory T cells in HBV infection. *J Leukoc Biol*. (2015) 98.6: 1071–80.
113. Ikeno Y, Ohara D, Takeuchi Y, Watanabe H, Kondoh G, et al. Foxp3<sup>+</sup> regulatory T cells inhibit CCl<sub>4</sub>-induced liver inflammation and fibrosis by regulating tissue cellular immunity. *Front Immunol*. (2020) 11.October: 1–11.
114. Russi AE, Shivakumar P, Luo Z, and Bezerra JA. Plasticity between type 2 innate lymphoid cell subsets and amphiregulin expression regulates epithelial repair in biliary atresia. *Hepatology*. (2023) 78.4: 1035–49.
115. Schneider MR and Wolf E. The epidermal growth factor receptor ligands at a glance. *J Cell Physiol*. (2009) 218.3: 460–6.
116. Komposch K and Sibilía M. EGFR signaling in liver diseases. *Int J Mol Sci*. (2015) 17.1: 30.
117. Zaiss DMW, van Loosdregt J, Gorlani A, Bekker CPJ, Gröne A, et al. Amphiregulin enhances regulatory T cell-suppressive function via the epidermal growth factor receptor. *Immunity*. (2013) 38.2: 275–84.
118. Holbro T and Hynes NE. ErbB receptors: Directing key signaling networks throughout life. *Annu Rev Pharmacol Toxicol*. (2004) 44: 195–217.
119. Yarden Y and Shilo BZ. SnapShot: EGFR signaling pathway. *Cell*. (2007) 131.5: 1018.e1-1018.e2.



120. Komurasaki T, Toyoda H, Uchida D, and Nemoto N. Mechanism of growth promoting activity of epiregulin in primary cultures of rat hepatocytes. *Growth Factors*. (2002) 20.2: 61–9.
121. Lee D, Pearsall RS, Das S, Dey SK, Godfrey VL, et al. Epiregulin is not essential for development of intestinal tumors but is required for protection from intestinal damage. *Mol Cell Biol*. (2004) 24.20: 8907–16.
122. Toyoda H, Komurasaki T, Uchida D, Takayama Y, Isobe T, et al. Epiregulin: A novel epidermal growth factor with mitogenic activity for rat primary hepatocytes. *J Biol Chem*. (1995) 270.13: 7495–500.
123. Block GD, Locker J, Bowen WC, Petersen BE, Katyal S, et al. Population expansion, clonal growth, and specific differentiation patterns in primary cultures of hepatocytes induced by HGF/SF, EGF and TGFalpha in a chemically defined (HGM) medium. *J Cell Biol*. (1996) 132.6: 1133–49.
124. Ito N, Kawata S, Tamura S, Kiso S, Tsushima H, et al. Heparin-binding EGF-like growth factor is a potent mitogen for rat hepatocytes. *Biochem Biophys Res Commun*. (1994) 198.1: 25–31.
125. De Juan C, Benito M, Alvarez A, and Fabregat I. Differential proliferative response of cultured fetal and regenerating hepatocytes to growth factors and hormones. *Exp Cell Res*. (1992) 202: 495–500.
126. McGowan JA, Strain AJ, and Bucher NLR. DNA synthesis in primary cultures of adult rat hepatocytes in a defined medium: Effects of epidermal growth factor, insulin, glucagon, and cyclic-AMP. *J Cell Physiol*. (1981) 108.3: 353–63.
127. Shing Y, Christofori G, Hanahan D, Ono Y, Sasada R, et al. Betacellulin: A mitogen from pancreatic beta cell tumors. *Science* (1979). (1993) 259.5101: 1604–7.
128. Strachan L, Murison JG, Prestidge RL, Sleeman MA, Watson JD, et al. Cloning and biological activity of epigen, a novel member of the epidermal growth factor Superfamily. *J Biol Chem*. (2001) 276.21: 18265–71.
129. Berasain C, García-Trevijano EE, Castillo J, Erroba E, Santamaría M, et al. Novel role for amphiregulin in protection from liver injury. *J Biol Chem*. (2005) 280.19: 19012–20.
130. Dai K, Huang L, Chen J, Yang L, and Gong Z. Amphiregulin promotes the immunosuppressive activity of intrahepatic CD4+ regulatory T cells to impair

- CD8<sup>+</sup> T-cell immunity against hepatitis B virus infection. *Immunology*. (2015) 144.3: 506–17.
131. Burzyn D, Kuswanto W, Kolodin D, Shadrach JL, Cerletti M, et al. A special population of regulatory T cells potentiates muscle repair. *Cell*. (2013) 155.6: 1282–95.
  132. Arpaia N, Green JA, Molledo B, Arvey A, Hemmers S, et al. A distinct function of regulatory T cells in tissue protection. *Cell*. (2015) 162.5: 1078–89.
  133. Monticelli LA, Sonnenberg GF, Abt MC, Alenghat T, Ziegler CGK, et al. Innate lymphoid cells promote lung-tissue homeostasis after infection with influenza virus. *Nat Immunol*. (2011) 12.11: 1045–54.
  134. Monticelli LA, Osborne LC, Noti M, Tran S V., Zaiss DMW, et al. IL-33 promotes an innate immune pathway of intestinal tissue protection dependent on amphiregulin-EGFR interactions. *Proc Natl Acad Sci U S A*. (2015) 112.34: 10762–7.
  135. Meulenbroeks C, Van Weelden H, Schwartz C, Voehringer D, Redegeld FAM, et al. Basophil-derived amphiregulin is essential for UVB irradiation-induced immune suppression. *J Invest Dermatol*. (2015) 135.1: 222–8.
  136. Barnard JA, Graves-Deal R, Pittelkow MR, DuBois R, Cook P, et al. Auto- and cross-induction within the mammalian epidermal growth factor-related peptide family. *J Biol Chem*. (1994) 269.36: 22817–22.
  137. Castillo J, Erroba E, Perugorria MJ, Santamaría M, Lee DC, et al. Amphiregulin contributes to the transformed phenotype of human hepatocellular carcinoma cells. *Cancer Res*. (2006) 66.12: 6129–38.
  138. Zvibel I, Brill S, Halpern Z, and Papa M. Amphiregulin and hepatocyte-derived extracellular matrix regulate proliferation and autocrine growth factor expression in colon cancer cell lines of varying liver-colonizing capability. *J Cell Biochem*. (2000) 76.2: 332–40.
  139. Kato M, Inazu T, Kawai Y, Masamura K, Yoshida M, et al. Amphiregulin is a potent mitogen for the vascular smooth muscle cell line, A7r5. *Biochem Biophys Res Commun*. (2003) 301.4: 1109–15.
  140. Guo S and Luo Y. Brain Foxp3<sup>+</sup> regulatory T cells can be expanded by Interleukin-33 in mouse ischemic stroke. *Int Immunopharmacol*. (2020) 81: 106027.

141. Halvorsen EC, Franks SE, Wadsworth BJ, Harbourne BT, Cederberg RA, et al. IL-33 increases ST2<sup>+</sup> Tregs and promotes metastatic tumour growth in the lungs in an amphiregulin-dependent manner. *Oncoimmunology*. (2019) 8.2: e1527497.
142. Schmitz J, Owyang A, Oldham E, Song Y, Murphy E, et al. IL-33, an interleukin-1-like cytokine that signals via the IL-1 receptor-related protein ST2 and induces T helper type 2-associated cytokines. *Immunity*. (2005) 23.5: 479–90.
143. Carriere V, Roussel L, Ortega N, Lacorre DA, Americh L, et al. IL-33, the IL-1-like cytokine ligand for ST2 receptor, is a chromatin-associated nuclear factor in vivo. *Proc Natl Acad Sci U S A*. (2006) 104.1: 282–7.
144. Chackerian AA, Oldham ER, Murphy EE, Schmitz J, Pflanz S, et al. IL-1 receptor accessory protein and ST2 comprise the IL-33 receptor complex. *J Immunol*. (2007) 179.4: 2551–5.
145. Villarreal DO and Weiner DB. Interleukin 33: A switch-hitting cytokine. *Curr Opin Immunol*. (2014) 28.1: 102–6.
146. Moussion C, Ortega N, and Girard JP. The IL-1-like cytokine IL-33 is constitutively expressed in the nucleus of endothelial cells and epithelial cells in vivo: A novel “Alarmin”? *PLoS One*. (2008) 3.10: e3331.
147. Arshad MI, Piquet-Pellorce C, L’Helgoualc’h A, Rauch M, Patrat-Delon S, et al. TRAIL but not FasL and TNF $\alpha$ , regulates IL-33 expression in murine hepatocytes during acute hepatitis. *Hepatology*. (2012) 56.6: 2353–62.
148. Arshad MI, Patrat-Delon S, Piquet-Pellorce C, L’Helgoualc’h A, Rauch M, et al. Pathogenic mouse hepatitis virus or poly(I:C) induce IL-33 in hepatocytes in murine models of hepatitis. *PLoS One*. (2013) 8.9: 1–10.
149. Cayrol C and Girard JP. IL-33: An alarmin cytokine with crucial roles in innate immunity, inflammation and allergy. *Curr Opin Immunol*. (2014) 31: 31–7.
150. Salimi M, Barlow JL, Saunders SP, Xue L, Gutowska-Owsiak D, et al. A role for IL-25 and IL-33-driven type-2 innate lymphoid cells in atopic dermatitis. *J Exp Med*. (2013) 210.13: 2939–50.
151. Siede J, Fröhlich A, Datsi A, Hegazy AN, Varga D V., et al. IL-33 receptor-expressing regulatory T cells are highly activated, Th2 biased and suppress CD4 T Cell proliferation through IL-10 and TGF $\beta$  release. *PLoS One*. (2016) 11.8: 1–15.

152. Schiering C, Krausgruber T, Chomka A, Fröhlich A, Adelmann K, et al. The alarmin IL-33 promotes regulatory T-cell function in the intestine. *Nature*. (2014) 513.7519: 564–8.
153. Delacher M, Imbusch CD, Weichenhan D, Breiling A, Hotz-Wagenblatt A, et al. Genome-wide DNA-methylation landscape defines specialization of regulatory T cells in tissues. *Nat Immunol*. (2017) 18.10: 1160–72.
154. Abe K, Takahashi A, Fujita M, Hayashi M, Okai K, et al. Interleukin-33/ST2-mediated inflammation plays a critical role in the pathogenesis and severity of type I autoimmune hepatitis. *Hepatol Commun*. (2019) 3.5: 670–84.
155. Gao Y, Liu Y, Yang M, Guo X, Zhang M, et al. IL-33 treatment attenuated diet-induced hepatic steatosis but aggravated hepatic fibrosis. *Oncotarget*. (2016) 7.23: 33649–61.
156. Liang M, Liwen Z, Yun Z, Yanbo D, and Jianping C. Serum levels of IL-33 and correlation with IL-4, IL-17A, and hypergammaglobulinemia in patients with autoimmune hepatitis. *Mediators Inflamm*. (2018) 2018.1: 7964654.
157. Roth GA, Zimmermann M, Lubczyk BA, Pilz J, Faybik P, et al. Up-regulation of interleukin 33 and soluble ST2 serum levels in liver failure. *J Surg Res*. (2010) 163.2: e79–83.
158. Wang J, Cai Y, Ji H, Feng J, Ayana DA, et al. Serum IL-33 levels are associated with liver damage in patients with chronic hepatitis B. *J Interferon Cytokine Res*. (2012) 32.6: 248–53.
159. Wang J, Zhao P, Guo H, Sun X, Jiang Z, et al. Serum IL-33 levels are associated with liver damage in patients with chronic hepatitis C. *Mediators Inflamm*. (2012) 2012.1: 819636.
160. Wang M, Shen G, Xu L, Liu X, Brown JM, et al. IL-1 receptor like 1 protects against alcoholic liver injury by limiting NF- $\kappa$ B activation in hepatic macrophages. *J Hepatol*. (2018) 68.1: 109–17.
161. Chen J, Duan L, Xiong A, Zhang H, Zheng F, et al. Blockade of IL-33 ameliorates Con A-induced hepatic injury by reducing NKT cell activation and IFN- $\gamma$  production in mice. *J Mol Med*. (2012) 90.12: 1505–15.
162. Volarevic V, Mitrovic M, Milovanovic M, Zelen I, Nikolic I, et al. Protective role of IL-33/ST2 axis in Con A-induced hepatitis. *J Hepatol*. (2012) 56.1: 26–33.
163. Noel G, Arshad MI, Filliol A, Genet V, Rauch M, et al. Ablation of interaction between IL-33 and ST2<sup>+</sup> regulatory T cells increases immune cell-mediated

- hepatitis and activated NK cell liver infiltration. *Am J Physiol Gastrointest Liver Physiol.* (2016) 311.2: G313–23.
164. Wan YY and Flavell RA. Identifying Foxp3-expressing suppressor T cells with a bicistronic reporter. *Proc Natl Acad Sci U S A.* (2005) 102.14: 5126–31.
  165. Kamanaka M, Kim ST, Wan YY, Sutterwala FS, Lara-Tejero M, et al. Expression of interleukin-10 in intestinal lymphocytes detected by an interleukin-10 reporter knockin tiger mouse. *Immunity.* (2006) 25.6: 941–52.
  166. McGill MR. The past and present of serum aminotransferases and the future of liver injury biomarkers. *EXCLI J.* (2016) 15: 817–28.
  167. Shah K and Maghsoudlou P. Enzyme-linked immunosorbent assay (ELISA): the basics. *Br J Hosp Med.* (2016) 77.7: C98–101.
  168. Bos ES, van der Doelen AA, van Rooy N, and Schuurs AHW. 3,3',4,5'-Tetramethylbenzidine as an Ames test negative chromogen for horse-radish peroxidase in enzyme-immunoassay. *J Immunoassay.* (1981) 2.3–4: 187–204.
  169. Adams G. A beginner's guide to RT-PCR, qPCR and RT-qPCR. *Biochem (Lond).* (2020) 42.3: 48–53.
  170. Bustin SA and Mueller R. Real-time reverse transcription PCR (qRT-PCR) and its potential use in clinical diagnosis. Vol. 109, *Clin Sci.* (2005) 109.4: 365–79.
  171. Dibal NI, Garba SH, and Jacks TW. Histological stains and their application in teaching and research. *Asian J Health Sci.* (2022) 8.2: 43–43.
  172. Kiernan JA. Does progressive nuclear staining with hemalum (alum hematoxylin) involve DNA, and what is the nature of the dye-chromatin complex? *Biotech Histochem.* (2018) 93.2: 133–48.
  173. Meloan SN and Puchtler H. "Harris Hematoxylin," What Harris really wrote and the mechanism of Hemalum stains. *J Histotechnol.* (1987) 10.4: 257–61.
  174. Junqueira LCU, Bignolas G, and Brentani RR. Picrosirius staining plus polarization microscopy, a specific method for collagen detection in tissue sections. *Histochem J.* (1979) 11: 447–55.
  175. Miltenyi S, Müller W, Weichel W, and Radbruch A. High gradient magnetic cell separation with MACS. *Cytometry.* (1990) 11.2: 231–8.
  176. Radbruch A, Mechtold B, Thiel A, Miltenyi S, and Pflugert E. High-gradient magnetic cell sorting. In: *Methods Cell Biol.* 2nd ed. Editors: Darzynkiewicz Z, Robinson JP, Crissman HA. Academic Press, San Diego. (1994) 42: 387–403.

177. Liu ZX, Govindarajan S, Okamoto S, and Dennert G. NK cells cause liver injury and facilitate the induction of T cell-mediated immunity to a viral liver infection. *J Immunol.* (2000) 164.12: 6480–6.
178. Pertoft H. Fractionation of cells and subcellular particles with Percoll. *J Biochem Biophys Methods.* (2000) 44: 1–30.
179. Goetz C, Hammerbeck C, Wyman A, and Huh JB. Cell enrichment. In: *Flow Cytometry Basics for the Non-Expert*. 1st ed. Editor: Kalyuzhny AE. Springer, Cham. (2018): 149–55.
180. Bonnevier J, Hammerbeck C, and Goetz C. Flow cytometry: Definition, history, and uses in biological research. In: *Flow Cytometry Basics for the Non-Expert*. 1st ed. Editor: Kalyuzhny AE. Springer, Cham. (2018): 1–11.
181. Herzenberg LA, Parks D, Sahaf B, Perez O, Roederer M, et al. The history and future of the fluorescence activated cell sorter and flow cytometry: A view from Stanford. *Clin Chem.* (2002) 48.10: 1819–27.
182. Bonnevier J, Huh JB, Hammerbeck C, and Goetz C. Physics of a flow cytometer. In: *Flow Cytometry Basics for the Non-Expert*. 1st ed. Editor: Kalyuzhny AE. Springer, Cham. (2018): 13–24.
183. Hammerbeck C, Goetz C, Peng LJ, and Huh JB. Experimental considerations with data sets as examples. In: *Flow Cytometry Basics for the Non-Expert*. 1st ed. Editor: Kalyuzhny AE. Springer, Cham. (2018): 103–48.
184. Otto GP, Rathkolb B, Oestereicher MA, Lengger CJ, Moerth C, et al. Clinical chemistry reference intervals for C57BL/6J, C57BL/6N, and C3HeB/FeJ mice (*Mus musculus*). *J Am Assoc Lab Anim Sci.* (2016) 55.4: 375–86.
185. Luan J, Zhang X, Wang S, Li Y, Fan J, et al. NOD-like receptor protein 3 inflammasome-dependent IL-1 $\beta$  accelerated ConA-induced hepatitis. *Front Immunol.* (2018) 9: 340323.
186. Mizuhara H, O'Neill E, Seki N, Ogawa T, Kusunoki C, et al. T cell activation-associated hepatic injury: mediation by tumor necrosis factors and protection by interleukin 6. *J Exp Med.* (1994) 179.5: 1529–37.
187. Wang L, Tu L, Zhang J, Xu K, and Qian W. Stellate cell activation and imbalanced expression of TGF- $\beta$  1/TGF- $\beta$  3 in acute autoimmune liver lesions induced by ConA in mice. *Biomed Res Int.* (2017) 2017: 2540540.

188. Berasain C, Perugorria MJ, Latasa MU, Castillo J, Goñi S, et al. The epidermal growth factor receptor: A link between inflammation and liver cancer. *Exp Biol Med.* (2009) 234.7: 713–25.
189. Berasain C, Nicou A, Garcia-Irigoyen O, Latasa MU, Urtasun R, et al. Epidermal growth factor receptor signaling in hepatocellular carcinoma: Inflammatory activation and a new intracellular regulatory mechanism. *Dig Dis.* (2012) 30.5: 524–31.
190. Woodworth CD, McMullin E, Iglesias M, and Plowman GD. Interleukin 1 $\alpha$  and tumor necrosis factor  $\alpha$  stimulate autocrine amphiregulin expression and proliferation of human papillomavirus-immortalized and carcinoma-derived cervical epithelial cells. *Proc Natl Acad Sci U S A.* (1995) 92.7: 2840–4.
191. Asano K, Nakamura H, Lilly CM, Klagsbrun M, and Drazen JM. Interferon  $\gamma$  induces prostaglandin G/H synthase-2 through an autocrine loop via the epidermal growth factor receptor in human bronchial epithelial cells. *J Clin Invest.* (1997) 99.5: 1057–63.
192. Liu FL, Wu CC, and Chang DM. TACE-dependent amphiregulin release is induced by IL-1 $\beta$  and promotes cell invasion in fibroblast-like synoviocytes in rheumatoid arthritis. *Rheumatology.* (2014) 53.2: 260–9.
193. Wang SE, Xiang B, Guix M, Olivares MG, Parker J, et al. Transforming growth factor  $\beta$  engages TACE and ErbB3 to activate phosphatidylinositol-3 kinase/Akt in ErbB2-overexpressing breast cancer and desensitizes cell to trastuzumab. *Mol Cell Biol.* (2008) 28.18: 5605–20.
194. Basset L, Chevalier S, Danger Y, Arshad MI, Piquet-Pellorce C, et al. Interleukin-27 and IFN $\gamma$  regulate the expression of CXCL9, CXCL10, and CXCL11 in hepatitis. *J Mol Med.* (2015) 93.12: 1355–67.
195. Collison LW and Vignali DAA. In vitro Treg suppression assays. *Methods Mol Biol.* (2011) 707: 21–37.
196. Venken K, Thewissen M, Hellings N, Somers V, Hensen K, et al. A CFSE based assay for measuring CD4+CD25+ regulatory T cell mediated suppression of auto-antigen specific and polyclonal T cell responses. *J Immunol Methods.* (2007) 322.1–2: 1–11.
197. Parish CR. Fluorescent dyes for lymphocyte migration and proliferation studies. *Immunol Cell Biol.* (1999) 77.6: 499–508.

198. Lyons AB and Parish CR. Determination of lymphocyte division by flow cytometry. *J Immunol Methods*. (1994) 171.1: 131–7.
199. Fabregat I, Moreno-Càceres J, Sánchez A, Dooley S, Dewidar B, et al. TGF- $\beta$  signalling and liver disease. *FEBS Journal*. (2016) 283: 2219–32.
200. Castillo J, Goñi S, Latasa MU, Perugorria MJ, Calvo A, et al. Amphiregulin induces the alternative splicing of p73 into its oncogenic isoform  $\Delta$ Ex2p73 in human hepatocellular tumors. *Gastroenterology*. (2009) 137.5: 1805–15.
201. Latasa MU, Salis F, Urtasun R, Garcia-Irigoyen O, Elizalde M, et al. Regulation of amphiregulin gene expression by  $\beta$ -catenin signaling in human hepatocellular carcinoma cells: A novel crosstalk between FGF19 and the EGFR system. *PLoS One*. (2012) 7.12: e52711.
202. Yuan CH, Sun XM, Zhu CL, Liu SP, Wu L, et al. Amphiregulin activates regulatory T lymphocytes and suppresses CD8<sup>+</sup> T cell-mediated anti-tumor response in hepatocellular carcinoma cells. *Oncotarget*. (2015) 6.31: 32138–53.
203. Awad AE, Ebrahim MA, Eissa LA, and El-Shishtawy MM. Dickkopf-1 and amphiregulin as novel biomarkers and potential therapeutic targets in hepatocellular carcinoma. *Int J Hematol Oncol Stem Cell Res*. (2019) 13.3: 153–63.
204. Lin HH, Peng YJ, Tsai MJ, Wu YY, Tsai TN, et al. Upregulation of amphiregulin by retinoic acid and Wnt signalling promotes liver cancer cell proliferation. *J Cell Physiol*. (2020) 235.2: 1689–99.
205. Isaac A, Mohamed SM, Ahmed OA, Hassan AGM, and Rasmy HS. Amphiregulin as a novel diagnostic and prognostic biomarker of hepatocellular carcinoma before and after locoregional treatment. *Egypt J Intern Med*. (2021) 33: 46.
206. Chang YC, Li CH, Chan MH, Chen MH, Yeh CN, et al. Regorafenib inhibits epithelial-mesenchymal transition and suppresses cholangiocarcinoma metastasis via YAP1-AREG axis. *Cell Death Dis*. (2022) 13.4: 391.
207. Takemura T, Yoshida Y, Kiso S, Saji Y, Ezaki H, et al. Conditional knockout of heparin-binding epidermal growth factor-like growth factor in the liver accelerates carbon tetrachloride-induced liver injury in mice. *Hepatol Res*. (2013) 43.4: 384–93.
208. Liu Q, Rehman H, Krishnasamy Y, Haque K, Schnellmann RG, et al. Amphiregulin stimulates liver regeneration after small-for-size mouse liver transplantation. *Am J Transplant*. (2012) 12.8: 2052–61.



209. Tomita K, Haga H, Mizuno K, Katsumi T, Sato C, et al. Epiregulin promotes the emergence and proliferation of adult liver progenitor cells. *Am J Physiol Gastrointest Liver Physiol*. (2014) 307.1: 50–7.
210. Kiso S, Kawata S, Tamura S, Higashiyama S, Ito N, et al. Role of heparin-binding epidermal growth factor-like growth factor as a hepatotrophic factor in rat liver regeneration after partial hepatectomy. *Hepatology*. (1995) 22.5: 1584–90.
211. Kiso S, Kawata S, Tamura S, Ito N, Tsushima H, et al. Expression of heparin-binding EGF-like growth factor in rat liver injured by carbon tetrachloride or D-galactosamine. *Biochem Biophys Res Commun*. (1996) 220.2: 285–8.
212. Kiso S, Kawata S, Tamura S, Umeki S, Ito N, et al. Effects of exogenous human heparin-binding epidermal growth factor-like growth factor on DNA synthesis of hepatocytes in normal mouse liver. *Biochem Biophys Res Commun*. (1999) 259.3: 683–7.
213. Kiso S, Kawata S, Tamura S, Ito N, Takaishi K, et al. Alteration in growth regulation of hepatocytes in primary culture obtained from cirrhotic rat: Poor response to transforming growth factor- $\beta$ 1 and interferons. *Hepatology*. (1994) 20.5: 1303–8.
214. Mitchell C, Nivison M, Jackson LF, Fox R, Lee DC, et al. Heparin-binding epidermal growth factor-like growth factor links hepatocyte priming with cell cycle progression during liver regeneration. *J Biol Chem*. (2005) 280.4: 2562–8.
215. Yamada A, Kawata S, Tamura S, Kiso S, Higashiyama S, et al. Plasma heparin-binding EGF-like growth factor levels in patients after partial hepatectomy as determined with an enzyme-linked immunosorbent assay. *Biochem Biophys Res Commun*. (1998) 246.3: 783–7.
216. Kiso S, Kawata S, Tamura S, Inui Y, Yoshida Y, et al. Liver regeneration in heparin-binding EGF-like growth factor transgenic mice after partial hepatectomy. *Gastroenterology*. (2003) 124.3: 701–7.
217. Khai NC, Sakamoto K, Takamatsu H, Matsufuji H, and Kosai KI. Recombinant soluble form of heparin-binding epidermal growth factor-like growth factor protein therapy drastically inhibits Fas-mediated fulminant hepatic failure: Implications in clinical application. *Hepatol Res*. (2011) 41.6: 594–6.
218. Khai NC, Takahashi T, Ushikoshi H, Nagano S, Yuge K, et al. In vivo hepatic HB-EGF gene transduction inhibits Fas-induced liver injury and induces liver

- regeneration in mice: A comparative study to HGF. *J Hepatol.* (2006) 44.6: 1046–54.
219. Sakamoto K, Khai NC, Wang Y, Irie R, Takamatsu H, et al. Heparin-binding epidermal growth factor-like growth factor and hepatocyte growth factor inhibit cholestatic liver injury in mice through different mechanisms. *Int J Mol Med.* (2016) 38.6: 1673–82.
  220. Padiadpu J, Garcia-Jaramillo M, Newman NK, Pederson JW, Rodrigues R, et al. Multi-omic network analysis identified betacellulin as a novel target of omega-3 fatty acid attenuation of western diet-induced nonalcoholic steatohepatitis. *EMBO Mol Med.* (2023) 15: e18367.
  221. Moon WS, Park HS, Yu KH, Park MY, Kim KR, et al. Expression of betacellulin and epidermal growth factor receptor in hepatocellular carcinoma: implications for angiogenesis. *Hum Pathol.* (2006) 37.10: 1324–32.
  222. Takemura T, Yoshida Y, Kiso S, Kizu T, Furuta K, et al. Conditional loss of heparin-binding EGF-like growth factor results in enhanced liver fibrosis after bile duct ligation in mice. *Biochem Biophys Res Commun.* (2013) 437.2: 185–91.
  223. Guo Y, Ding Q, Chen L, Ji C, Hao H, et al. Overexpression of heparin-binding epidermal growth factor-like growth factor mediates liver fibrosis in transgenic mice. *Am J Med Sci.* (2017) 354.2: 199–210.
  224. Kiso S, Kawata S, Tamura S, Miyagawa JI, Ito N, et al. Expression of heparin-binding epidermal growth factor-like growth factor in the hepatocytes of fibrotic rat liver during hepatocarcinogenesis. *J Gastroenterol Hepatol.* (1999) 14.12: 1203–9.
  225. Huang G, Besner GE, and Brigstock DR. Heparin-binding epidermal growth factor-like growth factor suppresses experimental liver fibrosis in mice. *Lab Invest.* (2012) 92.5: 703–12.
  226. Chen WY, Wu YH, Tsai TH, Li RF, Lai ACY, et al. Group 2 innate lymphoid cells contribute to IL-33-mediated alleviation of cardiac fibrosis. *Theranostics.* (2021) 11.6: 2594–611.
  227. Liu Q, Dwyer GK, Zhao Y, Li H, Mathews LR, et al. IL-33-mediated IL-13 secretion by ST2<sup>+</sup> Tregs controls inflammation after lung injury. *JCI Insight.* (2019) 4.6.
  228. Matta BM, Lott JM, Mathews LR, Liu Q, Rosborough BR, et al. IL-33 is an unconventional alarmin that stimulates IL-2 secretion by dendritic cells to

- selectively expand IL-33R/ST2<sup>+</sup> regulatory T cells. *J Immunol.* (2014) 193.8: 4010–20.
229. Kawai K, Uchiyama M, Hester J, and Issa F. IL-33 drives the production of mouse regulatory T cells with enhanced in vivo suppressive activity in skin transplantation. *Am J Transplant.* (2021) 21.3: 978–92.
  230. Han JM, Wu D, Denroche HC, Yao Y, Verchere CB, et al. IL-33 reverses an obesity-induced deficit in visceral adipose tissue ST2<sup>+</sup> T regulatory cells and ameliorates adipose tissue inflammation and insulin resistance. *J Immunol.* (2015) 194.10: 4777–83.
  231. Biton J, Khaleghparast Athari S, Thiolat A, Santinon F, Lemeiter D, et al. In vivo expansion of activated Foxp3<sup>+</sup> regulatory T cells and establishment of a type 2 immune response upon IL-33 treatment protect against experimental arthritis. *J Immunol.* (2016) 197.5: 1708–19.
  232. Matta BM, Reichenbach DK, Zhang X, Mathews L, Koehn BH, et al. Peri-alloHCT IL-33 administration expands recipient T-regulatory cells that protect mice against acute GVHD. *Blood.* (2016) 128.3: 427–39.
  233. Popovic B, Golemac M, Podlech J, Zeleznjak J, Bilic-Zulle L, et al. IL-33/ST2 pathway drives regulatory T cell dependent suppression of liver damage upon cytomegalovirus infection. *PLoS Pathog.* (2017) 13.4: e1006345.
  234. Xie D, Miao W, Xu F, Yuan C, Li S, et al. IL-33/ST2 axis protects against traumatic brain injury through enhancing the function of regulatory T cells. *Front Immunol.* (2022) 13: 860772.
  235. Xu L, Li W, Wang X, Zhang L, Qi Q, et al. The IL-33-ST2-MyD88 axis promotes regulatory T cell proliferation in the murine liver. *Eur J Immunol.* (2018) 48.8: 1302–7.
  236. Han M, Rajput C, Hong JY, Lei J, Hinde JL, et al. The innate cytokines IL-25, IL-33, and TSLP cooperate in the induction of type 2 innate lymphoid cell expansion and mucous metaplasia in rhinovirus-infected immature mice. *J Immunol.* (2017) 199.4: 1308–18.
  237. Long A, Dominguez D, Qin L, Chen S, Fan J, et al. Type 2 innate lymphoid cells Impede IL-33-mediated tumor suppression. *J Immunol.* (2018) 201.11: 3456–64.
  238. Barlow JL, Bellosi A, Hardman CS, Drynan LF, Wong SH, et al. Innate IL-13-producing nuocytes arise during allergic lung inflammation and contribute to airways hyperreactivity. *J Allergy Clin Immunol.* (2012) 129.1: 191–8.

239. Wolterink RGJK, Kleinjan A, van Nimwegen M, Bergen I, de Bruijn M, et al. Pulmonary innate lymphoid cells are major producers of IL-5 and IL-13 in murine models of allergic asthma. *Eur J Immunol.* (2012) 42.5: 1106–16.
240. Ngo Thi Phuong N, Palmieri V, Adamczyk A, Klopfleisch R, Langhorst J, et al. IL-33 drives expansion of type 2 innate lymphoid cells and regulatory T cells and protects mice from severe, acute colitis. *Front Immunol.* (2021) 12: 669787.
241. Kotas ME, Dion J, Dyken S Van, Ricardo-Gonzalez RR, Danel CJ, et al. A role for IL-33-activated ILC2s in eosinophilic vasculitis. *JCI Insight.* (2021) 6.11: e143366.
242. Halim TYF, Steer CA, Mathä L, Gold MJ, Martinez-Gonzalez I, et al. Group 2 innate lymphoid cells are critical for the initiation of adaptive T helper 2 cell-mediated allergic lung inflammation. *Immunity.* (2014) 40.3: 425–35.
243. Trautwein C, Rakemann T, Malek NP, Plümpe J, Tiegs G, et al. Concanavalin A-induced liver injury triggers hepatocyte proliferation. *J Clin Invest.* (1998) 101.9: 1960–9.
244. Kaija H, Pakanen L, Kortelainen ML, and Porvari K. Hypothermia and rewarming induce gene expression and multiplication of cells in healthy rat prostate tissue. *PLoS One.* (2015) 10.5: e0127854.
245. Zhou Y, Lee JY, Lee CM, Cho WK, Kang MJ, et al. Amphiregulin, an epidermal growth factor receptor ligand, plays an essential role in the pathogenesis of transforming growth factor- $\beta$ -induced pulmonary fibrosis. *J Biol Chem.* (2012) 287.50: 41991–2000.
246. Cook PW, Piepkorn M, Clegg CH, Plowman GD, Mark DeMay J, et al. Transgenic expression of the human amphiregulin gene induces a psoriasis-like phenotype. *J Clin Invest.* (1997) 100.9: 2286–94.
247. Cook PW, Brown JR, Cornell KA, and Pittelkow MR. Suprabasal expression of human amphiregulin in the epidermis of transgenic mice induces a severe, early-onset, psoriasis-like skin pathology: Expression of amphiregulin in the basal epidermis is also associated with synovitis. *Exp Dermatol.* (2004) 13.6: 347–56.
248. Amin K, Yaqoob U, Schultz B, Vaughn BP, Khoruts A, et al. Amphiregulin in intestinal acute graft-versus-host disease: a possible diagnostic and prognostic aid. *Modern Pathology.* (2019) 32.4: 560–7.

249. Qi CF, Liscia DS, Normanno N, Merlo G, Johnson GR, et al. Expression of transforming growth factor  $\alpha$ , amphiregulin and cripto-1 in human breast carcinomas. *Br J Cancer*. (1994) 69.5: 903–10.
250. Panico L, D'Antonio A, Salvatore G, Mezza E, Tortora G, et al. Differential immunohistochemical detection of transforming growth factor  $\alpha$ , amphiregulin and CRIPTO in human normal and malignant breast tissues. *Int J Cancer*. (1996) 65.1: 51–6.
251. Martini A, Marioni G, Zanoletti E, Cappellesso R, Stramare R, et al. YAP, TAZ and AREG expression in eighth cranial nerve schwannoma. *Int J Biol Markers*. (2017) 32.3: e319–24.
252. Karlmark KR, Wasmuth HE, Trautwein C, and Tacke F. Chemokine-directed immune cell infiltration in acute and chronic liver disease. *Expert Rev Gastroenterol Hepatol*. (2008) 2.2: 233–42.
253. Sahin H, Borkham-Kamphorst E, Do O NT, Berres ML, Kaldenbach M, et al. Proapoptotic effects of the chemokine, CXCL 10 are mediated by the noncognate receptor TLR4 in hepatocytes. *Hepatology*. (2013) 57.2: 797–805.
254. Ito M, Komai K, Mise-Omata S, Iizuka-Koga M, Noguchi Y, et al. Brain regulatory T cells suppress astrogliosis and potentiate neurological recovery. *Nature*. (2019) 565.7738: 246–50.
255. Qin L, Tamasi J, Raggatt L, Li X, Feyen JHM, et al. Amphiregulin is a novel growth factor involved in normal bone development and in the cellular response to parathyroid hormone stimulation. *Journal of Biological Chemistry*. (2005) 280.5: 3974–81.
256. Wang S, Zhang Y, Wang Y, Ye P, Li J, et al. Amphiregulin confers regulatory T cell suppressive function and tumor invasion via the EGFR/GSK-3 $\beta$ /Foxp3 axis. *J Biol Chem*. (2016) 291.40: 21085–95.
257. Rauber S, Lubber M, Weber S, Maul L, Soare A, et al. Resolution of inflammation by interleukin-9-producing type 2 innate lymphoid cells. *Nat Med*. (2017) 23.8: 938.
258. Rigas D, Lewis G, Aron JL, Wang B, Banie H, et al. Type 2 innate lymphoid cell suppression by regulatory T cells attenuates airway hyperreactivity and requires inducible T-cell costimulator–inducible T-cell costimulator ligand interaction. *J Allergy Clin Immunol*. (2017) 139.5: 1468-1477.e2.

259. Krishnamoorthy N, Burkett PR, Dalli J, Abdulnour REE, Colas R, et al. Cutting edge: Maresin-1 engages regulatory T cells to limit type 2 innate lymphoid cell activation and promote resolution of lung inflammation. *J Immunol.* (2015) 194.3: 863–7.
260. Behary J, Raposo AE, Amorim NML, Zheng H, Gong L, et al. Defining the temporal evolution of gut dysbiosis and inflammatory responses leading to hepatocellular carcinoma in Mdr2  $-/-$  mouse model. *BMC Microbiol.* (2021) 21: 113.

## Danksagung

An dieser Stelle möchte ich mich bei allen bedanken, die durch ihre fachliche oder persönliche Unterstützung zur Entstehung und Umsetzung dieser Arbeit beigetragen haben.

Zunächst gilt mein Dank meiner Betreuerin, Frau PD Dr. Katrin Neumann, die dieses Projekt geplant und die Finanzierung organisiert hat. Darüber hinaus hat sie mich während aller Phasen meiner Arbeit mit wertvollem Rat und stetiger Unterstützung begleitet. Sie hat mich fachkundig in die experimentellen und analytischen Methoden des Projekts eingeführt und mich zu selbstständigem Arbeiten angeleitet. Besonders schätze ich ihr Vertrauen in meine fachliche Kompetenz, auch nach Misserfolgen, und ihre sachliche und ruhige Art, mit stressigen Situationen umzugehen. Trotz ihres oft sehr vollen Terminkalenders hat sie sich immer die Zeit genommen, wichtige Entscheidungen und Fortschritte des Projektes zu besprechen. Ich danke ihr auch sehr für die hilfreichen Anmerkungen zu Postern, Präsentationen und vor allem zu dieser Dissertation.

Weiterhin geht mein Dank an Frau PD Dr. Katrin Neumann und Herrn PD Dr. Hartwig Lüthen für die Übernahme der Gutachten und den damit verbundenen zeitlichen Aufwand.

Ganz besonderer Dank geht ebenfalls an Frau Prof. Dr. Gisa Tiegs für die freundliche Aufnahme in ihrer Arbeitsgruppe am Institut für Experimentelle Immunologie und Hepatologie des UKE, und die Bereitstellung dieses interessanten Forschungsprojektes. Ich hatte eine sehr schöne und lehrreiche Zeit in einer optimalen Forschungsumgebung. Ich danke ihr auch für die Möglichkeit der Teilnahme an so vielen Konferenzen, auf denen ich meine vorläufigen Daten vorstellen und viel Wissen im Bereich Immunologie und Hepatologie sammeln konnte. Weiterhin danke ich Frau Prof. Dr. Gisa Tiegs, dass sie mir die Teilnahme am Graduiertenkolleg „Entzündung und Regeneration“ des SFB 841 ermöglicht hat. Ich danke außerdem allen Vortragenden und Lehrenden, die das Graduiertenkolleg mit ihrem Wissen bereichert und mir wertvolle Kompetenzen in den Bereichen gute wissenschaftliche Praxis, wissenschaftliches Schreiben, wissenschaftliche Methoden, Präsentationstechniken

und Biostatistik vermittelt haben. Im Besonderen Danke ich den Mitgliedern meiner Betreuungskommission des Graduiertenkollegs, Herrn Prof. Dr. Hans-Willi Mittrücker und Herrn Prof. Dr. Johannes Herkel, für das konstruktive Feedback und die hilfreichen Anregungen.

Ich danke zudem den Co-Autoren meiner veröffentlichten Arbeit, Fitriasari Jonin, Dr. Aaron Ochel, Fabian Heinrich, Prof. Dr. Astrid M. Westendorf, Prof. Dr. Gisa Tiegs und PD Dr. Katrin Neumann, für ihre bedeutenden wissenschaftlichen Beiträge, die enge Zusammenarbeit und die fachliche Unterstützung.

Darüber hinaus danke ich allen ehemaligen Mitgliedern der Arbeitsgruppe, die während meiner Promotionszeit das Labor mit Leben erfüllt haben, darunter Prof. Dr. Gisa Tiegs, PD Dr. Katrin Neumann, PD Dr. Andrea Horst, Dr. Claudia Wegscheid, Dr. Laura Berkhout, Dr. Gevitha Ravichandran, Dr. Sana Javed, Dr. Kingsley Gideon Kumashie, Dr. Anne Müller, Mareike Kellerer, Fitriasari Jonin, Charlotte Rumer, Elena Tasika, Carsten Rothkegel und Martina Lüneburg. Ihr habt durch die angenehme, motivierende, freundschaftliche und spaßige Arbeitsatmosphäre viele produktive Tage ermöglicht und darüber hinaus unvergessliche Momente geschaffen, sei es durch spannende Gespräche, lustige Streiche, gemeinsames Eis essen an heißen Sommertagen oder gesellige Abende außerhalb der Arbeitszeit. Mein ganz großer Dank gilt den technischen Assistenten Elena Tasika und Carsten Rothkegel für die Organisation des Labors und die Einführung in viele labortechnische Methoden. Bei Elena bedanke ich mich besonders für ihre außerordentliche und sehr zuverlässige Unterstützung bei allen aufwändigen Tierversuchen und bei Carsten für seine großartige Hilfe im Bereich Histologie. Ich bin sehr froh, Teil eines so wunderbaren Teams gewesen zu sein. Weiterhin möchte ich mich bei den Kollegen der FACS Core Facility des Universitätsklinikums Eppendorf für ihre Unterstützung bedanken.

Zu guter Letzt möchte ich meiner Familie und meinen Freunden danken, die mich immer unterstützt und gerade in schwierigen Zeiten motiviert und ermutigt haben. Insbesondere danke ich Ammar Alabdo, Emma-Maria Efremova, Charlotte Rumer und Carolin Wachtendorf für die zahlreichen Stunden, die sie gemeinsam mit mir in der Bibliothek oder daheim am Schreibtisch verbracht haben. Dank ihnen wurden diese Stunden zu wunderschönen Tagen.



## Affidavit

I hereby declare and affirm that this doctoral dissertation is my own work and that I have not used any aids and sources other than those indicated.

If electronic resources based on generative artificial intelligence (gAI) were used in the course of writing this dissertation, I confirm that my own work was the main and value-adding contribution and that complete documentation of all resources used is available in accordance with good scientific practice. I am responsible for any erroneous or distorted content, incorrect references, violations of data protection and copyright law or plagiarism that may have been generated by the gAI.

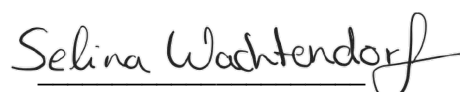
## Eidesstattliche Versicherung

Hiermit versichere ich an Eides statt, die vorliegende Dissertationsschrift selbst verfasst und keine anderen als die angegebenen Hilfsmittel und Quellen benutzt zu haben.

Sofern im Zuge der Erstellung der vorliegenden Dissertationsschrift generative Künstliche Intelligenz (gKI) basierte elektronische Hilfsmittel verwendet wurden, versichere ich, dass meine eigene Leistung im Vordergrund stand und dass eine vollständige Dokumentation aller verwendeten Hilfsmittel gemäß der Guten wissenschaftlichen Praxis vorliegt. Ich trage die Verantwortung für eventuell durch die gKI generierte fehlerhafte oder verzerrte Inhalte, fehlerhafte Referenzen, Verstöße gegen das Datenschutz- und Urheberrecht oder Plagiate.

Hamburg, den 14.11.2024

Ort und Datum



Selina Wachtendorf